Ph.D. Thesis 2023

Coastal aquifers and processes related to Global Change: Wetlands, heat transport and floodings

Ángela María Blanco Coronas

UNIVERSIDAD DE GRANADA

Programa Doctorado
Ciencias de la Tierra

Universidad de Granada

Departamento de Geodinámica

Coastal aquifers and processes related to Global Change: Wetlands, heat transport and floodings

Memoria de Tesis Doctoral presentada por la Licenciada en Geología Dña. Ángela María Blanco Coronas para optar al Grado de Doctor con Mención Internacional por la Universidad de Granada.

Granada, 31 de Enero de 2023.

V°B° de los Directores   La Doctoranda

Fdo. Dr. Manuel López Chicano   Fdo. Ángela María Blanco Coronas

Fdo. Dra. María Luisa Calvache Quesada

Fdo. Dr. Carlos Duque

La doctoranda / *The doctoral candidate* **[Angela María Blanco Coronas]** y los directores de la tesis / *and the thesis supervisors:* **[Manuel López Chicano, María Luisa Calvache Quesada y Carlos Duque]**

Garantizamos, al firmar esta tesis doctoral, que el trabajo ha sido realizado por la doctoranda bajo la dirección de los directores de la tesis y hasta donde nuestro conocimiento alcanza, en la realización del trabajo, se han respetado los derechos de otros autores a ser citados, cuando se han utilizado sus resultados o publicaciones.

/

Guarantee, by singing this doctoral thesis, that the work has been done by the doctoral candidate under the direction of the thesis supervisor/s and, as far as our knowledge reaches, in the performance of the work, the rights of other authors to be cited (when their results or publications have been used) have been respected.

Lugar y fecha / *Place and date*:

Granada, a 31 de Enero de 2023

Directores de la Tesis / *Thesis supervisors;*   Doctoranda / *Doctoral candidate:*

Firma / Signed   Firma / Signed

Firma / Signed

Firma / Signed

"No hay que temer nada en la vida, sólo hay que entender. Ahora es el momento de entender más, para poder temer menos."

Maria Skłodowska

Agradecimientos

Esta tesis doctoral no se hubiese podido llevar a cabo sin la colaboración de todas y cada una de las personas que se citan a continuación. No tengo palabras suficientes para expresar mi agradecimiento.

En primer lugar, me gustaría dar las gracias a mis directores por acogerme en su grupo de investigación y darme la oportunidad de realizar este trabajo. A Manuel López Chicano, por su amabilidad y por su compañía durante las largas jornadas de trabajo de campo. A María Luisa Calvache, por su optimismo y por la confianza depositada en mí. A Carlos Duque, por su paciencia y su total disponibilidad. Además, me gustaría agradecerle el haberme hecho más amena una estancia en Dinamarca de lo más "catastrófica".

Al personal y a los voluntarios de La Charca de Suárez y a Fernando Alcalde, por su ayuda en la instalación de la red de control y en la toma de datos. Quisiera dar mi más sincero agradecimiento a Pepe Larios, por su ayuda desinteresada y su entera disposición.

Agradecer también a todos los integrantes del Departamento de Geodinámica de la Universidad de Granada. A Pepe Benavente, mi tutor del programa de doctorado, por estar siempre dispuesto a escucharme y darme consejos. A Jesús Galindo, por introducirme en el mundo de la investigación y por ser siempre tan atento conmigo. A Ángel Perandrés, por su ayuda con la construcción y la instalación de los equipos de medida. A Patricia, por las tardes en el tejado de la facultad enseñándome a calibrar el GPS.

No podría faltar mi agradecimiento a todos mis compañeros y amigos de la becaría. A la anterior generación de doctorandos (Irene, Ángel, Juampe, Manuel y Fran) por los sabios consejos al inicio de esta aventura. A Cris, Víctor, Cristinilla, Alex, Mayte, por todos los momentos compartidos y por haber sido un gran apoyo en cada una de las etapas. También agradecer a Asier y Marcos que, aunque hayamos coincidido menos, me han brindado su ayuda en todo lo que he necesitado. A Lourdes le doy las gracias por todos los consejos y su grandísimo apoyo desde que nos conocimos.

A Rogelio, por todas las vivencias en campo mientras estaba realizando su trabajo de fin de grado. Al personal del IGME de Granada, en especial a Crisanto y Jorge por su simpatía y disposición, y a José Antonio Navarro por llevar todo tipo de herramientas a campo con las que sacarme de unos cuantos apuros. Al grupo de hidrogeología de la Universidad de Málaga, por los consejos durante mi primera etapa del doctorado y por los buenos momentos vividos en cursos y congresos. A Ana Fernández Ayuso, por ser un apoyo fundamental en lo personal y lo profesional.

Gracias también a todas amigas, a Ángela, Ceci y Jenni, y a mis geólogos asturianos (Ana, Cris, Gus e Irene), que han sabido entender mis prolongadas ausencias y me han animado en todo momento. A mis compañeros de Tragsatec, en especial a Yaiza por hacerme más llevadero este último año.

Por supuesto, agradecer a mis padres y a mi hermana. Sin su comprensión e inestimable apoyo no hubiese encontrado las fuerzas para seguir con este proyecto. A mi familia política, a Vicky y José por darme tanto ánimo durante todo este tiempo.

A mi compañero de vida, José, por su apoyo incondicional y comprensión, especialmente en los momentos más difíciles. Convivir con una estudiante de doctorado no es tarea fácil. Sin su soporte, este trabajo no se habría finalizado y, por eso, es también suyo.

Por último, y no menos importante, a Kiara y Roger, mis fieles compañeros de teletrabajo. No podría haber tenido un mejor apoyo emocional.

A todos, muchas gracias.

Abstract

This Ph.D. Thesis investigates the hydrodynamic processes of the detrital coastal aquifers related to: (i) groundwater-surface water interactions in wetlands, (ii) the temperature distribution of the groundwater near the freshwater-saltwater interface, and (iii) coastal flooding events associated with hydrogeological processes. The aim is to advance in the knowledge of aquifers to understand their behavior under the effect of external factors (climatic, marine, and anthropic), which are expected to have more impact under the context of Global Change. The Motril-Salobreña aquifer was selected as experimental site due to its relatively good state and its location on the Mediterranean coast, which is exposed to human action and the effect of Climate Change.

Regarding the groundwater-surface water interactions, the water connection of "La Charca de Suárez" wetlands with the Motril-Salobreña aquifer was determined, because of the interest related to the high degree of anthropization of the wetlands and the conservation threats. The combination of different methodologies allowed the estimation of the water balance of the lake complex, the determination of the flow directions, and the hydrochemical characteristics of the water. The obtained results showed the complex hydrological functioning of the system and the existence of variations controlled by climate conditions and human activity.

In the study of the temperature distribution near the freshwater-saltwater interface in coastal aquifers, the effect of different heat sources (surface water recharge, sea infiltration, and geothermal heat) was included for the first time in the scientific literature. A numerical model was developed to propose a synthetic theoretical model of temperature distribution in coastal aquifers, which was tested in a case study with the calibration of temperature field data. Furthermore, the impact of different hydraulic and thermal parameters was determined based on a sensitivity analysis. The models indicated the connection between groundwater temperature and salinity in coastal aquifers and established the basis for future research in this field. A more detailed analysis was conducted to study groundwater temperature and salinity fluctuations in the deep zone of coastal aquifers induced by sea tides and changes in recharge. For that purpose, statistical analysis of the field data obtained at different depths was combined with numerical modeling. This methodology provided the conceptual mechanism that produces temperature oscillations and disclosed the importance of having a first picture of the temperature and salinity distribution in the aquifer. Furthermore, the most susceptible zones to temperature variations were identified as well as some of the hydrogeological characteristics of the aquifer that conditioned them.

Concerning coastal floodings associated with hydrogeological processes, the role of the groundwater for the existence and the durability of these inundations was analyzed, which is frequently ignored in most flood-risk studies. The groundwater level data obtained over two years was compared to hydrometeorological data and sea wave height records to identify different types of events depending on the climatic conditions. Finally, a more detailed study of the changes in the hydrodynamics of "La Charca de Suárez"

wetlands due to coastal events complemented the acquired knowledge of the functioning of the lakes during extreme climatic events.

Resumen

La presente Tesis Doctoral investiga los procesos hidrodinámicos de los acuíferos detríticos costeros relacionados con: (i) la interacción entre el agua subterránea y el agua superficial en humedales, (ii) la distribución de la temperatura del agua cerca de la interfase agua dulce-agua salada y (iii) los eventos de inundación costera asociados con procesos hidrogeológicos. Con ello, se pretende avanzar en el conocimiento de los acuíferos para entender cómo se comportan debido a determinados factores externos (climáticos, marinos y antrópicos) que se espera que tengan mayor protagonismo bajo un contexto de Cambio Global. El acuífero Motril-Salobreña ha sido elegido como emplazamiento experimental debido a su relativo buen estado actual y a su localización en la Costa Mediterránea, que hace que esté expuesto a la acción del hombre y a los efectos del Cambio Climático.

En relación a la interacción entre el agua subterránea y el agua superficial en humedales, se ha determinado la conexión hídrica de las lagunas de la reserva natural de La Charca de Suárez con el acuífero de Motril-Salobreña, considerándose de gran interés científico debido al alto grado de antropización del humedal y a las amenazas de conservación a las que se enfrenta. El uso combinado de diferentes metodologías ha permitido la estimación del balance hídrico del complejo lagunar, la determinación de las direcciónes de flujo y las características hidroquímicas del agua. Los resultados obtenidos ponen de manifiesto el complejo funcionamiento del sistema además de la existencia de alteraciones del funcionamiento hídrico debido a las condiciones climáticas y a la actividad humana.

En el estudio de la distribución de la temperatura cerca de la interfase agua dulce-agua salada en acuíferos costeros, se ha llevado a cabo un análisis incluyendo el efecto de las diferentes fuentes de calor (recarga del acuífero, infiltración del agua marina y calor geotérmico) por primera vez en la literatura científica. Se ha propuesto un modelo teórico de distribución de temperatura mediante la modelización numérica, validando su aplicación en un acuífero real mediante la calibración con datos de temperatura del agua subterránea obtenidos experimentalmente. Asimismo, se ha evaluado el impacto de diferentes parámetros hidráulicos y térmicos mediante un análisis de sensibilidad. Estos resultados han puesto de manifiesto la estrecha relación existente entre la temperatura y la salinidad del agua subterránea en un acuífero costero y establecen las bases para el desarrollo de futuras investigaciones en este campo. Se ha llevado a cabo un análisis más detallado para las fluctuaciones de temperatura y salinidad del agua en la zona profunda de los acuíferos costeros inducidas por las mareas y por cambios en la recarga. Con este objetivo, se ha combinado el análisis estadístico de datos obtenidos en campo a diferentes profundidades con la construcción de modelos numéricos. A partir de esta metodología, se ha propuesto el mecanismo conceptual que explica cómo se producen las oscilaciones de temperatura y se ha constatado la importancia de conocer previamente la distribución de temperatura y salinidad dentro del acuífero. Además, se han identificado las zonas más propensas a que existan variaciones de temperatura, condicionadas por determinadas características hidrogeológicas del acuífero.

En la temática de inundación costera asociada con procesos hidrogeológicos, se ha analizado el papel que juegan las aguas subterráneas en la ocurrencia y permanencia en el tiempo de las inundaciones costeras, algo frecuentemente ignorado en estudios de inundabilidad. Se ha realizado un análisis de los datos de nivel piezométrico recogidos durante dos años en comparación con datos hidrometeorológicos y de altura del oleaje que ha permitido identificar diferentes tipologías de eventos dependiendo de las condiciones climáticas. Finalmente, se ha llevado a cabo un estudio más detallado de los cambios de la hidrodinámica de las lagunas de La Charca de Suárez debido a eventos costeros conectando el conocimiento adquirido en el estudio de las lagunas, con los efectos de eventos climáticos extremos.

Index

Chapter 3: Temperature Distribution in Coastal Aquifers: Insights from Groundwater Modelling and Field Data

Chapter 4: Salinity and Temperature Variations near the Freshwater-Saltwater Interface in Coastal Aquifers Induced by Ocean Tides and Changes in Recharge
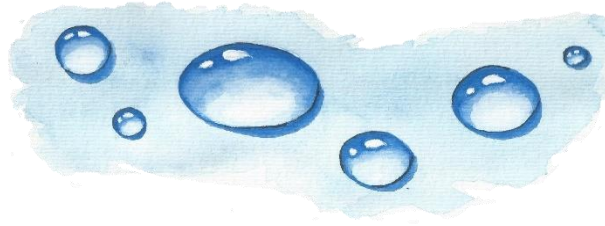
Chapter 5: Coastal Floodings in the Guadalfeo River Plain: The Role of Groundwater

Chapter 6: Conclusions

Appendix

CHAPTER 1

Introduction

1. Problem Statement

1.1. Coastal Aquifers: Effects of Global Change

Coastal areas have developed a rapid population growth compared to other regions of the world (Lu et al., 2017; Shi et al., 2020). It entails a prompt social-economic development that causes an increase in water demand. Surface water is scarce in semi-arid or arid regions, and thus, groundwater resources have been seriously overexploited or contaminated (Werner et al., 2013; Cuthbert et al., 2019; McDonough et al., 2020) which is expected to be aggravated in the future (Hoekstra and Mekonnen, 2012; Greve et al., 2018).

In coastal aquifers, fresh groundwater encounters salt groundwater and the mixing of both fluids develops the freshwater-saltwater interface (FSI). Under natural conditions, the density difference between the two fluids disturbs the freshwater flow that takes a vertical upward direction toward the ocean, what is known as fresh submarine groundwater discharge (SGD). Saltwater intrusion (SWI) occurs when the hydraulic gradient changes, e.g. when an excessive withdrawal of groundwater (van Camp et al., 2014; Houben and Post, 2017), and the saltwater intrudes into the aquifer replacing the freshwater (Morgan and Werner, 2015). In addition, climate change effects, such as frequent droughts, sea level rise, and increasing temperatures magnify the deterioration of coastal aquifers (Werner et al., 2013; Neumann et al., 2015).

In the year 2100, 95% of the coastal areas in the world will be highly affected by sea level rise (SLR) (Pearce et al., 2014), increasing the SWI in coastal aquifers and the risk of inundation of the land (Siarkos et al., 2017). The rise of the sea level moves the FSI upward and landward due to a reduction in the land-sea hydraulic gradient (Werner and Simmons, 2009; Yechieli et al., 2010). Furthermore, marine floodings produce vertical salinization due to infiltration of surface saltwater (Paldor and Michael, 2021). Given that SLR is a worldwide problem, small-scale variations in the sea level (tidal effects and surge events) can provide insights of its impact in the future.

About 60% of coastal aquifers in Spain have SWI problems, commonly found on the Mediterranean coast of the Iberian Peninsula and on the Balearic Isles (Gómez-Gómez et al., 2003). The present Ph.D. thesis aims to improve the understanding of coastal hydrodynamic processes taking as experimental site the Motril-Salobreña coastal aquifer, located on the southeastern coast of Spain. The hydraulic properties of the aquifer and the amount of water inputs propitiate the relatively good state of the aquifer. However, it could be transitory and conditioned by the climate change and the increase of the tourism. Thus, the experimental site not only provides the perfect conditions to study natural coastal patterns under undisturbed or barely disturbed situation, but also a previous scenario to the construction of pending projects, which are potentially polluting activities of coastal areas.

A dam, located upstream of the aquifer, was constructed to control the risk of downstream floods and to supply water for irrigation and urban needs. However, the dam is not fully operational due to the temporary delay in the construction of the pipelines for the delivery of water. Continuous discharge from the dam also contains a surplus of water that runs downstream as an ecological flow and reaches the Motril-Salobreña aquifer.

Downstream from the dam, water is derived from the river to a complex network of irrigation channels that cross the surface of the aquifer. The water demand for irrigation is satisfied, but a large volume of water is not being used by the farmers: water that flows by the channels is infiltrated into the aquifer, being the main water entrance of the aquifer, and also discharged into the sea. This fact led to the proposal of a project by farmers' associations to make the channels impermeable to reduce water waste and costs. Thus, an important decrease in groundwater recharge can be expected.

Urbanistic planning near the coastal strip has been paralyzed by the economic crisis and the declaration of flood hazard area near the Guadalfeo river mouth (Figure 1.2), although interest in construction persists. One of the most important construction projects of the area is planned to be located in the former delta of the river: an inner harbor for recreational boats designed to attract more tourists and, thus, the increase of the economic activity in the area due to the construction of new hotels and the creation of employment opportunities. However, the construction of the harbor threaten the shape of the coastline and therefore the freshwater-saltwater balance. Furthermore, the entailed economic activities would lead to an increase in demand of freshwater resources and fostering saltwater intrusion.

Understanding the current situation and the future trends of affecting factors (Figures 1.1 and 1.2) is the most viable solution to face the future of the aquifer taking into account Global Change.
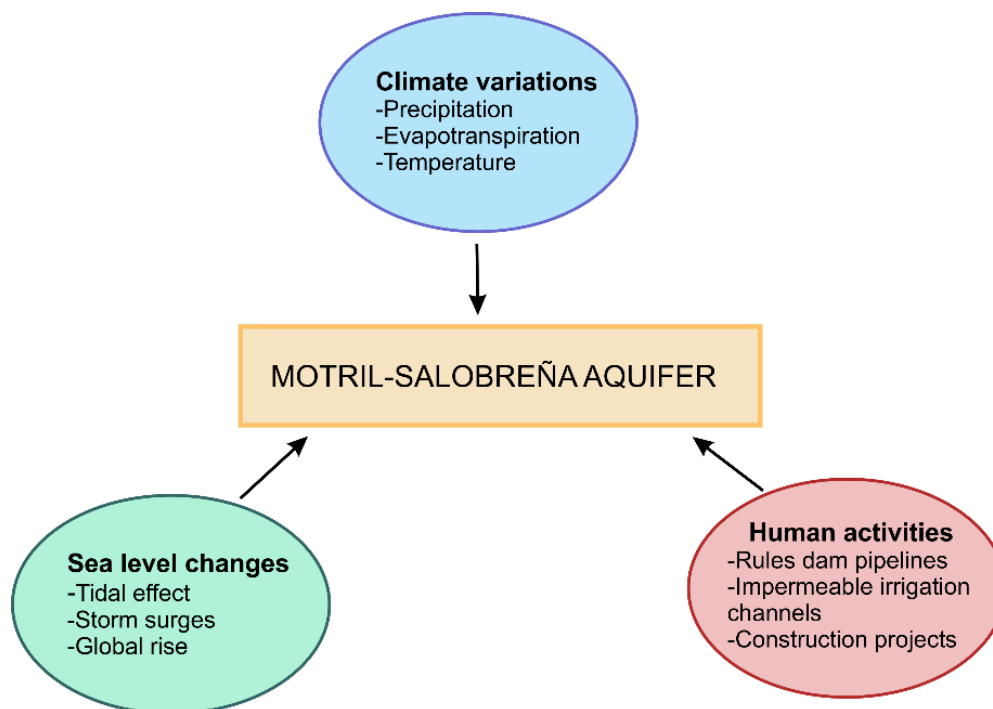
Figure 1.1.- Impact factors on the Motril-Salobreña aquifer due to Global Change.

Figure 1.2.- Photo of the Guadalfeo river plain showing some of the factors that stress the water resources: Urbanism, agriculture, the sea level and coastal erosion. The Guadalfeo river mouth was declared as flood hazard area.

1.2. Wetlands: Surface Water-Groundwater Interactions

Wetlands constitute one of the most important ecosystems in the world. However, in the past several decades, they were highly damaged by human activities. Thorslund et al. (2017) identified a continued and fast reduction of wetland areas globally. In recent decades, groundwater-dependent ecosystems obtained worldwide recognition (Richardson et al., 2011), and more emphasis has been put on their protection and sustainable management (Rohde et al., 2017). Various studies manifested their different benefits for society, such as water quality improvement (Verhoeven et al., 2006), coastal protection (Gedan et al., 2011; Temmerman et al., 2013), flood regulation (Acreman and Holden, 2013), groundwater level and soil moisture regulation (Hefting et al., 2004), and carbon sequestration (Mitsch et al., 2013). Despite all the updated information, many regions are still suffering rapid wetland loss (Davidson, 2014; Mitsch and Gosselink, 2015).

It has multiple practical implications understanding the hydrodynamics between wetlands and groundwater to offer protection and maintain stability, especially in semi-arid regions (Li et al., 2016, Su et al., 2016). The understanding of the water input to the system remains a challenge because of the difficulty to measure small rates of flow, the heterogeneity of the exchange in space and time, and the influence of surface-water hydrodynamics that can hinder measurements (Duque and Rosenberry, 2022). Groundwater (GW) and surface water (SW) interactions occur under natural conditions but also in response to human activities (Sánchez-Martos et al., 2021), such as water withdrawal and agricultural land extension (Parish et al., 2008; Kløve et al., 2011; Malek et al., 2018). The losses are expected to be exacerbated by climate change. Thus, it is crucial to distinguish and quantify the impact of the human and climate influences on the GW-SW interactions for adequate water resources management (Wang et al., 2021).

Wetlands located in coastal areas must face another phenomenon: the sea and its constant changes. Coastal wetlands are among the most fluctuating and threatened ecosystems in the world due to their critical location between the terrestrial and marine environments (Bruland, 2008). Their degradation associated with modifications in hydrological functioning has been accelerated by saline intrusion processes, common in littoral areas.

In the Mediterranean, the loss of wetland surface was estimated to be 48% (Gardner et al., 2018). The progressive aridity of the climate and the increase of water pressures in coastal areas (an increase in the inhabitants, urbanization, and the demand for hydrological resources) are expected to seriously harm the coastal Mediterranean wetlands in the future. Various authors showed coastal wetlands degradation in the south of Spain: the Punta Entinas wetland (Sánchez-Martos et al., 2021), the Doñana wetlands (Fernández-Ayuso et al., 2018), and Guadalhorce Delta wetlands (Nieto-López et al., 2020). These studies manifested the lack of consideration of the groundwater resources by the authorities and demonstrated the importance in determining the hydrological interactions between wetlands and groundwater to effectively manage surface water ecosystems.

La Charca de Suárez (LCS) Nature Reserve is the only coastal wetland in the province of Granada. Thanks to the growing interest in the protection of the environment by the society of Motril and different environmental groups, LCS wetland is nowadays a protected space and is progressively winning the expansion that was reduced during previous decades. The last attempt was made in the 90s due to the increasing interest in agriculture and urbanization in the area, although the workers of LCS and the inhabitants managed to stop the dewatering project (Figure 1.3). Despite the many factors that seriously threaten the conservation of the reserve, there are no previous studies about the relationship between the wetlands and the Motril-Salobreña aquifer.

Figure 1.3.- Wetlands dewatering project stopped by workers of LCS reserve and the inhabitants of Motril.

1.3. Coastal Aquifers: Temperature Distribution

Heat was recognized to be a relevant tracer for a wide variety of hydrogeological studies (Anderson et al., 2005) as in rivers, wetlands, and lakes (Constantz, 2008; Kurylyk et al., 2009; Ozotta and Gerla, 2021; Li et al., 2021), in lagoons (Swain and Prinos, 2018; Tirado-Conde et al., 2019), or in coastal aquifers (Taniguchi, 2003). In the upper meters of the aquifer, groundwater temperature fluctuates depending on the environmental temperature (Pollack et al., 2005; Duque et al., 2010). Surface water is heated or cooled and infiltrated into the aquifer producing a thermal signal to a maximum depth of a few tens of meters (Pollack and Huang, 2000; Smerdon et al. 2003). Thus, the use of heat is generating interest in the study of climate change and anthropogenic activities due to the modification of the groundwater temperature pattern in addition to increase the stress on the groundwater resources. Changes in temperature are pronounced in urbanized and industrial areas (Epting et al., 2017; Bayer et al., 2019; Hemmerle et al., 2019) and cause important heat anomalies in the aquifers (Tissen et al., 2019). In rural areas, groundwater temperature has slowly increased in response to recent climate change (Kurylyk et al., 2014; Menberg et al., 2014; Colombani et al., 2016).

Global Change can impact the temperature of coastal zones, partially induced by human activity in the most densely populated areas in the world. Surface warming is higher in urban areas than in rural surroundings, and in addition it increases with the city size (Liu et al., 2022). In coastal areas, another factor to consider is the influence of the sea. Several authors studied thermal signals associated with the exchanged temperature groundwater-seawater (Vandenbohede and Van Houtte, 2012; Befus et al., 2013; Debnath et al., 2015). However, few studies focused on the deeper zones of coastal aquifers, where groundwater temperature is subject to a linear increase due to the influence of the geothermal heat. Kim et al. (2008, 2009) and Vallejos et al. (2015) identified temperature variations at deep zones of the aquifer where recharge temperature cannot induce them. However, there is still no explanation of the process due to the lack of knowledge about temperature distribution of coastal aquifers affected by the geothermal heat.

Some authors (Hughes and Sanford, 2004; Dausman et al., 2010; Thorne et al., 2006; Langevin et al., 2010) simulated the laboratory experiment of Henry and Hilleke (1972), which suggested that infiltrated seawater is heated by the geothermal heat, driving to thermal convection in addition to variable-density effects. However, there is no benchmark model of temperature distribution based on field measurements that incorporates all the possible heat sources (surface water recharge, sea infiltration, and geothermal heat). Therefore, to ensure the understanding of the impact of climate and anthropic changes on groundwater temperature, it is necessary to establish the basis of heat distribution for coastal aquifers. Furthermore, the knowledge of the behavior of temperature and its mixing processes could indicate the location of preferential flow zones in coastal areas which are potential saltwater intrusion pathways. Thus, heat could be used as a tracer in coastal areas to prevent and remediate marine intrusion problems.

1.4. Study Area Background

The Motril-Salobreña aquifer had been studied since the 70s when its importance was highlighted due to its abundant resources and its water quality. Several hydrogeological studies have been conducted in the area like Bachelor's thesis (Castillo, 1975; Benavente, 1982; Calvache, 1981; Soto, 1998) and doctoral thesis (Al Alwani, 1997; Ibáñez, 2005; Duque, 2009; Sánchez-Úbeda, 2017).

The absence of marine intrusion was manifested by the first hydrochemistry study conducted by Castillo and Fernández Rubio (1976). Also, Castillo and Fernández Rubio (1978) made the first estimation of the groundwater reserves. The Spanish Geological Survey (IGME) developed its first studies of the aquifer and published them in IGME (1983; 1985) and ITGE (1988; 1989). ITGE (1991) published the first numerical model of the aquifer.

Pulido-Bosch et al. (1980) analyzed the possible contamination sources of the aquifer. Benavente and Calvache (1981) studied the dominant hydrochemical facies of the system, distinguishing two sectors with different hydrogeological behavior: the western and the eastern. In 1983, the General Direction of Hydraulic Works performed various hydrogeological studies in the area (DGOH-CHSE 1983; 1988; 1993). Pulido-Bosch and Rubio (1988) compiled all the existing information on the aquifer until that moment. In 1995, the area suffered a severe drought and, hence, the Hydrographic Confederation of Southern Spain (DGOH) performed an emergency campaign of water supply wells to distribute water to the population (CHSE, 1995). Soto (1998) analyzed the evolution of the piezometric levels and electrical conductivity logs. Furthermore, the study indicated that the paleochannel of the Guadalfeo river was the area of the aquifer with higher transitivity values and highly threatened by marine intrusion in times of drought. In IGME (1999), a constant density model was developed taking into account the heterogeneity of the aquifer.

Before the construction of the Rules dam in 2003, the Government of Andalucía conducted studies on the management of water resources in the basin and the effects of regulating the flow of the Guadalfeo river. Calvache et al. (2003) analyzed the situation of the Motril-Salobreña aquifer before the startup of the dam. Calvache et al. (2004) and Duque et al. (2005) described the relationship between the river and the aquifer from a detailed study of electrical conductivity and temperature vertical logs. Ibáñez (2005) simulated different scenarios with a numerical model of the aquifer and studied the possible effects of the Rules dam on the saltwater intrusion process. Calvache et al. (2006) studied the changes in the land use that had taken place over the years and their relationship with the effects of the Rules dam. Duque et al. (2007, 2008) completed a geophysical campaign, combining TDEM soundings and gravimetry, to determine the position of the saline wedge and delimit the aquifer basement. As a result of the previous studies, an approximate volume of the reserve was proposed (Duque et al., 2007). Martín-Rosales et al. (2007) evaluated the effects of the Rules dam on the flow of the Guadalfeo river and correlated them with the piezometric levels of the aquifer. The mathematical simulation using flow and transport models allows the evaluation of different scenarios concerning marine intrusion (Calvache et al., 2009).

Duque and Calvache (2010) updated the water balance of the aquifer and compared the new values with those obtained in previous studies. Vertical logs of temperature and the numerical model of heat transport (Duque et al., 2010) and Calvache et al. (2011) delved into the river-aquifer interactions. Pretel et al. (2010) showed the dramatic decrease in the traditional crops of sugarcane and the elevated increases of the greenhouses and subtropical trees agriculture extent in the previous 50 years. Duque et al. (2011) studied the effect of the irrigation returns and the river on the groundwater recharge through the analysis of stable isotopes. Crespo et al. (2012) performed a hydrochemical analysis of the salinization sources of the aquifer, and Reolid et al. (2013) calculated the water entrance from the alluvium of the Guadalfeo river in the northern sector of the aquifer. Sánchez-Úbeda et al. (2013) investigated for the first time the influence of sea tides on the piezometric levels nearby the shoreline. Sánchez-Úbeda (2017) and Calvache et al. (2016) calculated the transmissivity and the storage coefficient through modern methods. Hódar-Pérez et al. (2015) measured nitrate concentrations of groundwater and detected contamination in the eastern sector of the aquifer. Corral-Rubio (2018) detected a salinity anomaly in central sector of the aquifer and determined the origin of high concentrations of chlorides, sulfates and nitrates. Sánchez-Úbeda et al. (2018a) and Calvache et al. (2020) estimated the age of groundwater through environmental tracers to determine the predominant flow patterns, the mixing processes, and the residence time in the aquifer. The previously obtained data was used to complete a numerical model of groundwater age distribution (Sánchez-Úbeda et al., 2018b). Duque et al. (2019) indicated that the salinity in groundwater could be produced during the formation of the delta of the Guadalfeo river and simulated the flushing time of salinity by freshwater with a paleohydrogeological model. Acosta-Rodriguez (2019) analyzed the effluent-influent behaviour of the Guadalfeo river with differential flow gaugings.

2. Research Objectives and Structure

The Motril-Salobreña aquifer has been the subject of research by a wide range of authors contributing to an excellent knowledge of hydrodynamics and marine intrusion processes of the study area. However, there were no previous studies dealing with the role of groundwater on the prevalence of the unique preserved coastal wetlands in the study area and on the existence of flooding, which is becoming increasingly common. Likewise, the groundwater temperature at deeper areas of the aquifer was not previously studied in detail and, thus, there was a lack of awareness regarding the temperature distribution of the Motril-Salobreña aquifer that can be also applied to any other aquifer. There are also no precedents studying the connection of coastal floodings, which are becoming increasingly frequent events, with groundwater.

The present Ph.D. Thesis is organized as a compendium of papers focused on those questions never studied before (Figure 1.4.). The objectives are framed within the research project CGL2016-77503-R "*Respuesta del acuífero costero Motril-Salobreña al cambio climático y a los cambios de uso del suelo*" from the Ministry of Economy and Competitiveness (MINECO), being provided in the following order:

- ▪ Chapter 2 presents the hydrological functioning of LCS lagoons and their relationship with the Motril-Salobreña aquifer.

- Chapter 3 proposes the theoretical model of temperature distribution in coastal aquifers, considering all possible sources of heat.

- Chapter 4 shows the influence of ocean tides and groundwater recharge on the salinity and temperature distribution of coastal aquifers.

- Chapter 5 describes the flooding episodes produced in the deltaic plain of the Guadalfeo River and the factors that induced them.

- Chapter 6 summarizes the conclusions obtained in this Ph.D. thesis.
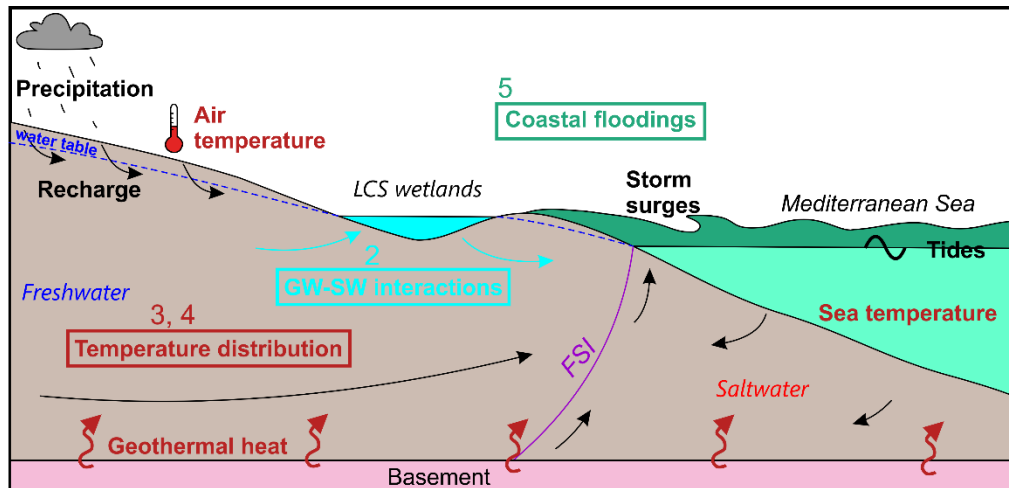
Figure 1.4.- Research topics of the Motril-Salobreña aquifer (Chapter 2: Groundwater-Surface water interactions, Chapters 3 and 4: Temperature distribution, Chapter 5: Coastal floodings) and processes involved.

3. Location of the Study Area

The Motril-Salobreña aquifer is located in the southeast of Spain, within the province of Granada (Figure 1.5). It is delimited by the Mediterranean Sea at the south and by mountain ranges at the north: Sierra of Lújar (more than 2000 m altitudes) and Sierras of Almijara and Tejeda (more than 2000 m altitudes). However, the highest is Sierra Nevada with a maximum altitude of 3482 m a.s.l.

The Guadalfeo river, with a drainage basin of 1290 km^2, is the main surface watercourse that runs through the aquifer. It begins in the peaks of Sierra Nevada and collects the waters from various tributaries, such as Ízbor, Lanjarón Trevélez, and Poqueira. The river has a high gradient due to the big difference in altitude (more than 3400 m) from its headwaters to its mouth in a small distance of 50 km. Thus, the Guadalfeo river had a relevant role in the formation of the aquifer due to the erosion, transport, and deposition of large amounts of sediments from Sierra Nevada. As a result, the Motril-Salobreña aquifer is considered the most important coastal detrital aquifer of the province due to its extension (42 km^2) and its water resources by several authors (Castillo and Fernández Rubio, 1978; Pulido-Bosch and Rubio, 1988; ITGE, 1991).

The largest urban areas located on the aquifer are Motril and Salobreña. Motril has 58460 inhabitants (INE, 2020) and Salobreña 12513 inhabitants (INE, 2020). During the summer months, the population figures drastically increase due to tourism, and

consequently, the stress on water resources is intensified. The main economic activities of the area are related to the urbanism, agriculture, tourism, and fishing sectors.

Figure 1.5.- Geographical location of the Motril Salobreña aquifer and the Guadalfeo river catchment.

The Guadalfeo river plain was highly modified by human interventions focused on the management of water resources. The changes in land uses, the channelization of the river and the construction of the Rules dam are mostly related to the intense agricultural activity, which endangers the aquifer. In the past, the flood irrigation practices for the crops of sugarcane ensured the balance of the economic activity and the water resources of the area (Pretel et al., 2010). However, the traditional crops were progressively replaced by tropical and subtropical fruit crops, such as custard apple, avocado, and mango, and by greenhouses horticulture (Figure 1.6).

Figure 1.6.- Aerial photography of the Guadalfeo river plain, where it is seen the intense agricultural activity of tropical fruit crops and greenhouses horticulture.

4. Geological and Hydrogeological Setting

The Motril-Salobreña aquifer is located in the Internal Zones of the Betic Cordillera (Figure 1.7), the Iberian zone of the Betic-Rif Mountain Range (Vera and Martín-Algarra, 2004). They represent the core of the Betic Cordillera, which is the most intensely deformed region of the orogeny. It is essentially constituted by metamorphic rocks from the Middle/Upper Trias and Paleozoic. The Internal Zones are divided into three metamorphic complexes: Nevado-Filábride, Alpujárride, and Maláguide. The Motril-Salobreña aquifer is constituted by Quaternary detrital materials, which lie discordantly over the Alpujárride complex which comprises a basement of schists, quartzites, phyllites, and marbles with Paleozoic and Triassic ages (Castillo, 1975; Duque, 2009).
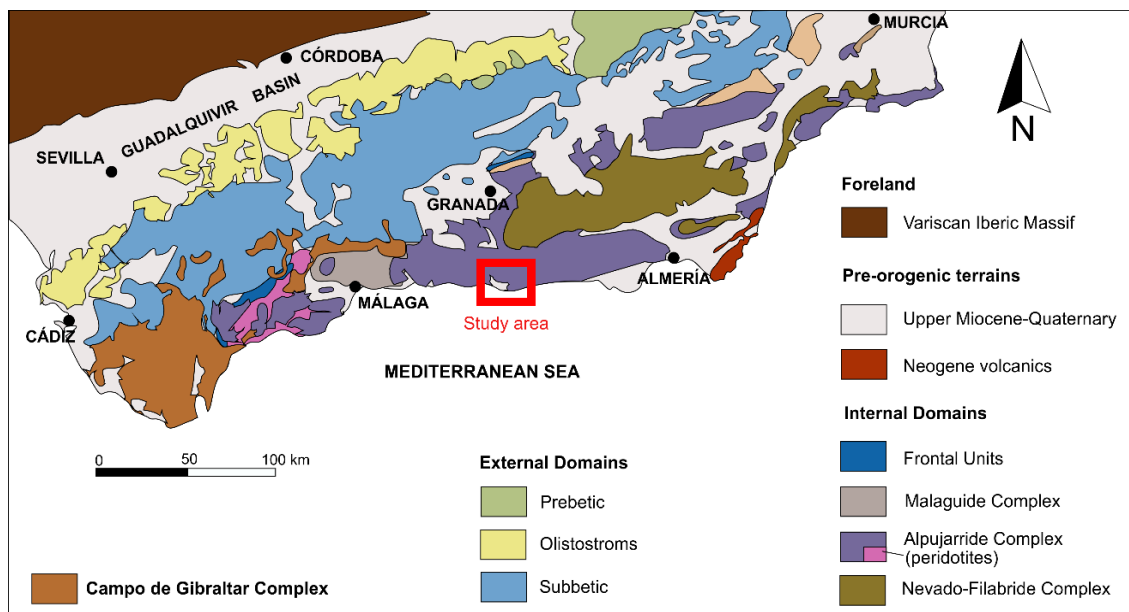
Figure 1.7.- Schematic geological map of the Betic Cordilleras and location of the study area. Modified from Vera and Martín-Algarra (2004).

The structural setting of the area is characterized by predominantly E-W-oriented normal and strike-slip faults and folds. The relief uprising was developed mostly since Middle Miocene, associated with the oblique convergent character of the Eurasian–African plate boundary (Galindo-Zaldivar et al., 2013). The faults show recent tectonic activity, which conditioned the configuration of the drainage pattern of the Motril-Salobreña aquifer setting (Pérez-Peña, 2009).

The aquifer thickness ranges from 30 to 50 m in the north to more than 250 m in the south near the coastline (Duque et al., 2008). Except for the Escalate carbonate formation in the north, the lateral boundaries and the basement are made of schists and phyllites of very low permeability (Figure 1.8). The western sector is composed, from the deepest to the shallowest part of the aquifer, of marine lithofacies (dominated by clay and silt with some gravel), estuary lithofacies (finer-grained sediments, mainly silt and sand with some gravel), channel fill (very coarse-grained material, mainly gravel with some sand) and deltaic lithofacies (mostly gravel and silt or sand) (cross section A-A´, Figure 1.9) (Olsen, 2016). The eastern area is composed of coastal plain materials (silt/sand with some gravels) and alluvial sediments transported by *ramblas* during storms and intense rainfall

11

(mostly sand and gravel) (cross section B-B´, Figure 1.9). The depositional processes produced a decrease in hydraulic conductivity from north to south and east to west (Duque et al., 2005) and estimated values ranged from 12 to 300 m/d (Calvache et al., 2009; Duque et al., 2018). The general direction of the groundwater flow is from north to south with a hydraulic gradient estimated between 1.6×10^{-3} and 7×10^{-3} (Duque et al 2010; Blanco-Coronas et al., 2021).

The Gualdalfeo river has a catchment of 1294 km^2 and reaches very high altitudes of the Sierra Nevada. It has a mean discharge of 7700 L/s (Duque et al., 2011) and a mixed rainfall/snowfall hydrologic regime. The course of the river is altered by the intersection of the Rules dam (15 km from the aquifer) and by two weirs (azudes del Vínculo and Vélez). The river is influent throughout its course, except near the river mouth where the river gains water from the aquifer (Benavente 1982; Calvache et al., 2006; Duque et al., 2008; Blanco-Coronas et al., 2021). A complex net of channels, that covers the entire surface of the Motril-Salobreña aquifer, collects the derived water from the weirds and distributes it to use for irrigation purposes. An important part of the excess water from the irrigation is infiltrated into the aquifer, and the other part is collected again by the channels that discharge into the sea.
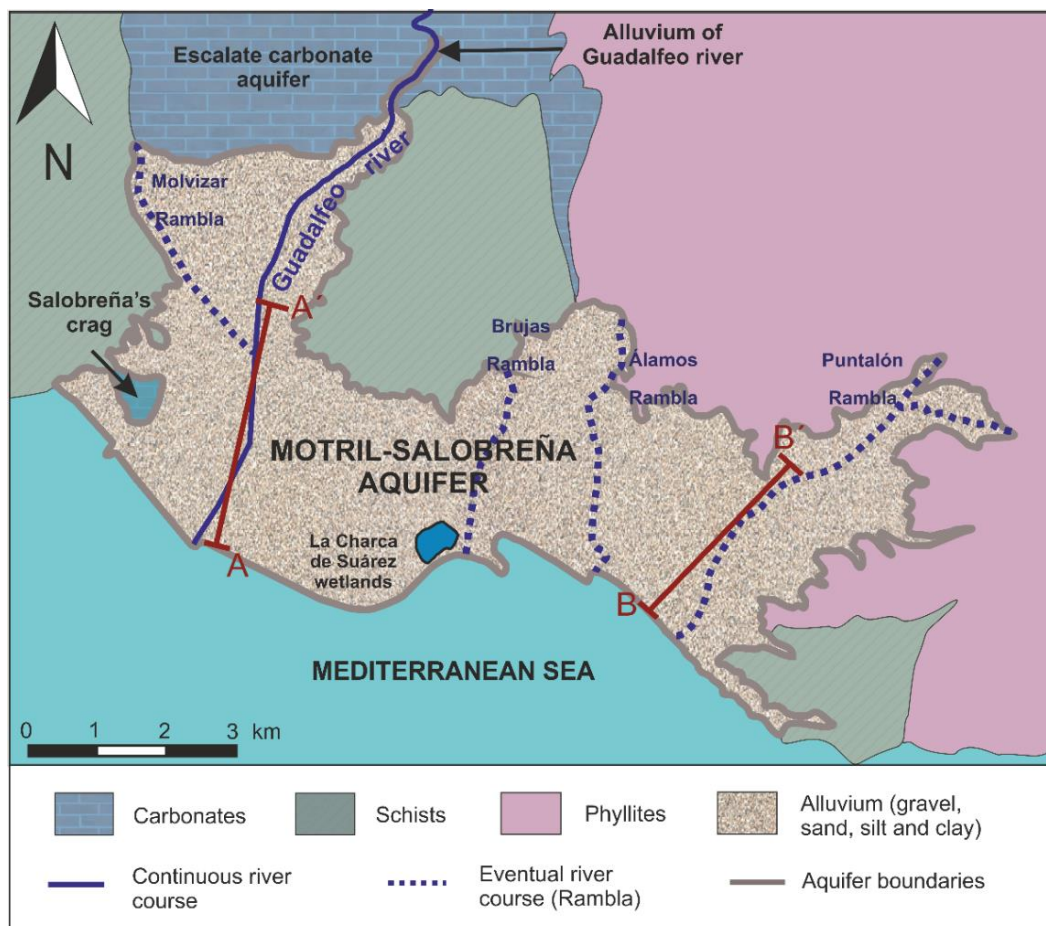

Figure 1.8.- Hydrogeological setting of the Motril-Salobreña aquifer and the location of the cross sections showed in figure 1.9.
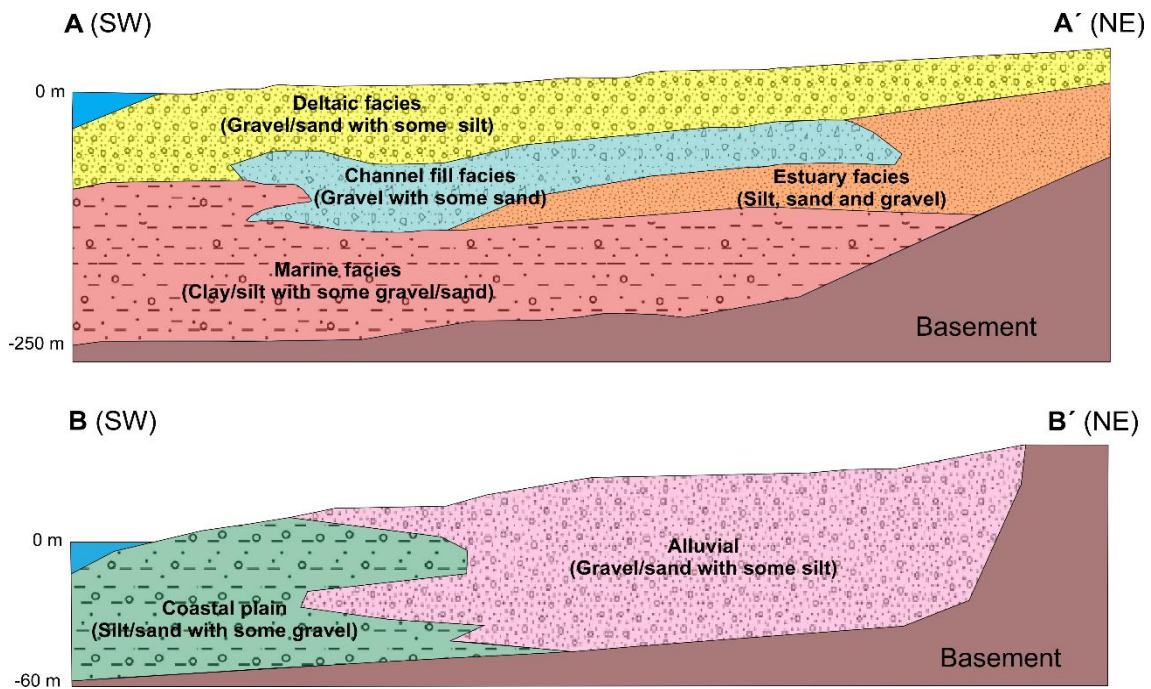
Figure 1.9.- Interpretation of the depositional environments of the western delta area (cross-section A-A´) and eastern area (cross-section B-B´). Modified from Olsen (2016).

The main water entrance of the Motril-Salobreña aquifer is produced by the infiltration from irrigation excess (16 Mm^3/year), and by the infiltration from the Guadalfeo river (11 Mm^3/year) (Calvache et al., 2009; Duque et al., 2011). Other minor contributions are the lateral inlets from the Escalate carbonate aquifer in the northern area (4 Mm^3/year) and the rain infiltration (3-6 Mm^3/year) (Calvache et al., 2009), and the hidden recharge by the Guadalfeo river alluvial-aquifer in the northern area (1 Mm^3/year) (Reolid et al., 2012). The most important outlet of the system is the discharge of fresh groundwater along the sea border in its contact with the Mediterranean Sea, which is estimated to range from 17 to 26 Mm^3/year (Calvache et al., 2009; Heredia et al., 2002; Ibáñez, 2005; Duque, 2009). The extraction by pumping wells and occasional river gains in its final stretch are other minor outlets. The last studies estimated a mean groundwater reserve of 190 Mm^3 (Duque, 2009) and a mean available groundwater resource between 35 Mm^3/year (Heredia et al. 2003; Ibáñez 2005) and 28 Mm^3/year (Duque and Calvache 2010), that satisfy the water consumption of the population and the economic activities of the area.

5. Marine Intrusion

The Motril-Salobreña aquifer is one of the few Mediterranean coastal aquifers to remain relatively unaffected by contamination from marine intrusion (Calvache et al., 2009). The study of elements, such as chloride, bromide, iodine, and strontium, concluded that the concentrations are very low to consider the existence of saltwater intrusion (Duque, 2007). The FSI has been established at a distance less than 500 m from the coastline. EC profiles obtained 300 m from the coastline indicated that the FSI is restricted to the deeper zone of the aquifer, and it is located at a depth of 130 m approximately. The aquifer hydraulic conductivity changes determine the shape of the FSI. In the western sector, greater hydraulic conductivity favors sharper changes in salinity, whereas, in the eastern sector, lower hydraulic conductivity causes a broader interface with a larger

mixing zone (Duque et al., 2008). Also, the Guadalfeo river has a significant role in the sharpness of the FSI: the higher fresh groundwater discharge towards the sea in the vicinity of the river reduces the thickness of the mixing zone. In the eastern sector, the groundwater recharge is lower and hence, the FSI is wider. In remote areas from the coastline, the existence of saline water is probably linked to old marine seawater trapped within sediments of low permeability during the shoreline progradation (Duque et al., 2008) and to the difficulty of flushing it by freshwater (Duque et al., 2018).

6. La Charca de Suárez Wetlands

LCS wetlands are the unique humid zone on the coast of the province of Granada, being on the route for migratory birds between Europe and Africa. It encompasses several lagoons located in topographically depressed areas of the old Guadalfeo river mouth, at a distance of 300 m from the shoreline (Figure 1.10 A). Its extension was reduced from 1000 hm^2 to 14 hm^2 due to numerous human interventions and, currently, it is surrounded by buildings, an industrial park, and crop fields (Figure 1.10 B, C). It was classified as a Protected Nature Reserve by the regional government of Andalusia in 2009 due to its high ecological value and to protect it from the existing pressures. The lagoon complex encompasses several waterbodies, but only five of them are located within the protected perimeter (Figure 1.10 C).

The wetlands are located in the discharge zone to the sea of the Motril-Salobreña aquifer. The local lithology can vary widely but it mainly consists of alluvial sediments (fine sands and some pebbles) and prodeltaic silty sediments. The wetlands are fed with surface water with the main channel that collects the surplus irrigation from the Guadalfeo river plain. The channel crosses the protected area from north to south, performing a water exchange with the flood meadows and the lagoons. In the south, the main and other minor channels collect the surplus water of the lagoons and flow directly to the sea. Concerning the groundwater inputs, there no information neither previous works about the interaction between wetlands and the aquifer.

7. Climatology of the Study Area

The climate of the Guadalfeo River catchment is extremely variable in space (Figure 1.11.) due to the steep topographic gradient of the catchment, but also in time due to the alternation of dry and wet periods throughout the year.

At the highest altitude of Sierra Nevada, there is a high-mountain climate with a mean annual temperature of 6°C and average annual precipitation of 1000 mm, frequently as snow, concentrated from October to March. However, intense precipitation events have been recorded with values of 400 mm in 24 hours (Jiménez-Sánchez et al., 2008). The mean annual potential evapotranspiration rate is 460 mm.

Near the coastline, the climate is warm dry Mediterranean, and semi-arid Mediterranean (Figure 1.11 A) with mean annual precipitation slightly lower than 400 mm, concentrated mostly during autumn and spring, and a mean annual temperature of 18.5 °C. The warmest months are July and August with mean temperatures of 25 °C and

the coolest months are January and February with mean temperatures of 10-12°C (Duque et al., 2010). The mean annual potential evapotranspiration rate is 920 mm.
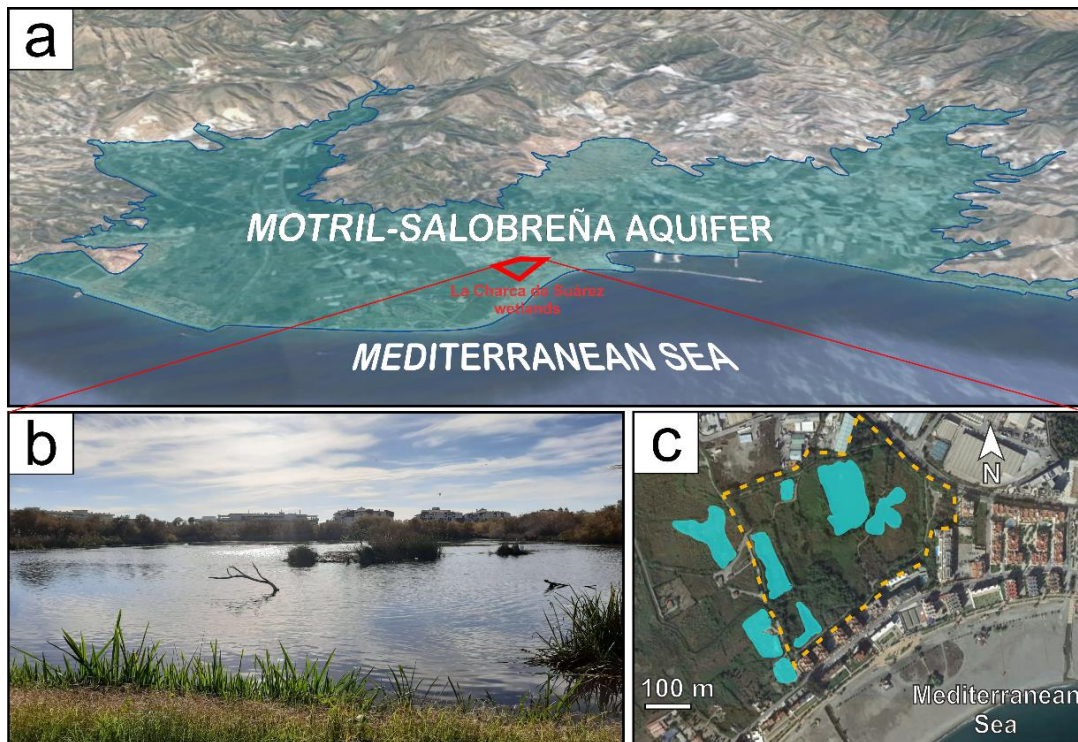
Figure 1.10.- (A) Location of the LCS wetlands in the Motril-Salobreña aquifer. (B) Picture of one of the lagoons surrounded by vacation buildings. (C) Current lagoons within and without the protected area (yellow dashed line).
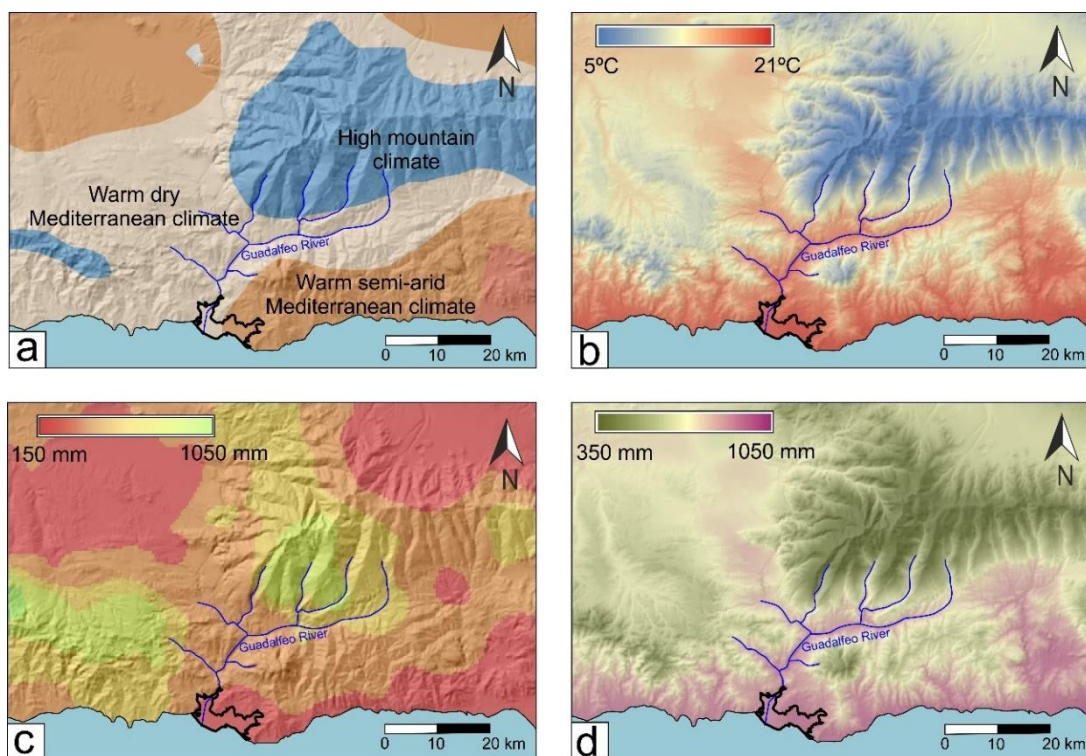
Figure 1.11.- Distribution maps of (A) Climate types, (B) Temperature, (C) Precipitation, and (D) Potential evapotranspiration. Annual average data in the period between 1971 and 2000 (Obtained from The Environmental Information Network of Andalucía, REDIAM).

The historical rainfall data (Figure 1.12 A), recorded from 1966 to 2021, shows the alternation of humid with wet periods that characterize the study area. During this period, the annual precipitation was higher than the average precipitation (385 mm) for 18 years and the wettest and driest years were 1996 and 1981, respectively. During the last 10 years (2011-2021), the annual precipitation rate of three of them was above the average precipitation rate. From 2013, a dry period was recorded related to precipitation rates lower than 348 mm/year until 2018, the time when the trend was broken with annual precipitation of 582 mm.

The historical temperature record (Figure 1.12 B) shows a repetitive pattern of temperatures leading to annual cycles. During the 1960's, the annual maximum values were closer to the mean temperature than the minimum values. However, the pattern changed at the end of the records: the annual minimum values were closer to the mean temperature than the maximum values. Thus, a gradual increment of the historical temperature was recorded in the study area from 1966 to 2021.
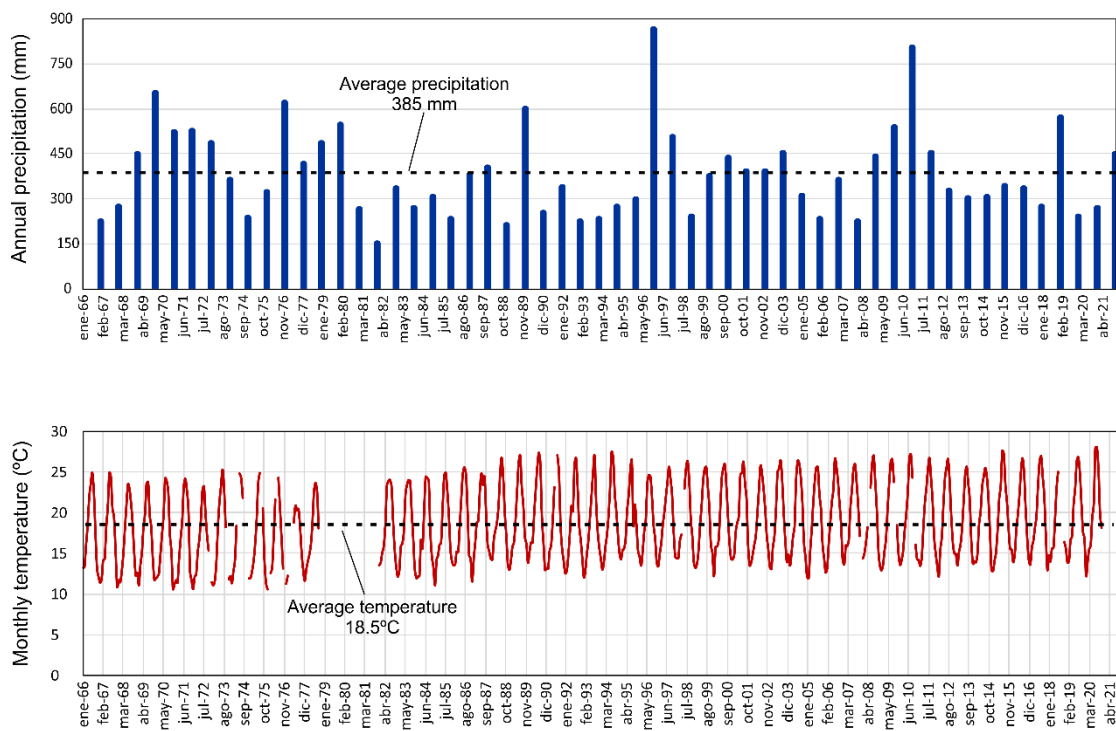
Figure 1.12.- Evolution of (A) Annual mean precipitation and (B) Monthly temperature during the period between 1966 and 2021. Data were obtained from the meteorological stations of the Spanish Meteorological Agency (AEMET) located on Motril and Salobreña.

REFERENCES

Acosta-Rodriguez, R., 2019. Relaciones entre el río Guadalfeo y el acuífero Motril-Salobreñañ mediante aforos diferenciales. Bachelor's tesis. University of Granada, 35 pp.

Acreman, M., Holden, J., 2013. How wetlands affect floods. Wetlands 33, 773-786. https://doi.org/10.1007/s13157-013-0473-2

Al Alwani, G., 1997. Hidrología e hidrogeología de la cuenca del río Guadalfeo. Doctoral thesis. University of Granada. 315 pp.

Anderson, M.P., 2005. Heat as a groundwater tracer. Groundwater. https://doi.org/10.1111/j.1745-6584.2005.00052.x.

Bayer, P., Attard, G., Blum, P., Menberg, K., 2019. The geothermal potential of cities. Renew. Sustain. Energy Rev. 106, 17–30. http://doi.org/10.1016/j.rser.2019.02.019

Befus, K.M., Cardenas, M.B., Erler, D.V., Santos, I.R., Eyre, B.D., 2013. Heat transport dynamics at a sandy intertidal zone. Water Resour. Res. 49, 3770–3786. https://doi.org/10.1002/wrcr.20325.

Benavente, J., 1982. Contribución al conocimiento hidrogeológico de los acuíferos costeros de la provincia de granada. Doctoral thesis. University of Granada. 571 pp.

Benavente, J., and Calvache, A. 1981. Aspectos hidrogeoquímicos de algunos acuíferos detrîticos costeros en la provincia de granada. Simp Agua Andalucía, 731-753.

Blanco-Coronas, A.M., López-Chicano, M., Acosta-Rodriguez, R., Calvache, M.L., 2021. Groundwater recharge-discharge estimation with differential flow gaugings in the final stretch of the Guadalfeo river (Granada). Geogaceta, 69, 91–94.

Bruland G.L., 2008. Coastal wetlands: function and role in reducing impact of land-based management. Natural Resources and Environmental Management Department, University of Hawaii Manoa, USA. pp 1-39

Calvache, A., 1981. Estudio hidroquímico del acuífero de Motril-Salobreña (provincia de Granada). Bachelor's thesis. University of Granada 125 pp.

Calvache, M., Rubio, J., López-Chicano, M., González-Ramón, A., Ibáñez, S., Martín-Rosales, W., Soler, R., Díaz-Losada, E., Peinado Parra, T., 2003. Estado actual del acuífero costero de Motril-Salobreña previo a la puesta en funcionamiento de la presa de rules. Proceedings of Coastal Aquifers Intrusion Technology: Mediterranean Countries, IGME, Madrid, 77-85.

Calvache, M., Cerón, J., Rubio, J., Martın-Rosales, W., López-Chicano, M., González-Ramón, A., Ibánez, S., Duque, C., 2004. Caracterización de las relaciones río acuífero en el sistema Motril–Salobreña (Granada) Proceedings of VIII Simposio de Hidrogeología, Zaragoza, Spain, 433-442.

Calvache, M., Martın-Rosales, W., López-Chicano, M., Rubio-Campos, J., González-Ramón, A., Duque, C., Cerón, J., 2006. Repercusión de la presa de rules sobre el acuífero detrítico costero Motril–Salobreña (granada) in el agua subterránea en los países mediterráneos. Guía de las excursiones AquainMed-06, 285

Calvache, M., Ibáñez, S., Duque, C., Martín-Rosales, W., López-Chicano, M., Rubio, J., González, A., Viseras, C., 2009. Numerical modelling of the potential effects of a dam on a coastal aquifer in s. Spain. Hydrol. Proc. 23, 1268-1281

Calvache, M., Duque, C., Fontalva, J. G., Crespo, F., 2011. Processes affecting groundwater temperature patterns in a coastal aquifer. International J. Environ. Sci.Technol. 8, 223-236.

Calvache, M., Sánchez-Úbeda, J., Duque, C., López-Chicano, M., de la Torre, B., 2016. Evaluation of analytical methods to study aquifer properties with pumping tests in coastal aquifers with numerical modelling (Motril-Salobreña aquifer). Water Resour. Manag. 30, 559-575.

Calvache, M.L., Sánchez-Úbeda, J.P., Purtschert, R., López-Chicano, M., Martín-Montañés, C., Sültenfuβ, J., Blanco-Coronas, A.M., Duque, C., 2020. Characterization of the functioning of the Motril–Salobreña coastal aquifer (SE Spain) through the use of environmental tracers. Environ. Earth Sci. 79, 141.

Castillo, E., 1975. Hidrogeología de la vega de Motril-Salobreña y sus bordes. Master's thesis University of Granada, 184 pp.

Castillo, E. and Fernández Rubio, R., 1976. Hidroquímica de los acuíferos del río Guadalfeo y sectores adyacentes (Motril, Granada). I Simposio Nacional de Hidrogeología, Valencia, 951-964.

Castillo, E., and Fernández-Rubio, R., 1978. Hidrogeología del acuífero de la vega de Motril-Salobreña. Bol Geol Min,.39-48.

C.H.S.E., 1995. Estudio para la ubicación de sondeos de abastecimiento a las poblaciones de la costa granadina. Unpublished.

Colombani, N., Giambastiani, B. M. S., Mastrocicco, M., 2016. Use of shallow groundwater temperature profiles to infer climate and land use change: interpretation and measurement challenges. Hydrol. Process. 30, 2512–2524. http://orcid.org/10.1002/hyp.10805

Constantz, J., 2008. Heat as a tracer to determine streambed water exchanges. Water Resour. Res. 44, 1–20. https://doi.org/10.1029/2008WR006996

Corral-Rubio, N. 2018. Análisis de la anomaía de salinidad del acuífero Motril-Salobreña en el entorno de la Rambla de las Brujas. Bachelor´s thesis. University of Granada. 34 pp.

Crespo, F. J., López Chicano, M., Calvache Quesada, M. L., Sánchez Úbeda, J. P., Duque, C., Martín Rosales, W., 2012. Estudio de las fuentes de salinización en el acuífero costero Motril-Salobreña (Granada).

Cuthbert, M.O., Gleeson, T., Moosdorf, N., Befus, K.M., Schneider, A., Hartmann, J., Lehner, B., 2019. Global patterns and dynamics of climate–groundwater interactions. Nat. Clim. Chang. 9, 137–141. https://doi.org/10.1038/s41558-018-0386-4

Dausman, A.M., Doherty, J., Langevin, C.D., Sukop, M.C., 2010. Quantifying data worth toward reducing predictive uncertainty. Ground Water 48, 729–740. https://doi.org/10.1111/j.1745-6584.2010.00679.x

Davidson, N.C., 2014. How much wetland has the world lost? Long-term and recent trends in global wetland area. Mar. Freshwater Res. 65, 934-941.

Debnath, P., Mukherjee, A., Singh, H.K., Mondal, S., 2005. Delineating seasonal porewater displacement on a tidal flat in the Bay of Bengal by thermal signature: Implications for submarine groundwater discharge. J. Hydrol. 529, 1185–1197. https://doi.org/10.1016/j.jhydrol.2015.09.029

D.G.O.H.-C.H.S.E. 1983. Estudios básicos para la redacción del Plan Hidrológico de la Cuenca Hidrográfica del Sur de España, 1ª fase. Unpublished.

D.G.O.H.-C.H.S.E. 1988. Plan Hidrológico Cuenca Sur. Documentación básica. Unpublished.

D.G.O.H.-C.H.S.E. 1993. Plan Hidrológico Cuenca Sur. Borrador del proyecto de directrices. Unpublished.

Duque, C., Calvache, M. L., Campos, J. C. R., Rosales, W. M., López-Chicano, M., Ramón, A. G., García, J. C. C., Ibáñez, S., 2005. Influencias de las litologías en los procesos de recarga del río Guadalfeo al acuífero de Motril-Salobreña. VI Simposio del Agua en Andalucía, Sevilla, 343-354.

Duque, C., Calvache, M. L., Pedrera, A., Martín-Rosales, W., López-Chicano, M., 2008. Combined time domain electromagnetic soundings and gravimetry to determine marine intrusion in a detrital coastal aquifer (southern Spain). J. Hydrol. 349, 536-547.

Duque, C., 2009. Influencia antrópica sobre la hidrogeología del acuífero Motril-Salobreña. Doctoral thesis. University of Granada. 196 pp.

Duque, C., and Calvache, M. L., 2010. El balance hídrico del acuífero Motril-Salobreña: Estudios previos y cálculo mediante modelación numérica. Geogaceta 48, 119-122

Duque, C., Calvache, M. L., Engesgaard, P., 2010. Investigating river–aquifer relations using water temperature in an anthropized environment (Motril-Salobreña aquifer). J. Hydrology 381, 121-133.

Duque, C., López-Chicano, M., Calvache, M., Martín-Rosales, W., Gómez-Fontalva, J., Crespo, F., 2011. Recharge sources and hydrogeological effects of irrigation and an influent river identified by stable isotopes in the Motril-Salobreña aquifer (southern Spain). Hydrol.Proc. 25, 2261-2274.

Duque, C., Olsen, J.T., Sánchez-Úbeda, J.P., Calvache, M.L., 2018. Paleohydrogeological model of the groundwater salinity in the Motril-Salobrena ˜ aquifer. In: Calvache, M., Duque, C., Pulido-Velazquez, D. (Eds.), Groundwater and Global Change in the Western Mediterranean Area. Environmental Earth Sciences. Springer, Cham. https://doi.org/10.1007/978-3-319-69356-9_14.

Duque, C., Olsen, J.T., Sánchez-Úbeda, J.P., Calvache, M.L., 2019. Groundwater salinity during 500 years of anthropogenic-driven coastline changes in the Motril-Salobreña aquifer (South East Spain). Environ. Earth Sci. 78, 471.

Duque, C., Rosenberry, D.O., 2022. Advances in the Study and Understanding of Groundwater Discharge to Surface Water. Water, 14, 1698. https://doi.org/10.3390/w14111698

Epting, J., Scheidler, S., Affolter, A., Borer, P., Mueller, M. H., Egli, L., García-Gil, A., Huggenberg, P., 2017. The thermal impact of subsurface building structures on urban groundwater resources–a paradigmatic example. Sci. Total Environ. 596-597, 87–96. http://doi.org/10.1016/j.scitotenv.2017.03.296

Fernández-Ayuso, A., Rodríguez-Rodríguez, M., Benavente, J., 2018. Assessment of the hydrological status of Doñana dune ponds: a natural World Heritage Site under threat. Hydrol. Sci. J. 63, 2048–2059. https://doi.org/10.1080/02626667.2018.1560449

Galindo-Zaldívar J. Gil A.J., Borque M.J., González-Lodeiro F., Jabaloy A., Marín-Lechado, Ruano P., Sanz de Gadeano C., 2003. Active faulting in the internal zones of the Betic Cordilleras (SE Spain). J. Geodyn. 36, 239-250.

Gardner, R.C. and Finlayson, C.M., 2018. Perspectives mondiales des zones humides: état des zones humides à l'échelle mondiale et des services qu'elles fournissent à l'humanité. Secrétariat de la Convention de Ramsar. Gland, Suisse.

Gedan, K.B., Kirwan, M.L., Wolanski, E., Barbier, E.B., Silliman, B.R., 2011. The present and future role of coastal wetland vegetation in protecting shorelines: Answering recent challenges to the paradigm. Clim. Change 106, 7–29. https://doi.org/10.1007/s10584-010-0003-7

Gómez-Gómez, J.D., López-Geta, J.A., Garrido-Schneider, E., 2003. The state of seawater intrusion in Spain. II TIAC, Alicante, II, pp 169–186

Greve, P., Kahil, T., Mochizuki, J., Schinko, T., Satoh, Y., Burek, P., Fischer, G., Tramberend, S., Burtscher, R., Langan, S., Wada, Y., 2018. Global assessment of water challenges under uncertainty in water scarcity projections. Nat. Sustain. 1, 486–494. https://doi.org/10.1038/s41893-018-0134-9

Hefting, M., Clément, J.C., Dowrick, D., Cosandey, A.C., Bernal, S., Cimpian, C., Tatur, A., Burt, T.P., Pinay, G., 2004. Water table elevation controls on soil nitrogen cycling in riparian wetlands along a European climatic gradient. Biogeochemistry 67, 113–134. https://doi.org/10.1023/B:BIOG.0000015320.69868.33

Hemmerle, H., Hale, S., Dressel, I., Benz, S. A., Attard, G., Blum, P., Bayer, P., 2019. Estimation of Groundwater Temperatures in Paris, France. Geofluids. 1–11. http://doi.org/10.1155%2F2019%2F5246307

Henry, H.R., Hilleke, J.B., 1972. Exploration of multiphase fluid flow in a saline aquifer system affected by geothermal heating. (Final report). Tech. rep. Alabama Univ., University (USA).

Heredia, J., Murillo, J., García-Aróstegui, J., Rubio, J., and Lopez-Geta, J., 2002. Construcción de presas e impacto sobre el régimen hidrológico de los acuíferos situados aguas abajo. Presa de Rules y acuífero costero de Motril-Salobreña-Granada, sur de España. Boletín Geológico y Minero 113: 165-184

Heredia J., Murillo J.M., García-Aróstegui J.L., Rubio J.C., López-Geta J.A., 2003. Influencia antrópica en un acuífero costero. Consideraciones sobre la gestión hídrica del acuífero de Motril-Salobreña (España). Revista Latino-Americana de Hidrogeología 3, 73-83.

Hódar-Pérez, A., López-Chicano, M., Calvache, M.L., Duque, C., Sánchez-Úbeda, J.P., Martín-Montañés, C., 2015. Evolución del contenido en nitratos en el acuífero de Motril-Salobreña durante la década 2001-2011. IX Simposio del Agua en Andalucía, Málaga, 165-175.

Hoekstra, A.Y., Mekonnen, M.M., 2012. The water footprint of humanity. Proc. Natl. Acad. Sci. U. S. A. 109, 3232–3237. https://doi.org/10.1073/pnas.1109936109

Houben, G., Post, V.E.A., 2017. The first field-based descriptions of pumping-induced saltwater intrusion and upconing. Hydrogeol. J. 25, 243–247. https://doi.org/10.1007/s10040-016-1476-x

Hughes, J.D., Vacher, H.L., Sanford, W.E., 2007. Three-dimensional flow in the Florida platform: Theoretical analysis of Kohout convection at its type locality. Geology 35, 663–666. https://doi.org/10.1130/G23374A.1.

Ibáñez, S., 2005. Comparación de la aplicación de distintos modelos matemáticos sobre los acuíferos costeros detríticos. Doctoral thesis. University of Granada, 304 pp.

IGME., 1983. Investigación Hidrogeológicas de las cuencas del Sur de España (sector occidental). PIAS. Informe técnico realizado por ENADIMSA.

IGME, 1985. Estudio hidrogeológico de la Cuenca del Guadalfeo y sectores costeros adyacentes (1a y 2a fases).

IGME, 1999. Plan de integración de los recursos hídricos subterráneos en los sistemas de abastecimiento público de Andalucía. Sector de acuíferos en relación con el abastecimiento de los núcleos situados en la cuenca del Guadalfeo y sectores costeros adyacentes (Almuñécar, Albuñol y Castell de Ferro) Granada. Actualización del conocimiento hidrogeológico de la unidad 06.21. Motril-Salobreña y modelización matemática del acuífero. Tomo de memoria, 169 pp.

ITGE, 1988. Investigación hidrogeológica para apoyo a la gestión hidrológica en las cuencas del río Guadalfeo (Cuenca Sur de España).

ITGE, 1989. Estudio hidrogeológico de la cuenca del Guadalfeo y sectores costeros adyacentes (3 fase).

ITGE, 1991. Investigación hidrogeológica para apoyo a la gestión hidrogeológica en la Cuenca del río Guadalfeo (Granada).

Jiménez-Sánchez, J., Martín-Rosales, W., Fernández-Chacón, F., Rubio-Campos, J.C., González-Ramón, A., López-Chicano, M., Calvache, M.L., Duque, C. 2008. Variabilidad temporal de las precipitaciones en la cuenca del río Guadalfeo (Provincia de Granada). VII Simposio del Agua en Andalucía, Baeza, 159-168.

Kim, K. Y., Chon, C. M., Park, K. H., Park, Y. S., Woo, N. C., 2008. Multi-depth monitoring of electrical conductivity and temperature of groundwater at a multilayered coastal aquifer: Jeju Island, Korea. Hydrol. Proc. 22, 3724–3733. https://doi.org/10.1002/hyp.6976

Kim, K. Y., Park, Y. S., Kim, G. P., Park, K. H., 2009. Dynamic freshwater-saline water interaction in the coastal zone of Jeju Island, South Korea. Hydrogeol. J., 17, 617–629. https://doi.org/10.1007/s10040-008-0372-4

Kløve, B., Allan, A., Bertrand, G., Druzynska, E., Ertürk, A., Goldscheider, N., Henry, S., Karakaya, N., Karjalainen, T.P., Koundouri, P., Kupfersberger, H., Kværner, J., Lundberg, A., Muotka, T., Preda, E., Pulido-Velazquez, M., Schipper, P., 2011. Groundwater dependent ecosystems. Part II. Ecosystem services and management in Europe under risk of climate change and land use intensification. Environ. Sci. Policy 14, 782–793. https://doi.org/10.1016/j.envsci.2011.04.005

Kurylyk, B.L., Irvine, D.J., Bense, V.F., 2019. Theory, tools, and multidisciplinary applications for tracing groundwater fluxes from temperature profiles. WIREs Water. https://doi.org/10.1002/wat2.1329

Kurylyk, B. L., MacQuarrie, K. T. B., McKenzie, J. M., 2014. Climate change impacts on groundwater and soil temperatures in cold and temperate regions: Implications, mathematical theory, and emerging simulation tools. Earth Sci. Rev. 138, 313–334. http://doi.org/10.1016/j.earscirev.2014.06.006

Langevin, C.D., Dausman, A.M., Sukop, M.C., 2010. Solute and heat transport model of the Henry and Hilleke laboratory experiment. Ground Water 48, 757–770. https://doi.org/10.1111/j.1745-6584.2009.00596.x

Li, Y., Li, N., Feng, J., Qian, J., Shan, Y., 2021. Temporal Temperature Distribution in Shallow Sediments of a Large Shallow Lake and Estimated Hyporheic Flux Using VFLUX 2 Model. Water. 13, 300. https://doi.org/10.3390/w13030300

Li, P., Wu, J., Qian, H., 2016. Preliminary assessment of hydraulic connectivity between river water and shallow groundwater and estimation of their transfer rate during dry season in the Shidi River, China. Environ. Earth Sci. 75, 1–16. https://doi.org/10.1007/s12665-015-4949-7

Lu, C., Shi, W., Xin, P., Wu, J., Werner, A.D., 2017. Replenishing an unconfined coastal aquifer to control seawater intrusion: Injection or infiltration? Water Resour. Res. 53, 4775–4786. https://doi.org/10.1002/2016WR019625

Liu, Z., Zhan, W., Bechtel, B., Voogt, J., Lai, J., Chakraborty, T., Wang, Z.H., Li, M., Huang, F., Lee, X. 2022. Surface warming in global cities is substantially more rapid than in rural background areas. Commun. Earth Environ. 3, 219. https://doi.org/10.1038/s43247-022-00539-x

Malek, Ž., Verburg, P.H., Geijzendorffer, I.R., Bondeau, A., Cramer, W. 2018. Global change effects on land management in the Mediterranean region. Glob. Environ. Chang. 50, 238-254.

Martín-Rosales, W., Duque, C., Calvache, M.L., López-Chicano, M., González, A., Rubio-Campos, J.C., 2007. Modificaciones recientes del régimen hidrológico en el río Guadalfeo. Agua y Cultura. IGME. Madrid, 149-156.

McDonough, L.K., Santos, I.R., Andersen, M.S., O'Carroll, D.M., Rutlidge, H., Meredith, K., Oudone, P., Bridgeman, J., Gooddy, D.C., Sorensen, J.P.R., Lapworth, D.J., MacDonald, A.M., Ward, J., Baker, A., 2020. Changes in global groundwater organic carbon driven by climate change and urbanization. Nat. Commun. 11, 1–10. https://doi.org/10.1038/s41467-020-14946-1

Menberg, K., Blum, P., Kurylyk, B. L., Bayer, P., 2014. Observed groundwater temperature response to recent climate change. Hydrol. Earth Sys. Sci. 18, 4453–4466. http://orcid.org/10.5194/hess-18-4453-2014

Mitsch, W.J., Bernal, B., Nahlik, A.M., Mander, Ü., Zhang, L., Anderson, C.J., Jørgensen, S.E., Brix, H., 2013. Wetlands, carbon, and climate change. Landsc. Ecol. 28, 583–597. https://doi.org/10.1007/s10980-012-9758-8

Mitsch, W.J. and Gosselink, J.G., 2015. Wetlands (5th edition), John Wiey & Sons, INC, Hoboken, N. 744 pp.

Morgan, L.K., Werner, A.D., 2015. A national inventory of seawater intrusion vulnerability for Australia. J. Hydrol. Reg. Stud. 4, 686–698. https://doi.org/10.1016/j.ejrh.2015.10.005

Neumann, B., Vafeidis, A.T., Zimmermann, J., Nicholls, R.J., 2015. Future coastal population growth and exposure to sea-level rise and coastal flooding - A global assessment. PLoS One 10, 131375. https://doi.org/10.1371/journal.pone.0118571

Nieto-López, J.M., Barberá, J.A., Andreo, B., Ramírez-González, J.M., Rendón-Martos, M., 2020. Hydro-environmental changes assessment after Guadalhorce River mouth channelization. An example of hydromodification in southern Spain. Catena 189, 104461. https://doi.org/10.1016/j.catena.2020.104461

Olsen, J.T., 2016. Modeling the evolution of salinity in the Motril-Salobreña aquifer using a paleo-hydrogeological model. Master´s thesis. University of Oslo. 92 pp.

Ozotta, O., Gerla, P.J., 2021. Mapping Groundwater Seepage in a Fen Using Thermal Imaging. Geosci. 11, 29. https://doi.org/10.3390/geosciences11010029

Paldor, A., Michael, H. A. 2021. Storm surges cause simultaneous salinization and freshening of coastal aquifers, exacerbated by climate change. Water Resour. Res., 57, e2020WR029213. https://doi.org/10.1029/2020WR029213

Parish, F., Sirin, A., Charman, D., Joosten, H., Minayeva, T., Silvius, M., Stringer, L., 2008. Assessment on Peatlands, Biodiversity and Climate Change: Main Report. Global Environment Centre, Kuala Lumpur and Wetlands International, Wageningen., Assessment on peatlands, biodiversity and climate change: main report.

Pearce, W., Holmberg, K., Hellsten, I., Nerlich, B., 2014. Climate change on twitter: Topics, communities and conversations about the 2013 IPCC Working Group 1 report. PLoS One 9, 1–11. https://doi.org/10.1371/journal.pone.0094785

Pérez-Peña J.V., 2009. GIS-Based tools and methods for landscape analysis and evaluation of active tectonics. Doctoral thesis. University of Granada. 143 pp.

Pollack, H.N., Huang, S., 2000. Climate Reconstruction from Subsurface Temperatures, Annu. Rev. Earth Planet. Sci. 28, 339-365. https://doi.org/10.1146/annurev.earth.28.1.339

Pollack, H.N., Smerdon, J.E., van Keken, P.E., 2005. Variable seasonal coupling between air and ground temperatures: A simple representation in terms of subsurface thermal diffusivity. Geophys. Res. Lett. 32. https://doi.org/10.1029/2005GL023869

Pretel, R.M., Duque, C., Calvache, M.L., 2010. Efecto de los cambios de usos del suelo sobre la recarga del acuífero Motril-Salobreña. Geogaceta. 49, 111-114.

Pulido-Bosch, A., García Gómez, J., Benavente, J., 1980. Las fuentes potenciales de contaminación en los acuíferos de Salobreña (Granada). Tecniterrae. 33, 31-38.

Pulido-Bosch, A., and Rubio, J. 1988. Los acuíferos costeros de Motril-Salobreña. TIAC 88, 209-238.

Reolid, J., López Chicano, M., Calvache Quesada, M. L., Duque, C., Sánchez Úbeda, J. P., 2013. Estimación de las aportaciones del aluvial del río Guadalfeo al acuífero Motril-Salobreña. Geogaceta, 52, 231-234.

Richardson, S., Irvine, E., Froend, R., Boon, P., Barber, S., Bonneville, B., 2011. Australian groundwater-dependent ecosystems toolbox part 1: assessment framework, Waterlines report.

Rohde, M.M., Froend, R., Howard, J., 2017. A Global Synthesis of Managing Groundwater Dependent Ecosystems Under Sustainable Groundwater Policy. Groundwater 55, 293–301. https://doi.org/10.1111/gwat.12511

Sánchez-Martos, F., López-Martos, J.M., Sánchez, L.M., Gisbert-Gallego, J., Navarro-Martínez, F., 2021. Influence of groundwater discharge on temporal evolution in two wetlands of an intensely anthropized area: Analysis using an integrated approach. Water (Switzerland) 13, 1–15. https://doi.org/10.3390/w13050697

Sánchez Úbeda, J. P., Calvache Quesada, M. L., Duque Calvache, C., López Chicano, M., Martín Rosales, W., 2013. Influence of tidal fluctuations in the water table and methods applied in the calculation of hydrogeological parameters. The case of Motril-Salobreña coastal aquifer. EGU General Assembly Conference Abstracts.

Sánchez-Úbeda, J.P., 2017. Procesos hidrodinámicos en la zona de descarga de los acuíferos costeros. Doctoral thesis. Universidad de Granada. 198 pp.

Sánchez-Úbeda, J. P., López-Chicano, M., Calvache, M. L., Purtschert, R., Engesgaard, P., Martín-Montañés, C., Sültenfub, J., Duque, C., 2018a. Groundwater Age Dating in Motril-Salobreña Coastal Aquifer with Environmental Tracers (18O/2H, 3H/3He, 4He, 85Kr, and 39Ar). Groundwater and Global Change in the Western Mediterranean Area, Environ.Earth Sci., 287-295.

Sánchez-Úbeda, J. P., Calvache, M. L., Engesgaard, P., Duque, C., López-Chicano, M., Purtschert, R., 2018b. Numerical Modeling of Groundwater Age Distribution in Motril-Salobreña Coastal Aquifer (SE Spain). Groundwater and Global Change in the Western Mediterranean Area, Environ. Earth Sci., 277-285.

Shi, L., Lu, C., Ye, Y., Xie, Y., Wu, J., 2020. Evaluation of the performance of multiple-well hydraulic barriers on enhancing groundwater extraction in a coastal aquifer. Adv. Water Resour. 144. https://doi.org/10.1016/j.advwatres.2020.103704

Siarkos, I., Latinopoulos, D., Mallios, Z., Latinopoulos, P., 2017. A methodological framework to assess the environmental and economic effects of injection barriers against seawater intrusion. J. Environ. Manage. 193, 532–540. https://doi.org/10.1016/j.jenvman.2017.02.051

Smerdon, J.E., Pollack, H.N., Enz, J.W., Lewis, M.J., 2003. Conduction-dominated heat transport of the annual temperature signal in soil. J. Geophys. Res. Solid Earth 108. https://doi.org/10.1029/2002jb002351

Soto, J.M., 1998. Aportaciones al conocimiento del acuífero detrítico de Motril-Salobreña (Granada). Bachelor's thesis. University of Granada. 135 pp.

Su, X., Cui, G., Du, S., Yuan, W., Wang, H., 2016. Using multiple environmental methods to estimate groundwater discharge into an arid lake (Dakebo Lake, Inner Mongolia, China). Hydrogeol. J. 24, 1707–1722. https://doi.org/10.1007/s10040-016-1439-2

Swain, E. D., Prinos, S. T., 2018. Using heat as a tracer to determine groundwater seepage in the Indian river Lagoon, Florida, April - November 2017. Reston, VA: U.S. Geological Survey Open File Report 2018-1151.

Taniguchi, M., Turner, J.V., Smith, A.J., 2003. Evaluations of groundwater discharge rates from subsurface temperature in Cockburn Sound, Western Australia. Biogeochem. 66, 111–124.

Temmerman, S., Meire, P., Bouma, T.J., Herman, P.M.J., Ysebaert, T., De Vriend, H.J., 2013. Ecosystem-based coastal defence in the face of global change. Nature 504, 79–83. https://doi.org/10.1038/nature12859

Thorne, D., Langevin, C.D., Sukop, M.C., 2006. Addition of simultaneous heat and solute transport and variable fluid viscosity to SEAWAT. Comput. Geosci. 32, 1758–1768. https://doi.org/10.1016/j.cageo.2006.04.005

Thorslund, J., Jarsjo, J., Jaramillo, F., Jawitz, J.W., Manzoni, S., Basu, N.B., Chalov, S.R., Cohen, M.J., Creed, I.F., Goldenberg, R., Hylin, A., Kalantari, Z., Koussis, A.D., Lyon, S.W., Mazi, K., Mard, J., Persson, K., Pietro, J., Prieto, C., Quin, A., Van Meter, K., Destouni, G., 2017. Wetlands as large-scale nature-based solutions: Status and challenges for research, engineering and management. Ecol. Eng. 108, 489–497. https://doi.org/10.1016/j.ecoleng.2017.07.012

Tirado-Conde, J., Engesgaard, P., Karan, S., Müller, S., Duque, C., 2019. Evaluation of temperature profiling and seepage meter methods for quantifying submarine groundwater discharge to coastal lagoons: Impacts of saltwater intrusion and the associated thermal regime. Water. 11, 1648. https://doi.org/10.3390/w11081648

Tissen, C., Benz, S. A., Menberg, K., Bayer, P., and Blum, P., 2019. Groundwater temperature anomalies in central Europe. Environ. Res. Lett. 14, 104012. http://doi.org/10.1088/1748-9326/ab4240

Vallejos, A., Sola, F., Pulido-Bosch, A., 2015. Processes Influencing Groundwater Level and the Freshwater-Saltwater Interface in a Coastal Aquifer. Water Res. Manag., 29, 679–697. https://doi.org/10.1007/s11269-014-0621-3

Van Camp, M., Mtoni, Y., Mjemah, I.C., Bakundukize, C., Walraevens, K., 2014. Investigating seawater intrusion due to groundwater pumping with schematic model simulations: The example of the Dar es Salaam coastal aquifer in Tanzania. J. African Earth Sci. 96, 71–78. https://doi.org/10.1016/j.jafrearsci.2014.02.012

Vandenbohede, A., Van Houtte, E., 2012. Heat transport and temperature distribution during managed artificial recharge with surface ponds. J. Hydrol. 472–473, 77–89. https://doi.org/10.1016/j.jhydrol.2012.09.028

Vera, J., Martín-Algarra, A., 2004. Cordillera Bética y Baleares. Divisiones mayores y nomenclatura. In Geología de España. Vera, J., Ed. SGE-IGME, Madrid, Spain. 347–350 pp.

Verhoeven, J.T.A., Arheimer, B., Yin, C., Hefting, M.M., 2006. Regional and global concerns over wetlands and water quality. Trends Ecol. Evol. 21, 96–103. https://doi.org/10.1016/j.tree.2005.11.015

Werner, A.D., Bakker, M., Post, V.E.A., Vandenbohede, A., Lu, C., Ataie-Ashtiani, B., Simmons, C.T., Barry, D.A., 2013. Seawater intrusion processes, investigation and management: Recent advances and future challenges. Adv. Water Resour. 51, 3–26. https://doi.org/10.1016/j.advwatres.2012.03.004

Werner, A.D., Simmons, C.T., 2009. Impact of sea-level rise on sea water intrusion in coastal aquifers. Ground Water 47, 197–204. https://doi.org/10.1111/j.1745-6584.2008.00535.x

Wang, Z., Yang, Y., Chen, G., Wu, Jianfeng, Wu, Jichun, 2021. Variation of lake-river-aquifer interactions induced by human activity and climatic condition in Poyang Lake Basin, China. J. Hydrol. 595, 126058. https://doi.org/10.1016/j.jhydrol.2021.126058

Yechieli, Y., Shalev, E., Wollman, S., Kiro, Y., Kafri, U., 2010. Response of the Mediterranean and Dead Sea coastal aquifers to sea level variations. Water Resour. Res. 46, 1–11. https://doi.org/10.1029/2009WR008708

CHAPTER 2
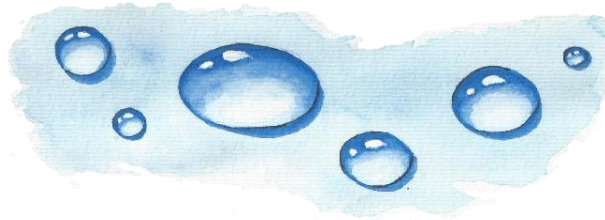
Groundwater-Surface Water Interactions in "La Charca de Suárez" Wetlands, Spain

Ángela M. Blanco-Coronas[1], Manuel López-Chicano[1], María Luisa Calvache[1], José Benavente[1] and Carlos Duque[2]

[1] Departamento de Geodinámica, Universidad de Granada, Avenida Fuente Nueva s/n., 18071 Granada, Spain

[2] WATEC, Department of Geoscience, Aarhus University, Høegh-Guldbergs Gade 2, 8000 Aarhus C, Denmark

Abstract

La Charca de Suárez (LCS) is a Protected Nature Reserve encompassing 4 lagoons located 300 m from the Mediterranean coast in southern Spain. LCS is a highly anthropized area, and its conservation is closely linked to the human use of water resources in its surroundings and within the reserve. Different methodologies were applied to determine the hydrodynamics of the lagoons and their connection to the Motril-Salobreña aquifer. Fieldwork was carried out to estimate the water balance of the lagoon complex, the groundwater flow directions, the lagoons-aquifer exchange flow and the hydrochemical characteristics of the water. The study focussed on the changes that take place during dry-wet periods that were detected in a 7-month period when measurements were collected. The lagoons were connected to the aquifer with a flow-through functioning under normal conditions. However, the predominant inlet to the system was the anthropic supply of surface water which fed one of the lagoons and produced changes in its flow pattern. Sea wave storms also altered the hydrodynamic of the lagoon complex and manifested a future threat to the conservation status of the wetland according to predicted climate change scenarios. This research presents the first study on this wetland and reveals the complex hydrological functioning of the system with high spatially and temporally variability controlled by climate conditions and human activity, setting a corner stone for future studies.

Keywords

_____

1. Introduction

Wetlands are considered some of the most productive and beneficial ecosystems in the world because of their high biological diversity (Misch and Gosselink, 1993) and the regulation of surface runoff, decreasing the risk of flooding and purifying inflowing waters (Richardson, 1995; Misch and Gosselink, 2000). However, many wetlands in Europe were considered low-production and unhealthy areas for humans for centuries and thus were drained (Jones and Hughes, 1993; McCovie and Christopher, 1993). Currently, wetlands are threatened, primarily due to the increase in economic activities and urban development.

Wetlands are particularly sensitive to changes affecting surface water (SW) or groundwater (GW) in their vicinity (Suso and Llamas, 1993; Syphard and Garcia, 2001). Knowledge of SW-GW interactions is essential for understanding their hydrodynamics (Richter et al., 1996; Shaffer et al., 1999; Zedler, 2000) and to improve the management and protection. GW-SW fluxes have been traditionally quantified using field measurements or estimating each component of the water budget (Doss, 1993; Mills and Zwarich, 1986; Ramberg et al., 2006; Mendoza-Sanchez et al., 2013). The connexion between a wetland system and an aquifer can change over the short term, controlled by the relative SW and GW heads (Rosenberry and Winter, 1997; Amoros and Bornette,

2002). Important variations can be produced by factors such as climate change (Wurster et al., 2003) and to modifications on the water management due to regulation, channelization, upstream water abstractions (Walker et al., 1992; Jolly, 1996). Aquifer heterogeneities often generate irregular flow patterns, hindering the identification of groundwater inputs to wetlands (e.g., (Freeze and Witherspoon, 1967; Krabbenhoft and Anderson, 1986). Additionally, groundwater exchange impacts on the water quality of wetlands (Lewandowski et al., 2015).

La Charca de Suárez (LCS) is one of the few wetlands of south-east Spain (Junta de Andalucía, 2017) and the only coastal wetland in the region. LCS is a prime habitat for the wintering, nesting and migration of water birds that cross the Strait of Gibraltar, as well as for amphibian reproduction. In addition, LCS supports a number of endangered species in Spain, such as Fulica cristata (del Hoyo et al., 2014). It was classified as a Protected Nature Reserve by the regional government of Andalusia in 2009 owing to its high ecological value.

The LCS extension, like in other wetlands from Spain and Europe, has been considerably reduced since its appearance in the 14th–15th century (Menotti and O'Sullivan, 2013). The wetland was drained to increase the area of arable land and to eradicate diseases such as malaria. Also, from 1918 to 1985, the "Cambó" law was active in Spain, which granted the piece of land occupied by the wetland to anyone who drains it causing a loss of 60% of the wetlands in Spain since the 70s (European Community, 2007). For these reasons, LCS wetland was decreased from more than 1000 ha registered in the XVIII century to 14 ha at the present. From 1980 to 2000, LCS was almost entirely disappeared due to urban development for tourism and the lack of water inlets due to infrastructure construction such as dams and irrigation channels. In 2000, a plan to recover the wetland was implemented and in 2009 it was recognized as Protected Nature Reserve (Consejería de Medio Ambiente, 2004).

One of the main characteristics of LCS is that it requires human intervention to maintain the sheet of water for the sustainability of the ecological system. The system receives inputs from surface water from irrigation channels generating highly variable conditions that can change regardless the weather conditions. Also, the management of the protected area requires a deep understanding of the water budget. So far, there is no information about the groundwater-surface water interaction of LCS or its water budget, and this is the first time that a study has focused on this area from a hydrological perspective. Because this system is affected by human management, during dry periods, the use of water is optimized to supply irrigation water reducing the inputs to the lagoons. The reaction of the system to these changes from and hydrological or chemical perspective can be considered as test anticipating predicted climate change scenarios in the long run (IPCC, 2014).

The objective of this study is to determine the hydrological functioning of the LCS wetland and its interaction with Motril-Salobreña aquifer. As short-term changes can play an important role in the system, dry and wet periods will be analyzed and the methods for the local evaluation of the fluxes and water budget will be examined for a 7- and 5-month period of data collected, respectively.

2. Materials and Methods

2.1. Hydrological Settings

The Motril-Salobreña aquifer is located on the Mediterranean coast of south-east Spain in the province of Granada (Figure 2.1 A). It is a detrital coastal aquifer with an extension of 42 km^2 and means annual resources of 35 Mm^3 (Calvache et al., 2009). It consists of poorly consolidated Quaternary detrital sediments discordantly overlying metamorphic rocks (Aldaya, 1981).

The aquifer is hydrogeologically bounded to the north by the alluvium of the Guadalfeo River and the Escalate carbonate aquifer and to the south by the Mediterranean Sea. Its lateral boundaries and the basement are composed of schists and phyllites of very low permeability (Figure 2.1 B) (Duque et al., 2008). The aquifer thickness ranges from 30 to 50 m in the northern sector in the northern sector (alluvial sedimentary environment) to more than 250 m in areas near the coastline (deltaic sedimentary environment) (Duque et al., 2008). The lithology of the aquifer is characterized by alternating clays, silts, sand and gravel. In addition, the proportion of materials with higher hydraulic conductivity decrease north to south and east to west (Duque et al., 2005). The direction of groundwater flow is north-south with a hydraulic gradient estimated between 1.6×10^{-3} and 5×10^{-3} (Duque et al., 2010). The main natural recharge of the aquifer is produced by infiltration from Guadalfeo River (Calvache et al., 2009; Duque et al., 2011) and by irrigation return flows (Calvache et al., 2009; Duque et al., 2011), estimated at 11 Mm^3/year and 16 Mm^3/year, respectively. Other minor contributions are produced by lateral inlets from the Escalate aquifer (4 Mm^3/year) and rainfall recharge (3–6 Mm^3/year) (Calvache et al., 2009) and by the alluvium from the river (1 Mm^3/year) (Reolid et al., 2012).

The main outlet is groundwater discharge from the aquifer to the sea, which is estimated to range from 17 to 26 Mm^3/year (Calvache et al., 2009; Heredia et al., 2002; Ibañez, 2005; Duque, 2009). Pumped outflows and, to a lesser extent, occasional river gains, in its final stretch, are also important.

The Guadalfeo River, with a drainage basin of 1290 km^2, is the main watercourse that runs through the aquifer, with a mixed pluvio-nival regime. It collects a large part of the waters that drain the southern slope of the Sierra Nevada mountain massif (3482 m a.s.l. of maximum altitude).

The Guadalfeo River Plain is an area with intense agricultural activity. A complex network of irrigation channels covers the entire surface of the Motril-Salobreña aquifer and transports the waters previously derived from the Guadalfeo River. In this region, the flood irrigation method is commonly applied, which uses more water than that required by plants (Duque et al., 2010). Part of the excess water infiltrates and becomes part of irrigation return flows, and the other part flows as surface runoff and is recovered again by the irrigation channels that ultimately discharge it into the sea.
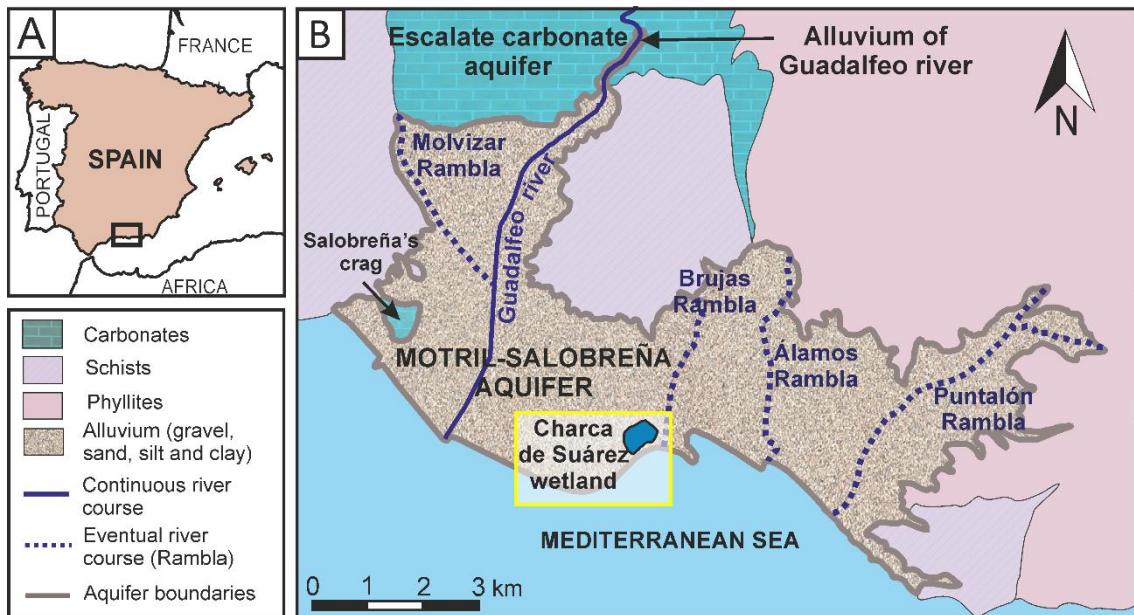
Figure 2.1.- (A) Location of the study area; (B) Hydrogeological location of the Motril-Salobreña aquifer and the La Charca de Suárez (LCS) wetland.

The climatic characteristics of the basin are highly variable over time and space. Its climate ranges from subtropical Mediterranean in the coast to high-mountain Mediterranean in high-altitude areas. The average precipitation is 400 mm/year in the coast and 1000 mm/year in the high-altitude areas of Sierra Nevada, primarily as snow. The wet seasons occur during the autumn and winter months, whereas summer months are extremely dry.

The LCS wetland is located in the southern border of the Motril-Salobreña aquifer, in its discharge zone to the sea. This specific area of the aquifer belongs to the former Guadalfeo river mouth. The local lithology of the first 75 meters of the aquifer is known based on a 75 m deep well (Well DW) (Figure 2.2 B). It consists of alluvial sediments (fine sands and some pebbles) and prodeltaic silty sediments. Although the sediments are the same for all the study area, the proportion and spatial distribution can vary widely as it is normal in these sedimentary environments. The lagoon complex encompasses several waterbodies, but this study focuses on those within the perimeter of the protected area (Figure 2.2 A), namely, Aneas (AW), Lirio (LW), Taraje (TAW) and Trébol (TW). The lagoons have various sizes ranging from 11,400 m^2 to 1800 m^2 and maximum depths ranging from 3.5 m to 1.2 m. These lagoons are surrounded by topographically low areas that sporadically flood during wet periods and that can even connect the lagoons.

Surface water inlets occur north of the reserve due to the main channel that collects surplus irrigation water from the Guadalfeo River Plain and surface runoff from the drainage basin. This channel crosses the protected area from north to south and feeds vegetation-covered areas naturally prone to flooding known as flood meadows. The water moves by surface runoff until reaching some of the lagoons, depending on the degree of flooding of the flood meadows. The main channel and others collect the water surplus of the lagoons, merging south of the reserve and flowing directly to the sea (Figure 2.2 C). These channels are directly excavated without any impermeabilization and can contribute to the interaction with the groundwater. The channels are 0.7 m deep and they would

require very high water table conditions, close to the groundwater flooding of the area to participate in this interaction. In this study, they have not been studied as it has been not observed a major impact over the system functioning but they remain as a research question to explore in the future.

2.2. Monitoring Network

A set of measuring stations was established to monitor changes in surface water, groundwater and weather conditions. This was the first time that the water inputs to LCS were quantified and required of several additional measuring points after the initial monitoring net design. One of the challenges working in protected areas with endangered species is the restriction for fieldwork activities and the limitation in the time periods that access to the lagoons is granted. This affected directly to the research activities in the lagoons to reduce the ecological disturbance (i.e., nesting periods).

Hydrometeorological data: These data were collected from a Davis Vantage Pro2 Plus wireless weather station. Precipitation, atmospheric pressure, temperature, wind speed and direction and solar radiation measurements were taken every 30 min (Figure 2.2 C) with a resolution and accuracy of each parameter represented in Table 2.1.
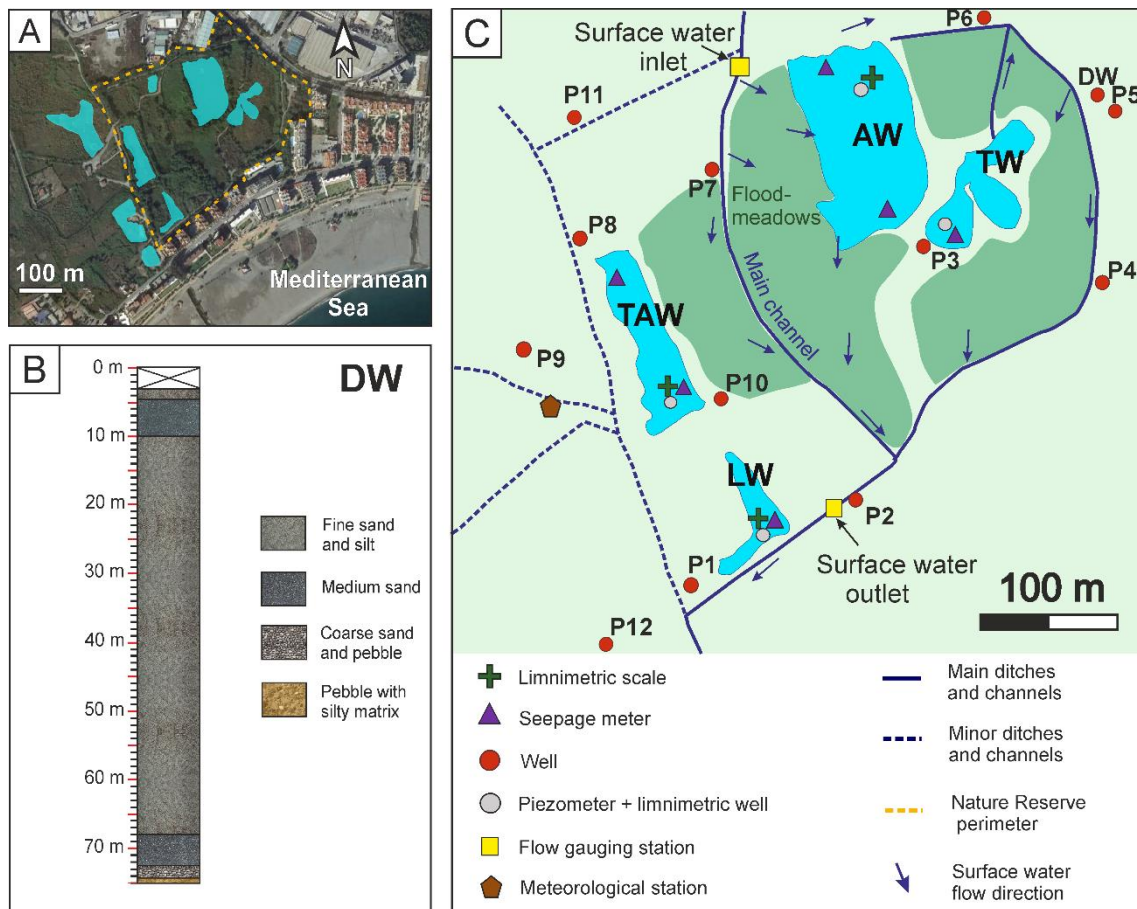

Figure 2.2.- (A) Location of the lagoon complex of LCS; (B) Lithological core of DW well; (C) Points of the new monitoring network.

Sensor	Resolution	Accuracy	Units
Barometric Pressure	0.1	±1	hPa
Rainfall	0.2	±0.2	mm
Solar Radiation	1	±90	W/m^2
Temperature	0.1	±0.3	°C
Wind Speed	0.4	±0.9	m/s
Humidity	100	±2	%

Table 2.1.- Resolution and accuracy of each integrated sensors of the meteorological station.

Discharge data: Two gauging stations were built to measure the inflow and outflow discharge of the reserve. They consisted of a V-shaped weir and of a limnimetric scale. In addition, a pressure sensor was installed to measure the water surface height every hour. These data were transformed into discharge using rating curves constructed with measurements taken manually at each station. The correlation coefficients (R^2) of the rating curves are 0.78 for inflow and 0.92 for outflow.

Groundwater level data: A total of 10 wells, 7 with depths of 3 m, 1 with a depth of 7 m and 2 with depths of 20 m, all 11 cm in diameter, were drilled using the rotary core drilling technique specifically for this project. In addition, 4 piezometers 11 cm in diameter were also installed at the bottom of each lagoon by nailing them to the bed at a depth of 0.5 m to estimate vertical hydraulic gradients. The wells are screened in their entire length and the lagoon piezometers have a 30 cm screen. Due to the lack of stability of the sediments, it was assumed that the screens were sealed immediately by to the collapsing during the drilling. In spite of the proximity to the groundwater discharge zone to the sea it was not observed vertical flow, likely because of the shallow depth reached in most of the wells. In wells P1, P2, P3, P4, P5, P6, P7 and P8 (Figure 2.2 C), pressure sensors were installed to measure the groundwater level hourly. Monthly measurements were taken in P9, P10, P11 and P12 and in the lagoon piezometers.

Limnimetric data: Water level variations in each lagoon were assessed using sensors installed in limnimetric tubes slotted throughout their length. Hourly readings were taken and verified using measurements taken from the monthly limnimetric scales.

Water level data from gauging stations, lagoons, wells and piezometers were recorded by Seametrics LevelSCOUT smart pressure sensors (Resolution: 0.34 mm; Accuracy: ±5 mm). These data loggers were complemented with a BaroSCOUT barometric pressure sensor (Resolution: 0.34 mm; Accuracy: ±5 mm) and were calibrated with manual level measurements taken with an OTT HydroMet KL010 contact gauge. All measurements were referenced to the absolute zero of the mean sea level with a GPS Leica System 1200+ (Vertical resolution: 6mm; Accuracy: ±0.55–2 cm).

Direct measurements of exchange flow: 6 Lee-type seepage meters (Lee, 1977) were installed inside the lagoons, 4–15 m distance from the shoreline. Due to the verticality of the lagoon margins, seepage meters were 0.7–1 m below the water surface. A 3 m long tube separated each seepage meter from the collection bag to avoid footsteps near the measurement of the affection to vertical hydraulic conductivity (Rosenberry et al., 2010).

Each bag was half-filled with tap water prior to the installation and a valve remained it closed during removal and while unattached. The weight variation was measured at the same 6 sites once per month, recording gains or losses as a function of the predominant relationships between the surface and groundwater. In each field campaign, measurements were repeated at approximately the same time of the day. In this work, the flow was considered positive or negative from the point of view of the lagoons. Positive if there was water inflow from the aquifer to the lagoons and negative if there was water outflow from the lagoons to the aquifer.

Water sampling for hydrochemical analysis: Water samples were collected at 5 points (in surface and groundwater inlets and outlets and in lagoons AW and TW), and in situ measurements of physicochemical water parameters (electrical conductivity, EC, temperature, T, pH, Eh, O_2) were performed. Chemical analysis of major and some minor components was performed at the Centre of Hydrogeology of the University of Málaga using a Compact IC Pro 881 ion chromatograph and a Shimadzu TOC-VCSN + TNM– 1 carbon analyzer.

Seawaves height information: The hourly data of sea-waves height were obtained from State Harbours (Spanish Ministry of Development) from the SIMAR point close to the study area. The data was obtained from a high-resolution numerical modelling which integrates the basic transport equation: WAN wave generation model (The WADMI Group, 1988).

2.3. Evaporation Calculation

Penman equation (Equation (1)) (Penman, 1956), which estimates evaporation from free water surfaces by combining the energy balance with the mass transfer method, has been applied to accurately estimate evaporation from shallow wetlands (McMahon et al., 2013):

$$E_P = \frac{\Delta}{\Delta+\gamma} \frac{R_{nw}}{\lambda} + \frac{\gamma}{\Delta+\gamma} E_a \tag{1}$$

Where E_P is the daily evaporation, Δ is the slope of the daily mean saturated vapour pressure, R_{nw} is the daily net radiation on the evaporation surface, γ is the psychrometric constant, λ is the latent heat of vaporisation, and E_a is the correction factor of wind action. The parameters were calculated using the climatic variables collected from the weather station. Both evaporation and precipitation were applied to the extension of the wetlands, but also to the flood meadows. The main channel feeds them in the north and collects water in the south; Therefore, gains by precipitation and losses by evaporation over the flood meadows must be considered in the calculation of the water balance.

2.4. Water Balance of the Lagoons

The water balance of the lagoons was calculated from January 2019 to May 2019, considering the principle of mass conservation:

$$Q_{in} + P + GWF_{in} - (Q_{out} + E_P + GWF_{out}) = \Delta S \tag{2}$$

where Q_{in} and Q_{out} are the surface water inflow and outflow to the lagoon complex, P is precipitation, E_P is evaporation, ΔS is the variation in water storage in the lagoons, and GWF_{in} and GWF_{out} are groundwater flow into and out of the lagoons, respectively. ΔS is positive when water storage increases in the lagoons and negative when water is lost. Given that:

$$GWF = GWF_{in} - GWF_{out} \qquad (3)$$

where GWF is the net exchange flow between the lagoons and the aquifer. GWF is positive when most groundwater flow was produced from the aquifer to the lagoons ($GWF_{in} > GWF_{out}$) and negative when most groundwater flow was produced from the lagoons to the aquifer ($GWF_{out} > GWF_{in}$). Substitution into (2) results in the following equation:

$$Q_{in} + P - Q_{out} - E_P - \Delta S = -GWF \qquad (4)$$

All variables of the equation were measured, except for GWF, which is commonly estimated indirectly or by residual approximation (Scanlon et al., 2002). In this study, the soil water storage variation was disregarded due to the permanent state of high moisture.

2.5. Groundwater Contour Maps

Groundwater level elevation data were used to draw detailed groundwater contour maps by natural neighbour interpolation (ArcGIS 10.1). The maps were compared with specific measurements taken in the lagoons and with the estimated water balances as an additional tool to verify the results.

3. Results

3.1. Water Balance of the Lagoons

The water balance from January to May 2019 was calculated using average daily data (Figure 2.3). Surface water flow records (Figure 2.3 A,B) showed differences in discharge between inlet and outlet stations. SW inflow (Q_{in}) ranged from 0 to 50 L/s in short periods of time, and these variations were related to precipitation and to the irrigation management of the basin upstream of the reserve. SW outflow (Q_{out}) did not experience the recorded short-term variations in Q_{in}), and it ranged from 0 to 15 L/s. Only major and long-term increases in discharge were recorded, albeit less pronounced and with a few days lag because the wetlands temporarily retained surface water, which delayed the transfer of the water mass from the inlet to the outlet (Carleton, 2002). The calculated daily evaporation (E_P) (Figure 2.3 C) ranged from 0.8 to 6.7 mm, reaching its highest values in May and the lowest values in January, marking an increasing trend. Daily data on storage variation (ΔS) (Figure 2.3 D) were similar to those on Q_{in}. The increase in inflow triggered a rapid response of the water level height in the lagoons and an increase in the amount of storage water. The daily findings of net exchange flow between surface water and groundwater (GWF) are mostly positive (Figure 2.3 E); that is, the aquifer fed the lagoons. In turn, sporadic negative peaks that coincided with periods of precipitation and/or sudden increases of Q_{in} were recorded. These peaks were inverse to those of Q_{in} and ΔS. When there were precipitation and a great contribution of surface water, the

groundwater level was overcome by the limnimetric level and the net exchange flow was from the wetland to the aquifer.
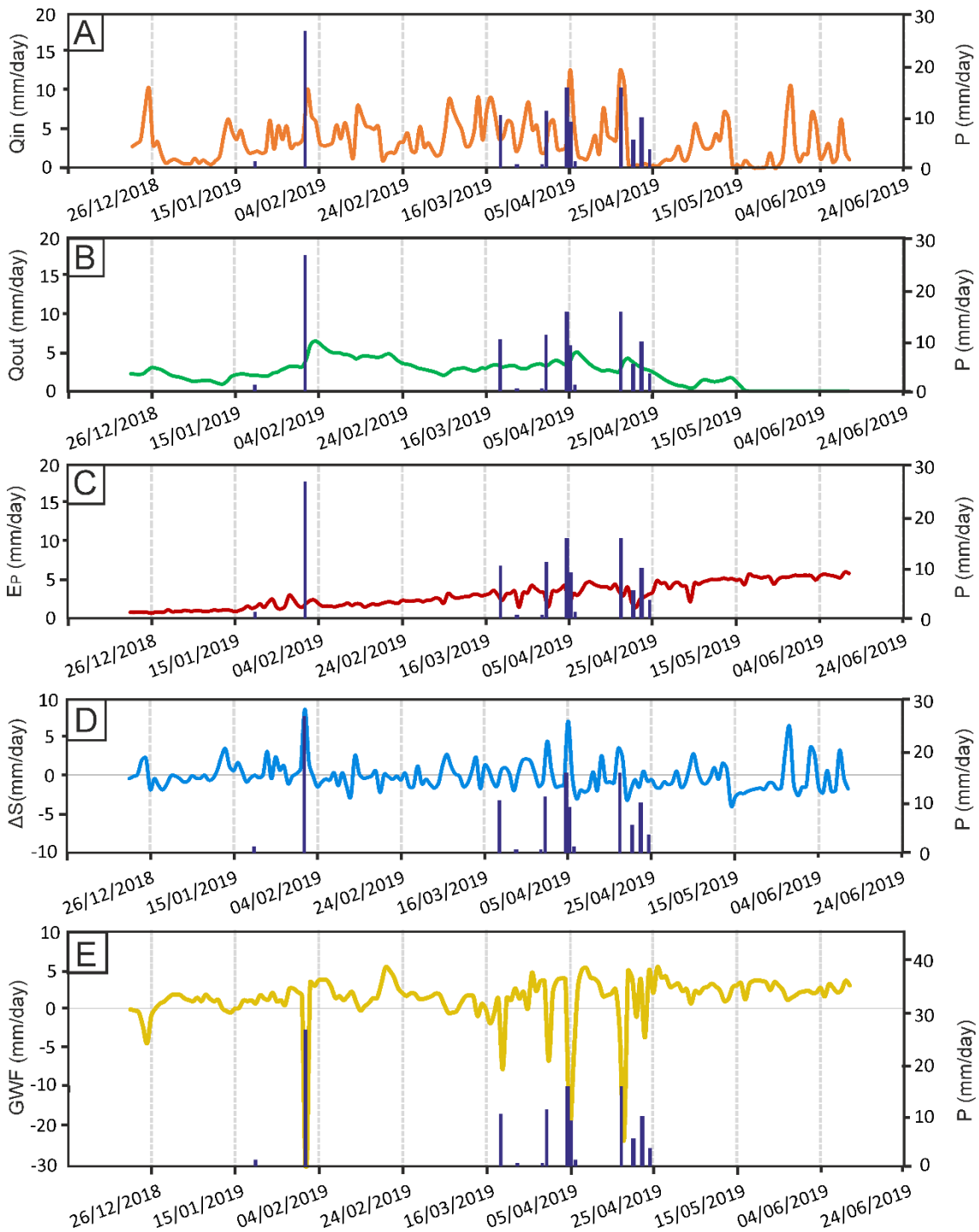

Figure 2.3.- Daily values (mm) of water balance components of the lagoon complex. (A) Inflow discharge and precipitation. (B) Outflow discharge and precipitation. (C) Evaporation and precipitation. (D) Variation of the four lagoons water storage and precipitation. (E) Net exchange flow between lagoons and aquifer, and precipitation.

The total monthly values of the variables of the water balance equation (Equation (4)) in the 5 study months show that Q_{in} was the main water inlet to the system (Table 2.2). P accounted for 9% of the total inflow during the 5 months. April was the rainiest month, and P reached 57% of the total inflow. Except in March, the total monthly values of GWF were always positive because GWF_{in} exceeded GWF_{out} most days of the month. This results from the fact that GWF was only negative for short periods of time and it did not modify the sign of the monthly value of GWF. In March, the combined value of Q_{in} and P increased, and GWF was negative. Q_{out} was the main outlet of the system until May, when flow ceased. E_P, however, progressively increased to become the main outlet of the system (83%). ΔS was highly variable, with positive and negative oscillations throughout the study period.

Date (month-year)	Q_{in} (mm)	P (mm)	Q_{out} (mm)	E_P (mm)	ΔS (mm)	GWF (mm)
Jan-19	142	1	109	46	19	30
Feb-19	207	26	222	57	-4	47
Mar-19	262	21	162	93	9	-19
Apr-19	164	57	165	112	-32	25
May-19	132	0	31	156	-40	13

Table 2.2.- Total monthly values (mm) of inflow and outflow discharge (Q_{in} and Q_{out}) precipitation (P), evaporation (E_P), storage variation (ΔS) and exchange flow between surface and groundwater (GWF).

Errors in measuring and estimating hydrologic components were analyzed in the estimation of water balance because the results could vary widely (Winter, 1981). The mean absolute errors calculated were: 41 mm for Q_{in}, 0.2 mm for P, 10 mm for Q_{out}, 13 mm for E_P and 2 mm for ΔS. The water balances calculated with extreme errors (minimum inputs and maximum outputs or maximum inputs and minimum outputs) differed from the results of the Table 2.2 and the range in the water-balance uncertainty is shown in the Table 2.3.

	Component					
	Q_{in}	P	Q_{out}	E_P	ΔS	GWF
Mean absolute percent error	24	8	12	17	6	154

Table 2.3.- Total mean absolute error of each hydrologic component (%).

3.2. Characterization of the Lagoon Functioning

3.2.1. Lagoon Levels

The records of limnimetric levels (Figure 2.4) showed that the absolute levels of the lagoons were not equal, decreasing from north to south. The lagoon with the highest level was AW, followed by TW and TAW, with LW having the lowest level. LW and TAW

had very gentle curves, excluding the sporadic peaks of LW (see the explanation of Figure 2.5). The AW level was more varied, with sporadic peaks identified in Q_{in} records. TW showed an intermediate behavior between AW and TAW-LW.
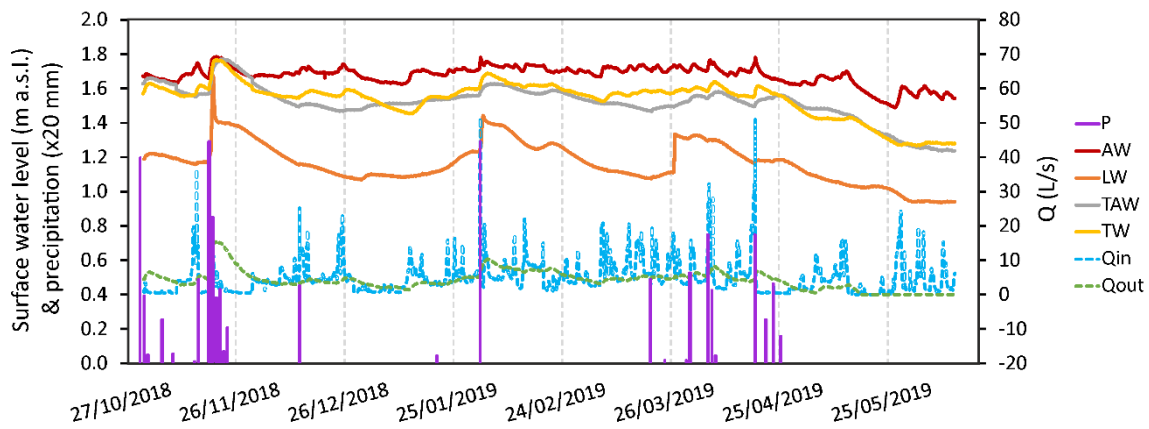

Figure 2.4.- Hourly data of water level height (meters above sea level (m.a.s.l.)) of each lagoon, inflow and outflow discharge (Q_{in} and Q_{out} in L/s) and precipitation (P in mm/d).
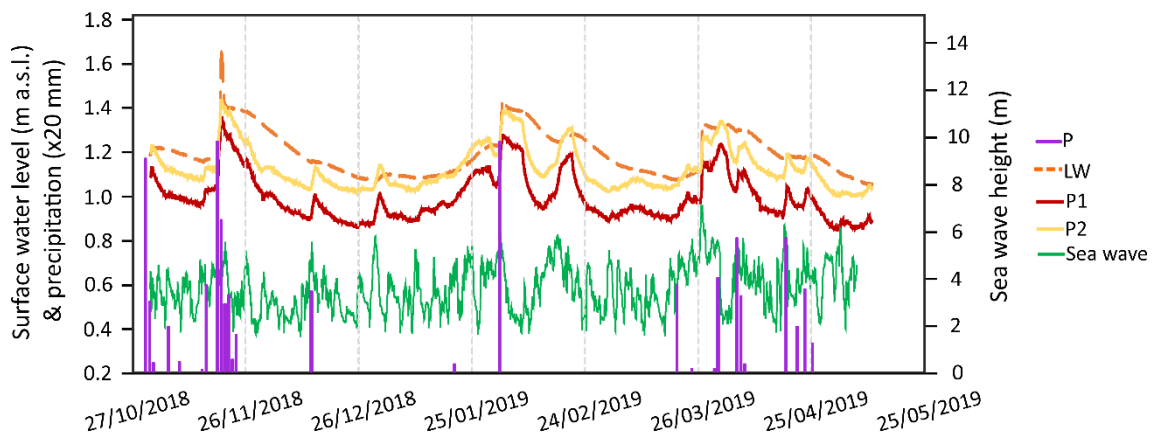

Figure 2.5.- Hourly data of water level height in the LW lagoon and in wells P1 and P2 (meters above sea level (m a.s.l), wave height (m) and precipitation (mm/d).

Lagoon levels increased with the Q_{in}, but the reaction rate was not the same in all lagoons. The AW level instantaneously increased on the same day when inflow peaks. TW reacted more slowly, and its level peaks approximately two days later than AW. Finally, the LW and TAW levels showed no response to the increase in Q_{in} most times, and when it did, it took more days to react than the other lagoons.

However, three instantaneous and sudden jumps in the water level were recorded in the LW lagoon (the lagoon located closest to the coastal edge), which were not recorded in the other lagoons. In addition, these jumps were even more clearly identified in wells P1 and P2 (Figure 2.5). Field observations showed increases in water levels on days when flooding occurred in the coastal strip. Coastal floods are usually related to precipitation and/or wind and wave storms (Nicholls et al., 1999; Ferrarin et al., 2015; Karim and Mimura, 2008). Comparisons between limnimetric records in LW and water table records in P1 and P2, as well as precipitation and wave records in the sector (Figure 2.5), show

that these sudden increases in the lagoon LW were clearly related to episodes of strong waves that cause floods near the coast and a local sea-level rise that was also transmitted to the water table, as recorded by wells located closer to the sea. Peaks 1 and 2 also coincided with intense rainfall; however, no precipitation was recorded in peak 3; therefore, the lagoon water level rise resulted exclusively from wave action. This action must have occurred locally because it was not recorded in other lagoons or wells.

3.2.2. Groundwater Levels

The water table elevation recorded in the wells (Figure 2.6) decreased from north to south, similarly to the limnimetric levels (Figure 2.4). In general, surface and groundwater levels varied similarly throughout the study period. They showed a constant trend until early May 2019, when they clearly began to decline.
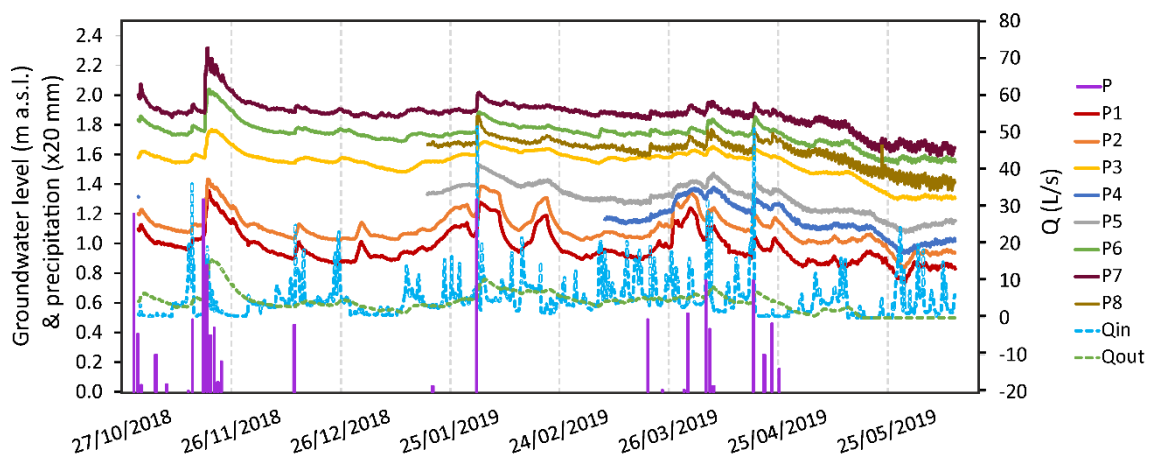

Figure 2.6.- Hourly data of groundwater level height (m. a. s. l.), inflow discharge (Q_{in} in L/s) and precipitation (P in mm/d).

Normally, short-term abrupt increases were preceded by an increase in Q_{in}, which in turn depended on P and irrigation return flows. The response in the groundwater level was faster in northern wells than in southern wells. The groundwater level responded a few hours slower than the AW water level, albeit from 1 to 4 days faster than the other lagoons.

The groundwater contour map shows the flow when both surface and groundwater levels were high (November 2018) and low (May 2019) (Figure 2.7). The general flow patterns were similar in both cases. According to the maps, the lagoons were connected to the aquifer, despite spatial variations in the interaction between the two bodies of water. Discharge to the lakes occurred in the northern boundary of the lagoons and recharge to the aquifer in the southern boundary; therefore, they are flow-through lagoons. The differences between high and low water levels resulted from variations in the hydraulic gradient because the gradient was higher in November than in May.

3.2.3. Direct Measurements of Exchange Flow

The 6 seepage meters installed in the LCS wetland showed differences in *GWF* depending on their positioning (Figure 2.7). The AWS1 and TAWS1 seepage meters highlighted that the aquifer fed the lagoons in the northern section of the lagoons.

Conversely, the AWS2, TWS and LWS seepage meters indicated negative flow; that is, recharge from the lagoons to the aquifer occurred in the southern section of the lagoons. In addition, temporal variations were observed, as shown in TAWS2, which measured a positive flow in November 2018 (inflow to the lakes) and a negative flow in May 2019 (outflow from the lakes). Therefore, the field data supported the groundwater contour maps and the groundwater flow patterns of the isopotential maps.
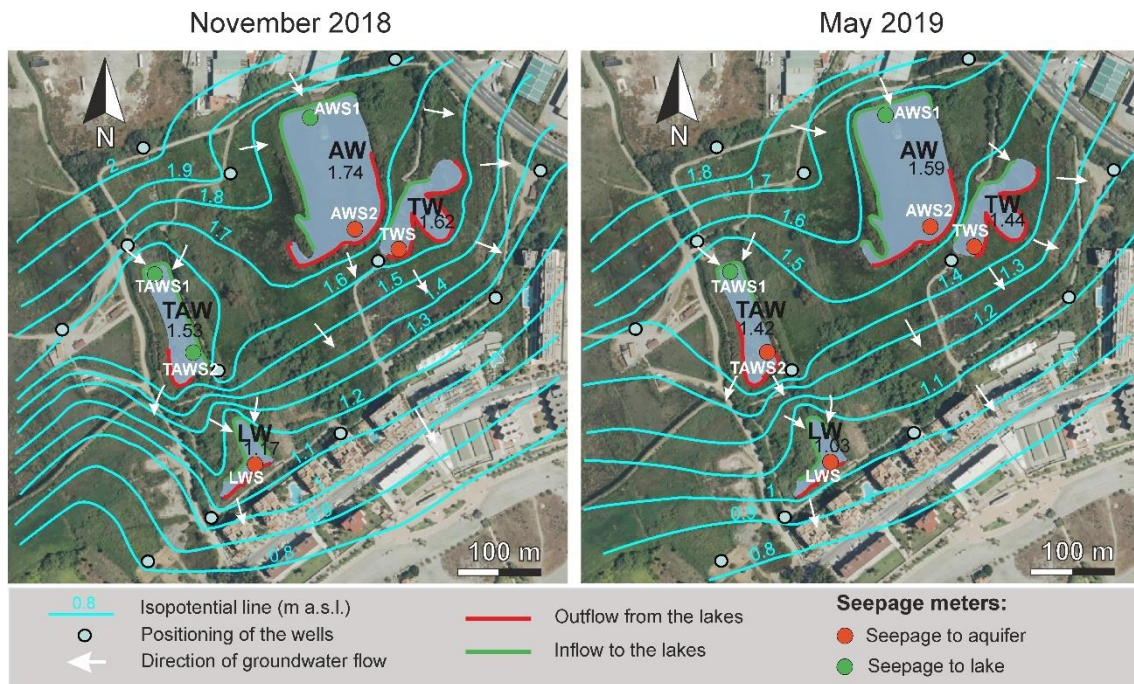

Figure 2.7.- Groundwater contour maps, location of the seepage meters and type of exchange flow between the aquifer and the lagoons in (A) November 2018 and (B) May 2019.

3.3. Hydrochemistry

The concentration of elements in water samples was similar in all sampling points (Figure 2.8), which indicated a close correlation between surface and groundwater throughout the aquifer. The salinity of lagoon AW was similar to that of surface water inlets (SW Inlet) and outlets (SW outlet), which confirms the fast connection between surface water and said lagoon that had already been revealed by the water level and Q_{in} measurements. Groundwater (GW) had a lower concentration of elements than the other sampling points. Last, the TAW lagoon was the sampling point with the highest salinity. This may seem contradictory since their feeding depended exclusively on groundwater; therefore, they should have had more similar concentration values. The higher concentration of the lagoons fed by the aquifer may be due to the fact that they underwent less water renewal (longer residence time) and that evaporation produced an enrichment in salts in those lagoons (e.g., Skrzypek et al., 2013). These variations in water composition indicated that in detail, there were notable differences in hydrological functioning between the different lagoons of the study area.
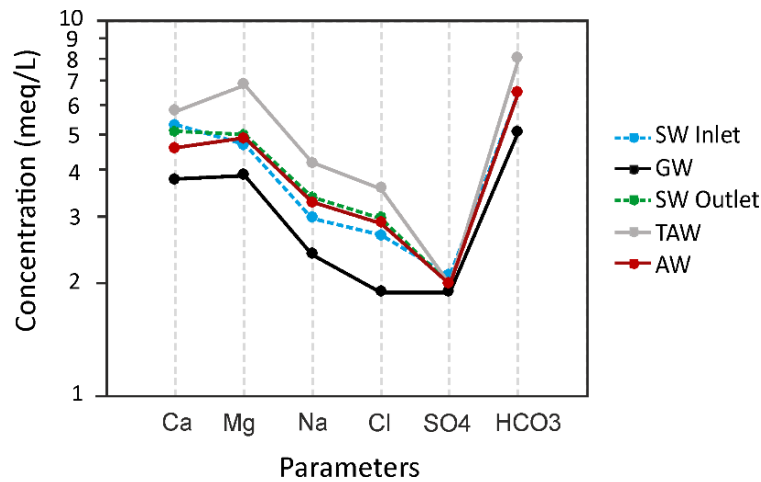
Figure 2.8.- Schöeller diagram representing the concentrations of elements in the surface water inlet (SW Inlet), groundwater (GW), surface water outlet (SW Outlet) and TAW and AW lagoons. Water-samples collected on 14 February 2019.

4. Discussion

The water balance of the wetland shows that surface water flow was the main inlet to the system, accounting for 82% of the total feeding of the lagoons during the five-month study period. Net groundwater exchange was calculated in every study month and accounted for 9% of the inlet to the lagoons. Precipitation accounted for 9% of the total inlet, although no precipitation occurred in some months. Evaporation and surface water outflow were the outlets of the system with similar total percentages of 60% and 40% respectively. Significant changes in the values of water balance components occurred in March that was especially wet during 2019. The main inlet to the system was Q_{in} which increased up to 93%, and GWF became an outlet of the system (19%). Therefore, it could be deduced that recharge to the aquifer dominated in the especially wet months when surface-water levels were high, as it has been shown in other wetlands (Michot et al., 2011; Sulula et al., 2001). The results of the water balance are based on the mean values of each balance component. The analysis of the errors indicates a high degree of uncertainty under the most extreme consideration of error. Despite this, the best-estimated balance is near to the mean.

This water balance is only considering 5 months so it might not be totally representative of a full hydrological year. However, during the period studied, wet and dry short periods have been identified and the quantitative and qualitative differences between both indicate the need for longer-term studies in these areas due to the high climatic seasonality. This region is characterized by periods of several years with alternation of climatic conditions, for example droughts can be extended for several years while wet periods can exceed or be shorter than a hydrological year. This has been shown by calculating Standardized Precipitation Indexes (SPI) (Duque et al., 2009) or by the analysis of water table elevations trends (Duque et al., 2009) that usually do not return to the starting level after a hydrological year. Considering this, the time period presented here was sufficient to cover dry and wet short periods and represented a starting point for understanding seasonality over LCS. Longer-term studies are required to evaluate the

effect of droughts and longer wet periods and to compare water budgets in LCS for different hydrological years.

Although flow patterns with vertical upward components have been studied in other parts of the Motril-Salobreña aquifer (Duque et al., 2010; Calvache et al., 2016), but in this study we did not identify these patterns. The explanation could be due to the shallow depth of the wells and the lagoons and therefore, the regional discharge of the aquifer to the coast did not impact the water level measurements neither the groundwater-surface water interactions. The low-permeability sediments deposited on the lagoon-aquifer interface could have greatly influenced seepage rates (Rosenberry et al., 2010), as well as the presence of organic sediments observed in other locations (Kidmose et al., 2015; Duque et al., 2018). These could be the causes of the low percentage of the net groundwater exchange obtained in the water balance. The measurements of groundwater level and limnimetric levels (Figures 2.4 and 2.6) reveal that the four lagoons were connected to the Motril-Salobreña aquifer, although they depended on groundwater differently. The LW, TAW and TW lagoons responded more strongly to changes in groundwater levels; therefore, it can be argued that their feeding mainly depended on groundwater. Lagoon AW, located in a more northern position and closer to the surface water inlet channel, must have had a considerable surface water feeding because variations in limnimetric levels were correlated with the inlet channel and with precipitation. Water from the channel flowed along the flood meadow as surface runoff and reaches AW. The small differences in the hydrochemical characteristics between TW lagoon and SW inlet also supported the existence of a fast connection between the AW lagoon and the surface water. However, the lagoons exclusively fed by groundwater, like TAW, were characterized by higher salinities, even higher than groundwater, showing the slow water renewal.

Daily data on water balance components of the lagoons (Figure 2.3) highlight that net groundwater flow to the wetland reacted inversely to SW inflow, precipitation and water storage. Precipitation and the surface discharge peaks produced limnimetric level increases in the AW lagoon. The net groundwater flow value calculated for the entire reserve, which was usually positive and low values (0–7 mm/d), decreased. Because AW is the largest lagoon in the reserve, in those cases when the water level at AW increased largely and the hydraulic gradient inverted sharply, the net groundwater flow drastically decreased and became negative (with values up to −20 mm/d). Discharge of great magnitude occurred from the lagoons complex to the aquifer for a few days. Inversions ended when the infiltration to the aquifer stabilized the groundwater and limnimetric levels at the same height. This was the reason why there was a sequence of rises in the limnimetric levels of the wetlands: the water level increased instantaneously in AW when the SW inflow increased, followed by the increased in the groundwater level due to the flow from AW to the aquifer and, ultimately, to the lagoons that depended on groundwater feeding (Figures 2.4 and 2.6). The water level at TW increased faster than those at LW and TAW due to the proximity of TW to AW.

An anomalous phenomenon occurred on the coast and altered the hydrodynamic of the lagoon complex. The functioning of LW changed when there were flooding episodes in the coastal strip, caused by precipitation and/or sea wave storms. Sea level rises produced jumps in the water level that was also transmitted to the limnimetric level of the LW

lagoon (Figure 2.5). However, this signal was barely recorded in the limnimetric level data of the remaining lagoons, probably because they are few more meters inland from the coast. On the other hand, all the lagoons may be affected in the near future according to the sea level rise forecasts due to climate change (IPCC, 2014).

The groundwater contour maps and the seepage measurements (Figure 2.7) indicate that the lagoons received groundwater in the northern section of their basins and lost surface water to the aquifer in the southern section. Therefore, they were flow-through lagoons under normal conditions (Figure 2.9).
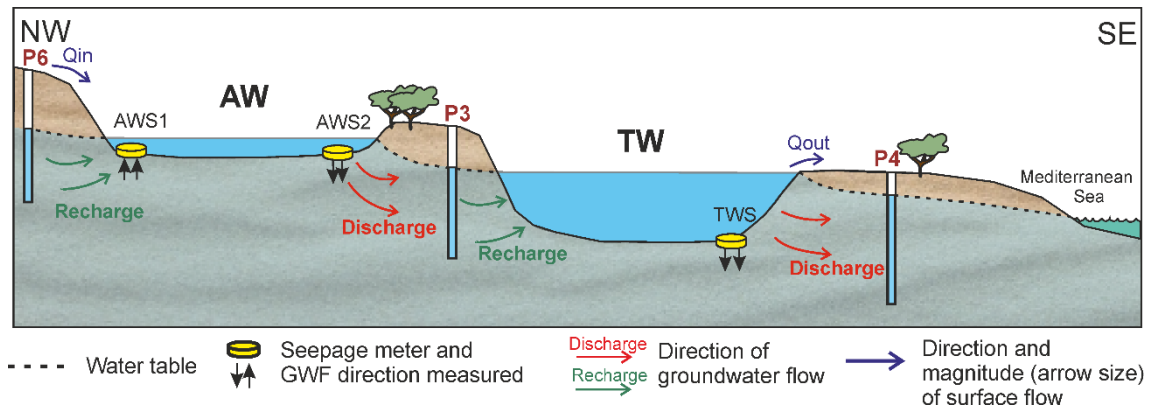

Figure 2.9.- Hydrodynamic functioning of lagoons Aneas (AW) and Trébol (TW): flow-through lagoons under normal conditions.

Starting at the end of April, the groundwater and limnimetric levels decreased continuously, reaching their minima since the beginning of the study period (Figures 2.4 and 2.6). Under these conditions of very low water levels, the flow pattern in the AW lagoon changed from flow-through lagoon to influent lagoon. Similar changes in the interactions between wetlands and groundwater have been observed in other studies (Sacks et al., 1992; Winter, 1999). When Q_{in} increased, surface water feeding of the AW lagoon increased, reflected in a sudden rise in water level, even exceeding the groundwater level in all sectors of the lagoon. The main channel behaved like an influent stream and produced a local high water table in the western sector of AW (Figure 2.10). Thereby inverting the hydraulic gradient in the northern sector of the lagoon, which became an aquifer feeding point. Drastic changes of groundwater flow direction were studied by other authors indicating temporal variations in the hydrodynamic functioning of lagoons (Hayashi et al., 1998).

Thus, the climate variability impacted on the interactions between GW-SW directly, mostly through changes in precipitation and evaporation. Indirectly, through changes in the inlets surface water. The SW availability was also strongly linked with the management of the basin water resources. Human activity controls the Guadalfeo river flow and the crop water, on which the two main recharge sources of the aquifer depends (infiltration from the river and the irrigation return flow). Successively, GW was an important inlet to the wetland, along with the surplus irrigation water. Then, LCS-Motril-Salobreña aquifer system is very sensitive to temporal variation caused by climate conditions and anthropic influence.
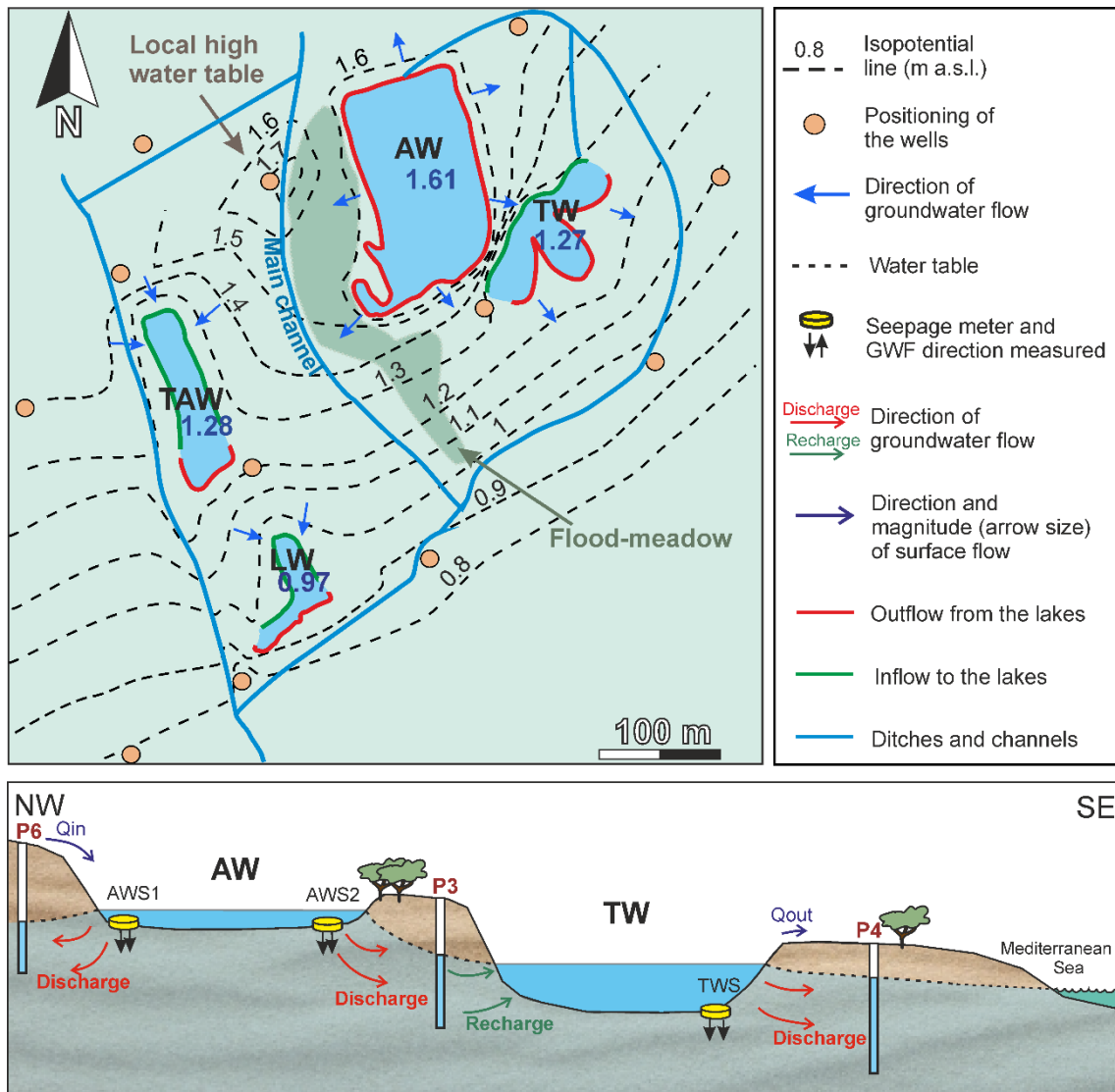
Figure 2.10.- Groundwater contour map of the LCS lagoon complex and hydrodynamic functioning of lagoons AW and TW at inversion, 29 May 2019.

5. Conclusions

The groundwater-surface water interaction in LCS wetlands presented a variety in the distribution of both spatially and temporally. The LW, TAW and TW lagoons (groundwater-fed only) always showed a flow-through functioning with groundwater inflows in the northern section and the aquifer recharged in the southern section. The AW lagoon (mixed water inlets) showed different flow patterns depending on the hydrological conditions. Under normal conditions, it behaved as a flow-through lagoon; however, during wet periods, the rise in the limnimetric level changed AW to an influent lagoon.

During the study period, the net exchange flow, which is the total water that remains in the system, indicated that surface water was the predominant inlet to the system (82%) compared with the groundwater (9%). This proportion remained even during the driest periods. Nevertheless, the seepage meters and the hydrochemical analysis suggested that groundwater was dominant for most of the lagoons (LW, TAW and TW) while only AW lagoon had a mixed input of groundwater and surface water. This means that surface water

inflow in AW lagoon played a highly relevant role in the water budget of the system. AW lagoon recharged the aquifer and might have even been partially the origin of the groundwater that later would recharge the other lagoons.

The anthropic water supply conducted through the main channel produced changes in the flow pattern of AW lagoon, which would have been flow-through type under natural conditions. The extra supply of water associated with human activity increased the water storage of the wetland, recharged the subjacent aquifer and prevented saltwater intrusion due to the proximity to the coastline.

LCS is an example of how the anthropic influence may affect a wetland in different manners. While human actions were responsible for almost the disappearance of the wetland by draining it and changing the land uses reducing its extension, the current management is maintaining the required hydrological conditions for sustaining the ecological equilibrium and also protects Motril-Salobreña aquifer from saltwater intrusion.

REFERENCES

Aldaya, F., 1981. Mapa Geológico Y Memoria Explicative De La Hoja 1056 (Albuñol) Del Mapa Geológico De España Escala 1:50000; IGME: Madrid, Spain.

Amoros, C., Bornette, G., 2002. Connectivity and bioicomplexity in waterbodies of riverine floodplains. Freshw. Biol. 47, 761–776. https://doi.org/10.1046/j.1365-2427.2002.00905.x

Calvache, M.L., Ibáñez, S., Duque, C., Martín-Rosales, W., López-Chicano, M., Rubio, J., Gónzález, A., Viseras, C., 2009. Numerical modelling of the potential effects of a dam on a coastal aquifer in s. Spain. Hydrol. Proc. 23, 1268–1281 https://doi.org/10.1002/hyp.7234

Calvache, M.L., Sánchez-Úbeda, J.P., Duque, C., López-Chicano, M., De la Torre, B., 2016. Evaluation of analytical methods to study aquifer properties with pumping test in coastal aquifers with numerical modelling (Motril-Salobreña aquifer). Water Resor. Manag. 30, 559–575. https://doi.org/10.1007/s11269-015-1177-6

Carleton, J.N., 2002. Damköler number distributions and constituent removal in treatment wetlands. Ecol. Eng. 19, 233–248. https://doi.org/10.1016/S0925-8574(02)00094-0

Consejería de Medio Ambiente, 2004. Inventario de Humedales de Andalucía Charca de Suárez.

del Hoyo, J., Collar, N.J., Christie, D.A., Elliott, A., Fishpool, L.D.C., 2014. HBW and BirdLife International Illustrated Checklist of the Birds of the World; Lynx Editions BirdLife International: Barcelona, Spain; Cambridge, UK.

Doss, P.K., 1993. The nature of a dynamic water table in a system of non-tidal, freshwater coastal wetlands. J. Hydrol. 141, 107–126. https://doi.org/10.1016/0022-1694(93)90046-C

Duque, C., 2009. Influencia Antrópica Sobre La Hidrogeología Del Acuífero Motril-Salobreña. Ph.D. Thesis, University of Granada, Granada, Spain.

Duque, C., Calvache, M.L., Engesgaard, P., 2010. Investigating river-aquifer relations using water temperature in an anthropized environment (Motril-Salobreña aquifer. J. Hydrol. 381, 121–133. https://doi.org/10.1016/j.jhydrol.2009.11.032

Duque, C., Calvache, M.L., Pedrera, A., Martín-Rosales, W., López-Chicano, M., 2008. Combined time domain electromagnetic soundings and gravimetry to determine marine intrusion in a detrital coastal aquifer (Southern Spain). J. Hydrol. 349, 536–547. https://doi.org/10.1016/j.jhydrol.2007.11.031

Duque, C., Calvache, M.L., Rubio, J.C., López-Chicano, M., González-Ramón, A., Martín-Rosales, W., Cerón, J.C., 2005. Influencia de las litologías en los procesos de recarga del río Guadalfeo al acuífero de Motril-Salobreña. In Proceedings of the VI SIAGA, Sevilla, Spain. 343–547.

Duque, C., López-Chicano, M., Calvache, M.L., Martín-Rosales, W., Gómez-Fontalva, J., Crespo, F., 2011. Recharge sources and hydrogeological effects of irrigation and an influent river identified by stable isotopes in the Motril-Salobreña aquifer (southern Spain). Hydrol. Proc. 25, 2261–2274. https://doi.org/10.1002/hyp.7990

Duque, C., Haider, K., Sebok, E., Sonnenborg, T.O., Engesgaard, P., 2018. A conceptual model for groundwater discharge to a coastal brackish lagoon based on seepage measurements (Ringkøbing Fjord, Denmark). Hydrol. Process. 32, 3352–3364. https://doi.org/10.1002/hyp.13264

European Community., 2007. LIFE and Europe's Wetlands. Publiic Office European Union, Luxembourg.

Ferrarin, C., Tomain, A., Bajo, M., Petrizzo, A., 2015. Tidal changes in a heavily modified coastal wetland. Cont. Shelf Res. 101, 22–33. https://doi.org/10.1016/j.csr.2015.04.002

Freeze, R.A.; Witherspoon, P.A., 1967. Theoretical analysis of regional groundwater flow 3: Quantitative interpretations. Water Resour. Res. 4, 581–590. https://doi.org/10.1029/WR004i003p00581

Hayashi, M., Van der Kamp, G., Rudolph, D.L., 1998. Water and solute transfer between a praire wetland and adjacent upland, 1. Water balance. J. Hydrol. 207, 42–55. https://doi.org/10.1016/S0022-1694(98)00098-5

Heredia, J., Murillo, J., García-Aróstegui, J., Rubio, J., López-Geta, J., 2002. Construcción de presas e impacto sobre el régimen hidrológico de los acuíferos situados aguas abajo. In Presa De Rules Y Acuífero Costero De Motril-Salobreña Granada, Sur De España. Boletín Geológico y Minero. 113, 165–184.

Ibañez, S., 2005. Comparación De La Aplicación De Distintos Modelos Matemáticos Sobre Acuíferos Costeros Detríticos. Ph.D. Thesis, University of Granada, Granada, Spain.

IPCC, 2014. Climate Change 2014: The Scientific Basis; Cambridge University Press: Cambridge, UK.

Jolly, I.D., 1996. The effect of river management on the hydrology and hydroecology of arid and semi-arid floodplains. In Floodplain Processes; Anderson, M.G., Walling, D.E., Bates, P.D., Eds.; John Wiley and Sons: New York, NY, USA, 577–609.

Jones, T.A., Hughes, J.M.R. 1993. Wetland inventories and wetland loss studies: A European perspective. In Waterfowl and Wetland Conservation in the 1990s. Moser, M., Prentice, R.C., van Vessem, J., Eds. IWRB Special Publication No. 26. IWRB: Slimbridge, UK. 164–170.

Junta de Andalucía, 2017. Memoria De Actuaciones En Materia De Humedales.

Karim, F., Mimura, N., 2008. Impacts of climate change and sea-level rise on cyclonic storm surge floods in Bangladesh. Glob. Environ. Change. 18, 490–500. https://doi.org/10.1016/j.gloenvcha.2008.05.002

Kidmose, J., Engesgaard, P., Ommen, D.A.O., Nilsson, B., Flindt, M.R., Andersen, F.Ø., 2015. The Role of Groundwater for Lake-Water Quality and Quantification of N Seepage. Groundwater. 53, 709–721. https://doi.org/10.1111/gwat.12281

Krabbenhoft, D.P., Anderson, M.P., 1986. Use of a numerical ground-water flow model for hypothesis testing. Groundwater. 24, 49–55. https://doi.org/10.1111/j.1745-6584.1986.tb01458.x

Lee, D.R., 1977. A device for measuring seepage flux in lakes and estuaries. Limnol. Oceanogr. 22, 140–147. https://doi.org/10.4319/lo.1977.22.1.0140

Lewandowski, J., Meinikmann, K., Nützmann, G., Rosenberry, D., 2015. Groundwater-the disregarded component in lake water and nutrient budgets. Part 2: Effects of groundwater on nutrients. Hydrol. Proc. 29, 2922–2955. https://doi.org/10.1002/hyp.10384

McCovie, M.R.; Christopher, L.L., 1993. Drainage District Formation and the Loss of Midwestern Wetlands, 1850–1930. Agric. Hist. 67, 13–39.

McMahon, T.A., Peel, M.C., Lowe, L., Srikanthan, R., McVicar, T.R., 2013. Estimating actual, potential, reference crop and pan evaporation using standard meteorological data: A pragmatic synthesis. Hydrol. Earth Syst. Sci. 17, 1331–1363. https://doi.org/10.5194/hess-17-1331-2013

Mendoza-Sanchez, I., Phanikumar, M.S., Niu, J., Masoner, J.R., Cozzarelli, I.M., McGuire, J.T., 2013. Quantifying wetland-aquifer interactions in a humid subtropical climate region: An integrated approach. J. Hydrol. 498, 237–253. https://doi.org/10.1016/j.jhydrol.2013.06.022

Menotti, F., O'Sullivan, A., 2013. The Oxford Handbook of Wetland Archaeology; Oxford University Press: Oxford, UK. https://doi.org/10.1093/oxfordhb/9780199573493.001.0001

Michot, B., Meselhe, E.A., Rivera-Monroy, V.H., Coronado-Molina, C., Twilley, R.R., 2011. A tidal creek water Budget: Estimation of groundwater discharge and overland flow using hydrologic modeling in the southern Everglades. Estuar. Coast. Shelf Sci. 93, 438–448. https://doi.org/10.1016/j.ecss.2011.05.018

Mills, J.G., Zwarich, M.A., 1986. Transient groundwater flow surrounding a recharge slough in a till plain. Can. J. Soil Sci. 66, 121–134. https://doi.org/10.4141/cjss86-012

Misch, W.J., Gosselink, J.G., 1993. Wetlands, 2nd ed. Van Nostrand Reinhold: New York, NY, USA. https://doi.org/10.1002/ldr.3400050107

Misch, W.J., Gosselink, J.G., 2000. Wetlands, 3rd ed.; John Wiley & Sons: Hoboken, NJ, USA. https://doi.org/10.1002/rrr.637

Nicholls, R.J., Hoozemans, F.M.J., 1999. Marchand, M. Increasing flood risk and wetland losses due to global sea-level rise: Regional and global analyses. Glob. Environ. Chang. 9, S69–S87. https://doi.org/10.1016/S0959-3780(99)00019-9

Penman, H.L., 1956. Evaporation: An introductory survey. Neth. J. Agric. Sci. 4, 9–29.

Ramberg, L., Wolski, P., Krah, M., 2006. Water balance and infiltration in seasonal floodplain in the Okavango delta, Bostwana. Wetlands. 26, 677–690.

Reolid, J., López-Chicano, M., Calvache, M.L., Duque, C., Sánchez-Úbeda, J.P., 2012. Estimación de las aportaciones del aluvial del río Guadalfeo al acuífero Motril-Salobreña. Geogaceta. 52, 141–144.

Richardson, C.J.,1995. Wetlands ecology. In Encyclopedia of Environmental Biology; Nierenberg, W.A., Ed.; Academic Press: New York, NY, USA. 3, 535–550.

Richter, B.D., Baumgartner, J.V., Powell, J., Braun, D.P., 1996. A method for assessing hydrologic alteration within ecosystems. Conserv. Biol. 10, 1163–1174. https://doi.org/10.1046/j.1523-1739.1996.10041163.x

Rosenberry, D.O., Toran, L., Nyquist, J.E., 2010. Effect of surficial disturbance on exchange between groundwater and surface water in nearshore margins. Water Resour. Res. 46. https://doi.org/10.1029/2009WR008755

Rosenberry, D.O., Winter, T.C., 1997. Dynamics of water-table fluctuation in an upland between two praire potholes wetlands in North Dakota. J. Hydrol. 191, 266–289. https://doi.org/10.1016/S0022-1694(96)03050-8

Sacks, L.A., Herman, J.S., Konikow, L.F., Vela, A.L., 1992. Seasonal dynamics of groundwater-lake interactions at Doñana National Park, Spain. J. Hydrol. 136, 123–154. https://doi.org/10.1016/0022-1694(92)90008-J

Scanlon, B.R., Healy, R.W., Cook, P.G., 2002. Choosing appropriate techniques for quantifying groundwater recharge. Hydrogeol. J. 10, 18–39. https://doi.org/10.1007/s10040-001-0176-2

Shaffer, P.W., Kentula, M.E., Gwin, S.E., 1999. Characterization of wetland hydrology using hydrogeomorphic classification. Wetlands. 19, 490–504. https://doi.org/10.1007/BF03161688

Skrzypek, G., Dogramaci, S., Grierson, P.F., 2013. Geochemical and hydrological processes controlling groundwater salinity of a large inland wetland of northwest Australia. Chem. Geol. 357, 164–177. https://doi.org/10.1016/j.chemgeo.2013.08.035

Suso, J., Llamas, M.R., 1993. Influence of groundwater development on the Doñana National Park ecosystems. Hydrol. J. 141, 239–269. https://doi.org/10.1016/0022-1694(93)90052-B

Sutula, M., Day, J.W., Cable, J., Rudnick, D., 2001. Hydrological and nutrient budgets of freshwater and estuarine wetlands of Taylor Slough in southern Everglades, Florida (USA). Biogeochem. 56, 287–310. https://doi.org/10.1023/A:1013121111153

Syphard, A.D., Garcia, M.W., 2001. Human- and beaver- induced wetland changes in the Chickahominy River watershed from 1953 to 1993. Wetlands. 21, 342–353.

The WADMI Group., 1988. The WAM Model- A Third Generation Ocean Wave Prediction Model. J. Phys. Oceanogr. 18, 1775–1810. https://doi.org/10.1175/1520-0485(1988)018<1775:TWMTGO>2.0.CO;2

Walker, K.F., Thoms, M.C., Sheldon, F., 1992. Effects of weirs on the littoral environment of the River Murray, South Australia. In River Conservation and Management; Boon, P.J., Calow, P., Petts, G.E., Eds.; John Wiley and Sons: New York, NY, USA. 271–292

Winter, T.C., 1981. Uncertainties in estimating the water balance of lakes. J. Am. Water Resour. Assoc. 17, 82–115. https://doi.org/10.1111/j.1752-1688.1981.tb02593.x

Winter, T.C., 1999. Relation of streams, lakes, and wetlands to groundwater flow systems. J. Hydrol. 7, 28–45. https://doi.org/10.1007/s100400050178

Wurster, F.C., Cooper, D.J., Sanford, W.E., 2003. Stream/aquifer interactions at Great Sand Dunes National Monument, Colorado: Influences on interdunal wetland disappearance. J. Hydrol. 271, 77–100. https://doi.org/10.1016/S0022-1694(02)00317-7

Zedler, J.B., 2000. Progress in wetland restoration ecology. Trend Ecol. Evol. 15, 402–407. https://doi.org/10.1016/S0169-5347(00)01959-5
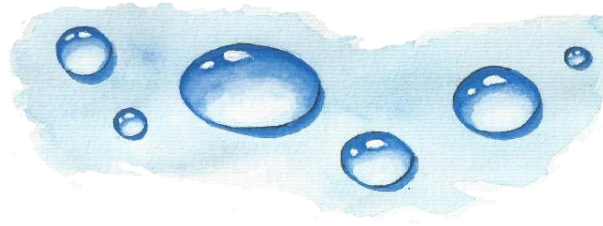
CHAPTER 3

Temperature Distribution in Coastal Aquifers: Insights from Groundwater Modeling and Field Data

Ángela M. Blanco-Coronas[1], Carlos Duque[2], María Luisa Calvache[1] and

Manuel López-Chicano[1]

[1] Departamento de Geodinámica, Universidad de Granada, Avenida Fuente Nueva s/n., 18071 Granada, Spain

[2] WATEC, Department of Geoscience, Aarhus University, Høegh-Guldbergs Gade 2, 8000 Aarhus C, Denmark

Abstract

The temperature distribution in coastal aquifers is determined by the effect of different heat sources: surface water recharge, sea infiltration, and geothermal heat. In previous studies, the signal generated in groundwater by each source was individually studied, and in the case of geothermal heat, it was often not considered. This research is the first in considering all possible sources of heat in a coastal aquifer simultaneously by using a combination of field data and numerical modeling to present a reference model based on the characteristics of a real aquifer. The position of the freshwater-saltwater interface (FSI) and its effect on temperature distribution have been modeled considering variable-density flow, coupled heat and solute transport. This study broadens the theoretical knowledge of temperature distribution in coastal aquifers based on a sensitivity analysis of hydraulic and thermic parameters. Furthermore, a case study (the Motril-Salobreña aquifer) was modeled with field data calibration to test the applicability to real aquifers. The new insights gained through this study provide integrated knowledge of the temperature distribution in coastal areas and establish the basis for future research using heat as a tracer in seaside aquifers.

Keywords

_____

1. Introduction

The use of heat as a groundwater tracer is growing in popularity and it has been extended in a wide range of hydrogeological studies (Anderson, 2005). Heat and solute transport have many similarities (deMarsily, 1986; Bear, 1972; Hopmans et al., 2002), which is the reason heat has been used as a tracer in groundwater systems. However, there are also differences in their behavior (Vandenbohede et al., 2009; Ma et al., 2012) due to the thermal exchange between water and aquifer solids, which depends on the heat properties of both (Bakker, 2015). This reflects a time delay of heat transport with respect to solute transport. For this reason, understanding the different aspects involved in both processes is important when including both solute transport and heat transport in the same model. Traditionally, the direct relationship of density and viscosity with temperature has been ignored in hydrogeological modeling because of its negligible effect over the results of variable density models; nevertheless, there is a broad area of research in groundwater systems where temperature is considered to play a significant role (e.g., sole-source aquifers and coastal aquifer/ocean interactions) (Thorne, 2006; Vandenbohede and Van Houtte, 2012; Befus et al., 2013; Debnath et al., 2015).

Studies about groundwater-surface water interaction have shown that thermal distribution in the aquifer can indicate the degree of connection with rivers that has seasonal and daily temperature fluctuations (Constantz, 1998; Duque et al., 2010; Keery et al., 2007; Lautz, 2012; McCallum et al., 2014; Sebok et al., 2015). Recharge processes can have an impact on temperature of the surficial zone of the aquifer to a maximum

depth of a few tens of meters as a consequence of atmospheric temperature (Pollack and Huang, 2000; Smerdon et al. 2003). Variations in environmental temperature produce groundwater temperature fluctuations due to the effect of cooling or heating of the surface water before infiltration (Pollack et al., 2005; Duque et al., 2010). The amplitude of fluctuations decreases with depth (Silliman and Booth, 1993; Kurylyk et al., 2013). As a result, the thermal signal has been used in analytical and numerical solutions to estimate groundwater recharge/discharge rates (Suzuki, 1960; Bredehoeft and Papadopulos, 1965; Stallman, 1965; Rushton, 2007; Duque et al., 2016). Taniguchi et al. (1999), Calvache et al. (2011), and Kurylyk et al. (2019) have described how the shape of temperature profiles is connected with discharge and recharge areas.

Apart from the surficial zone where temperature is affected by recharge and air temperature, aquifers can be affected by the geothermal gradient (Parsons, 1970). Temperature profiles within the geothermal zone are unaffected by seasonal variations and adopt a linear trend (Anderson, 2005). Domenico and Palciauskas (1973) indicated that the distribution of groundwater temperature can be disturbed by groundwater flow, and Stallman (1963) suggested that it depends directly on the velocity and direction of water flow. The geothermal gradient is greater in groundwater discharge areas than in recharge areas (Tóth, 1962; Domenico and Palciauskas, 1973; An et al., 2015), which results from the fact that a hot upwelling is forced by convection within the discharge zone (Szijártó et al., 2019). Hydraulic conductivity also plays an important role in the geothermal gradient, due to the high degree of convective heat transport with large hydraulic conductivity values (An et al., 2015). Other parameters such as anisotropy, heterogeneity, recharge rate, and the position of the water table have an important influence on the magnitude of the disturbance (Parsons, 1970; Smith and Chapman, 1983; Woodbury and Smith, 1988; Forster and Smith, 1989).

The groundwater flow pattern of coastal aquifers was initially studied in the 1950's and 1960's (Glover, 1959; Kohout, 1964). The intrusion of saline water into the deepest part of aquifers disturbs the freshwater flow due to the difference in density of the two fluids. Groundwater originated by recharge inland flows vertically upward resulting in fresh/terrestrial submarine groundwater discharge (SGD) across the seafloor, between land and sea. This process is intimately associated with the location of the freshwater-saltwater interface (FSI) and has been studied along many coasts of the world (Kinnear et al., 2013; Eissa et al., 2018; Duque et al., 2019; Zhang et al., 2020, Liu et al., 2021). Despite good knowledge about coastal areas, few studies have investigated heat distribution. A series of papers by the U.S. Geological Survey (USGS) in the 1960s hypothesized the existence of seawater circulation intensified by temperature-induced density gradients in a carbonate platform in southern of Florida (Kohout, 1965; Kohout, 1967; Henry and Kohout, 1972, Kohout et al. 1977). They hypothesized that infiltrated cold seawater could be heated by geothermal heat, driving to an open-cycle thermal convection in addition to variable-density effects. Subsequently, Henry and Hilleke (1972) tested Kohout's thermal convection with a laboratory experiment. Cold saltwater and warm freshwater were introduced in a glass tank with sand. For the first time, a laboratory experiment represented combined solute and heat transport and their effects on flow patterns were represented in porous media. The Henry and Hilleke problem was modeled with different numerical codes, such as SUTRA-MS (Hughes and Sanford, 2004), SEAWAT (Dausman et al., 2010), and HST3D (Thorne et al., 2006) showing very

similar results among them. The same benchmark problem was used to simulate this physical experiment with SEAWAT but also included variable-density groundwater flow (Langevin et al., 2010). Nevertheless, there are only a few studies that support their hypothesis with field measurements, such as Kim et al. (2008, 2009) who described the dynamics within the freshwater-saltwater interface in a volcanic island with a geothermal gradient. The vertical logs in boreholes situated close to the coastline in an aquifer in southeastern of Spain (Molina et al., 2002) did not show a normal increase in temperature with depth but revealed a sharp decrease in temperature at -160 m depth due to the entry of cooler seawater into the aquifer. Furthermore, time-series data of electrical conductivity and temperature at different depths showed variations due to two external influences: tidal fluctuation and recharge produced by rainfall. Beyond this, Vandenbohede and Lebbe (2011) observed yearly fluctuations in temperature in the surficial zone of a shallow detrital coastal aquifer and developed a density-dependent model to simulate how yearly temperature oscillations influence the distribution of groundwater temperature. They concluded that the thickness of the surficial zone and the amplitude of the temperature oscillations are dependent on the conduction/convection dominance on heat transport.

In most cases, research has focused on either surficial temperature processes (Vandenbohede and Lebbe, 2011; Befus et al., 2013; Debnath et al., 2015; Tirado-Conde et al., 2019) or geothermal effects (Taniguchi, 2000; Taniguchi et al., 1999), as the distance between these effects hinders the exchange between them. In coastal aquifers, the circulation patterns generated due to variable density of the fluid and the hydrodynamic dispersion can facilitate the interaction between shallow and deep groundwater but research has been limited thus far to a few theoretical (e.g. Thorne et al., 2006; Langevin et al., 2007, 2008, 2010) or field measurements in all the depth of shallow aquifers but without detection of geothermal gradient (e.g. Folch et al., 2020). The difficulties in obtaining temperature data in deep zones of coastal areas originate the scarcity of research focused on the geothermal effect.

This paper shows the temperature distribution in coastal aquifers, distinguishes the different thermal zones that can be found in coastal areas, and takes into consideration constant or variable temperature sources over. For this purpose and due to the scarcity of information in the scientific literature, a numerical model was developed to propose a generic synthetic theoretical model of temperature distribution in coastal aquifers. A detailed sensitivity analysis was applied to different parameters and properties for a range of realistic values in the study area. The results established the basis for the understanding of heat distribution for diverse types of coastal aquifers. Furthermore, the acquired knowledge was tested with field data obtained in the coastal aquifer of Motril-Salobreña, making it one of the few studies that combined heat modeling with temperature field data obtained near the discharge zone.

2. Research Area

2.1. Hydrogeological Setting

The Motril-Salobreña detrital aquifer is located on the southeastern coast of Spain in the province of Granada (Figure 3.1 A). It has an area of 42 km^2, and its thickness varies

from 30 to 50 m in the north to more than 250 m in the south (Duque et al., 2008). The aquifer is composed mostly of gravel, sand, silt, and clay of Quaternary age that overlay a very low permeability basement consisting of schist and phyllite (Figure 3.1 C). The hydraulic conductivity of the materials is widely variable (Calvache et al., 2015) due to the fluvial-deltaic depositional environment of the aquifer. In the vicinity of the mouth of the Guadalfeo River, the upper layers of the aquifer are characterized by gravel layers characterized by high hydraulic-conductivity; however, the ratio diminishes dramatically at a depth of 140 m due to the prevalence of clay layers (Figure 3.1 C). Numerical and sedimentological studies have estimated values of hydraulic conductivities, which ranged from 12 to 300 m/d (Calvache et al., 2009; Duque et al., 2018). The general flow direction in the aquifer is from north to south toward the Mediterranean Sea, with a hydraulic gradient estimated between 1.6×10^{-3} and 5×10^{-3} (Duque et al., 2010); although currently it reaches 7×10^{-3} in the northern part of the aquifer. The main water entrance to the aquifer is supplied by the Guadalfeo River, which provides direct infiltration along the riverbed and indirect infiltration from irrigation return flows, estimated at 11 Mm^3/year and 16 Mm^3/year, respectively (Calvache et al., 2009; Duque et al., 2011).

In the study area, several wells were drilled from north to south (W10, W250, W60, and W180) at distances of 285 m, 300 m, 700 m, and 1900 m from the shoreline (Figure 3.1 B). W10, W60, and W180 are three full-screened wells 10 m, 60 m, and 180 m deep respectively, and W250 is a deep well 250 m deep with one screen that is 6 m and 11 screens that are 3 m each at the depths indicated in Figure 3.1 C. W250 is an artesian well with an average flow of 18 L/s, providing evidence of the presence of vertical flows in this area of the aquifer (Calvache et al., 2015) according to the flow pattern of the discharge zone proposed by Glover (1959) and Kohout (1964) for a coastal aquifer. Duque et al. (2008) indicated slight marine intrusion in the aquifer by using gravitational and electromagnetic sounding methods, which were supported by the low electrical conductivity (EC) data obtained in W180. Additionally, well W250 intersected the FSI, which was approximately 135-200 m deep (Calvache et at., 2015).

The area is characterized by a subtropical climate with scarce rainfall and mild temperature. The average precipitation is 420 mm/year, and the mean annual temperature is 18°C. The mean air temperature follows a regular pattern each year: a maximum of 25°C in July-August and a minimum of 10-12°C in January-February (Duque et al., 2010). A similar pattern was observed in the temperature of water in the river with almost identical values to the atmospheric temperature but with an approximate delay of 1 month. On the other hand, the Mediterranean Sea in this area is characterized by a warm temperature that fluctuates between a maximum of 24°C in August and a minimum of 14°C in February (data supplied by the State Harbors, Spanish Ministry of Development). The temperature pattern in the upper section of the aquifer and in the proximity of the FSI was disturbed due to the influence of the thermal signal from the river (Duque et al., 2010) and the influence of the sea temperature respectively.
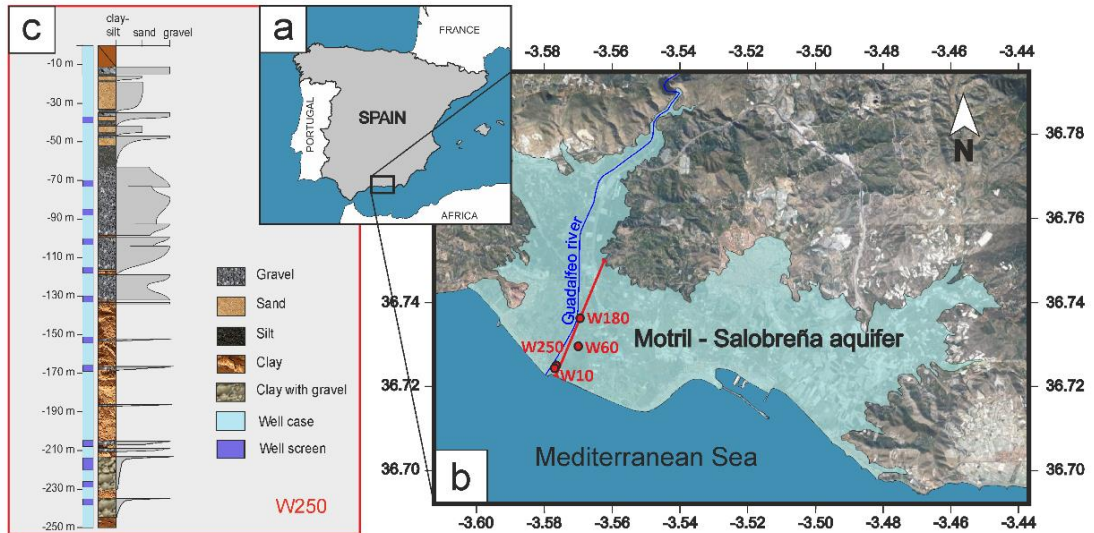
Figure 3.1.- (A) Location map of the research area; (B) Location of the Motril-Salobreña aquifer, research boreholes and cross section; (C) Lithological core of the W250 well and depths of the screens and installed sensors.

The collected data from well W180 represented the vertical heat distribution in the Motril-Salobreña aquifer (Figure 3.2). Three zones can be identified: the surficial zone, intermediate zone, and deep zone. The surficial zone is subject to seasonal changes in temperature. The intermediate zone does not have any significant seasonal variations and remains practically constant. The deep zone has a constant increase in temperature due to geothermal heat.

Figure 3.2.- Temperature vertical profiles measured in W180 collected monthly in 2005.

2.2. Temperature Conceptual Model

The conceptual model (Figure 3.3) was created from the field data information. The measurements obtained in W180 (Figure 3.2) were used to establish the initial temperature distribution within the freshwater domain. A surficial zone 23 m deep with an o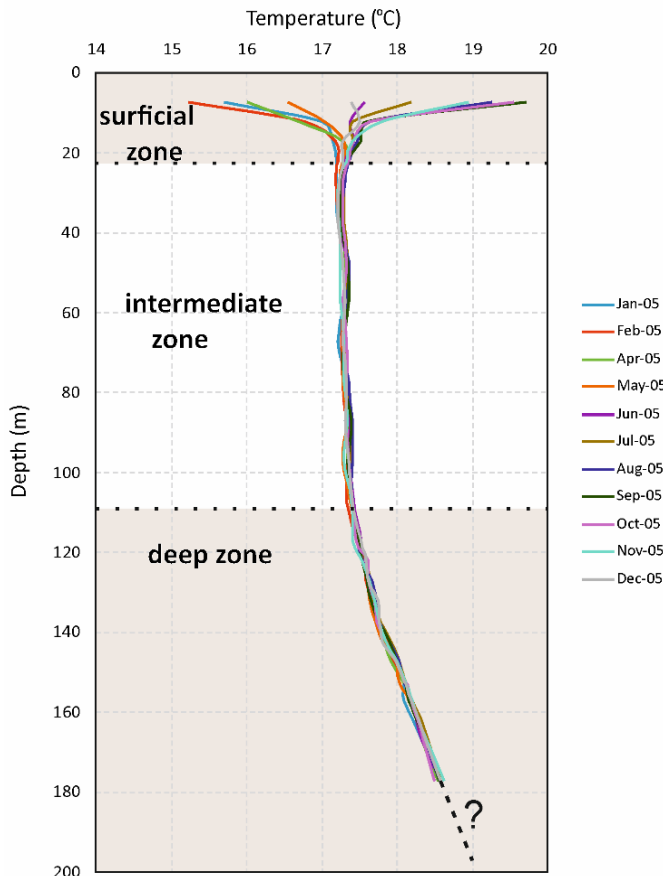scillating thermal signal could be distinguished due to infiltration of the river flow and air temperature influence. Below the surficial zone, the intermediate zone is differentiated because temperature had no oscillations and remained at 17.2°C until a depth of approximately 110 m. In the deep zone, an increment in temperature of 0.02°C per meter was calculated, which represents 20°C at −250 m. The temperature of the sea oscillated seasonally in the same manner as the temperature of the river flow. This conceptualization was used for assigning boundary conditions in the numerical model, and temperature and head measurements in W10, W250 and W60 were used for calibration and verification of the model.
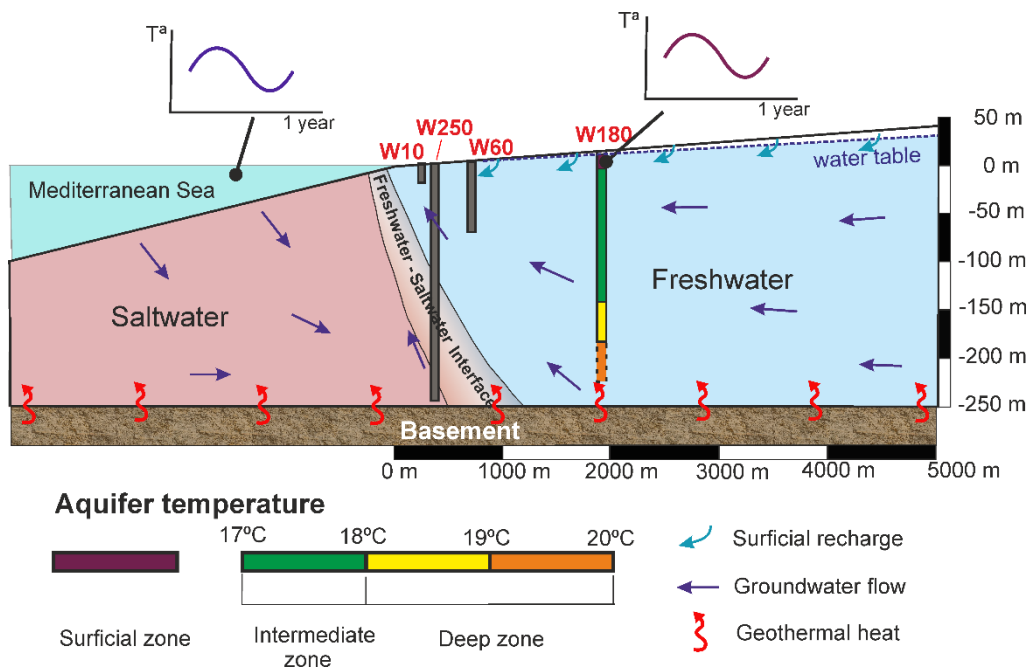
Figure 3.3.- Conceptual model of the temperature distribution of the Motril-Salobreña aquifer.

3. Methodology

3.1. Solute and Heat Transport Equation, Numerical Model and Model Indicators

In the present study, SEAWAT v.4 (Langevin et al. 2007) was used to simulate simultaneous multispecies solute and heat transport. This software couples MODFLOW (Harbaugh et al., 2000) and MT3DMS (Zheng and Wang, 1999) and solves the following form of the variable-density groundwater flow equation:

$$\left(1 + \frac{\rho_b K_d^k}{\theta}\right)\frac{\partial(\theta C^k)}{\partial t} = \nabla\left[\theta\left(D_m^k + \alpha\frac{q}{\theta}\right)\nabla C^k\right] - \nabla(qC^k) - q'_s C_s^k \qquad (1)$$

where ρ_b is the bulk density (mass of the solids divided by the total volume) [ML^{-3}], K_d^k is the distribution coefficient of species k [L^{3}M^{-1}], θ is porosity [-], C^k is the concentration of species k [ML^{-3}], t is time [t], D_m^k is the molecular diffusion coefficient [L^{2}t^{-1}] for species k, α is the dispersivity tensor [L], q is specific discharge [Lt^{-1}], q'_s is a fluid source or sink [t^{-1}], and C^k is the source or sink concentration [ML^{-3}] of species k. Dimensions include length [L], mass [M], time [t] and temperature [T].

Temperature is represented as one of the species of MT3DMS. Given that heat transport is analogous to solute transport in groundwater modeling, Thorne et al. (2006) adapted equation 1 to assign suitable thermal parameters for temperature species:

$$\left(1 + \frac{1-\theta}{\theta}\frac{\rho_s}{\rho}\frac{C_{Psolid}}{C_{Pfluid}}\right)\frac{\partial(\theta T)}{\partial t} = \nabla\left[\theta\left(\frac{k_{Tbulk}}{\theta\rho c_{Pfluid}} + \alpha\frac{q}{\theta}\right)\nabla T\right] - \nabla(qT) - q'_s T_s \qquad (2)$$

where ρ_s is the density of the solid (mass of the solid divided by the volume of the solid) [ML^{-3}], ρ is the fluid density [ML^{-3}], C_{Psolid} is the specific heat capacity of the solid [L^{2}t^{-2}T^{-1}], C_{Pfluid} is the specific heat capacity of the fluid [L^{2}t^{-2}T^{-1}], T is temperature [T], k_{Tbulk} is the bulk thermal conductivity of the aquifer material [MLt^{-3}T^{-1}] and T_s is source temperature [T]. Bulk density is calculated by $\rho_b = \rho_s(1 - \theta)$.

Equations 1 and 2 show that heat transport is controlled by convection and conduction, which are mathematically equivalent to advection and diffusion for solute transport, respectively. Both transport equations incorporate a retardation term. The adsorption of solutes by the aquifer matrix generates retardation in solute transport, whereas the thermal transfer between the fluid and solid aquifer matrix produces retardation in heat transport. A linear sorption isotherm was applied to the model to represent the thermal retardation by calculating the distribution coefficient (K_d) for temperature species:

$$K_d^t = \frac{C_{Psolid}}{\rho C_{Pfluid}} \qquad (3)$$

The thermal conduction term for temperature species D_m^T [L^2/T], is mathematically equivalent to molecular solute diffusion for the solute species. Heat and solute transfer are related to a gradient, from high-concentration areas to low-concentration areas. Bulk thermal diffusivity is calculated from the relationship between equations 1 and 2:

$$D_m^T = \frac{k_{Tbulk}}{\theta\rho c_{Pfluid}} \qquad (4)$$

In turn, bulk thermal conductivity k_{Tbulk} is obtained solving the following equation (Hughes and Sanford, 2004):

$$k_{Tbulk} = \theta k_{Tfluid} + (1 - \theta)k_{Tsolid} \qquad (5)$$

Thermal dispersion in heat transport is frequently ignored in most analytical solutions (Langevin et al., 2010) because heat conduction often dominates thermal dispersion in heat transport (Anderson, 2005; Ferguson, 2007). However, SEAWAT (version 4) includes the thermal dispersion term in the code formulation; therefore, it has been included in our models.

To interpret the temperature distribution within the aquifer and to quantitatively compare the model results, we used the following indicators:

1. $D(B, tc_i)$ is the vertical distance from the aquifer basement to each thermal contour:

$$D(B, tc_i) = -(Z_B - Z_{tc_i}) \tag{6}$$

2. R is the dimensionless factor obtained from the division of the vertical distance from sea surface level to each thermal contour and the location of the arbitrary observation point:

$$R = \frac{Z_{sl} - Z_{tc_i}}{X_{obs}} \tag{7}$$

where i is the temperature of the thermal contour [T], Z_B is the elevation of the aquifer basement [L] using sea level as a reference, Z_{tc_i} is the elevation of the thermal contour [L] using sea level as a reference, Z_{sl} is the elevation of sea level [L], and X_{obs} is the position of the observation point on the x-axis [L].

The coefficient of determination (R^2) and the root mean squared error (RMSE) were calculated on the basis of the comparison of the observed data with the field measurements:

$$R^2 = 1 - \frac{\sum(T_m - T_s)}{\sum(T_m - \bar{T})}$$

$$RMSE = \sqrt{\frac{1}{n} \sum_{i=1}^{n} (T_m - T_s)^2}$$

where T_m is the measured temperature [T], T_s is the simulated temperature [T], $\bar{T}$ is the mean of the temperature values [T] and n is the number of observations.

3.2. Field Data

Four research wells were used to study the temperature distribution of the aquifer. Vertical temperature profiles were logged monthly at W180 and, W60 and sporadically at W250 using the multiparameter probe KLL-Q-2 (accuracy: ±0.1°C; resolution 0.01°C) during the period 2005-2019. In W180, the profiles were obtained by measuring every five meters throughout the well. In W250, the measurement points of the logs were taken at the depths of the 12 screens (Figure 3.1 C). In W60, the observation points of the logs were obtained every 5 meters to a depth of 20 m. In W10, one pressure-temperature sensor was installed at a 5-m depth to measure at 1-hour intervals (Seametrics LevelSCOUT smart pressure sensors; accuracy: ± 0.1°C and resolution: ± 0.01°C). The collection of temperature profiles is subject to uncertainties. Water circulation inside the casing of the well affects the temperature distribution and the measurements could not be an exact replica of temperature into the aquifer. However, as the objective of this research was to focus on the major trends and general dynamics, this limitation was considered acceptable. Other methodologies to collect temperature profiles such as fiber-optic distributed temperature sensing (FO-DTS) directly inserted in the aquifer sediments prevent the problem of water circulation inside wells (del Val et al., 2021) but it requires specific design and construction of the monitoring system instead of using boreholes already drilled. The temperature dataset

of the Mediterranean Sea was supplied from monthly mean temperature by the State Harbors (Spanish Ministry of Development) on the coast at Málaga. This station was chosen because it was closer to the research area (75 km west) and because climatic conditions were practically the same: the same mean monthly temperature and mean precipitation. The measurement device was a TRIAXYS™ Directional Wave Buoy that measures temperature 0.5 m below the sea surface and provides real-time data via radio to a land station with hourly cadence.

3.3. Numerical Model Characteristics

The temperature distribution within the coastal aquifer was modeled with a finite-difference 2D model using SEAWAT, which solved the variable-density groundwater flow and heat transport equations. The 2D model (cross-section) was 8.5 km long (x-axis), of which 5 km were landward and 3.5 km seaward from the coastline, and 100 m wide (y-axis). The depth of the model (z-axis) varied from 150 m in the south (offshore boundary) to 290 m deep in the north (onshore boundary). The topography of the aquifer and seabed had slopes of 0.8% and 2.8% respectively, based on a groundwater age model of the study area (Calvache et al., 2020) and the seabed bathymetric information (Jabaloy-Sánchez et al., 2014). The grid was defined based on a mesh with 124 rows and 22 layers with cells of 85 x 12 m. It was refined near the FSI area (42 x 12 m) and surface area (42 x 6 m). These dimensions of the model were applied to the case study model and for the sensitivity analysis. However, depth, topography, and basement were modified to test how the size of the model affects the temperature distribution. The flow was solved using the Pre-Conditioned Conjugate Gradient (PCG) solver. The solution method for the advective term of the transport equation was the Generalized Conjugate Gradient (GCG) solver with Jacobi pre-conditioner. The Courant number used was 0.75. The simulation of models 1 and 2 requires between 1000-1600 years to reach the steady-state conditions. However, simulation of the model 3 was run during 15 years.

For the boundary conditions, the basement of the aquifer and the left border were defined as a nonflow boundary (Neumann boundary condition). In the sea bed and right boundary, constant hydraulic heads and salinities were defined (Dirichlet boundary condition). With respect to the thermal boundary conditions, temperature recorded data from W180 were used to establish them; on the other hand, temperature measurements of W60, W250, and W10 were used to calibrate the study model.

The workflow with the numerical models included a sensitivity analysis and a real case simulation. Sensitivity analysis was conducted to assess the effect of model parameters on heat transport in coastal aquifers. To reproduce the field observations with the real case study model, specific site characteristics, obtained from previous studies (Duque et al., 2008; Duque et al., 2018; Sánchez-Úbeda et al., 2018a) and fieldwork, were considered, such as aquifer geometry, hydraulic conductivity, heterogeneity, and hydraulic gradient. In the process, three different models (Models 1, 2, and 3) were constructed addressing the different purposes, and the boundary conditions were modified for each of them (Figure 3.4 and Table 3.1):
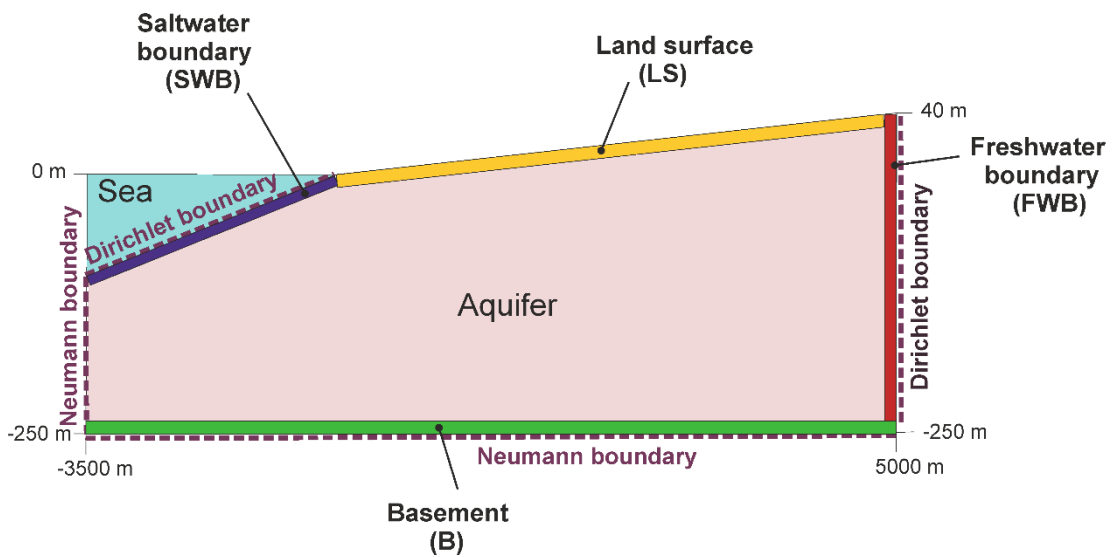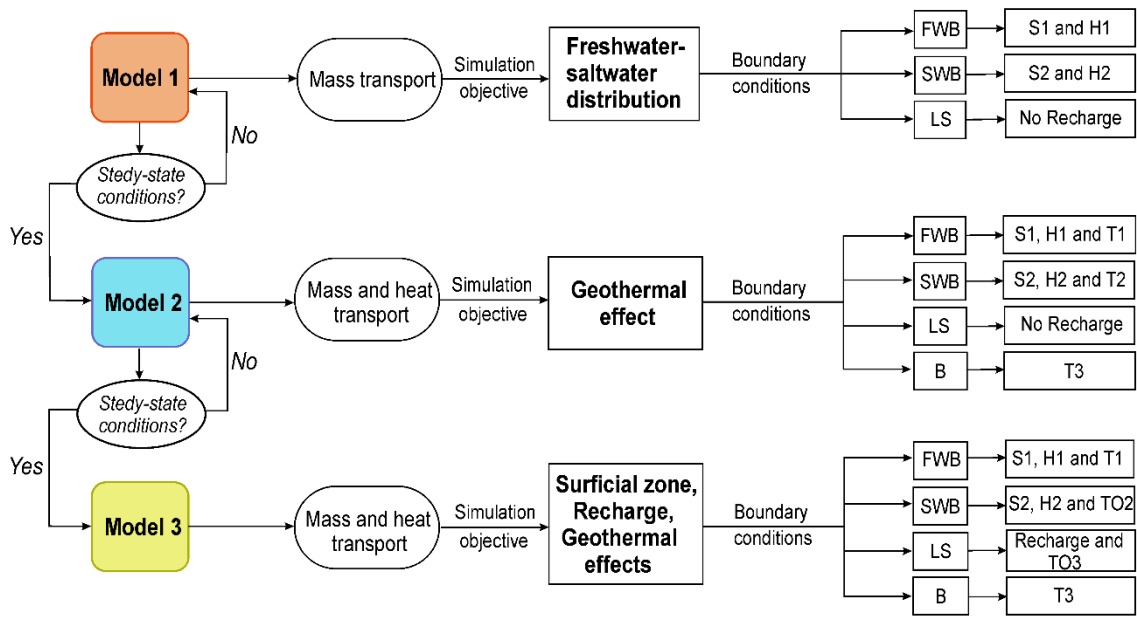
Figure 3.4.- Steps of the simulation and boundary conditions of the numerical model. The values of salinity, hydraulic head and temperature are specified in Table 3.1. FWB: Freshwater boundary, SWB: Saltwater boundary, LS: Land surface, B: Basement.

Input parameters	Sensitivity analysis	Case study model	Source
Specific storage	1E-5 m^{-1}	1E-5 m^{-1}	Calvache et al. (2015)
Specific yield	0.25	0.25	Similar value to Calvache et al. (2009)
Porosity θ	0.2-0.6	0.3	Duque et al. (2008)
Longitudinal dispersivity	1-100 m	10 m	Sauffer et al. (2013)
Horizontal transverse dispersivity	0.5-50 m	5 m	Sauffer et al. (2013)
Vertical transverse dispersivity	0.5-50 m	5 m	Sauffer et al. (2013)
Freshwater salinity S_1	350 mg/L	350 mg/L	Field observations
Saltwater salinity S_2	35000 mg/L	35000 mg/L	Field observations
Freshwater boundary head H_1	15-35 m	17 m	Field observations
Saltwater boundary head H_2	0 m	0 m	Field observations
Freshwater temperature T_1	17.2°C	16.7°C	Field observations
Saltwater temperature T_2	13°C	16.7°C	Manca et al. (2004)
Basement temperature T_3	19-30 °C	20.05°C	Field observations
River water temperature oscillation TO_1	-	Sinus function 12-26°C	Based on Duque et al. (2010)
Seawater temperature oscillation TO_2	-	Sinus function 14-24°C	State of Harbors (Spanish Ministry)
Molecular diffusion coefficient D_m^s	1E-10 m^2/d	1E-10 m^2/d	Langevin et al. (2007)
Thermal conductivity of water k_{Tfluid}	0.58 W/m°K	0.58 W/m°K	Langevin et al. (2007)
Thermal conductivity of sediments k_{Tsolid}	1-6 W/m°K	2.9 W/m°K	Approximate value for gravel (Xiaoqing, 2018)
Specific heat of water C_{Pfluid}	4186 J/kg°K	4186 J/kg°K	Langevin et al. (2007)
Specific heat of sediments C_{Psolid}	100-1000 J/kg°K	830 J/kg°K	Approximate value for gravel (Xiaoqing, 2018)
Thermal diffusivity D_m^T	0.06-0.3 m^2/d	0.15 m^2/d	Calculated using eq. 4
Bulk thermal conductivity k_{Tbulk}	0.87-4.37 W/m°K	1.8 W/m°K	Calculated using eq. 5
Thermal distribution factor K_d^t	2E-8 – 2E-7 L/mg	2E-7 L/mg	Calculated using eq. 3
Density change with concentration	0.7	0.7	Langevin et al. (2007)
Density change with temperature	-0.375 kg/(m^3 °C)	-0.375 kg/(m^3 °C)	Langevin et al. (2007)
Density vs pressure head slope	0.00446 kg/m^4	0.00446 kg/m^4	Langevin et al. (2007)
Bulk density ρ_b	1800 kg/m^3	1800 kg/m^3	Calculated with $\rho_b = \rho_s(1 - \theta)$
Reference temperature	25 °C	25 °C	Langevin et al. (2007)
Viscosity vs concentration slope	1.923E-6 m^4/d	1.923E-6 m^4/d	Langevin et al. (2007)
Reference viscosity	86.4 kg/ m d	86.4 kg/ m d	Langevin et al. (2007)

Table 3.1.- Input values of the parameters for the sensitivity analysis and study model.

4. Results

4.1. Temperature Distribution

An initial synthetic cross section of the temperature distribution of a coastal aquifer was obtained based on model 2, which was compared with model 1 (Figure 3.5). The hydraulic conductivity used was Kx=1 and the anisotropic ratio Kx/Kz = 10, and the boundary conditions and the rest of the input parameters are specified in Figure 3.4 and Table 3.1. Groundwater temperature increases with depth due to the geothermal gradient. However, temperature propagation and thermal contours are bent because of the change in flow direction (Figure 3.5 A), generating a hotter temperature plume along the FSI. At deeper locations in the aquifer, fresh groundwater is forced to ascend toward the sea due to the presence of the salt wedge, which implies greater heat transport than other parts of the aquifer where convection is less important. In turn, temperature also affects the position of the FSI. When adding temperature to the model (comparing model 1 and model 2), the FSI width changed, but it also rotated and moved its toe inland (Figure 3.5 B). The FSI toe moved tens of meters when temperature difference between the surface and basement is 1°C for our case study; however, it is also highly dependent on the aquifer properties. In general, an increase of temperature difference will favor the encroachment of seawater. This is consistent with Henry and Hilleke (1972) and Langevin et al. (2010), who indicated that convective cells are stronger when density is affected by temperature. Groundwater is heated at the bottom of the aquifer, rises because of the combination of the effect of the saline wedge and the buoyancy effect in warmer water, and saltwater replaces the heated upward water.
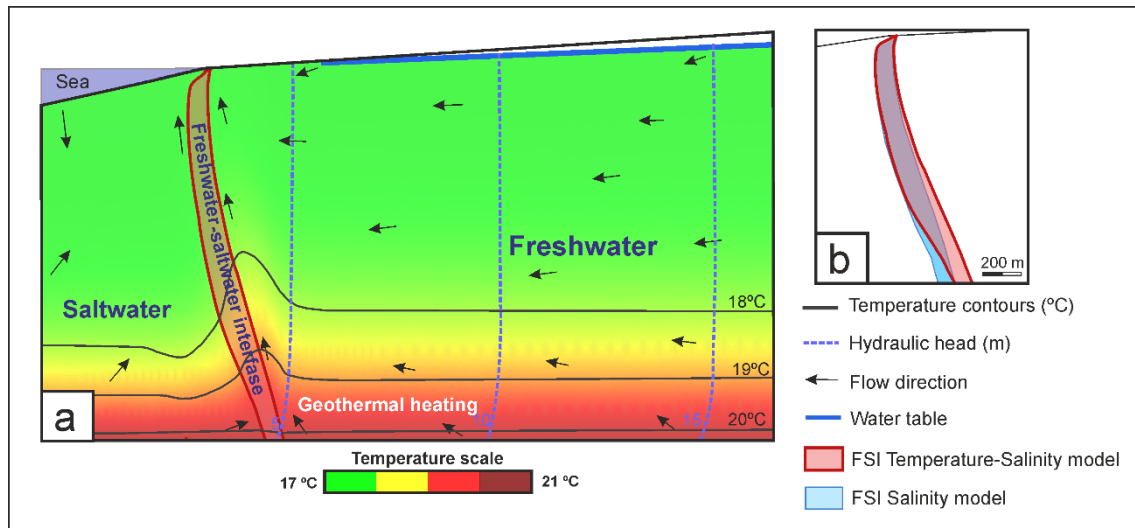
Figure 3.5.- (A) Synthetic cross section of the temperature distribution of a coastal aquifer; (B) Freshwater-saltwater interface (FSI) position simulated with a variable-density mass transport model with and without temperature.

4.2. Sensitivity Analysis

Heat transport is controlled by different parameters: hydraulic conductivity, porosity, dispersivity, thermal distribution coefficient, thermal diffusivity, hydraulic gradient, thermal boundary, seafloor slope, and depth of the basement. Sensitivity analysis of the variable-density groundwater flow and heat transport model showed the impact of each

parameter on thermal distribution. The sensitivity analysis was focused on heat transport within the deep zone of each model and especially around the area of the FSI. Thus, modeling of this section consisted of a variable-density model with geothermal heat input (Figure 3.4). The value of the parameters was changed for a range based on realistic values obtained in the literature (specified in Table 3.1). The assignation of maximum, mean, and minimum values to each parameter aimed to cover those parameters with scarce information and to show the differences associated with the natural variability in aquifers. Homogeneous conditions were assumed with a hydraulic conductivity of Kx= 1 m/d, a Kx/Kz ratio of 10, and the input parameter values of Table 3.1, except for the parameter that was tested in each case.

4.2.1. Hydraulic Conductivity

Four sets of hydraulic conductivities were tested obtained from the literature (Calvache et al., 2009; Duque et al., 2017): two with a lower hydraulic conductivity (Kx=1 m/d and changing anisotropic ratios Kx/Kz of 1 and 10) and two with higher hydraulic conductivity (Kx=300 m/d and anisotropic ratios Kx/Kz of 1 and 10). The resulting temperature distribution of the different scenarios showed changes in the order of magnitude of hundreds of meters, depending on the value of the hydraulic conductivity (Fig. 4.6). Lower hydraulic conductivity generated thermal contours distributed parallel to the base of the aquifer, while higher values related to more changes in the section. Anisotropy played a more important role in the area where the flow components were more vertical; that is, along the zone where the FSI is located. High hydraulic conductivities (300 m/d) produced a sharper rise in the thermal plume than low hydraulic conductivities (1 m/d).
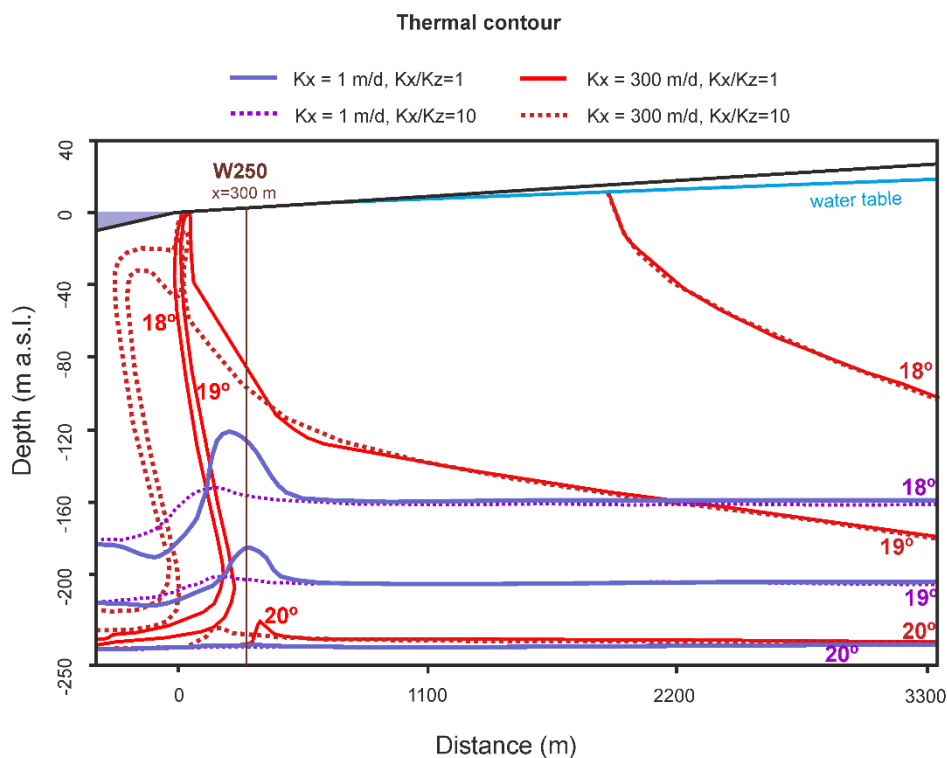

Figure 3.6.- Thermal contours distribution resulting from models with different values of hydraulic conductivity.

Anisotropy of Kx/Kz = 10 generated a higher horizontal than vertical component, hindering vertical heat transport and flattening the thermal contours. Anisotropy favored the horizontal flow thereby displacing the FSI seawards, and the thermal plume was affected in the same manner due to the direct relationship with the FSI. This test indicates that the anisotropy can cause a change on an order of magnitude of tens of meters in the thermal distribution under the boundary conditions selected.

4.2.2. Porosity (θ)

The sensitivity of temperature to porosity was evaluated by introducing two extreme values (0.2 and 0.6) to the model obtained from the literature (Freeze and Cherry, 1979). Although the depth of the thermal contours was very similar for both cases, there were slight differences in the shape of the isothermal lines (Figure 3.7 A). For θ = 0.6, the thermal contours became flattened and therefore, the geothermal gradient was practically the same for any observation point on the x-axis. For θ = 0.2, the thermal plume was slightly higher. Likewise, the FSI varied depending on the porosity value. For θ = 0.6, the FSI was narrower in the upper area in comparison with a θ = 0.2.

This indicates that a reduction in porosity is related to higher advective transport; hence, the buoyancy effect is larger, which causes a modification in the upper part of the FSI (fresh groundwater discharge zone) and, consequently, in the temperature distribution. Nevertheless, the effect of this parameter is very reduced considering the range of values tested. For the range of porosities commonly found in real aquifers, the differences would be minor.
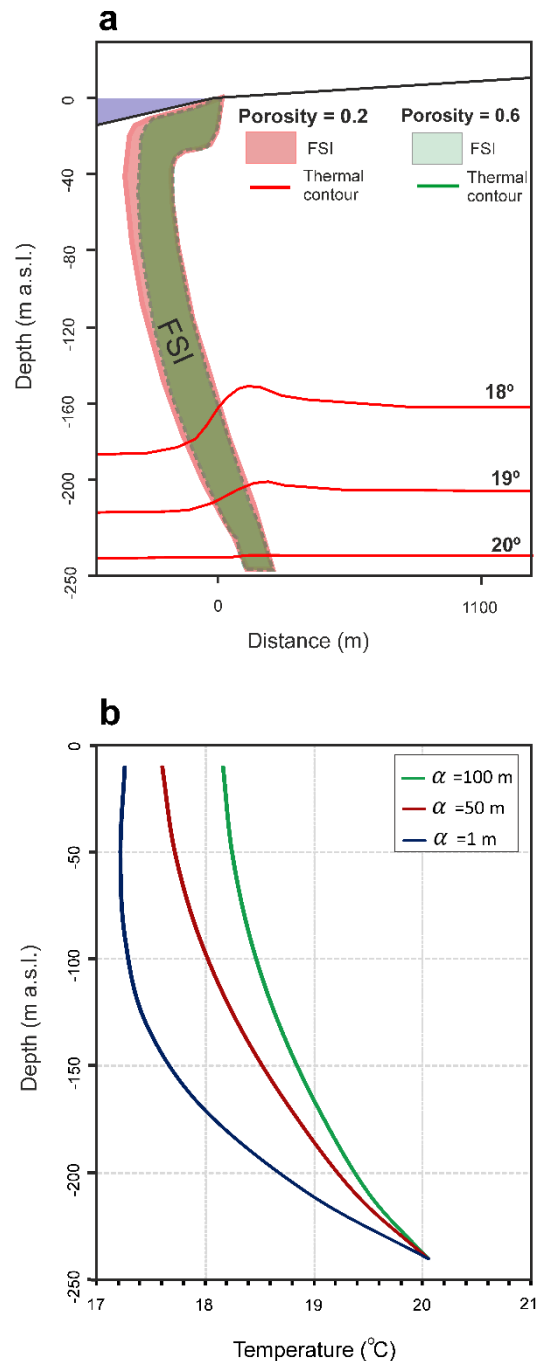
Figure 3.7.- (A) Position of the FSI and the thermal contours resulting from models with different values of porosity; (B) Temperature profiles at x=300 m (W250 location) obtained for different values of dispersivity.

4.2.3. Dispersivity (α)

Both salinity dispersivity and thermal dispersivity were considered, as they are modeled in an analogous manner (de Marsily, 1986); therefore, they have the same value (Bridger and Allen, 2010; Engelhardt et al., 2013). The thermal dispersivity of aquifers usually ranges from 0.1 to 100 m (Sauffer et al., 2013). The three values for the dispersivity tensor (α) were considered based on the dimensions of the model (1 m, 50 m, and 100 m). The temperature profiles obtained 300 m from the coastline showed that higher dispersivity (α = 100 m) increased temperature throughout the entire thickness of the aquifer (Fig. 3.7 B), as the heat effect from the geothermal source of heat can spread more easily. For α = 1 m, the trend of the temperature profile was more concave, whereas temperature increased more linearly with depth for α = 100 m. When thermal dispersivity played a more important role in heat transport, heat convection decreased. Hence, weaker convection (and thus dispersivity-dominant heat transfer) produced a linear increase in temperature, as demonstrated by An et al. (2015).

The temperature difference reached more than 1°C, which had significant relevance in the comparison with other parameters. A dispersivity of approximately 100 can move water with a temperature of 18°C upwards to the shallow part of the aquifer. This has not been possible to reach with the sensitivity analysis of the other parameters.

4.2.4. Thermal Distribution Coefficient (K_d^t)

K_d^t was estimated with equation 3 applying maximum, minimum, and mean values of C_{Psolid} for rocks and minerals reported in the literature (Schärli and Rybach, 2000; Clauser, 2011). The resulting values of K_d^t were 2.3 x 10^{-7}, 1.27 x 10^{-7} and 2.3 x 10^{-8} L/mg. The sensitivity analysis showed variations up to tens of meters in the distance from the basement to the thermal contours D(B, tc$_i$) (Figure 3.8 A): a low value of K_d^t (2.3 x 10^{-8} L/mg) generated a greater D(B, tc$_i$), i.e., a further propagation of the thermal signal compared with higher values of K_d^t. The shallowest thermal contour (18°C) was the one with greater displacement from the basement when changing the values of K_d^t. These results are consistent with the fact that K_d^t works as a retardation coefficient that causes the temperature changes to be slower than the linear flow velocity (Langevin et al., 2008). If more heat is necessary to increase the sediment temperature, the retardation of heat transport will increase (Ma et al., 2012). K_d^t had no direct effect on the salinity distribution but did on the heat distribution; therefore, the FSI can be affected by the buoyancy effect. However, the changes were so small that they were not appreciable in these simulations.

4.2.5. Thermal Diffusivity (D_m^T)

The thermal diffusivity D_m^T was calculated with equations 4 and 5 using the given value of k_{Tsolid}. The maximum and minimum values and a middle value of k_{Tsolid} were estimated for different lithologies and were obtained from Xiaoqing et al. (2018). The values assigned to D_m^T were 0.3, 0.15, and 0.06 m^2/d, corresponding to dolomites, marlstone, and mudstones, respectively. The results of each simulation were observed in different locations of the model and represented with the R parameter (Figure 3.8 B).
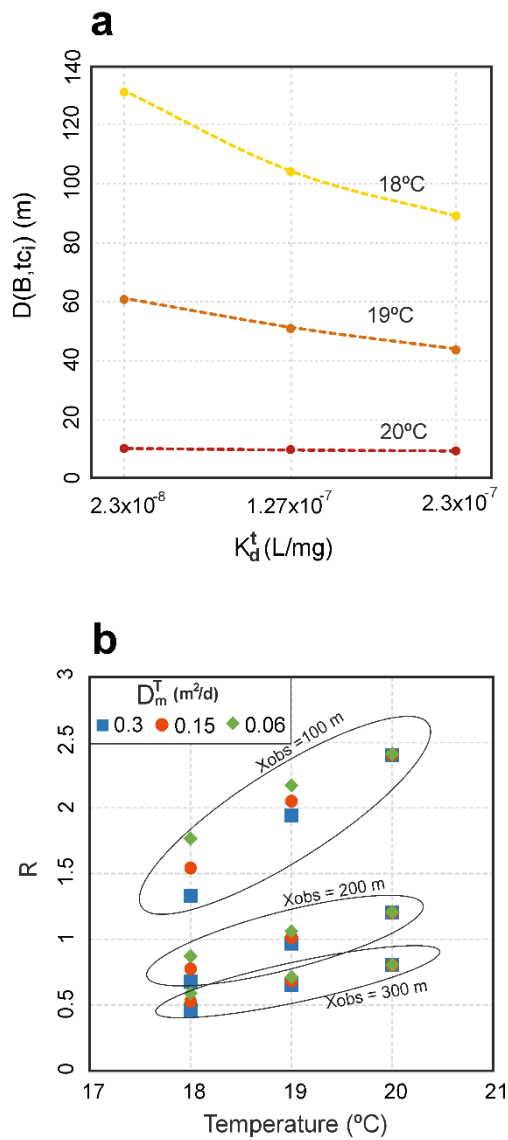
Modification of the values of D_m^T produced a greater variability in R for the thermal contour of 18°C. In contrast, R did not change for the thermal contour of 20 °C when changing D_m^T. For $D_m^T = 0.06$, the R value can reach 24 % higher than that for $D_m^T = 0.3$, as is the case of the thermal contour of 18°C observed at $X_{obs} = 100$ m. Just as K_d^t, the thermal contour of 18°C showed larger changes than the rest of the temperatures due to the greater vertical component of the flow at this depth. The variation in the FSI position was so small that it could not be detected while testing the different values of D_m^T.

4.2.6. Hydraulic Gradient (Δh)

The hydraulic gradient in aquifers is a variable parameter in time and space. Seasonal oscillation in recharge conditions can modify it in short periods. The impact on heat transfer was tested with a range between 0.003 and 0.007 from the lateral inflow. The constant head of the sea boundary was maintained at 0, and only the constant head of the freshwater boundary was changed (from 15 m to 35 m). These changes were on the same order of magnitude as observed in the Motril-Salobreña aquifer during the last 20 years (Duque et al., 2010). Δh changed the distribution of salinity moving the FSI hundreds of meters and temperature by changing the pattern (Figure 3.9). For Δh = 0.007, the FSI was positioned more seaward and vertical, and the temperature transport had a higher vertical component throughout the entire model compared with the results for Δh = 0.003. Additionally, the thermal plume in the discharge zone moved seaward and had a more pointy shape.

Figure 3.8.- (A) Model results for different values of thermal distribution coefficient (K_d^t) obtained at x= 300 m (W250 location). (B) Model results represented by R vs temperature of the thermal contours for different values of thermal diffusivity (D_m^T).
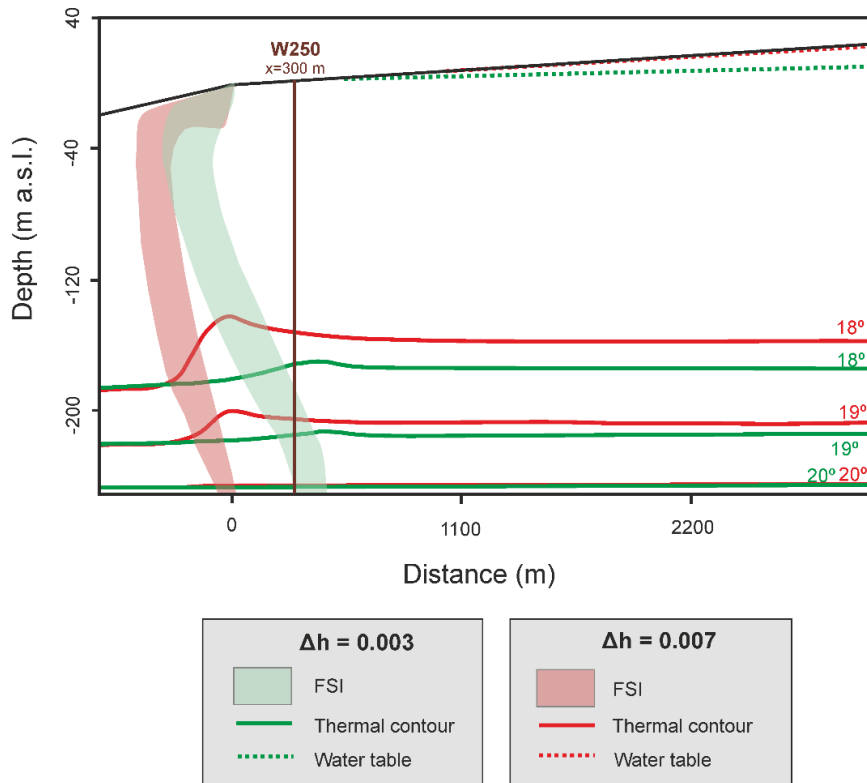
Figure 3.9.- Comparison of the thermal contours distribution and FSI position for two different hydraulic gradients.

4.2.7. Thermal Boundary

The effect of the input of geothermal heat was tested based on different rates. As the geothermal gradient increased 1°C per 20 to 40 m of depth (Anderson, 2005), and the model was 250 meters deep, the highest temperature difference between the surface and basement (ΔT) was 13°C. Additionally, a ΔT of 6°C and 2°C were also tested. As the shallow part of the aquifer was assigned 17.2°C, the basement of the model was 30°C, 23°C, and 19°C. The ΔT was compared with the temperature distribution at different depths (-30 m, -100 m, -160 m, and -230 m) at x = 300 m (Figure 3.10).

Figure 3.10.- Temperature variation by adding different geothermal inputs at different depths for three different values of geothermal gradients. Obtained at x = 300

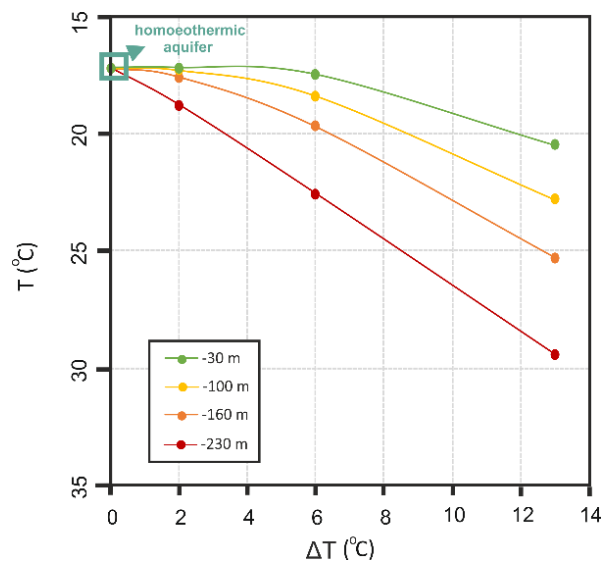The point where the resultant lines intersected the x-axis, represented the temperature of a homoeothermic aquifer in which temperature would be homogeneous regardless of depth. $\Delta T = 13°C$ produced an increase in temperature in the shallowest observation point (-30 m) of $3°C$ with respect to the homoeothermic aquifer. There were small changes in the FSI position: for higher ΔT, the FSI had more verticality (a few meters seaward of the FSI toe) and was wider than for smaller ΔT, although there were no large differences.

4.2.8. Seafloor Slope (SFS)

The seafloor geometry of the model was tested in order to study its relevance on temperature distribution. The different slope values used were: 2.8 % based on the estimated value for the Motril-Salobreña aquifer by bathymetric techniques (Jabaloy-Sánchez et al., 2014) and a minimum and maximum values of 0% and 5% respectively, to take account of other possible SFS representative of more study areas (Figure 3.11 A).

The starting point of the slope was the coastline, and the continental topography was not changed regarding previous models. For SFS=5%, the thermal contour had a larger R parameter in comparison with the rest of the inclinations, which indicates that the isotherms ascended less. For SFS = 5% the R value can reach 9% higher than that for SFS = 0%, as is the case of the thermal contour of 18°C observed at X_{obs} = 100 m. The thermal contour of 18°C, as it was located at a shallower location in the aquifer, was more affected by the change in slope than the other isotherms, and this sector had greater vertical flow components. Thus, the higher the seafloor slope is, the lower the elevation of the thermal contour. Moreover, the slope of the seafloor had an impact on the position of the FSI. For SFS=5%, the FSI is less vertical, and its toe is situated a few meters seaward than for SFS=0%.
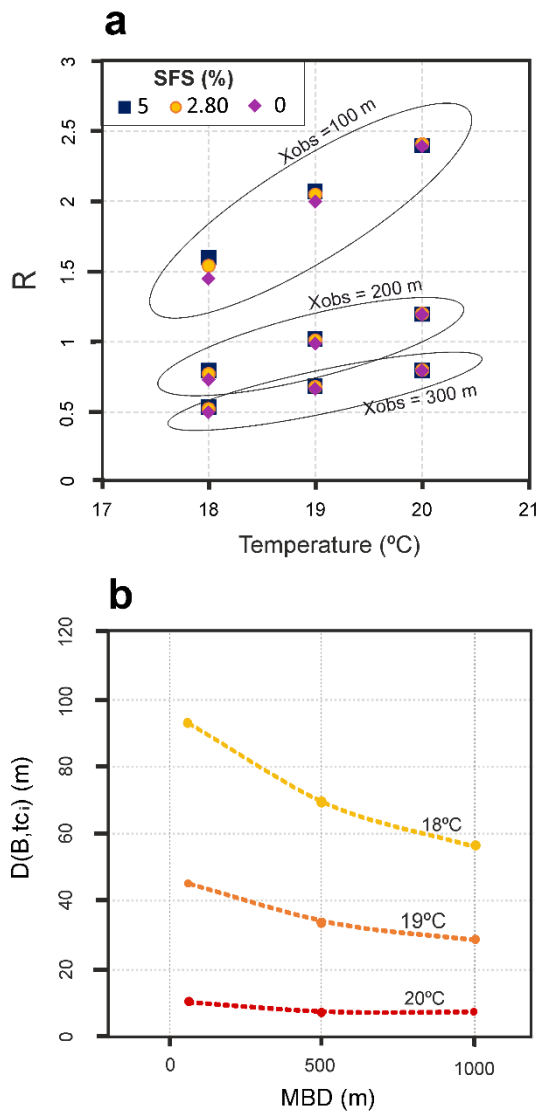
Figure 3.11.- (A) Model results represented by R vs temperature of the thermal contours for different seafloor slopes. (B) Distance of each thermal contour to the basement in different depth models.

4.2.9. <u>Model Basement Depth (MBD)</u>

Three model basement depths (MBD): 100 m, 500 m, and 1000 m, were considered (Figure 3.11 B). Although an increase in depth is usually associated with a major geothermal gradient, the temperature of the basement boundary was the same for all cases since the target was to understand their influence separately. The results showed important variations in the distance from the basement to the thermal contours $D(B, tc_i)$; for example for $D(B, tc_{18°C})$, the difference between a model of 100 and 1000 m was almost 40 m.

4.3. Case Study Model

The model had the same structure as the model used for sensitivity analysis but the parameters were adjusted based on the local knowledge of the areas (Table 3.1). Horizontal layers without lateral facies changes were defined as this is the major sedimentary architecture of the aquifer. Smaller scale heterogeneity was not introduced to focus on major aspects of the thermal distribution.

Hydraulic conductivity was initially defined based on previous studies (Calvache et al., 2009; Duque et al., 2018) and the lithological core of W250 (Figure 3.1). Model results were compared with the field measurements of temperature and salinity in W10, W250, and W60.

For temperature boundary conditions, a fixed temperature (20.05°C) was assigned to the base of the aquifer based on the expected temperature at −250 m due to the linear temperature increment in W180 (Figure 3.2). Temperature of the right boundary (freshwater entry) was 16.7°C, which is an approximate value for temperature in the intermediate zone. The temperature oscillation assigned to the seafloor fluctuated between 14 and 24°C. At the surface boundary, a constant recharge of 5000 mm/yr was assigned that represented the river inflow to the aquifer, as the observation wells were all located at a maximum distance of a few tens of meters from the trace of the river. The temperature of this recharge was a sinus function according to the seasonal oscillation of the river water temperature: 12-26°C (Duque et al., 2010). In the calibration, hydraulic conductivity of the different layers was adjusted as well as temperature in the right boundary and in the recharge. These changes were minor adjustments, as still the boundary conditions were coherent with the field measurements (i.e., temperature value of the right boundary was modified to 16.7°C, from 17.2°C). Additionally, the adjusted recharge was four times smaller than that estimated in previous studies. The model was run for a total of 15 years to give enough time to reach the semistability, which was reached in the 9th year of simulation. From this time, the FSI position and geothermal heat were in steady state, and the temperature of the surficial zone and saltwater had repeated seasonal oscillations annually. The results displayed below correspond once the steady-state condition had been reached.

The coefficient of determination (R^2) of the calculated rating curves was 0.81, and the RMSE was 0.37°C.

The vertical profiles of temperature at x=300 m are displayed with the field data obtained from W250 (Figure 3.12 A). The differences in the first few meters correspond with the seasonal temperature oscillation. From −50 m, these differences were buffered, indicating that recharge had no influence. However, in the field data, temporal variations were observed when W250 intersected the FSI (from −150 m). This issue is discussed in the next section. There is a strong connection between hydraulic conductivity values of the model (Table 3.2) and temperature distribution. The intermediate zone of the temperature profiles was related to a layer with high hydraulic conductivity (layer 2). This suggested that the temperature distribution is strongly dependent on the geology of the study area. The seasonal temperature oscillation in the surficial part of the aquifer was analyzed by the temperature logs at x=700 m (Figure 3.12 B) and compared with the envelopes of the field logs measured in W60. The results ranged between 17.3 and 19.1°C and were between the maximum and minimum envelopes (16.4-19.6°C) and had very similar shapes. The profile with the minimum value was slightly lower than the minimum field measurement.
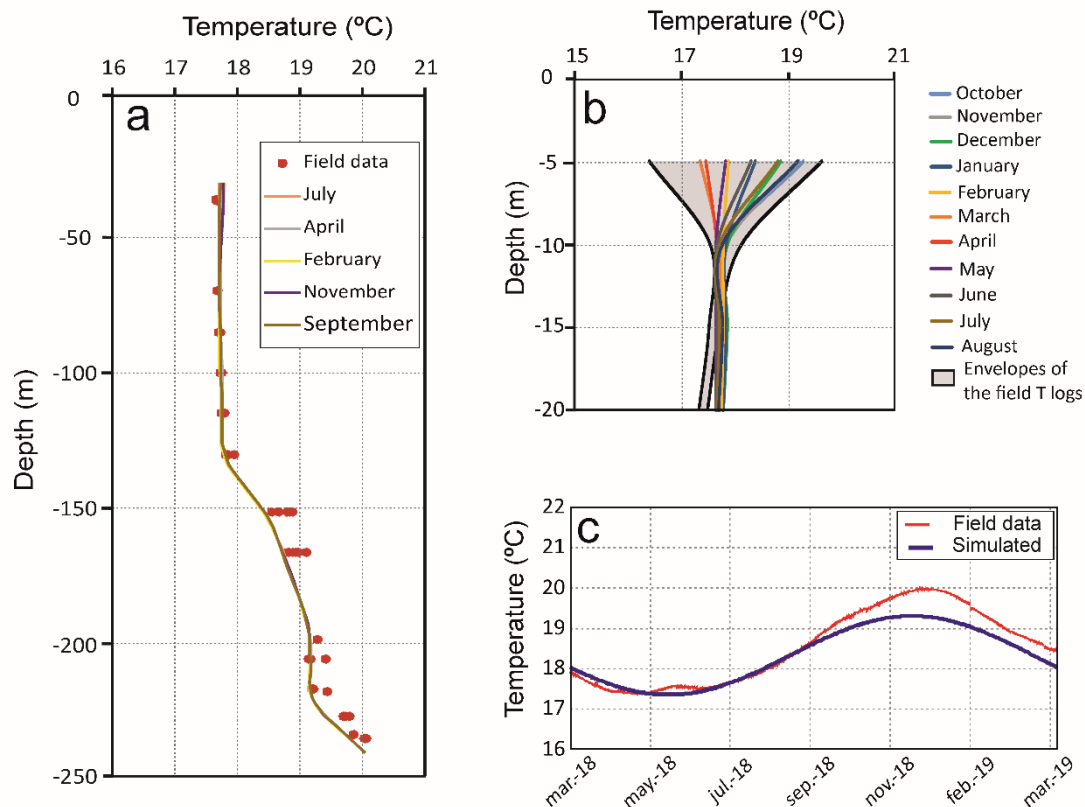

Figure 3.12.- Temperature results once the model reached the semisteady state: model simulation vs field data. (A) Deep temperature logs at W250; (B) Shallow temperature logs at W60; (C) Seasonal oscillation in the surficial zone obtained at W10.

	Thickness (m)	Hydraulic conductivity (m/d)
Layer 1	16	Kx = Ky = 5 and Kz = 0.5
Layer 2	121	Kx = Ky = 400 and Kz = 40
Layer 3	63	Kx = Ky = 30 and Kz = 5
Layer 4	12	Kx = Ky = 150 and Kz = 1
Layer 5	35	Kx = Ky = 20 and Kz = 2

Table 3.2.- Hydraulic conductivity values defined in each layer of the study model.

The thermal signal obtained at -5 m at x=285 m demonstrated that the model was able to simulate seasonal oscillations (Figure 3.12 C). The sensor installed in W10 showed temperature oscillations with a maximum of 20°C in December and a minimum of 17.5°C in May, and the simulated temperature oscillated from 17.3 to 19.3°C; therefore, the maximum value was slightly lower than the observed value.

For temperature distribution near the sea boundary, the simulated data obtained at x=-600 m (Figure 3.13 A) reflected the relevance of sea temperature to groundwater temperature in the saltwater domain. Groundwater under the sea followed the seasonal oscillation of sea temperature, but the amplitude was smaller and the delay increased with depth. At z=-50 m, oscillation could be observed, although the signal was poor. Cross sections of temperature distribution (Figures 3.13 B, C) showed that, below the surficial zone, the temperature of the freshwater domain was maintained at approximately 17°C during summer and winter. This means that FSI acted as a barrier for temperature distribution because fresh groundwater removed the sea thermal signal due to the significant vertical flux near the discharge zone to the sea. In the vicinity of the FSI on the left side, there was a high infiltration of seawater. Consequently, the thermal signal was transferred to a greater depth, and a temperature mixing zone of several tens of meters was generated. This indicates the presence of an interface for temperature along the FSI that does not allow the heat transfer between freshwater and saltwater.

5. Discussion

Sources of different temperatures and hydrodynamics established in coastal aquifers, including variable-density convective processes, generate a challenging scenario for developing temperature models. The availability of temperature data is scarce, as this parameter has not traditionally garnered extensive attention, but also because of the lack of deep wells in the proximity of the sea due to the dearth of salty water utilization.

The development of a numerical model improved the knowledge of temperature distribution within coastal aquifers and the generation of a prototype compiling the main characteristics of these areas regarding temperature and the interaction with variable density. Preliminary simulations disclosed the existence of thermal warm upwelling below the discharge area. An et al. (2015) and Szijártó et al. (2019) simulated this phenomenon with a groundwater flow model but in a freshwater setting, where flow moved upwards in discharge areas; however, coastal areas and variable density were not

considered. There was a lack of information about temperature distribution in coastal aquifers and the differences with other types of groundwater systems, such as the dependence of the warm plume on the position and shape of the FSI. Additionally, the FSI changes because of the buoyancy caused by temperature over density of water, which is consistent with the convective cells demonstrated in a laboratory experiment (Henry and Hilleke, 1972) and in a small dimensional model (Langevin et al., 2010) based on a previous experiment. Environmental tracers also indicated the rise of old deep groundwater nearby the FSI (i.e. Sánchez-Úbeda et al., 2018b; Calvache et al., 2020), indicating that the temperature distribution in coastal aquifers could be directly related to the age distribution.

Sensitivity analysis allowed us to quantify the order of magnitude of the impacts of the different parameters that are used for simulating temperature in coastal aquifers. These results are based on an aquifer that has been used as a reference (the Motril-Salobreña aquifer) and the implementation of much higher and lower values in the range of what can be considered common in natural settings (see section 3.4.2.). Therefore, the impact of each value (Table 3.3) can be used as a general indicator but in settings that differ extremely from our starting point (for example, karstified, highly heterogeneous, or extreme in size aquifers- i.e., a few meters deep aquifer) which should be used more carefully.

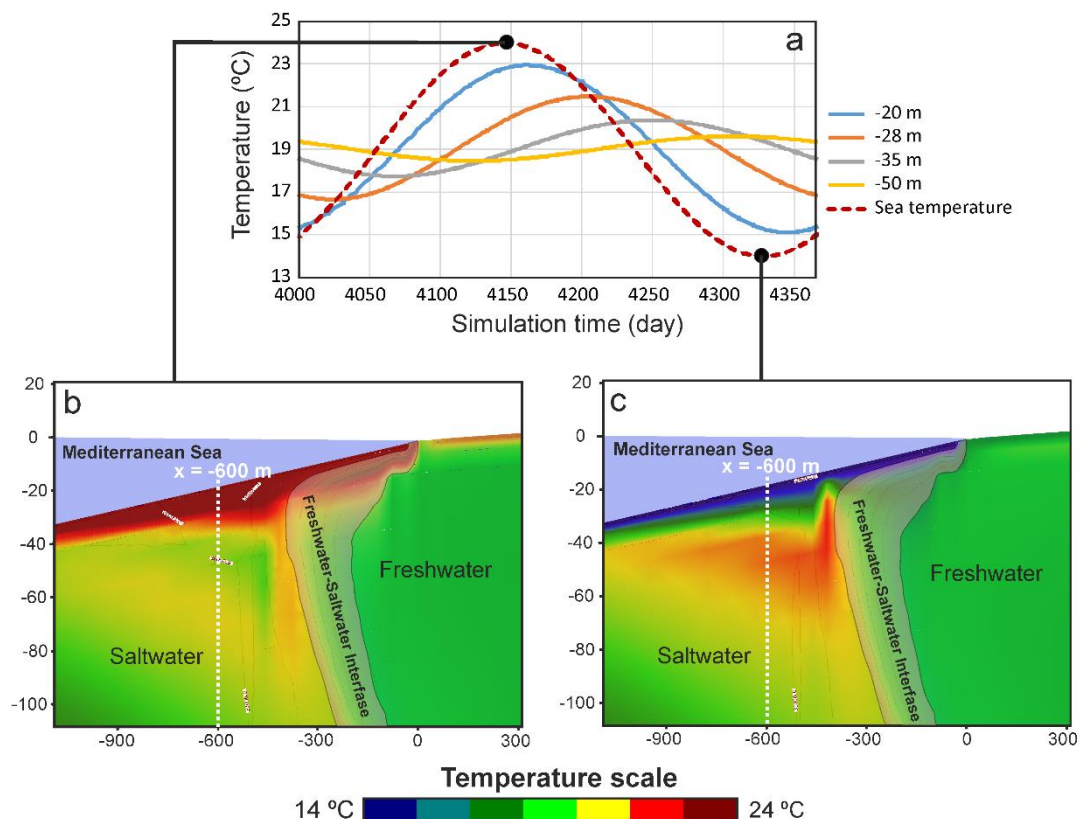
Figure 3.13.- Seawater temperature signal obtained by the study model. (A) Time series at different depths at x=−600 m; (B) Vertical section when the sea had the maximum temperature; (C) Cross section when the sea had the minimum temperature.

Parameters	Variation of the D(B, tc$_{19°C}$)	Variation of the FSI toe position
Hydraulic conductivity	100's of meters	100's of meters
Thermal boundary	100's of meters	Few meters
Dispersivity	Several 10's of meters	100's meters
Model basement depth	Several 10's of meters	1000's meters
Thermal distribution coefficient	10's of meters	Few meters
Thermal diffusivity	10's of meters	Few meters
Hydraulic gradient	10's of meters	100's meters
Seafloor slope	Meters	Meters
Porosity	Few meters	Meters

Table 3.3.- Influence of each parameter or boundary condition on sensitivity analysis: variations on the distance between the basement and the thermal contour of 19°C and in the position of the FSI toe.

K is the most controlling parameter in the temperature distribution of a coastal aquifer. This can be applied to noncoastal aquifers (Ma et al., 2012; An et al., 2015). The Kx/Kz ratio had a notable influence on the vertical component of heat transport. The importance of this parameter increased in coastal areas due to its impact on the position of the FSI, on which heat transport depends. Both of them must be considered the primary calibration parameters when modeling a coastal aquifer.

Heat distribution of the entire aquifer is influenced by the temperature established at the base of the model, which is associated with geothermal heat. Thus, ΔT should be treated with special attention in studies based on aquifers located in zones with positive anomalies in the geothermal gradient, such as tectonically and volcanically active zones (geothermal gradients > 40°C/km), as well as thin aquifers. Additionally, even thick aquifers with normal geothermal gradients (30°C/km) can have relatively high temperatures, such as the southern Permian Basin in Europe (Limberger et al., 2018).

There are conflicting points of view in the literature about the role of dispersivity in heat transport. Some authors (i.e., Bear, 1972; Ingebritsen and Sanford, 1998; Hopmans et al., 2002) have given greater weight to conduction and have ignored thermal dispersivity. While others (i.e., Molina-Giraldo et al., 2011; Park et al., 2015; Piga et al., 2017) have given a higher relevance to thermal dispersion in their studies. Our research showed how dissipation of heat energy leading to high dispersivity values in a coastal aquifer could change the temperature pattern.

An aquifer with a deeper basement kept the thermal contours closest to the bottom compared with a model with a small MBD and the same boundary conditions. Reduction in heat transport at a greater MBD is related to the findings of Szijártó et al. (2019), who suggested that flux decreased with the increase in deeper models.

Both K_d^t and D_m^T were the least sensitive parameters for temperature modeling in a previous study using a heat tracer test (Ma et al., 2012). However, our results showed that larger values of K_d^t and D_m^T maintained the temperature input generated by geothermal heat near the basement, preventing the ascent of thermal contours. This is because the

heat is dispersed quickly and cannot ascend to the upper layers of the aquifer. K_d^t and D_m^T depend on C_{Psolid} and k_{Tsolid} respectively; therefore, aquifer materials play an important role in conduction transfer when they reach higher values of K_d^t and D_m^T.

The effect of hydraulic gradient has a direct impact on the position of the FSI and hence the thermal plume. The same happened with the increase in hydraulic conductivity, although the magnitude of heat propagation was considerably lower for the hydraulic gradient. For this reason, Δh could play a more relevant role in areas with climatic variability (strong seasonality) where hydraulic heads will vary due to changes in recharge.

Geometry of the seafloor and its impact on the FSI has been previously studied, and a bigger SFS led to an augmentation of the intrusion (Abarca et al., 2007; Walther et al., 2017). In our case, the range of values considered based on the studies in the area, do not have a significant effect compared with other parameters considered. The verticality of the FSI for smaller SFS also impacts on the temperature distribution in coastal aquifers because it favors the vertical component of the flux and the thermal contours were positioned more towards the surface.

Porosity was the least controlling parameter in the temperature distribution. It had an effect on both advection and convection components but in opposite ways (Panteli, 2018; Piga et al., 2017). An increase in porosity resulted in a decrease in the effective velocity of groundwater and a reduction in plume length but also caused a decrease in thermal conductivity (groundwater is less conductive than the solid phase), which increased plume length. The opposite effects compensated for each other; however, porosity slightly affected the advection component, and the plume was slightly larger at lower porosities. Ranjan et al. (2004) found that a change in porosity does not lead to a change in the position of the FSI, but only leads to a change in the length of time to achieve the steady state of the interface. However, our results showed that when heat transport is added to the model, porosity could affect the FSI by thermal buoyancy, though only slightly. Analysis of the changes in porosity is, in this case, a theoretical example because in real aquifers, changes in porosity, such as the extremes considered in this study, would likely be associated with changes in hydraulic conductivity that, as has been explained before, could have a strong impact on temperature distribution within the aquifer.

The study model of the Motril-Salobreña aquifer is the first attempt, to our knowledge, of a model including temperature and variable density that is calibrated based on field temperature data. It is a synthetic model of the natural system that consider recharge and the hydraulic gradient constant but with seasonal changes in temperature inputs. Although the results were consistent with observations, there are three aspects that should be clarified with this model. (1) Recharge was assigned continuously, but there were dry periods that could reduce the flow even if there was a dam that regulated river flow upstream. Additionally, recharge from the river to the aquifer was four times less than the recharge estimated in previous studies from the river to the aquifer (Calvache et al., 2009; Duque et al., 2011). However, this model does not simulate all river tracks over the aquifer, and infiltration is higher in the northern stretch of the river, which was not included in the model. (2) The hydraulic gradient has seasonal and interannual oscillations with dry and wet periods that in the model were represented with a mean

value for both cases. (3) For the calibration of K, in line with the sedimentology in the study area (Figure 3.1 C), K was drastically reduced. The hydraulic conductivity value is due to the high topographic gradient (3482 m from the river head to the river mouth) that allows the deposition of coarse sediments. The geological and geometrical characteristics of the aquifer (depth, high K, and hydraulic gradient) are very relevant for the temperature pattern identified.

Comparison of the model results with the field observations showed some differences. The modeled temperature logs in W250 were constant over time (Figure 3.12 A); however, field measurements indicated slight variations at the depth where the FSI was intersected, i.e., at the intersection of the ascendant thermal plume. This contrasts with the field data in W180, where temporal variations were not observed (Figure 3.2). This demonstrates that temperature in the proximity of the FSI was more exposed to changes related to variations in water entry to the aquifer, such as hydraulic gradient or surficial recharge. This hypothesis is reinforced by the sensitivity analysis (Figure 3.9), indicating movement of the FSI on the order of magnitude of hundreds of meters and hence of the thermal plume due to changes in hydraulic gradient. Discrepancies between the model and field data regarding the movement of temperature are then due to the absence of changing recharge and hydraulic gradient in the model, and they can be the object of study in future research.

Oscillation of the recharge temperature allowed us to obtain a time series of temperature at x=285 m (Figure 3.12C) with better fitting than the vertical logs (Figure 3.12 B). Nevertheless, lateral changes in hydraulic conductivity would be needed to achieve a better calibration of the results. This model does not consider lateral changes in hydraulic conductivity that are likely to take place in the study area as it corresponds with a deltaic sedimentary architecture. However, it should be taken into consideration that there are field measurements that have been collected in different years and that climatic conditions are likely to be dissimilar. Therefore, both temperature data and model results must be considered general indicators of trends even if the results have achieved a very high degree of matching between observations and model results.

The recharge temperature was decided based on the average temperature of the air in this region. Nevertheless, for different seasons this temperature changes along the year with colder recharge during winter and warmer in summer. In this region, the temperature changes are relatively mild due to the proximity of the coast, also recharge is almost inexistent during the warmest months of the year. Still, a better characterization of recharge temperatures would be a useful input for further studies on this topic.

Changes in temperature generated by seawater infiltration are an infrequent parameter considered in previous studies. As hypothesized by Kohout (1965), seawater infiltrates the aquifer and is warmed by geothermal heating. However, he assumed a constant temperature. Our results demonstrated that seasonal oscillation of sea temperature created a thermal signal in the aquifer that only affected the saltwater domain. The FSI acts as a barrier for the thermal domains in freshwater, dominated by the temperature associated with the geothermal input and the temperature of the recharge and saltwater, affected by seawater infiltration and the deep processes associated with variable-density convection. Hydraulic conductivity and hydraulic gradient are clearly related favoring the flushing of

the seawater thermal signal due to the upwards fresh groundwater flux near to the FSI. The thermal barrier could be sharper in the case of the Motril-Salobreña aquifer in comparison with other aquifers due to the relatively high hydraulic conductivity and hydraulic gradient. However, temperature separation is also expected in other study areas, although the thermal barrier would be more or less evident depending on the conditions of the area, such as the temperature difference between the aquifer and sea. Temperature variations along the sea water column were not considered in the model; instead, the same value of temperature was established at all depths. Preliminary analysis indicated that other parameters had more influence on the groundwater temperature distribution, however, its impact was not studied in detail due to the limited availability of seawater temperature data in depth. Cross-disciplinary collaboration with both oceanographic and hydrogeologic viewpoints would strengthen the perspectives on this matter as has been highlighted previously (Duque et al., 2020).

Human activities, such as pumping, altered groundwater flow producing saline upconing beneath the pumping area, and enhancing the seawater intrusion. The geometry of the FSI can be modified significantly with this process, as has been the case of the Andarax coastal aquifer (Stein et al., 2020). Given the close connection of the FSI with temperature distribution, human-induced changes can have a direct impact on the heat plume described in this work.

One general issue in the development of groundwater temperature models is how to obtain reliable temperature data. Temperature profiles inside wells can be highly affected by water circulation inside the casing, and even the mixing of water when collecting data can generate problems if this is not performed carefully. This problem has been discussed in previous research that has suggested alternative methods for measuring temperature, such as Shalev et al. (2009), Carrera et al. (2010), and Levanon et al. (2016). Some of the temperature data collected in this investigation have been obtained in similar wells, but systematic collection with monthly campaigns and continued activity for years indicates that the temperature profiles are consistent. For example, Levanon et al. (2017) indicated how these types of measurements show significant trends and prevalent dynamics for salinity. It is not common to find deep wells in coastal areas well equipped for conducting research, and drilling prices are prohibitive; therefore, as long as drilling and measuring technology is in the current state, this type of temperature profile is our best approach for groundwater temperature research. A recent investigation using DTS fiber optic cables allowed us to obtain temperature profiles without flow inside the well (Folch et al., 2020), but still, the depth reached did not exceed 25 m. This also indicates the utility at the moment of the development of numerical models to further scientific knowledge in areas where it is challenging to collect high-quality data, such as sensitivity analysis conducted in this study. Further progress in the development of more realistic models, including lateral heterogeneity and seasonal hydrogeological processes, will contribute to a better knowledge of heat transport processes in coastal aquifers.

6. Conclusions

Heat sources for groundwater in coastal aquifers include surface water recharge, sea infiltration, and geothermal heat. Each source produces a thermal signal within the aquifer, generating changes in temperature at different depths. Recharge water temperature produces a surficial temperature zone that is highly variable throughout the year. Sea water temperature also produces a seasonal temperature oscillation within the saltwater domain. These two sources are affected by seasonal changes, while the Earth's internal heat induces a continuous geothermal gradient within the aquifer that increases with depth. In coastal aquifers, all these factors coalesce in the area where groundwater discharges to the sea. Geothermal heat ascends, boosted by variable-density processes that bring deep aquifer water to the surface where recharge water and sea infiltration all meet, generating a complex mix of different temperatures.

The variable density and temperature transport model using SEAWAT revealed that the effect of the geothermal gradient is strongly dependent on the FSI and that the heat plume ascends following the FSI (i.e., thermal contour of 19°C ascended 100 m in the proximity of the FSI for Kx=300 m/d and Kx/Kz=10). The shape and position of the thermal plume depend on different parameters, e.g. more flattened plumes affected by higher anisotropic ratios with the same values of Kx. In addition, temperature also influences water density; therefore, the FSI can be modified with respect to a model without temperature species. The FSI toe can be moved tens or even hundreds of meters depending on the aquifer properties by using or not using temperature.

The results indicated that the most sensitive parameters are hydraulic conductivity and thermal input at the base of the aquifer. These findings demonstrate the importance of convection on heat transport in an aquifer with these characteristics (high hydraulic conductivities and hydraulic gradient). The changes in parameters open a range of possibilities for research and work in this sector with a view on the application to other study areas.

The case study model integrates the three heat sources into the same model, which provides a better understanding of heat interactions with different origins, as there are no precedents on including all the different temperature sources in coastal aquifers. Furthermore, the model demonstrates the existence of a thermal barrier coinciding with the position of the FSI that separates the temperature of the saltwater and freshwater.

Despite our results are focused on one case study, many of our findings could be applied to other coastal aquifers as the temperature barrier of the FSI, the plume of higher temperature associated with geothermal heat, especially in aquifers with significant thickness, and the presence of different temperature sectors that can be identified at different depths. Still, geological conditions can play a fundamental role in these processes, and aquifers with higher heterogeneity, alternation of layers with high contrast in hydraulic conductivity or different temperature seasonality can generate a picture differing from what has been presented in this work. This is the first attempt at providing a full picture of temperature distribution in coastal aquifers but further research applying a similar methodology to other hydrogeological settings, climatic conditions, and with more focus on the simplified aspects that have been done in this study would help to provide answers to this emerging field of research. The use of heat as a tracer in

hydrogeological studies is growing in interest, as this is a reliable and inexpensive tracer. In this study, we discussed the major processes and the effect of parameters on the application of temperature in coastal aquifers, where a number of processes generate a different picture of what can be found in other coastal or non-coastal settings.

REFERENCES

Abarca, E., Carrera, J., Sánchez-Vila, X., Voss, C.I., 2007. Quasi-horizontal circulation cells in 3D seawater intrusion. J. Hydrol. 339, 118–129. https://doi.org/10.1016/j.jhydrol.2007.02.017

An, Ran, Xiao Wei Jiang, Jun Zhi Wang, Li Wan, Xu Sheng Wang, and Hailong Li., 2015. Analyse Théorique de La Distribution de La Température de L'eau Souterraine à L'échelle D'un Bassin. Hydrogeol. J. 23, 397–404. https://doi.org/10.1007/s10040-014-1197-y

Anderson, M.P., 2005. Heat as a ground water tracer. Groundwater. https://doi.org/10.1111/j.1745-6584.2005.00052.x

Bakker, M., Caljé, R., Schaars, F., Van Der Made, K.J., De Haas, S., 2015. An active heat tracer experiment to determine groundwater velocities using fiber optic cables installed with direct push equipment. Water Resour. Res. 51, 2760–2772. https://doi.org/10.1002/2014WR016632

Bear, J., 1972. Dynamics of Fluids in Porous Media. New York: American Elsevier Publishing Company Inc.

Befus, K.M., Cardenas, M.B., Erler, D.V., Santos, I.R., Eyre, B.D., 2013. Heat transport dynamics at a sandy intertidal zone. Water Resour. Res. 49, 3770–3786. https://doi.org/10.1002/wrcr.20325

Bredehoeft, J.D., Papadopulos, I.S., 1965. Rates of vertical groundwater movement estimated from the Earth's thermal profile. Water Resour. Res. 1, 325–328.

Bridger, D.W., Allen, D.M., 2010. Heat transport simulations in a heterogeneous aquifer used for aquifer thermal energy storage (ATES). Can. Geotech. J. 47, 96–115. https://doi.org/10.1139/T09-078

Calvache, M.L., Duque, C., Gomez Fontalva, J.M., Crespo, F., 2011. Processes affecting groundwater temperature patterns in a coastal aquifer. Int. J. Environ. Sci. Tech 8, 223–236.

Calvache, M.L., Ibáñez, S., Duque, C., Martín-Rosales, W., López-Chicano, M., Rubio, J.C., González, A., Viseras, C., 2009. Numerical modelling of the potential effects of a dam on a coastal aquifer in S. Spain. Hydrol. Process. 23, 1268–1281. https://doi.org/10.1002/hyp.7234

Calvache, M.L., Sánchez-Úbeda, J.P., Duque, C., López-Chicano, M., De La Torre, B., 2015. Evaluation of analytical methods to study aquifer properties with pumping tests in coastal aquifers with numerical modelling (Motril-salobreña aquifer). Water Resour. Manag. 30, 559–575. https://doi.org/10.1007/s11269-015-1177-6

Calvache, M.L., Sánchez-Úbeda, J.P., Purtschert, R., López-Chicano, M.L., Martín-Montañés, C, Sültenfuβ, J., Blanco-Coronas, A.M., Duque, C., 2020. Characterization of the functioning of the Motril–Salobreña coastal aquifer (SE Spain) through the use of environmental tracers. Environ. Earth. Sci. 79, 141. https://doi.org/10.1007/s12665-020-8852-5

Carrera, J., Hidalgo, J.J., Slooten, L.J., Vázquez-Suñé, E., 2010. Computational and conceptual issues in the calibration of seawater intrusion models. Hydrogeol. J. 18, 131–145. http://dx.doi.org/10.1007/s10040-009-0524-1.

Clauser C., 2011. Thermal Storage and Transport Properties of Rocks, I: Heat Capacity and Latent Heat. In: Gupta H.K. (eds) Encyclopedia of Solid Earth Geophysics. Encyclopedia of Earth Sciences Series. Springer, Dordrecht. https://doi.org/10.1007/978-90-481-8702-7_238

Constantz, J., 1998. Interaction between Stream Temperature, Streamflow, and Groundwater Exchanges in Alpine Streams. Water Resour. Res. 34, 7. 1609–15. https://doi.org/10.1029/98WR00998.

Constantz, J., Thomas. C.L., 1997. Stream bed temperature profiles as indicators of percolation characteristics beneath arroyos in the middle Rio Grande Basin, USA. Hydrol. Process., 11, 1621-1634. https://doi.org/10.1002/(SICI)1099-1085(19971015)11:12<1621::AID-HYP493>3.0.CO;2-X

Constantz, J., Thomas, C.L., Zellweger, G., 1994. Influence of diurnal variations in stream temperature on streamflow loss and groundwater recharge, Water Resour. Res., 30 , 3253– 3264, https://doi.org/10.1029/94WR01968

Dausman, A.M., Doherty, J., Langevin, C.D., Sukop, M.C., 2010. Quantifying data worth toward reducing predictive uncertainty. Groundwater 48, 729–740. https://doi.org/10.1111/j.1745-6584.2010.00679.x

Debnath, P., Mukherjee, A., Singh, H.K., Mondal, S., 2005. Delineating seasonal porewater displacement on a tidal flat in the Bay of Bengal by thermal signature: Implications for submarine groundwater discharge. J. Hydrol. 529,1185-1197. https://doi.org/10.1016/j.jhydrol.2015.09.029

deMarsily, G., 1986. Quantitative Hydrogeology: Groundwater Hydrology for Engineers, 440 pp., Academic, Orlando, Fla.

del Val, L., Carrera, J., Pool, M., Martínez, L., Casanovas, C., Bour, O., Folch, A., 2021. Heat Dissipation Test With Fiber-Optic Distributed Temperature Sensing to Estimate Groundwater Flux. Water Resour. Res. 57, 1–18. https://doi.org/10.1029/2020WR027228

Domenico, P.A., Palciauskas. V.V., 1973. Theoretical analysis of forced convective heat transfer in regional groundwater flow. GSA Bulletin 84, 3803–3814. https://doi.org/10.1130/0016-7606(1973)84<3803:TAOFCH>2.0.CO;2

Duque, C., Calvache, M.L., Engesgaard, P., 2010. Investigating river-aquifer relations using water temperature in an anthropized environment (Motril-Salobreña aquifer). J. Hydrol. 381, 121–133. https://doi.org/10.1016/j.jhydrol.2009.11.032

Duque, C., Calvache, M.L., Pedrera, A., Martín-Rosales, W., López-Chicano, M., 2008. Combined time domain electromagnetic soundings and gravimetry to determine marine intrusion in a detrital coastal aquifer (Southern Spain). J. Hydrol. 349, 536–547. https://doi.org/10.1016/j.jhydrol.2007.11.031

Duque, C., Knee, K.L., Russoniello, C.J., Sherif, M., Abu Risha, U.A., Sturchio, N.C., Michael, H.A., 2019. Hydrogeological processes and near shore spatial variability of radium and radon isotopes for the characterization of submarine groundwater discharge. J. Hydrol. 579, 124192. https://doi.org/10.1016/j.jhydrol.2019.124192

Duque, C., López-Chicano, M., Calvache, M.L., Martín-Rosales, W., Gómez-Fontalva, J.M., Crespo, F., 2011. Recharge sources and hydrogeological effects of irrigation and an influent river identified by stable isotopes in the Motril-Salobreña aquifer (Southern Spain). Hydrol. Process. 25, 2261–2274. https://doi.org/10.1002/hyp.7990

Duque, C., Michael, H.A., Wilson, A.M., 2020. The Subterranean Estuary: Technical Term, Simple Analogy, or Source of Confusion? Water Resour. Res. 56, 1–7. https://doi.org/10.1029/2019WR026554

Duque, C., Muller, S., Sebok, E., Haider, K., Engesgaard, P., 2016. Estimating groundwater discharge to surface waters using heat as a tracer in low flux environments: The role of thermal conductivity. Hydrol. Process. 30, 383-395. https://doi.org/10.1002/hyp.10568

Duque, C., Olsen, J.T., Sánchez-Úbeda, J.P., Calvache, M.L., 2018. Paleohydrogeological Model of the Groundwater Salinity in the Motril-Salobreña Aquifer. In: Calvache M., Duque C., Pulido-Velazquez D. (eds) Groundwater and Global Change in the Western Mediterranean Area. Environmental Earth Sciences. Springer, Cham. https://doi.org/10.1007/978-3-319-69356-9_14

Eissa, M.A., de Dreuzy, J.R., Parker, B., 2018. Integrative management of saltwater intrusion in poorly-constrained semi-arid coastal aquifer at Ras El-Hekma, Northwestern Coast, Egypt. Groundw. Sustain. Dev. 6, 57–70. https://doi.org/10.1016/j.gsd.2017.10.002

Engelhardt, I., Prommer, H., Moore, C., Schulz, M., Schüth, C., Ternes, T.A., 2013. Suitability of temperature, hydraulic heads, and acesulfame to quantify wastewater-related fluxes in the hyporheic and riparian zone. Water Resour. Res. 49, 426–440. https://doi.org/10.1029/2012WR012604

Ferguson, G., 2007. Heterogeneity and Thermal Modeling of Ground Water. Ground Water 45, 485–490. https://doi.org/10.1111/j.1745-6584.2007.00323.x

Folch, A., del Val, L., Luquot, L., Martínez-Pérez, L., Bellmunt, F., Le Lay, H., Rodellas, V., Ferrer, N., Palacios, A., Fernández, S., Marazuela, M.A., Diego-Feliu, M., Pool, M., Goyetche, T., Ledo, J., Pezard, P., Bour, O., Queralt, P., Marcuello, A., Garcia-Orellana, J., Saaltink, M.W., Vázquez-Suñé, E., Carrera, J., 2020. Combining fiber optic DTS, cross-hole ERT and time-lapse induction logging to characterize and monitor a coastal aquifer. J. Hydrol. 588, 125050. https://doi.org/10.1016/j.jhydrol.2020.125050

Forster, C., Smith, L., 1989. The influence of groundwater flow on thermal regimes in mountainous terrain: A model study, J. Geophys. Res., 94, 9439– 9451. https://doi.org/10.1029/JB094iB07p09439

Freeze, R. A., Cherry, J. A., 1979. Groundwater. Prentice-Hall. Inc. Englewood Cliffs, N.J.

Glover, R.E., 1959. The pattern of fresh-water flow in a coastal aquifer. J. Geophys. Res., 64, 457–459. https:// doi.org/10.1029/JZ064i004p00457.

Harbaugh, A.W., Banta, E.R., Hill, M.C., Mcdonald, M.G., 2000. MODFLOW-2000, The U.S. Geological Survey modular ground-water model user guide to modularization concepts and the ground-water flow procesS, Geological Survey. CO McDonald Morrissey Associates.

Henry, H.R., Kohout, F.A., 1972. Circulation patterns of saline groundwater affected by geothermal heating as related to waste disposal. In: Underground Water Management and Environmental Implications, Amer Assoc Pet Geol, Memoir 18, pp. 202-221.

Hopmans, J.W., Šimunek, J., Bristow, K.L., 2002. Indirect estimation of soil thermal properties and water flux using heat pulse probe measurements: Geometry and dispersion effects. Water Resour. Res. 38, 7-1-7–14. https://doi.org/10.1029/2000wr000071

Hughes, J.D., Vacher, H.L., Sanford, W.E., 2007. Three-dimensional flow in the Florida platform: Theoretical analysis of Kohout convection at its type locality. Geology 35, 663–666. https://doi.org/10.1130/G23374A.1.

Ingebritsen, S.E., Sanford, W.E., 1998. Groundwater in Geologic Processes. Cambridge, UK: Cambridge University Press.

Jabaloy-Sánchez, A., Lobo, F.J., Azor, A., Martín-Rosales, W., Pérez-Peña, J.V., Bárcenas, P., Macías, J., Fernández-Salas, L.M., Vázquez-Vílchez, M., 2014. Six thousand years of coastline evolution in the Guadalfeo deltaic system (southern Iberian Peninsula). Geomorphology 206, 374–391. https://doi.org/10.1016/j.geomorph.2013.08.037

Keery, J., Binley, A., Crook, N., Smith, J.W.N., 2007. Temporal and spatial variability of groundwater-surface water fluxes: Development and application of an analytical method using temperature time series. J. Hydrol. 336, 1-16. https://doi.org/10.1016/j.jhydrol.2006.12.003

Keys, W.S., MacCary. L.M., 1971. Application of borehole geophysics to water-resources investigations. In Techniques of Water Resources Investigations, Book 2, chap. E1. Washington, DC: USGS.

Kim, K.Y., Chon, C.M., Park, K.H., Park, Y.S., Woo, N.C., 2008. Multi-depth monitoring of electrical conductivity and temperature of groundwater at a multilayered coastal aquifer: Jeju Island, Korea. Hydrol. Process. 22, 3724–3733. https://doi.org/10.1002/hyp.6976

Kim, K.Y., Park, Y.S., Kim, G.P., Park, K.H., 2009. Dynamic freshwater-saline water interaction in the coastal zone of Jeju Island, South Korea. Hydrogeol. J. 17, 617–629. https://doi.org/10.1007/s10040-008-0372-4

Kinnear, J.A., Binley, A., Duque, C., Engesgaard, P.K., 2013. Using geophysics to map areas of potential groundwater discharge into Ringkøbing Fjord, Denmark. Lead. Edge. 32. https://doi.org/10.1190/tle32070792.1

Kohout, F.A., 1964. The flow of fresh water and salt water in the Biscayne aquifer of the Miami area, Florida. In: sea water in coastal aquifers: U.S.G.S. Water-Supply, 1613, 12– 32.

Kohout, F.A., 1965. Section of geological sciences: a hypothesis concerning cyclic flow of salt water related to geothermal heating in the Floridan aquifer. Trans. N. Y. Acad. Sci. 28, 249–271. https://doi.org/10.1111/j.2164-0947.1965.tb02879.x

Kohout, F.A., 1967. Groundwater flow and the geothermal regime of the Floridan Plateau. Trans Gulf Coast Assoc Geol Soc 17: 339-354

Kohout, F.A., Henry, H., Banks, J., 1977. Hydrogeology related to geothermal conditions of the Floridan Plateau. In: Smith D, Grien G (eds) The geothermal nature of the Floridan Plateau. Florida Dept Nat Resour Spec Publ 21 pp. 1-41

Kurylyk, B.L., Bourque, C.P.-A., MacQuarrie, K.T.B., 2013. Potential surface temperature and shallow groundwater temperature response to climate change: an example from a small forested catchment in east-central New Brunswick (Canada). Hydrol. Earth Syst. Sci. Discuss. 10, 3283–3326. https://doi.org/10.5194/hessd-10-3283-2013

Kurylyk, B.L., Irvine, D.J., Bense, V.F., 2019. Theory, tools, and multidisciplinary applications for tracing groundwater fluxes from temperature profiles. Wiley Interdiscip. Rev. Water 6, e1329. https://doi.org/10.1002/wat2.1329

Langevin, C.D., Dausman, A.M., Sukop, M.C., 2010. Solute and heat transport model of the Henry and Hilleke laboratory experiment. Groundwater 48, 757–770. https://doi.org/10.1111/j.1745-6584.2009.00596.x

Langevin, C.D., Dausman, A.M., Thorne, D., Sukop., M.C., 2008. Modeling solute and heat transport with SEAWAT. In MODFLOW and More 2008: Ground Water and Public Policy–Conference Proceedings, Golden, Colorado, 19–21 May 2008.

Langevin, C.D., Thorne , D.T., Dausman, A.M., Sukop, M.C., Guo. W., 2007. SEAWAT Version 4: A Computer Program for Simulation of multi-species Solute and Heat Transport. U.S. Geological Survey Techniques and Methods. book 6, chap. A22 Reston, Virginia: USGS.

Lautz, L.K., 2012. Observing temporal patterns of vertical flux through streambed sediments using time-series analysis of temperature records. J. Hydrol. 464–465, 199-215. https://doi.org/10.1016/j.jhydrol.2012.07.006

Levanon, E., Shalev, E., Yechieli, Y., Gvirtzman, H., 2016. Advances in Water Resources Fluctuations of fresh-saline water interface and of water table induced by sea tides in unconfined aquifers. Adv. Water Resour. 96, 34–42. https://doi.org/10.1016/j.advwatres.2016.06.013

Levanon, E., Yechieli, Y., Gvirtzman, H., Shalev, E., 2017. Tide-induced fluctuations of salinity and groundwater level in unconfined aquifers – Field measurements and numerical model. J. Hydrol. 551, 665–675. https://doi.org/10.1016/j.jhydrol.2016.12.045

Limberger, J., Boxem, T., Pluymaekers, M., Bruhn, D., Manzella, A., Calcagno, P., Beekman, F., Cloetingh, S., van Wees, J.D., 2018. Geothermal energy in deep aquifers: A global assessment of the resource base for direct heat utilization. Renew. Sustain. Energy Rev. https://doi.org/10.1016/j.rser.2017.09.084

Liu, J., Du, J., Yu, X., 2021. Submarine groundwater discharge enhances primary productivity in the Yellow Sea, China: Insight from the separation of fresh and recirculated components. Geosci. Front. 12, 101204. https://doi.org/10.1016/j.gsf.2021.101204

Ma, R., Zheng, C., Zachara, J.M., Tonkin, M., 2012. Utility of bromide and heat tracers for aquifer characterization affected by highly transient flow conditions. Water Resour. Res. 48. https://doi.org/10.1029/2011WR011281

Manca, B., Burca, M., Giorgetti, A., Coatanoan, C., García, M.J., Iona, A. 2004. Physical and biochemical averaged vertical profiles in the Mediterranean regions: an important tool to trace the climatology of water masses and to validate incoming data from operational oceanography. 48, 83-116.

McCallum, A.M., Andersen, M.S., Rau, G.C., Larsen, J.R., Acworth, R.I., 2014. Investigated Using Point and Reach Measurements. Water Resour. Res. 2815–2829. https://doi.org/10.1002/2012WR012922

Molina, L., Vallejos, A., Pulido-Bosch, A., Sánchez-Martos, F., 2002. Water temperature and conductivity variability as indicators of groundwater behaviour in complex aquifer systems in the south-east of Spain. Hydrol. Process. 16, 3365–3378. https://doi.org/10.1002/hyp.1105

Molina-Giraldo, N., Bayer, P., Blum, P., 2011. Evaluating the influence of thermal dispersion on temperature plumes from geothermal systems using analytical solutions. Int. J. Therm. Sci. 50, 1223–1231. https://doi.org/10.1016/j.ijthermalsci.2011.02.004

Ranjan, S.P., Kazama, S., Sawamoto, M., 2004. Modeling of the dynamics of saltwater–freshwater, interface in coastal aquifers. In: Proceedings of the joint AOGS annual meeting & APHW second conference. Singapore. 373–380.

Panteli, N.M., 2018. Assessment of the effect of groundwater flow on the performance of Borehole Thermal Energy Storage systems. MS thesis, Delft University of Technology, 59 p.

Park, B.H., Bae, G.O., Lee, K.K., 2015. Importance of thermal dispersivity in designing groundwater heat pump (GWHP) system: Field and numerical study. Renew. Energy 83, 270–279. https://doi.org/10.1016/j.renene.2015.04.036

Parsons, M.L., 1970. Groundwater thermal regime in a glacial complex. Water Resour. Res. 6, 1701–172.

Piga, B., Casasso, A., Pace, F., Godio, A., Sethi, R., 2017. Thermal impact assessment of groundwater heat pumps (GWHPs): Rigorous vs. simplified models. Energies 10. https://doi.org/10.3390/en10091385

Pollack, H.N., Huang, S., 2000. Climate Reconstruction from Subsurface Temperatures, Annu. Rev. Earth Planet. Sci. 28, 339-365. https://doi.org/10.1146/annurev.earth.28.1.339

Pollack, H.N., Smerdon, J.E., van Keken, P.E., 2005. Variable seasonal coupling between air and ground temperatures: A simple representation in terms of subsurface thermal diffusivity. Geophys. Res. Lett. 32. https://doi.org/10.1029/2005GL023869

Rorabaugh, M.I., 1956. Groundwater in northeastern Louisville, Kentucky with reference to induced infiltration. Water-Supply Paper 1360-B. Washington, DC: USGS.

Rushton, K., 2007. Representation in regional models of saturated river-aquifer interaction for gaining/losing rivers. J. Hydrol. 334, 262–281. https://doi.org/10.1016/j.jhydrol.2006.10.008 Sánchez-Úbeda, J.P., Calvache, M.L., Engesgaard, P., Duque, C., López-Chicano, M., Purtschert, R., 2018a. Numerical Modeling of Groundwater Age Distribution in Motril-Salobreña Coastal Aquifer (SE Spain). In: Calvache M., Duque C., Pulido-Velazquez D. (eds) Groundwater and Global Change in the Western Mediterranean Area. Environ. Earth Sci. Springer, Cham. https://doi.org/10.1007/978-3-319-69356-9_32

Sánchez-Úbeda, J.P., López-Chicano, M., Calvache, M.L., Purtschert, R., Engesgaard, P., Martín-Montañés, C., Sültenfuβ, J., Duque, C., 2018b. Groundwater Age Dating in Motril-Salobreña Coastal Aquifer with Environmental Tracers (δ18O/δ2H, 3H/3He, 4He, 85Kr, and 39Ar). In: Calvache M., Duque C., Pulido-Velazquez D. (eds) Groundwater and Global Change in the Western Mediterranean Area. Environ. Earth Sci. Springer, Cham. https://doi.org/10.1007/978-3-319-69356-9_33

Sebok, E., Duque, C., Engesgaard, P., Boegh, E., 2015. Application of Distributed Temperature Sensing for coupled mapping of sedimentation processes and spatio-temporal variability of groundwater discharge in soft-bedded streams. Hydrol. Process. 29, 3408–3422. https://doi.org/10.1002/hyp.10455

Schärli, U. and Rybach, L., 2001. Determination of specific heat capacity on rock fragments. Geothermics, 30, 1 93-110. https://doi.org/10.1016/S0375-6505(00)00035-3

Shalev, E., Lazar, A., Wollman, S., Kington, S., Yechieli, Y., Gvirtzman, H., 2009. Biased monitoring of fresh water-salt water mixing zone in coastal aquifers. Ground Water 47, 49–56. http://dx.doi.org/10.1111/j.1745-6584.20 08.0 0502.x

Silliman, S.E., Booth, D.F., 1993. Analysis of time-series measurements of sediment temperature for identification of gaining vs. losing portions of Juday Creek, Indiana, J. of Hydrol., 146, 131-148. https://doi.org/10.1016/0022-1694(93)90273-C

Smerdon, J.E., Pollack, H.N., Enz, J.W., Lewis, M.J., 2003. Conduction-dominated heat transport of the annual temperature signal in soil. J. Geophys. Res. Solid Earth 108. https://doi.org/10.1029/2002jb002351

Smith, L., Chapman., D.S., 1983. On the thermal effects of groundwater flow 1. Regional scale systems. J. Geophys. Res. 88, 593–608. https://doi.org/10.1029/JB088iB01p00593

Stallman, R.W., 1963. Computation of ground-water velocity from temperature data. In: Methods of Collecting and Interpreting Ground-Water Data, ed. R. Bentall, 36–46. Water Supply Paper 1544-H. Washington, DC: USGS.

Stallman, R.W., 1965. Steady one-dimensional fluid flow in a semi-infinite porous medium with sinusoidal surface temperature. J. Geophys. Res. 70, 12, 2821–2827. https://doi.org/10.1029/JZ070i012p02821

Stauffer, F., Bayer, P., Blum, P., Giraldo, N., Kinzelbach, W., 2014. Thermal Use of Shallow Groundwater. Boca Raton: CRC Press, https://doi.org/10.1201/b16239

Stein, S., Sola, F., Yechieli, Y., Shalev, E., Sivan, O., Kasher, R., Vallejos, A., 2020. The effects of long-term saline groundwater pumping for desalination on the fresh – saline water interface: field observations and numerical modeling. Sci. Total Environ. 732, 139249. https://doi.org/10.1016/j.scitotenv.2020.139249.

Suzuki, S., 1960. Percolation measurements based on heat flow through soil with special reference to paddy fields. J. Geophys. Res. 65, 2883–2885. https://doi.org/10.1029/JZ065i009p02883

Szijártó, M., Galsa, A., Tóth, Á., Mádl-Szőnyi, J., 2019. Numerical investigation of the combined effect of forced and free thermal convection in synthetic groundwater basins. J. Hydrol. 572, 364–379. https://doi.org/10.1016/j.jhydrol.2019.03.003

Taniguchi, M., Shimada, J., Tanaka, T., Kayane, I., Sakura, Y., Shimano, Y., Dapaah-Siakwan, S., Kawashima, S., 1999. Disturbances of temperature-depth profiles due to surface climate change and subsurface water flow: 1. An effect of linear increase in surface temperature caused by global warming and urbanization in the Tokyo metropolitan area, Japan. Water Resour. Res. 35, 1507–1517. https://doi.org/10.1029/1999WR900009

Taniguchi, M., 2000. Evaluations of the saltwater-groundwater interface from borehole temperatura in a coastal region. Geophys. Res. Lett. 27, 713-716.

Thorne, D., Langevin, C.D., Sukop, M.C., 2006. Addition of simultaneous heat and solute transport and variable fluid viscosity to SEAWAT. Comput. Geosci. 32, 1758–1768. https://doi.org/10.1016/j.cageo.2006.04.005

Tirado-Conde, J., Engesgaard, P., Karan, S., Müller, S., Duque, C., 2019. Evaluation of temperature profiling and seepage meter methods for quantifying submarine groundwater discharge to coastal lagoons: Impacts of saltwater intrusion and the associated thermal regime. Water. 11, 1648. https://doi.org/10.3390/w11081648

Tóth, J., 1962. A theory of groundwater motion in small basins in central Alberta, Canada. J. Geophys. Res., 67, 4375–43787. https://doi.org/10.1029/JZ067i011p04375

Vandenbohede, A., Lebbe, L., 2011. Heat transport in a coastal groundwater flow system near De Panne, Belgium. Hydrogeol. J. 19, 1225–1238. https://doi.org/10.1007/s10040-011-0756-8

Vandenbohede, A., Louwyck, A., Lebbe, L., 2009. Conservative solute versus heat transport in porous media during push-pull tests. Transp. Porous Media 76, 265–287. https://doi.org/10.1007/s11242-008-9246-4

Vandenbohede, A., Van Houtte, E., 2012. Heat transport and temperature distribution during managed artificial recharge with surface ponds. J. Hydrol. 472–473, 77–89. https://doi.org/10.1016/j.jhydrol.2012.09.028

Walther, M., Graf, T., Kolditz, O., Liedl, R., Post, V., 2017. How significant is the slope of the sea-side boundary for modelling seawater intrusion in coastal aquifers? J. Hydrol. 551, 648–659. https://doi.org/10.1016/j.jhydrol.2017.02.031

Woodbury, A.D., Smith. L., 1988. Simultaneous inversion of hydrogeologic and thermal data, 2. Incorporation of thermal data. Water Resour. Res. 23, 356–372. https://doi.org/10.1029/WR024i003p00356

Xiaoqing, S., Ming, J., Peiwen, X., 2018. Analysis Of The Thermophysical Properties And Influencing Factors Of Various Rock Types From The Guizhou Province, in: E3S Web of Conferences. EDP Sciences. https://doi.org/10.1051/e3sconf/20185303059.

Zhang, Y., Li, H., Guo, H., Zheng, C., Wang, X., Zhang, M., Xiao, K., 2020. Improvement of evaluation of water age and submarine groundwater discharge: A case study in Daya Bay, China. J. Hydrol. 586, 124775. https://doi.org/10.1016/j.jhydrol.2020.124775

Zheng, C., Wang., P.P., 1999. MT3DMS—A modular three-dimensional multispecies transport model for simulation of advection, dispersion and chemical reactions of contaminants in groundwater systems: Documentation and user's guide. U.S. Army Corps of Engineers Contract Report SERDP-99-1.

CHAPTER 4
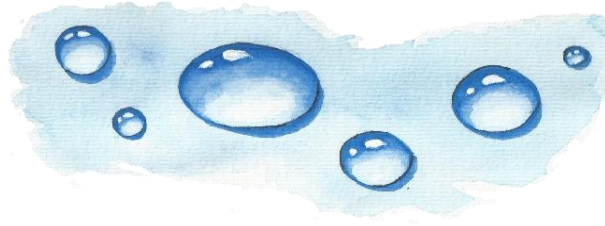
Salinity and Temperature Variations near the Freshwater-Saltwater Interface in Coastal Aquifers Induced by Ocean Tides and Changes in Recharge

Angela M. Blanco-Coronas[1], Maria L. Calvache[1,2], Manuel López-Chicano[1,2], Crisanto Martín-Montañés[3], Jorge Jiménez-Sánchez[3] and Carlos Duque[1,4]

[1] Departamento de Geodinámica, Universidad de Granada, Avenida Fuente Nueva s/n., 18071 Granada, Spain

[2] Instituto del Agua, Universidad de Granada, Calle Ramón y Cajal 4, Edificio Fray Luis, 18003 Granada, Spain

[3] CN-Instituto Geológico y Minero de España (IGME-CSIC), Unidad de Granada, Urb. Alcázar del Genil, 4 Edificio Zulema, Bajo, 18006 Granada, Spain

[4] Department of Geosciences, University of Oslo, Sem Sælands vei 1, 0371 Oslo, Norway

Abstract

The temperature distribution of shallow sectors of coastal aquifers are highly influenced by the atmospheric temperature and recharge. However, geothermal heat or vertical fluxes due to the presence of the saline wedge have more influence at deeper locations. In this study, using numerical models that account for variable density, periodic oscillations of temperature have been detected, and their origin has been attributed to the influence exerted by recharge and tides. The combined analysis of field data and numerical models showed that the alternation of dry and wet periods modifies heat distribution in deep zones (>100 m) of the aquifer. Oscillations with diurnal and semidiurnal frequencies have been detected for groundwater temperature, but they show differences in terms of amplitudes and delay with electrical conductivity (EC). The main driver of the temperature oscillations is the forward and backward displacement of the freshwater–saltwater interface, and the associated thermal plume generated by the upward flow from the aquifer basement. These oscillations are amplified at the interfaces between layers with different hydraulic conductivity, where thermal contours are affected by refraction.

Keywords

_____

1. Introduction

Coastal aquifers are characterized by the influence of tides that generate periodic changes in the groundwater table (Nielsen, 1990; Li et al., 2000). The study of tidal influences has allowed the authors to determine hydraulic properties (Rotzoll et al., 2013; Xun et al, 2015) and identify tens of tidal constituents with different fluctuation frequencies and amplitudes (Pawlowicz et al., 2002). Semidiurnal and diurnal frequencies, as well as fortnightly components, are the most important constituents in groundwater head time series measured in unconsolidated aquifers (Levanon et al., 2013; Sánchez-Úbeda et al., 2018). The amplitude of the fluctuation decreases exponentially with the distance from the shoreline (Carr and Kamp, 1969; Erskine, 1991), while the time-lag between the sea level and the water table increases (Nielsen, 1990; Raubenheimer et al., 1999).

The effect of tidal oscillations on the freshwater–saltwater interface (FSI) has been the subject of far fewer studies. Sea tides impact the width of the FSI and groundwater discharge (Robinson et al., 1998; Urish and McKenna, 2004; Heiss and Michael, 2014). Ataie-Ashtiani et al. (1999) showed that tidal oscillations favor seawater intruding further inland and result in a wider FSI than what would occur from the tidal effect alone. La Licata et al. (2011) compared the results of solute transport in the transition zone with and without tidal effects, concluding that contaminant and salinity concentration are more mixed under the influence of tidal variations. Using numerical simulations, Robinson et al. (2007) demonstrated that inland (freshwater discharge) and oceanic (tidal) forces

strongly affect mixing processes. Pool et al. (2014) showed that the impact of the tides depends largely on tidal amplitude, tidal period, and hydraulic diffusivity. Levanon et al. (2017) found a correlation between the time lags of the groundwater table and oscillations in salinity, indicating a simultaneous movement of the entire freshwater body. Yu et al. (2019) identified high-frequency tidal constituents (M2, S2, K1, and N2) but also lower frequency signals, which affected the recirculation cell at beaches and at the saltwater wedge. All the above studies used different methods to investigate the effect of tidal oscillations on the groundwater table and the FSI. However, the influence of tidal fluctuations on groundwater temperature has received considerably less attention. Most temperature studies are focused on the temperature variations in the first upper meters of the aquifer (Pollock and Hummon, 1971; Li et al., 2006; Vandenbohede and Lebbe, 2011), which are caused by the interaction between temperature, infiltrated seawater, fresh groundwater, and vertical heat conduction from the surface. Geng and Boufadel (2017) compared the response of pore water salinity and temperature to tidal signals in the intertidal zone of two beaches in Alaska. Nguyen et al. (2020) studied the effect of temperature on the flow, salinity distribution, and circulating seawater flux through laboratory experiments and numerical simulations subjected to tides. There are a few studies dealing with groundwater thermal oscillations produced in areas different from the surficial zone of the aquifer, where the infiltrated seawater cannot generate temperature variations. Kim et al. (2008; 2009) detected small variations in temperature, measured at depths of up to 120 m, which are produced by the force of tidal fluctuations, but they also found significant temperature changes coinciding with seasonal rainfall. Vallejos et al. (2015) identified the response of electrical conductivity (EC) and temperature to tidal cycles at a depth of 65 m. The scarcity of research dealing with temperature oscillations in deep areas of the FSI is related to the difficulty of finding deep wells in coastal aquifers that are well equipped for conducting research, the lack of data available associated with it, and prohibitive drilling prices only for research purposes, as wells in saltwater do not have a practical purpose. Other reasons are the complexity of measuring equipment specifically for salty water and high pressure, as well as the need for multiple piezometers to measure at different depths. In this sense, there is only a theoretical model for the heat distribution of coastal aquifers, considering all possible sources of heat simultaneously (Blanco-Coronas et al., 2021a).

The use of heat as a groundwater tracer is a useful tool in the estimation of groundwater fluxes (Anderson, 2005), but in coastal aquifers, it can also be applied to gauge the state of advancement of seawater intrusion (Del Val, 2020). Taniguchi (2000) monitored the dynamics of the FSI using vertical profiles of temperature. Fidelibus and Pulido-Bosch (2019) demonstrated that the trend of the isotherms in a karstic aquifer indicated the position of the saltwater and hence reflected groundwater vulnerability to salinization. Blanco-Coronas et al. (2021a) showed that when groundwater systems are affected by geothermal warming, an ascending thermal plume is generated relative to the position of the FSI. However, only LeRoux et al. (2021) connected the distribution of temperature in the aquifer with the tides. All these studies highlighted the applicability of heat as a natural tracer in coastal settings, the differences with noncoastal settings, and the usefulness of establishing thermal patterns in coastal aquifers.

Below the zone of surface temperature influence, groundwater temperature generally increases with depth due to the geothermal gradient (Parsons, 1970), which is unaffected

by seasonal variations (Anderson, 2005), although thermal trends can be reversed due to surface warming induced by climate change (Kurylyk et al., 2019). In discharge areas, the geothermal gradient in groundwater can be disturbed by the groundwater flow pattern (Tóth, 1962; Domenico and Palciauskas, 1973; An et al., 2015; Szijártó et al., 2019). The temperature distribution in coastal aquifers is defined by the interaction between different heat sources, such as sea water intrusion and surface water recharge (Befus et al., 2013; Tirado-Conde et al., 2019), but also by geothermal heating, especially when aquifers reach depths of over 100 m. The groundwater flow near the submarine freshwater discharge zone produces a warm thermal upwelling (Figure 4.1). This phenomenon occurs when freshwater heated at the bottom of the aquifer is forced to ascend towards the sea due to the presence of the saline wedge. This rising of heated freshwater causes a thermal plume that is dependent on the position and shape of the FSI (Blanco-Coronas et al., 2021a). Simultaneously, the difference in temperature between the top and the bottom of the aquifer produces changes in the width of the FSI and the position of its toe.

The goal of this work was to study the processes that occur in coastal aquifers at depths greater than 100 m by (1) determining how temperature oscillations are induced by tidal oscillations, (2) identifying the role played by aquifer recharge variation due to seasonal changes, and (3) comparing temperature and salinity oscillations. For this purpose, EC and temperature oscillations measured in a 250 m deep well near the coastline in the Motril-Salobreña aquifer (Spain) were compared to sea level and hydraulic head fluctuations. Since field data were limited to one single point, a numerical model was constructed in order to study other factors that might have affected temperature and EC.
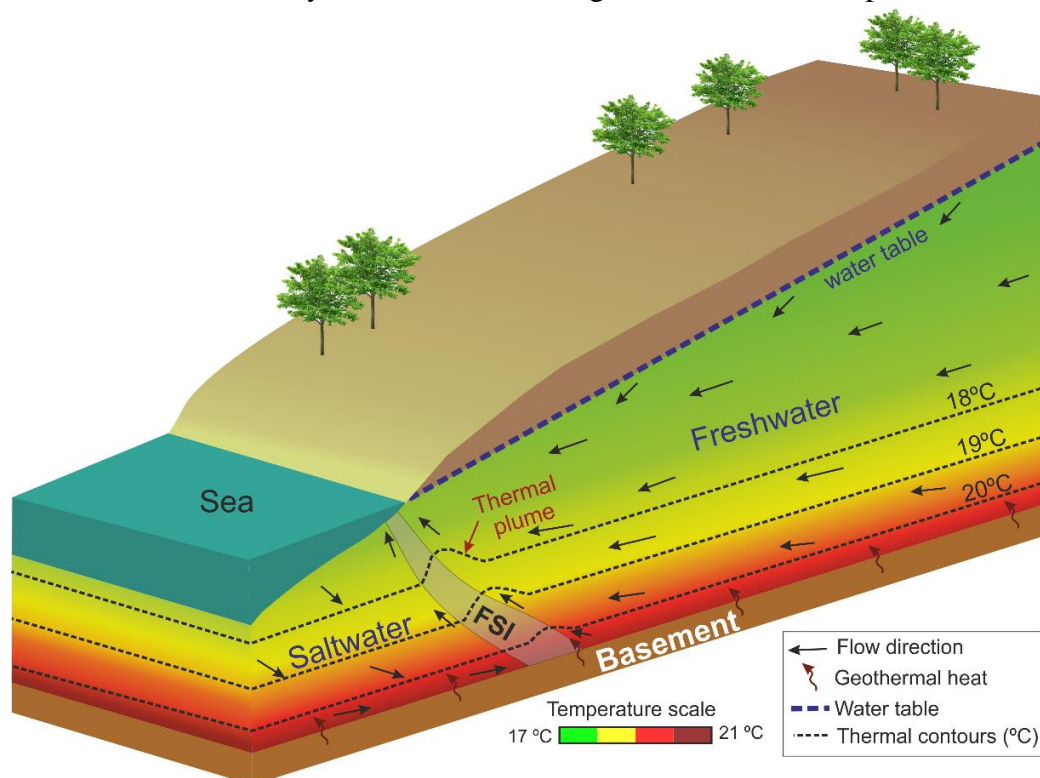

Figure 4.1.- Simplified schematic diagram of temperature distribution of a coastal aquifer affected by the geothermal gradient.

2. Study Area and Hydrogeological Setting

The Motril-Salobreña aquifer is located along the coast of the Mediterranean Sea in southeastern Spain (Figure 4.2). It extends over 42 km^2, and its thickness varies from 30 to 50 m in the northernmost sector to more than 250 m in the southern sector (Calvache et al., 2009). The aquifer is composed of Quaternary detrital sediments with highly variable grain sizes (gravels, sands, and silts), which lie over an impermeable basement of metapelitic materials (schists and phyllites). The hydraulic conductivity of the materials is highly variable, ranging from 1 to 300 m/d (Calvache et al., 2009; Duque, 2009), due to their fluvio-deltaic depositional environment.

The general flow direction in the aquifer is from north to south toward the Mediterranean Sea. The horizontal hydraulic gradients range between 1.6×10^{-3} and 7×10^{-3} (Duque et al., 2010; Blanco-Coronas et al., 2021b).

The main recharge of the aquifer is produced by irrigation return flows from agricultural activity, with water previously uptaken from the river, and direct infiltration along the Guadalfeo River course (Calvache et al., 2009; Duque et al., 2011). The Guadalfeo River is characterized by being influent in its upper sector, causing important fluctuations in the water table related to dry and wet periods and by being effluent in the sector near the coastline (Duque et al., 2010). Other minor recharges occur at groundwater lateral inlets and are due to rainfall infiltration (Calvache et al., 2009). The main outlet of the aquifer is groundwater discharge from the aquifer to the sea (Calvache et al., 2009).
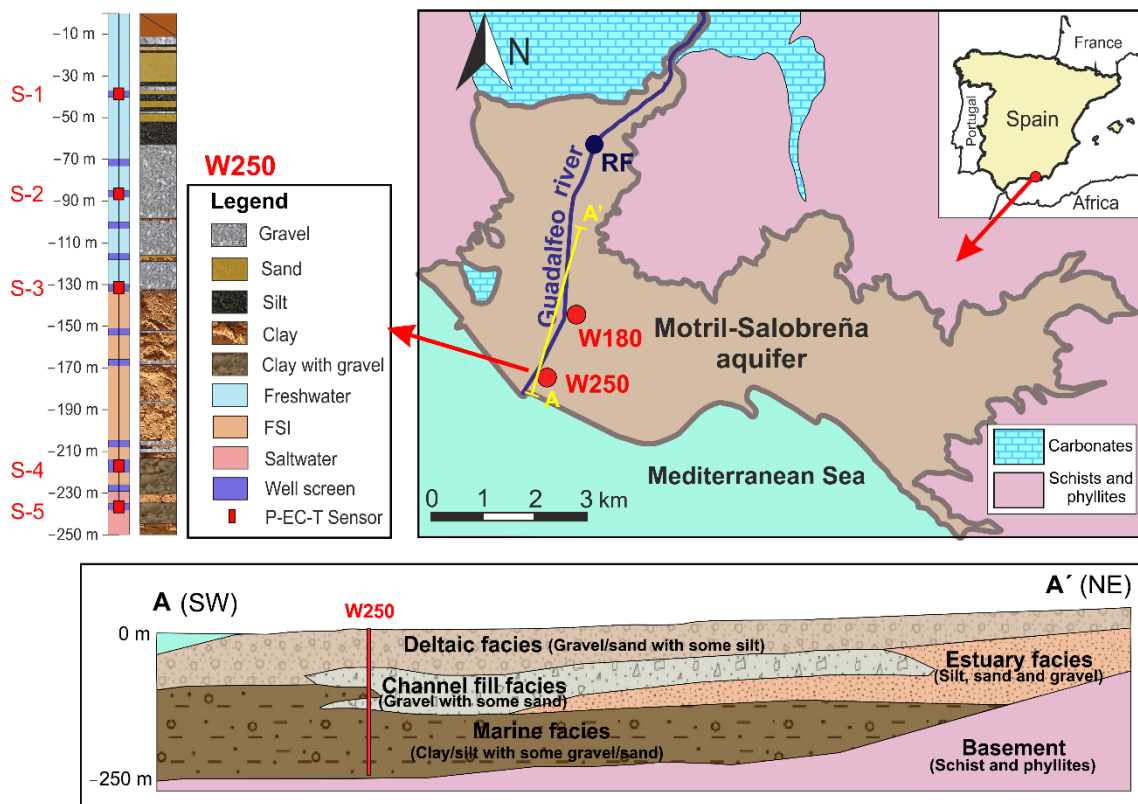

Figure 4.2.- Location of the Motril-Salobreña aquifer, research boreholes, and the measurement point of the river flow (RF). Cross section of the depositional environments at the study area (modified from Olsen et al., 2016).

The climate of the area is Mediterranean dry with mean air temperatures around 18°C and average precipitation of 400 mm/year. The catchment of the Guadalfeo River extends itself over 1290 km^2 and drains the southern slopes of the Sierra Nevada. The highest mountain peak reaches an elevation of 3482 m, and the average annual precipitation is more than 1000 mm in that area. The hydrologic regime of the Guadalfeo River is pluvio-nival with maximum flows reached from April to June. Upstream from the Motril-Salobreña aquifer (10 km), the Rules Dam interrupts the Guadalfeo River flow. The Motril-Salobreña aquifer has not shown any signs of marine intrusion yet, and the saline wedge does not penetrate more than 500 m (Duque et al., 2008; Calvache et al., 2009).

The groundwater temperature distribution in the aquifer shows three thermal zones (Calvache et al., 2011) based on temperature profiles (Figure 4.3): (1) a surficial zone, where temperature changes due to surface water recharge and air temperature changes; (2) an intermediate zone with a relatively constant temperature of 17.2°C; and (3) a deep zone characterized by a constant increase in temperature of 0.02°C per meter due to geothermal heat. The research area was located in the southern part of the coastal aquifer, in the discharge zone towards the sea. A well 250 m deep (W250) was drilled 300 m from the coastline, which has 12 screens, between 3 to 6 m in length, at different depths (Figure 4.2). The well is artesian and had an average flow of 0.018 m^3/s at the time of its opening, providing evidence of upward vertical flow in this area of the aquifer (Calvache et al., 2015). The well intersects the FSI and the three temperature zones described above. Previous studies showed fluctuations in groundwater head attributed to tidal forces (Sánchez-Úbeda et al., 2018; Sánchez-Úbeda et al., 2016).
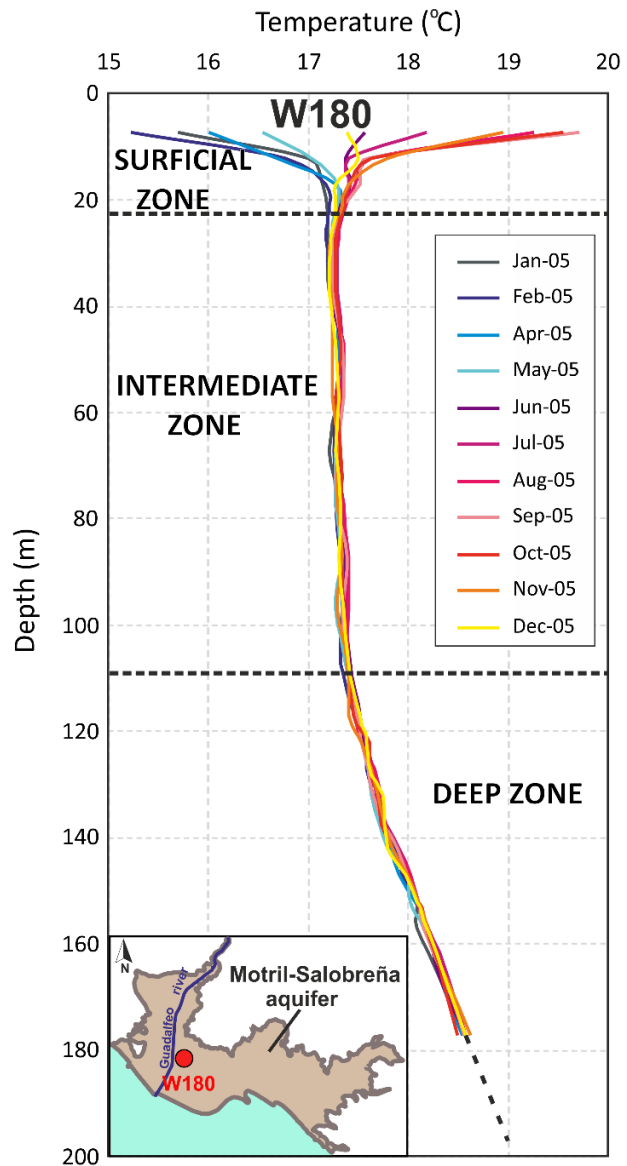

Figure 4.3.- Vertical temperature profiles measured in the Motril-Salobreña aquifer, obtained from the observation well W180 located in Figure 4.2.

3. Methodology

To study the factors that influence the distribution of temperature near the FSI, vertical logs of continuous hydraulic head, EC, and temperature data were collected at different depths of a multi-screened borehole over 1 year (W250) (Figure 4.2). A flowmeter was used to assess the direction and intensity of water circulation inside well W250. The hydraulic head and temperature values at different depths were compared with the Guadalfeo River flow and precipitation to determine their correlation with seasonal variations. Statistical analyses were applied to study temperature and EC changes related to the tidal cycle. A numerical model was constructed to test the information obtained from the field data and to simulate different scenarios to understand how changes in the water table and sea tides affect the groundwater temperature at depths of >100 m.

3.1. Field Monitoring

Hourly data of pressure, EC, and temperature were obtained with five Aqua TROLL 200 Data Loggers (In-situ, Inc. Fort Collins, CO, USA) during 2018. The EC sensor accuracy was ±0.5% of the reading, with a resolution of 0.1 µS/cm and the temperature sensor accuracy was ± 0.1°C, with a resolution 0.01°C. Two sensors were located within the freshwater domain (S-1 at −39 m and S-2 at −86 m) and three were within the freshwater–saltwater transition zone (S-3 at 132 m, S-4 at 217 m, and S-5 at −236 m) (Figure 4.2).

Vertical EC and temperature profiles in the aquifer were logged along the borehole length every 3 h, at W250, using a multiparameter probe KLL-Q-2 (Seba Hydrometrie. Kaufbeuren, Germany) during 1 day (30 September 2019). The EC sensor accuracy was ±1 µs/cm, with a resolution of 0.1 µs/cm and the T sensor accuracy was ±0.1°C with a resolution of 0.01°C. The measurement depths correspond to the 12 screens of W250. Because of the artesian nature of the borehole, the borehole pipe was extended 2 m above the height of the hydraulic head to avoid water outflow and the destabilization of the system.

The sea-tide dataset of the Mediterranean Sea was supplied by State Harbors (Spanish Ministry of Development) at a gauge station installed in Motril Harbor (300 m from the coastline). Tide measurements were monitored every five minutes and filtered to remove energy at high frequencies, noise, and instrument errors by applying a symmetric filter. Thereafter, the data were recalculated at hourly intervals. The sea tide was corrected in time to GMT+01 to allow an easier comparison with the obtained field data.

Precipitation data were obtained from the nearest hydrometeorological station (60. Motril) belonging to the Automatic Hydrological Information System (AHIS) of the Hidrosur Basin (Junta de Andalucía).

Downstream of the Rules Dam, the river flow was measured monthly throughout 2018 (Blanco-Coronas et al., 2021b). An electromagnetic water flow meter MF Pro (OTT HydroMet. Kempten, Germany) was used at the measurement point RF (Figure 4.2) to quantify the river flow. The accuracy of the velocity sensor was ±4% of the reading and the accuracy of the water level sensor was ±2% of the reading.

The vertical flow in well W250 was measured with a QL40-SFM Spinner Flowmeter probe (Mount Sopris Instruments. Denver, CO, USA). The probe used was magnetically coupled, and its quadrature sensing electronics detected flow direction changes instantaneously. Due to the artesian nature of W250, it was necessary to record the outflow with a portable gauging station H0.75 (Lynks Ingeniería. Cali, Colombia) and then to compare it with the fluid velocity at each depth of the borehole. Three series of tests were performed on well W250, logging down and logging up. Three different upload/download sensor speed values were kept constant for each series (2, 5, and 8 m/min) in order to generate a calibration curve. The obtained data were analyzed with the WellCAD v5.5 software, and the extreme peaks produced by measurement errors were eliminated. The count rate of the impeller was related to the fluid velocity and converted into fluid flow rate using a calibration curve. The sign of the fluid flow rate indicates the flow direction within the borehole: negative for ascendant flow and positive for descendant flow.

3.2. Time Series Analysis

Statistical methods were completed with commercial software (IBM SPSS software version 24.0) in order to analyze the tidal influence on temperature, hydraulic head, and EC time series and their correlations obtained at different depths of the well W250.

To determine the influence of the seasonal variations (wet-dry periods) on the parameters (hydraulic head, EC and temperature), the precipitation and river flow were compared with the borehole data. The data obtained during 1 year were normalized to the moving average (MA) (Equation(1)), in order to eliminate short period oscillations (with periods less than 5 days), and to produce an easier contrast for the major trends:

$$MA = \frac{\sum_{k=i-n}^{i} x_k}{n} \tag{1}$$

Where i is the total number of observations, n is the number of periods to be averaged, x_k is the single observed value in period k.

To detect the main tidal constituents in the sea level and temperature, harmonic analysis was conducted using the S_TIDE MATLAB 1.23 toolbox (Pan et al., 2018). One month (February 2018) was selected for the analysis because during this period, the groundwater temperature was stable. Furthermore, the spectral energy distribution of the tidal constituents was estimated by a periodogram $P\left(\frac{j}{n}\right)$, obtained from the decomposition of the time series into its harmonic components a_j and b_j (Shumway and Stoffer, 2006):

$$P\left(\frac{j}{n}\right) = a_j^2 + b_j^2 \tag{2}$$

The coefficients a_j and b_j represent the correlation of the field data with the model sinusoidal signal oscillating at j cycles in n time points.

$$a_j = \frac{2}{n}\sum_{t=1}^{n} x_t \; cos\left(\frac{2\pi t j}{n}\right) \tag{3}$$

$$b_j = \frac{2}{n}\sum_{t=1}^{n} x_t \; sin\left(\frac{2\pi t j}{n}\right) \tag{4}$$

The causal and non-causal relationships between sea level and temperature were evaluated with a cross-correlation analysis. The correlation and the time lag between sea level, hydraulic head, EC (as an input time series), and temperature (as an output time series) were studied. The most important tidal constituent detected in the datasets ('Principal lunar semidiurnal' constituent M2) was chosen to obtain the delay between the input and the output signals, so that the time series were noise-filtered to eliminate measurement errors and other unidentified non-tidal factors at high frequencies and hence to improve tidal detection.

The cross-correlation function $r_{xy}(k)$ was used to establish the link between the input time series x_t (sea level, hydraulic head, and EC) and the output time series y_t (temperature), solving the following equation (Larocque et al., 1998):

$$r_{xy}(k) = \frac{C_{xy}(k)}{\sigma_x \sigma_y} \tag{5}$$

$$C_{xy}(k) = \frac{1}{n} \sum_{t=1}^{n-k} (x_t - \bar{x})(y_{t+k} - \bar{y}) \tag{6}$$

Where $C_{xy}(k)$ is the cross-correlogram, σ_x and σ_y are the standard deviations of the time series. k is the time lag, n is the length of the time series and $\bar{x}$ and $\bar{y}$ are the mean of the input and output time series, respectively.

If $r_{xy}(k) > 0$ for $k > 0$, the input influences the output: while if $r_{xy}(k) > 0$ for $k < 0$, the output influences the input (Padilla and Pulido-Bosch, 1995; Larocque et al., 1998).

3.3. Numerical Modeling

SEAWAT v.4 (Langevin et al., 2008) was used to simulate simultaneous multispecies solute and heat transport. This software couples MODFLOW (Harbaugh et al., 2000) and MT3DMS (Zheng and Wang, 1999) and solves the following form of the variable-density groundwater flow and its adaptation to simulate heat transport. A fully saturated porous media was assumed with changes in the boundary conditions to replicate tidal oscillations to simplify the system. The model represented the effect of fluid density variations, which are caused by temperature and solute concentration variations (Yang et al., 2021; Tabrizinejadas et al., 2020). In a similar manner, fluid viscosity was considered using an equation of state that relates viscosity to concentration and temperature (Langevin et al., 2008).

Thermal diffusivity (D_m^T), thermal distribution coefficient (K_d), and bulk thermal conductivity (k_{Tbulk}) were calculated following the approach described by Langevin et al. (2008).

The model represents a 2 km cross-section (x-axis), of which 1.5 km extends on land and 0.5 km on the sea (Figure 4.4), with 180–215 m depth (z-axis). The slope of the aquifer and seabed were 1% and 4%, respectively. The grid was defined based on a mesh with 203 rows and 114 layers, with cells of 5.2 m × 20 m. After verifying the location of the FSI with a test model, the grid was refined along the FSI area (5.2 × 5 m) and at a depth of over 70 m (5.2 × 0.1 m). Because this study is focused on the discharge zone of the aquifer to the

sea, distant boundaries were imposed to minimize the influence of the boundary specifications on the flow in the interest area of the aquifer.

The model is based on the characteristics of the Motril-Salobreña aquifer in terms of dimensions, lithology, and boundary conditions. However, as most of the data for the analysis corresponded with one single well, it was not intended to exactly reproduce the functioning of the aquifer even if the results could be considered an approximation to the real case.
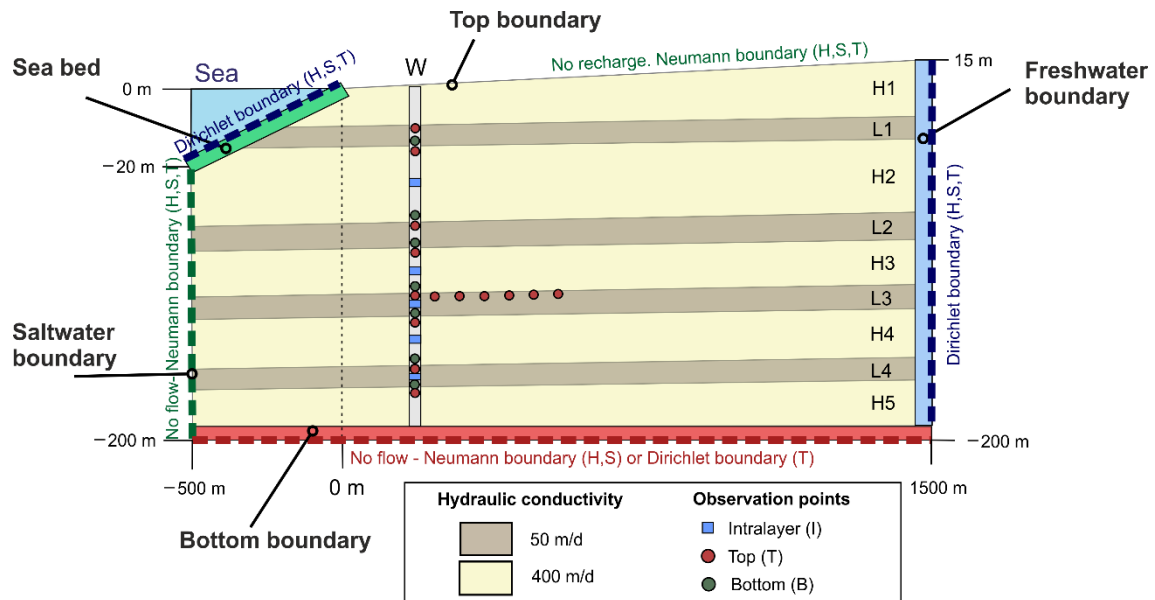

Figure 4.4.- Boundary conditions of the numerical model. The specified hydraulic conductivity values were considered for models B and C; however, in model A, the unique value considered was 100 m/d. H: hydraulic head, S: salinity, T: temperature.

3.3.1. Models

Three different numerical models with increasing complexity in hydrogeological characteristics and boundary conditions (specified in Figure 4.4 and Table 4.1) were tested to determine the impact of sea and water table oscillations on the distribution of temperature in the aquifer.

- Model A (Homogeneous model): the hydraulic conductivity was homogeneous (100 m/d).

- Model B (Heterogeneous layered model): nine layers with different hydraulic conductivity (50 and 400 m/d) were included to modify model A. The thickness of the layers was 15 m for the layers with lower hydraulic conductivity (L1, L2, L3 and L4) and 20–45 m for the layers with higher hydraulic conductivity (H1, H2, H3 and H4) (Figure 4.4). The alternation of layers with the two values of hydraulic conductivity represented the vertical heterogeneity often found in alluvial coastal aquifers.

- Model C (Changes in recharge conditions): the model parameters were the same as those of model B, but the recharge effect was simulated, modifying the boundary conditions to reproduce a gradually increasing hydraulic gradient, justified by fluctuations of the

water table in the upper sector of the aquifer (up to 5 m from summer to winter), and by the lack of recharge of the river near the coastline (Duque et al., 2010).

The rest of the parameters of the model were based on standard values presented in the literature or estimated based on previous local studies (specified in Section 3.3.3. Parameters and time discretization).

	Parameter	Freshwater	Sea Bed	Saltwater	Top	Bottom
Model A	H	Dirichlet 8 m	Dirichlet $H = A \sin\left(\frac{2\pi}{P} t - \varphi\right)$	Neumann No flow	Neumann No flow	Neumann No flow
	S	Dirichlet 350 mg/L	Dirichlet 35000 mg/L	Neumann No flow	Neumann No flow	Neuman No flow
	T	Dirichlet 17 °C	Dirichlet 13 °C	Neumann No flow	Neumann No flow	Dirichlet 24 °C
Model B	H	Dirichlet 8 m	Dirichlet $H = A \sin\left(\frac{2\pi}{P} t - \varphi\right)$	Neumann No flow	Neumann No flow	Neumann No flow
	S	Dirichlet 350 mg/L	Dirichlet 35000 mg/L	Neumann No flow	Neumann No flow	Neuman No flow
	T	Dirichlet 17 °C	Dirichlet 13 °C	Neumann No flow	Neumann No flow	Dirichlet 24 °C
Model C	H	Dirichlet 8 to 13 m	Dirichlet $H = A \sin\left(\frac{2\pi}{P} t - \varphi\right)$	Neumann No flow	Neumann No flow	Neumann No flow
	S	Dirichlet 350 mg/L	Dirichlet 35000 mg/L	Neumann No flow	Neumann No flow	Neuman No flow
	T	Dirichlet 17 °C	Dirichlet 13 °C	Neumann No flow	Neumann No flow	Dirichlet 24 °C

Table 4.1.- Values of hydraulic head (H), salinity (S) and temperature (T) given to each boundary of the models A, B and C.

3.3.2. Boundary Conditions

1. Freshwater boundary: this boundary is the main freshwater input to the aquifer. For models A and B, it had a constant head of 8 m above sea level; and for model C, the head was gradually raised from 8 m to 13 m over 40 days, which meant an increment of the hydraulic gradient from 0.0058 to 0.0087 (an increase of 41%) from the mean sea level (0 m). For the three models, the salinity was 350 mg/L, and the temperature was 17°C (Dirichlet boundary condition) based on field measurements.

2. Sea bed boundary: a sinusoidal oscillation head boundary was imposed using the expression:

$$H = A \sin\left(\frac{2\pi}{P} t - \varphi\right) \tag{7}$$

where H is the transient sea level at time t [L], A is the half of the tidal range [L], P is the period of tide oscillation [t], t is the time [t], and φ is the phase of the tide [rad]. Although different tidal constituents were detected in the field data, only the period of

the most important one ('Principal lunar semidiurnal' M2) was considered. The semidiurnal tide fluctuation was adjusted with three amplitudes, taking into account microtidal, mesotidal, and macrotidal ranges (0.75 m, 1.5 m, and 2.5 m, respectively) for models A and B. For model C, a mesotidal condition was selected to represent an intermediate value of tidal amplitude. A salinity of 35,000 mg/L and a temperature of 13°C were assigned, both based on field measurements.

3. Bottom boundary: the temperature imposed at the base of the model was 24 °C, based on the mean value of the geothermal gradient increment described in [29]. No flow boundary was applied for head and salinity.

4. Top boundary: no recharge. Neumann boundary condition (no flow) for temperature, salinity, and head.

5. Seawater boundary: Neumann boundary conditions for temperature, salinity, and head. The Dirichlet was not considered as preliminary analysis of the study indicated that a no flow boundary did not interfere with the salinity and temperature distribution of the FSI and freshwater domain where data was obtained.

3.3.3.   Parameters and Time Discretization

The model was run for a total of 500 days in order to stabilize the system, using as starting salinity and temperature distribution the steady-state solution of the model, with a constant head at the sea bed boundary, and without tidal oscillations (0 m). The results were used as initial conditions for models A and B, changing the boundary conditions (Table 4.1). For model C, the initial conditions were the results of model B.

The parameters used for the simulation were obtained from the literature and based on previous local studies (Table 4.2). The seawater and freshwater temperatures were assumed to be constant since they should not experience important seasonal variations due to the short period of simulation (40 days). The values of hydraulic conductivity differed between models (Section 3.3.1.), however, the rest of the input parameters did not change. The influence of K_d^t and D_m^T was found to be not as important as hydraulic conductivity (Blanco-Coronas et al., 2021a) and thus homogeneous values were given to both parameters.

The results of the three models were compared with several sets of observation points located 217 m from the shoreline (Figure 4.4) because both the FSI and the thermal plume were intersected at that location. The observation points were positioned at the top, middle, and bottom of the layers (Table 4.3) in order to compare the differences in temperature distribution. They were named according to the designated layer and the situation inside the layer (top T, bottom B, or intralayer I). In model B, six observation points at the top of layer L3 were added (Figure 4.4) to study the differences in temperature with respect to the distance from the shoreline.

Input parameters	Value	Source
Specific storage	1×10^{-5} m^{-1}	Calvache et al. (2015)
Specific yield	0.25	Similar value to Calvache et al. (2015)
Porosity θ	0.3	Duque et al. (2008)
Longitudinal dispersivity	20 m	Stauffer et al. (2014)
Vertical transverse dispersivity	10 m	Stauffer et al. (2014)
Molecular diffusion coefficient D_m^s	1×10^{-10} m^2/d	Langevin et al. (2008)
Thermal conductivity of water k_{Tfluid}	0.58 W/m °C	Langevin et al. (2008)
Thermal conductivity of sediments k_{Tsolid}	2.9 W/m °C	Approximate value for gravel (Xiaoqing et al., 2018)
Specific heat of water C_{Pfluid}	4186 J/kg °C	Langevin et al. (2008)
Specific heat of sediments C_{Psolid}	830 J/kg °C	Approximate value for gravel (Xiaoqing et al., 2018)
Thermal diffusivity D_m^T	0.15 m^2/d	Langevin et al. (2008)
Bulk thermal conductivity k_{Tbulk}	1.8 W/m °C	Langevin et al. (2008)
Thermal distribution factor K_d^t	2×10^{-7} L/mg	Langevin et al. (2008)
Density change with concentration	0.7	Langevin et al. (2008)
Density change with temperature	-0.375 kg/(m^3 °C)	Langevin et al. (2008)
Density vs pressure head slope	0.00446 kg/m^4	Langevin et al. (2008)
Bulk density ρ_b	1800 kg/m^3	Calculated with $\rho_b = \rho_s(1 - \theta)$
Reference temperature	25 °C	Langevin et al. (2008)
Viscosity vs concentration slope	1.923×10^{-6} m^4/d	Langevin et al. (2008)
Reference viscosity	86.4 kg/ m d	Langevin et al. (2008)

Table 4.2.- Input values of the parameters for the model.

L1-T	L1-I	L1-B	H2-T	H2-I	H2-B	L2-T	L2-I	L2-B	H3-T	H3-I
-20 m	-26 m	-31 m	-34 m	-70 m	-79 m	-80 m	-88 m	-96 m	-97 m	-110 m

H3-B	L3-T	L3-I	L3-B	H4-T	H4-I	H4-B	L4-T	L4-I	L4-B	H5-T
-122 m	-124 m	-131 m	-139 m	-140 m	-155 m	-168 m	-169 m	-175 m	-182 m	-183 m

Table 4.3.- Observation points of the model (nomenclature and depths) located at a distance of 217 m from the shoreline.

4. Results

4.1. Vertical Flow in the Borehole

The flowmeter measurements allowed us to distinguish two flow mechanisms within the borehole. From ground surface to −130 m, the flow was upward with a maximum accumulated flow velocity of 60 m/min at a depth of −50 m (Figure 4.5). Within those 130 m, the first 84 m had a highly variable velocity, and from −84 m to −130 m, the vertical flow velocity increased throughout the screens (Figure 4.5). The maximum increase in velocity was produced between −84 m and −87 m. From −130 m to the bottom, the vertical flow was almost non-existent. There were no variations in the velocity values at the depths of the screens where the sensors S-3, S-4, and S-5 were installed. This indicates that the data obtained at 130 m and below were not induced by mixing processes inside the well casing, while data obtained from S-1 and S-2 would be highly influenced by internal mixing due to the dominance of vertical flow velocity over lateral flow velocity. Based on the flowmeter results, the datasets obtained in S-1 and S-2 were discarded, while the datasets obtained in S-3, S-4, and S-5 were considered representative of the aquifer conditions.
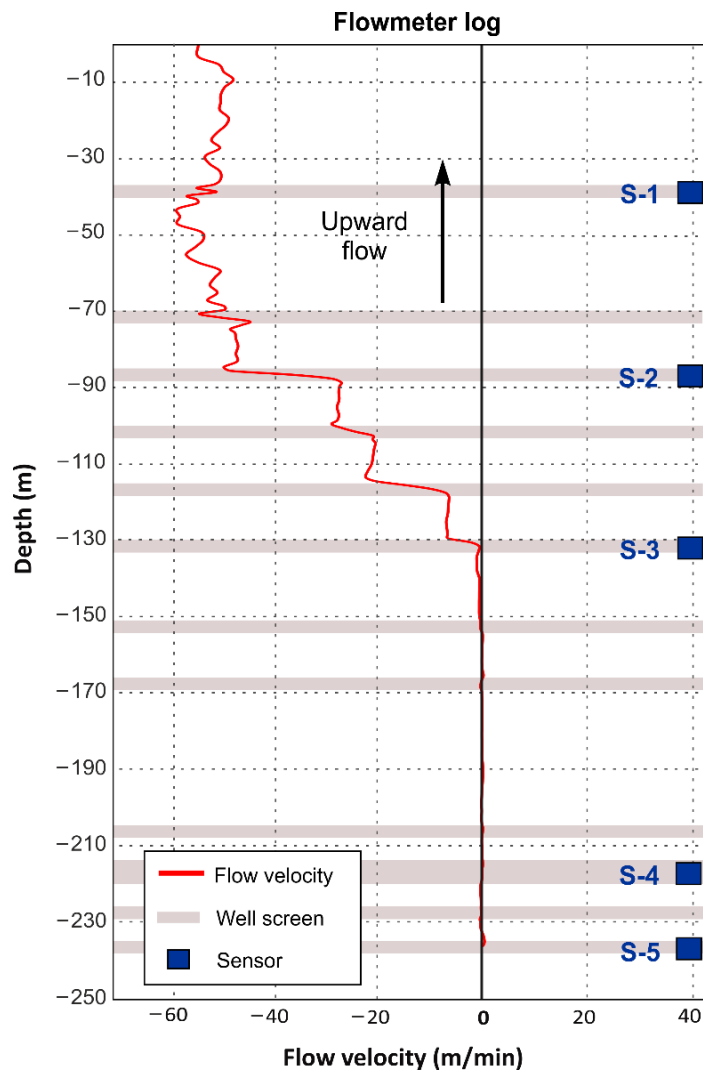

Figure 4.5.- Vertical flow velocity estimated from flowmeter logs in well W250.

4.2. Water Table Variation Effect on Temperature Oscillation in the FSI

To determine whether there was an influence from the seasonal variations of the groundwater recharge on the fluctuations of head, temperature, and EC, the precipitation and river flow data were compared to the recorded data from January to December 2018, using sensors S-4 and S-5 (Figure 4.6). At the end of 2017 and during the first two months of 2018, rainfall was scarce, and the river flow was less than 1 m^3/s. The lack of surface water prevented the recharge of the aquifer, and thus heads remained low in the aquifer. In March 2018, a period of continuous precipitation started. However, the peak river flow was not reached until May 2018 (7.5 m^3/s) due to the snowmelt in the nearby mountains and the management of river flow by a dam. Since May, the hydraulic heads increased due to the river flow recharge. In July 2018, with the beginning of the summer, a new dry period without precipitation started, and ended in October–November 2018.
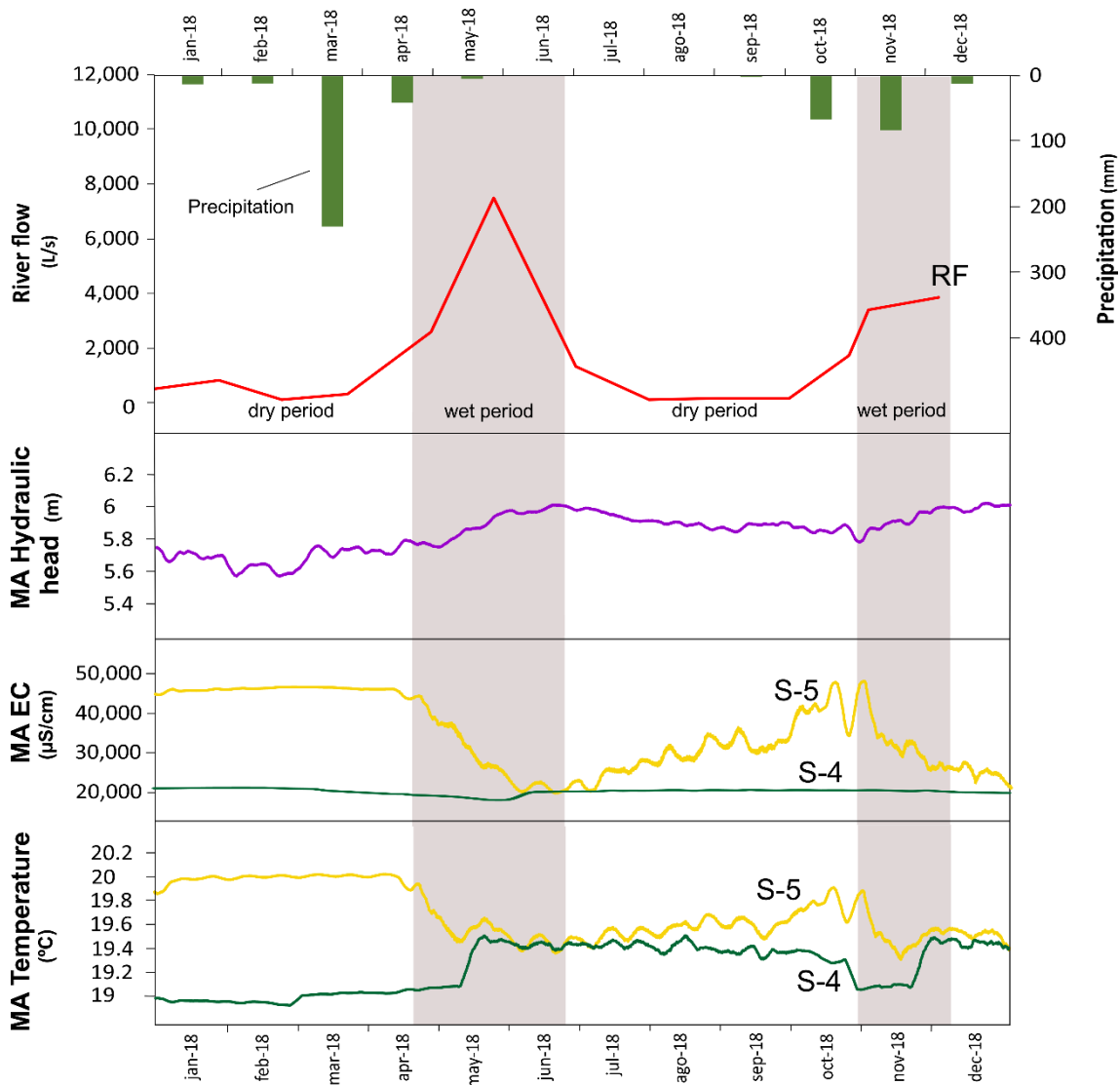

Figure 4.6.- Data during 2018: Monthly measurements of river water flow (red line) and moving average (*AM*) of hourly measurements of H obtained from S-4 and S-5 in purple (same values for both sensors), and EC and T obtained from S-4 (green lines) and S-5 (yellow lines). Wet periods are delimited by the grey areas coinciding with the increment of river flow.

EC and temperature within the aquifer also responded to wet periods. From January to April (first dry period), EC was approximately 21,000 µS/cm in S-4 and approximately 45,000 µS/cm in S-5. In May 2018, EC decreased to 17,000 and 20000 µS/cm in S-4 and S-5, respectively. However, when the wet period ended, EC recovered its initial values in S-4, but, in the case of S-5, it took longer for EC to reach the initial values. The same process can be observed in November 2018.

In S-5, temperature variations showed the same pattern as EC. Temperature oscillated between 19.8 and 20°C in the first period (from January to April), and then it was lower (19.4–19.7°C) starting from May 2018. Until October 2018, the temperature did not recover the values of the first period. After the second wet period, the temperature reached similar values to the first wet period. In S-4, the process was inverted and delayed with respect to the temperature measured in S-5: when the temperature decreased in S-5, it increased in S-4 about 1 month later. Temperature started with values around 19°C and then increased to 19.4–19.5°C starting from May 2018. Subsequently, a decrease in temperature was produced in early November 2018, related to the end of the dry period (19°C), and then at the end of November 2018, the temperature reached the same values as the first wet period (19.4–19.5°C). The comparison of the results in S-4 and S-5 indicated irregular patterns in temperature that differed depending on the locations of the observation point, but it still showed the same inverse relationship between S-4 and S-5. This irregularity seemed to be induced by changes in the groundwater recharge. However, the cause–effect relationship at the root of this behavior was still unclear and thus it was further studied, as explained in the next sections.

4.3. Sea Tides Effect on Temperature and EC Oscillations in the FSI

4.3.1. Vertical logs

The vertical logs obtained in well W250 during one tidal cycle (Figure 4.7) showed no changes over the first 130 m, excluding the most surficial zone of the aquifer (first 50 m) that was probably influenced by air temperature. The beginning of the FSI was located at 130 m, from which EC and temperature increased sharply until reaching 160 m (first step increment). The beginning of the increment in EC reflected the start of the FSI. However, from 160 m to 220 m of depth, EC was constant, and temperature increased slowly due to the geothermal gradient, which affects the groundwater temperature. From 220 m to the end of the well, the values of both parameters increased sharply again (a second step in the increment of their values).

The EC and temperature showed changes throughout the tidal cycle in the FSI domain. EC and temperature were highest during low tide (Log 1). At the mid-point of sea-level rise, EC and temperature decreased (Log 2). When high tide was reached (Log 3), EC and temperature generally decreased even more. At the mid-point of sea level fall (Log 4), EC had almost the same values as those of Log 3; however, temperature was slightly higher (by ~0.1°C), which was more evident in the deepest part of the aquifer.
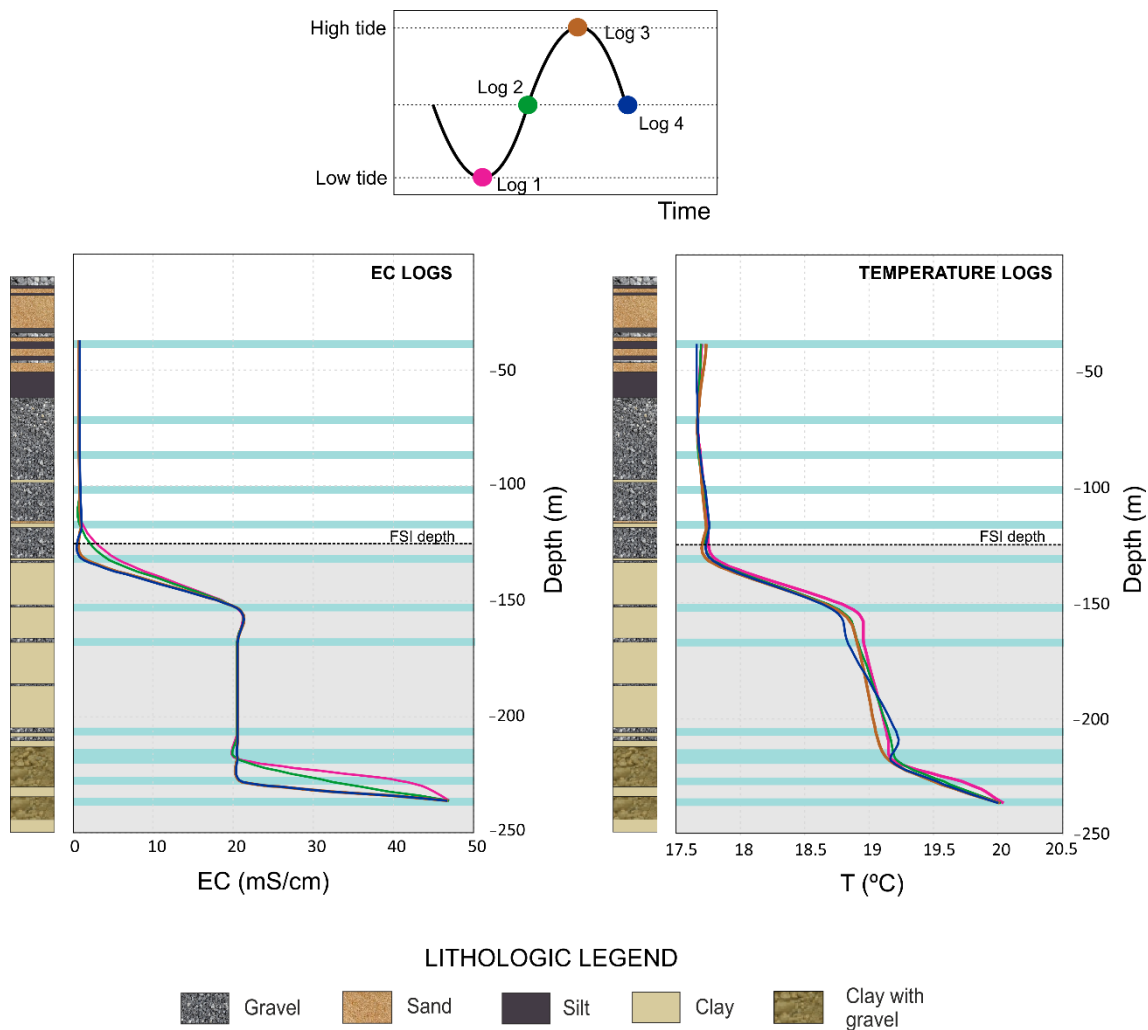
Figure 4.7.- Vertical logs of EC and T in well W250 during a tidal cycle and the position of the FSI (grey area) and location of the screens (grey bars) where the measurements were obtained (30 September 2019). Log 1 (pink line) during low tide, Log 2 (green line) during tidal rise, Log 3 (brown line) during high tide and Log 4 (blue line) during tidal fall.

4.3.2. Continuous Temperature Data

The effects of the sea tide on the groundwater temperature are visible in the time series of February 2018 (Figure 4.8 A). The Mediterranean Sea has a mixed tidal phenomenon with two cycles of high and low tide per day (Pugh, 1996), with a mean tidal amplitude of 0.54 m at the Motril coastline. The largest constituents obtained on the 1-month data of sea level were M2, S2, Msf, N2, K1, O1, M4, and OO1 (Table 4.4) and their average amplitudes ranged between 0.152 and 0.013 m. The magnitude of the temperature oscillations measured in the aquifer is highly dependent on the fortnightly spring–neap cycle. The temperature had a larger amplitude and perfectly sinusoidal pattern during the spring tides and smaller oscillations, with a squarer wave, during the neap tides.
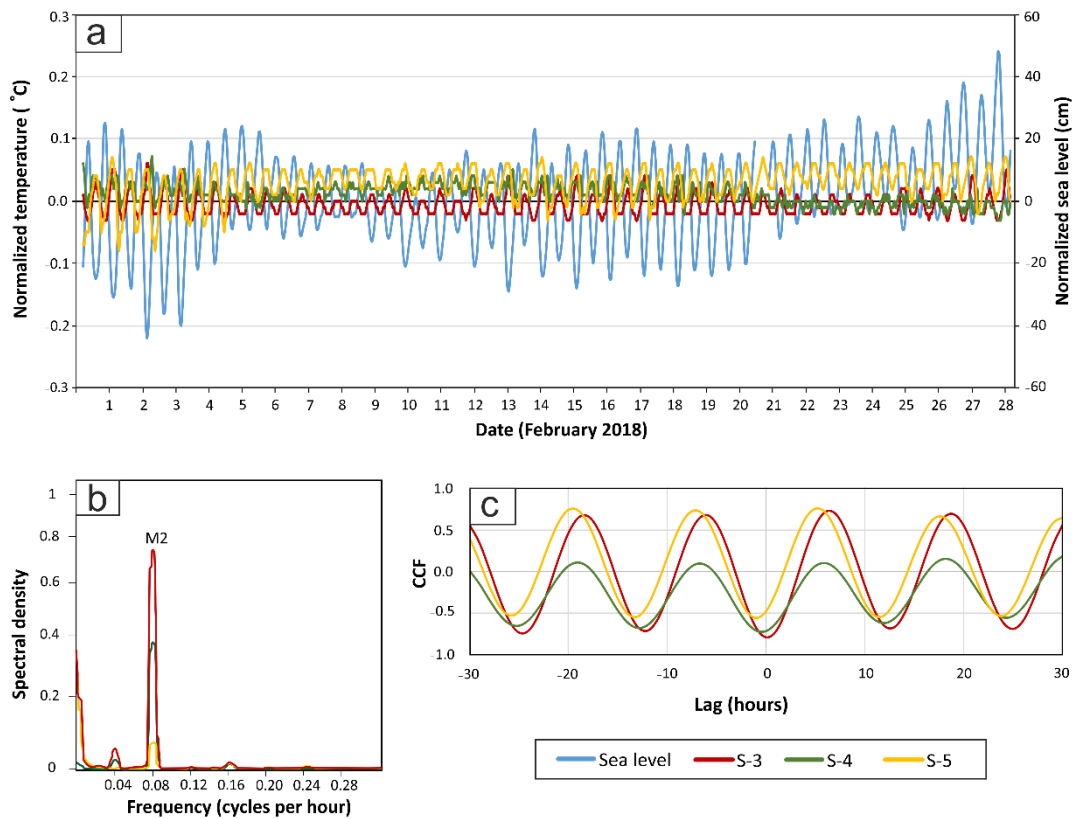
Figure 4.8.- (A) Continuous measurements of sea level and temperature were obtained from S-3, S-4, and S-5 during February 2018; (B) Density spectra (energy versus frequency) of the temperature data obtained during February 2018; (C) Cross-correlation functions of sea level as input and temperature measured in S-3, S-4 and S-5 as output for February 2018.

Harmonic constituent	Symbol	Amplitude (m)	Amplitude (°C)		
		Sea Level	S-3	S-4	S-5
Lunisolar synodic fortnightly	Msf	0.046	0.003	0.007	0.012
Principal lunar diurnal	O1	0.022	0.004	0.001	0.005
Luni-solar diurnal	K1	0.029	0.004	0.001	0.006
Lunar diurnal	OO1	0.013	0.001	0.002	0.001
Larger lunar elliptic semidiurnal	N2	0.031	0.004	0.002	0.006
Principal lunar semidiurnal	M2	0.157	0.021	0.009	0.027
Principal solar semidiurnal	S2	0.064	0.008	0.003	0.011
Shallow water overtides of principal lunar constituent	M4	0.016	0.001	0	0

Table 4.4.- Main tidal constituents of the Mediterranean Sea and the temperature measured in S-3, S-4, and S-5, obtained with S_TIDE toolbox.

The main constituents of the Mediterranean Sea were also detected in temperature (Table 4.4). The 'Principal lunar semidiurnal' constituent (M2) had the biggest amplitude at the depths of the sensor (S-3, S-4 and S-5). The spectral analysis (Figure 4.8 B) detected that M2 also had the largest spectra energy, as calculated previously for the groundwater head time series (Sánchez-Úbeda et al., 2018).

Temperatures obtained in S-3, S-4, and S-5 change with a symmetrical lag following the sea level signal (Figure 4.8 C). Temperature had a delay with respect to the tide ($t_{lag_{TIDE-T}}$) between 5.4–6.4 h (Table 4.5). The time-lags of temperature with respect to H ($t_{lag_{H-T}}$)) were slightly smaller compared to the tide: between 5.3–6.1 h. The delay of temperature with respect to EC ($t_{lag_{EC-T}}$) was negative, indicating that temperature oscillated faster than EC. However, the phase shifts were small: −0.7 and −1.1 h. $t_{lag_{EC-T}}$ could not be calculated at the depth of 217 m (sensor S-4), due to the irregular oscillations of the EC dataset. The amplitude of the temperature oscillations ranged between 0.02 °C and 0.06 °C at the three depths in February.

Depth	$t_{lag_{TIDE-T}}$ (hours)	$t_{lag_{H-T}}$ (hours)	$t_{lag_{EC-T}}$ (hours)	Amplitude (°C)	Range (°C)
132 m	6.4	6.1	−1.1	0.04	17.7–17.8
217 m	5.6	5.6	-	0.02	18.9–19.0
236 m	5.4	5.3	−0.7	0.06	19.9–20.0

Table 4.5.- Time-lags obtained from the cross-correlation analysis, average amplitudes of the temperature oscillations, and temperature ranges of the dataset for February 2018. $t_{lag_{TIDE-T}}$ is the delay between tide and temperature, $t_{lag_{H-T}}$ is the delay between hydraulic head and temperature, $t_{lag_{EC-T}}$ is the delay between electrical conductivity and temperature.

4.4. Numerical Model Results

4.4.1. Model A

The addition of sea oscillations to the homogeneous model did not produce significant variations in temperature and salinity at the observation points for microtidal, mesotidal, or macrotidal conditions. The maximum changes in salinity and temperature were at the observation point L4-T (Figure 4.9). However, other observation points located in the model (Figure 4.4) did not show any changes in temperature. Salinity variations had an amplitude of less than 0.1 g/L for the three tidal conditions. The temperature showed irregular squared fluctuations related to the time discretization of the model, with amplitudes of 10^{-3}°C. Still, these small temperature variations must have been generated by the tidal oscillation since, in the case of the mesotidal conditions, the minimum values of temperature and salinity occurred simultaneously, as shown in Figure 4.9.

4.4.2. Model B

The inclusion of heterogeneity generated higher temperature oscillations in the numerical model. The thermal contours had a different pattern with respect to the iso-

concentration lines because of the presence of an ascending thermal plume in the fresh groundwater domain, associated with the FSI, which increased sharply towards the surface (Figure 4.10). The alternation of layers with different hydraulic conductivity induced the bending of thermal contours, which were almost horizontal within the low hydraulic conductivity layers, and closer to vertical in the high hydraulic conductivity layers. The shape of the thermal plume was well defined near the surface, and then it gradually flattened towards the basement. This explains the presence of a horizontal thermal gradient in the nearest groundwater.

Temperature and salinity oscillations related to sea tides were registered at the boundaries between layers with different hydraulic conductivity. However, in the intralayer area, the temperature oscillations were irregular or even absent (Figure A1 in Appendix). Therefore, intralayer results were selected to be analyzed.
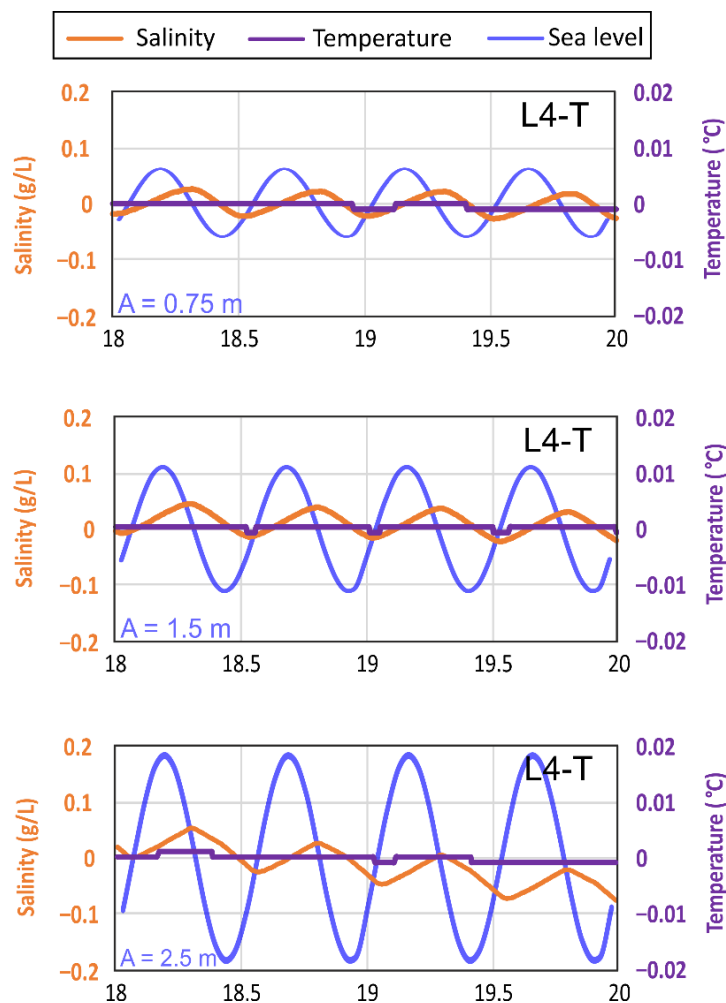
Figure 4.9.- Simulation results of the homogeneous model (Model A) for microtidal, mesotidal, and macrotidal conditions (semi-amplitudes of 0.75 m, 1.5 m, and 2.5 m, respectively) measured at the observation point L4-T.
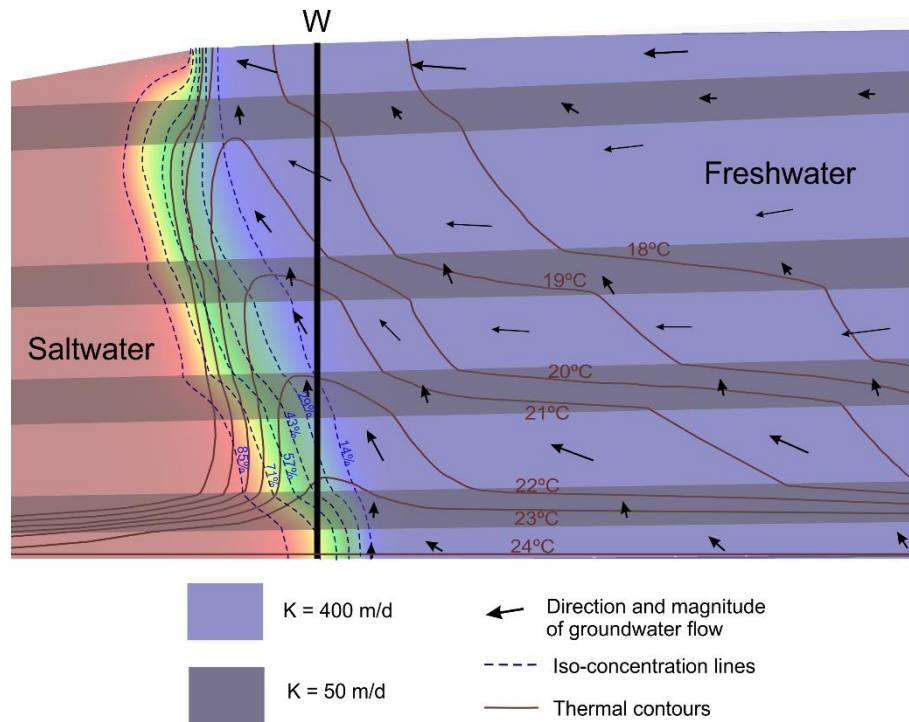
Figure 4.10.- Salinity and temperature distribution resulting from the multilayered model (model B).

The amplitude of temperature oscillations varied according to the condition of the tide (Figure 4.11): from 0.015°C to 0.004°C for microtidal conditions, 0.033°C to 0.014°C for mesotidal conditions, and from 0.029°C to 0.052°C for macrotidal conditions. The amplitude was maximum at a distance of 350 m from the shoreline and at the top of layer L3 (Figure 4.11 A). Thus, the model did not simulate a decreasing trend of the amplitude with distance from the shoreline or the FSI. However, the oscillation amplitude was related to the local horizontal thermal gradient ($\Delta T/d$), where the observation points were located (Figure 4.11 B). The maximum amplitude of temperature was registered at x = 350 m, where the thermal contours were the closest to each other; from that point on, the amplitude decreased landwards as the $\Delta T/d$ also decreased. The oscillations were produced by the horizontal displacements of the freshwater body due to sea tides and, consequently, the bigger the $\Delta T/d$, the greater the amplitude of groundwater temperature oscillations.
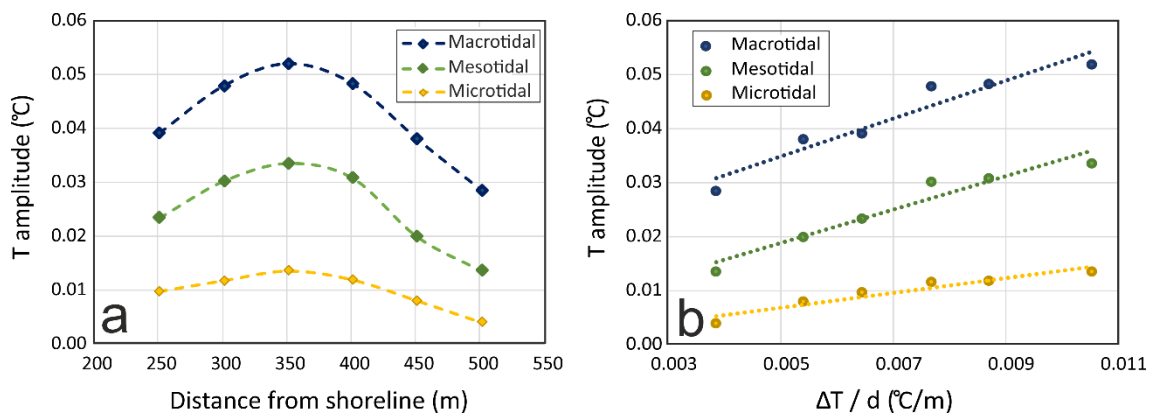

Figure 4.11.- Simulation results of model B for microtidal, mesotidal, and macrotidal conditions measured at the top of layer L3. (A) Temperature (T) amplitude measured at different distances from the shoreline; (B) T amplitude vs. local horizontal thermal gradient at each observation point $\Delta T/d$.

The salinity and temperature semidiurnal oscillations were analyzed for the mesotidal condition as an average value representative of other locations. Temperature and salinity almost oscillated together (Figure 4.12); the maximum and minimum peaks were reached at the same time for both parameters. However, comparing the top and the bottom of the same layer, they had an inverted evolution. For example, in layer L3, temperature and salinity reached their maximum values at the top of the layer (Figure 4.12 B), just when they reached their minimum values at the bottom (Figure 4.12 C). The maximum values of salinity and temperature had a lag of 2.5 h with respect to the sea tide, at the bottom of a layer with high hydraulic conductivity, and at the top of a layer with low hydraulic conductivity just below (Figure 4.12 A and Figure 4.12 B, respectively). However, the maximum value of salinity and temperature had a lag of 8.9 h with respect to the sea tide, as registered at the bottom of a layer with low hydraulic conductivity (L3-B) and at the top of a layer with high hydraulic conductivity just below (H4-T) (Figure 4.12 C and Figure 4.12 D, respectively). This means that the sequence of layers with different hydraulic conductivities determined the behavior of temperature and salinity with respect to the sea tides, as can be seen in many cases in the various layers presented in the model (Figure A1 in Appendix).
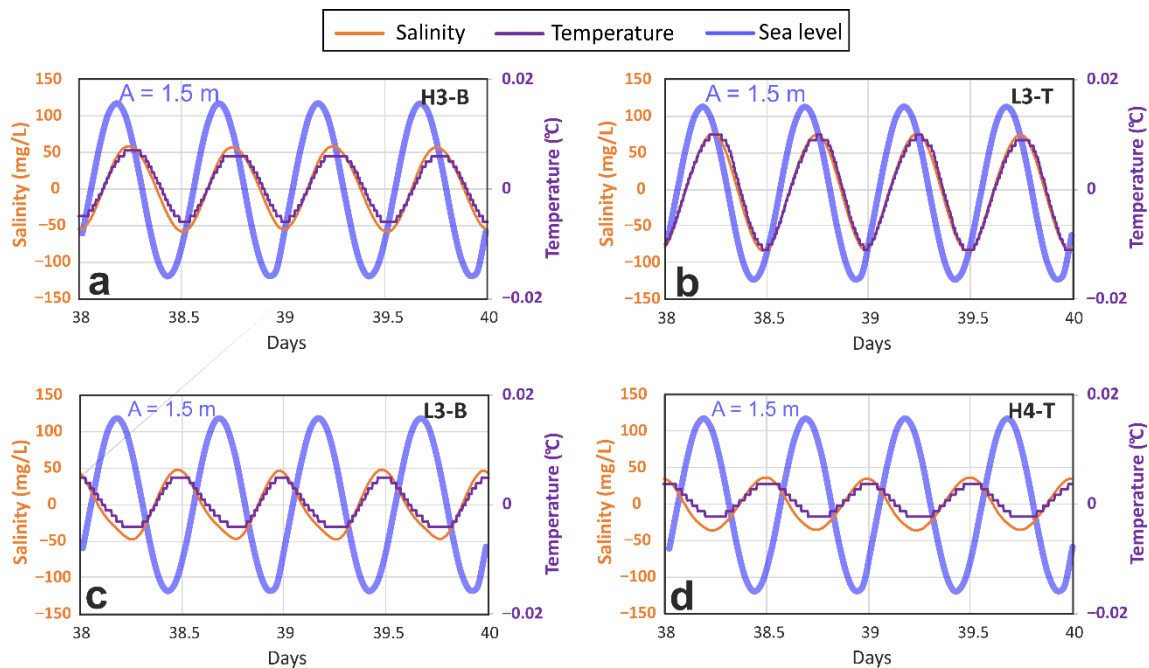

Figure 4.12.- Simulation results of model B at four depths of the well W for a mesotidal condition (semi-amplitude of 1.5 m): (A) At the observation point H3-B (−122 m); (B) At the observation point L3-T (−123 m); (C) At the observation point L3-B (−138 m); (D) At the observation point H4-T (−140 m).

The results obtained at the tops and bottoms of low and high hydraulic conductivity layers were used to analyze the impact of depth and hydraulic conductivity on the amplitude of temperature and salinity oscillations. Only temperature results were plotted, as salinity had an almost synchronous evolution. The same conditions of hydraulic conductivity and location within the layer were considered to compare the results. In all cases, the amplitude of temperature oscillations decreased with depth. The flattening of the thermal plume towards deeper areas of the aquifer caused the reduction in $\Delta T / d$ and, hence, the variations in temperature with horizontal movements due to the pushing of the FSI associated with sea tides were smaller. The oscillations of temperature and salinity were larger in low

hydraulic conductivity layers, compared with those obtained in layers with high hydraulic conductivity.

Temperature fluctuations were synchronized in all four cases (Figure 4.13), except for L4-B and H5-T, in which oscillations were delayed with respect to the other results. The desynchronization of the maximum-maximum peaks may be due to the position of the observation points on both sides of the thermal plume. The core of the thermal plume (the highest temperature area) moved landwards toward the observation points located on the right side of the thermal plume, and that is what made them register an increment in temperature. However, the observation points situated on the left side of the thermal plume registered a decrease in temperature due to the core of the plume moving away.
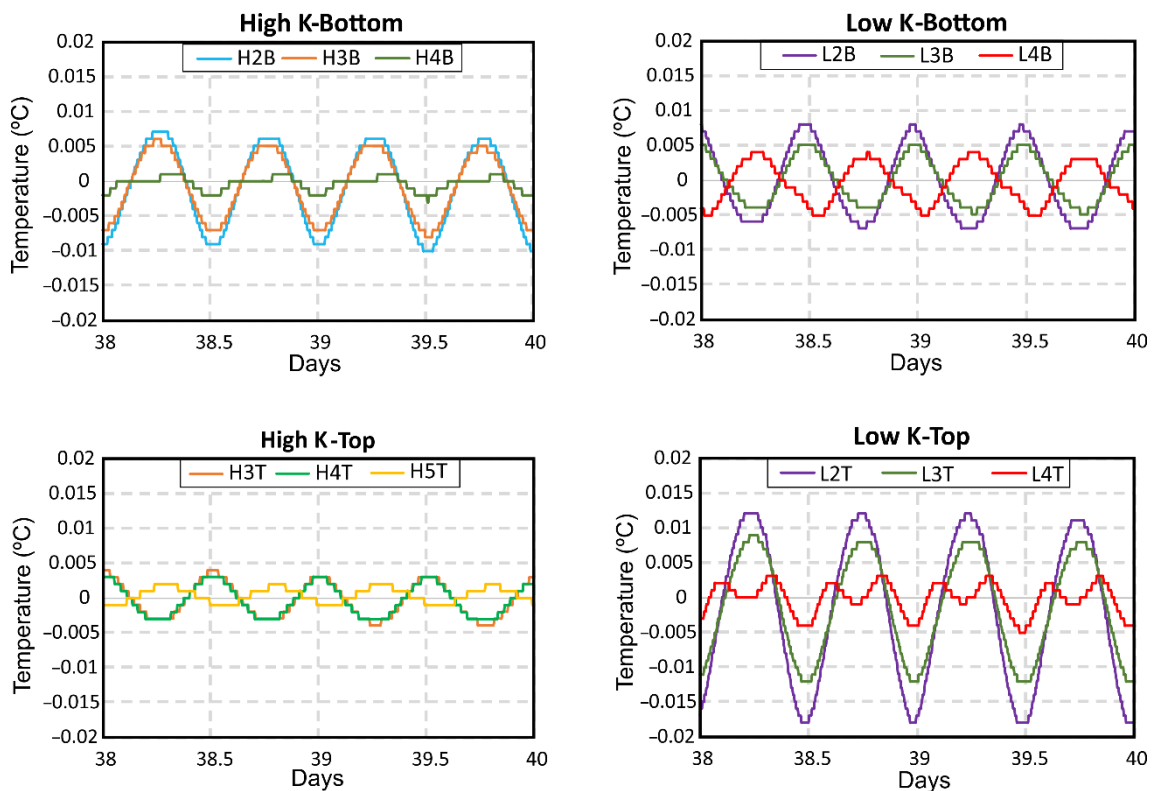

Figure 4.13.- Comparison of the simulation results depending of the location of the observation points (top and bottom of high and low hydraulic conductivity layers).

4.4.3. Model C

The increase in hydraulic gradient reflected how temperature and salinity changed during a gradual increase in groundwater recharge, until exceeding the initial value by 40%. The amplitude of the oscillation of both parameters became smaller over the simulation time due to the increase in recharge. However, the general trend of the time series had a different behavior: salinity and temperature decreased where a high hydraulic conductivity layer was above a low hydraulic conductivity layer (H3-B and L3-T, Figure 4.14 A and Figure 4.14 B, respectively), while salinity decreased and temperature increased where a low hydraulic conductivity layer was above a high hydraulic conductivity layer (L3-B and H4-T, Figure 4.14 C and Figure 4.14 D, respectively). Hence, the sequence of the layers

with different hydraulic conductivity generated a different temperature behavior. This phenomenon was also modeled at the top and bottom of other layers and also at the intralayer areas where temperature decreased together with salinity (Figure A2 in Appendix). These results confirmed that recharge variations did have an influence on salinity and temperature since the amplitude of the oscillations and the general trend of both parameters did not change in model B, where the hydraulic gradient remained constant over time.
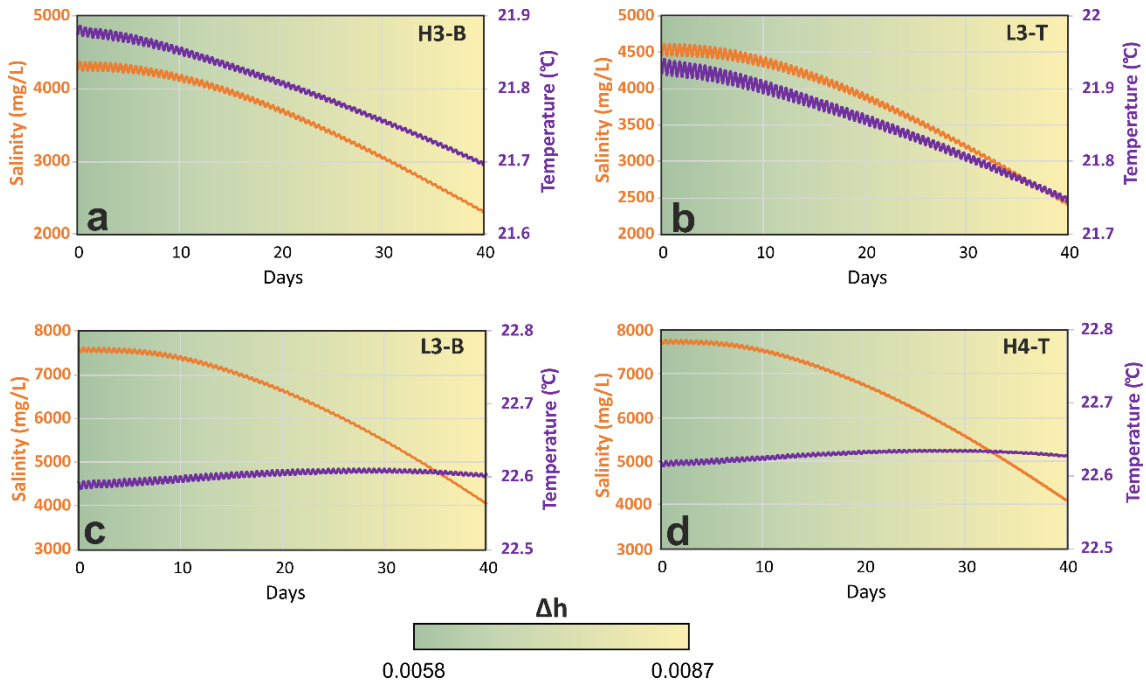
Figure 4.14.- Simulation results of model C at four depths of the well W for a mesotidal condition (semi-amplitude of 1.5 m): (A)At the observation point H3-B (−122 m); (B) At the observation point L3-T (−123 m); (C) At the observation point L3-B (−138 m); (D) At the observation point H4-T (−140 m).

5. Discussion

Temporal variations in temperature and EC distribution were identified by vertical logs and sensor monitoring in the Motril-Salobreña aquifer, near the FSI. The oscillations followed, in general terms, the tidal and recharge changes, but there were differences in the temperature and EC variations depending on the location of the measurement point. This relationship between observation point location and variations in temperature and EC required the use of numerical simulations in order to be properly analyzed and explained.

Time series analysis allowed us to detect the characteristics and relationships between temperature and EC measurements and sea level oscillations. Considering the 'principal lunar semidiurnal' constituent (M2), temperature and EC were synchronized with sea tides with a time lag that differs from what was reported by previous authors. The difference could be caused by a smaller well-to-shoreline distance, as Levanon et al. (2017) measured at a distance of 70 m from the shoreline (0.75–2 h) and Vallejos et al. (2015) were located at 7 m from the shoreline (2.8 h and 4.3 h). In the present study, the amplitudes of temperature oscillations measured were in the range of 0.02 °C to 0.06 °C; values that are about one order of magnitude smaller than those measured by Vallejos et al. (2015): 0.2 °C.

Temperature fluctuations were neither synchronized nor had the same amplitude at every depth. This is related to the hydraulic characteristics of the aquifer and especially to the alternation of lithological layers. Time lags obtained from field data tended to decrease with depth, but the difference between shallow and deep measurements was so small that it could be considered negligible. The analysis of the results of the model did not point to any specific relationship between time lag and depth; however, it did show a link between the position of the observation point and the lithology contrast.

The effect of hydraulic conductivity changes on temperature distribution can be used to explain the measurements obtained in the wells. The heterogeneity of hydraulic conductivity induced the bending of the thermal contours as shown in Figure 4.10, especially at the boundaries between different layers. The thermal contours were less close to vertical in low hydraulic conductivity layers compared to those with high hydraulic conductivity. Moreover, Saar (2011), Wang et al. (2021), and Ma & Zhou (2021) also associated the bending of the thermal contours with the refraction of the heat flow. They demonstrated that the variation of thermal conductivity within the aquifer materials produced the refraction. However, in the case of this study, the value of thermal conductivity was homogeneous across the three models. Therefore, the bending of thermal contours may be due to the different convective heat transport induced by the refraction of the flowlines at the interfaces between layers with different K values. This demonstrates the importance of the characterization of layering, hydraulic properties, and heterogeneity in studies focused on this topic.

Sea tides and recharge variations produced the displacement of the FSI and the associated thermal plume, inducing periodic oscillations of salinity and temperature. The oscillations of temperature measured at depths of over 100 m in the aquifer were related to the presence of the ascending thermal plume, which generated a local horizontal thermal gradient. Without the thermal plume, the thermal contours in the freshwater domain would be horizontal and, therefore, the landward-seaward movements of the FSI would produce salinity oscillations but not temperature oscillations.

The amplitude of the temperature oscillations did not decrease linearly landwards (Figure 4.11 A), as other authors have described for hydraulic head oscillations (Erskine, 1991; Sánchez-Úbeda et al., 2016; Levanon et al., 2016; Mao et al., 2006). Although the general trend showed decreasing amplitudes, an increment in amplitude was recorded from x = 250 m to x = 300 m, which shows a correlation between the oscillation amplitudes and the local horizontal thermal gradient produced by the thermal plume (Figure 4.11 B). These results indicate that temperature oscillations generated by tides could not be identified in every portion of the aquifer but only in those where temperature differences in the horizontal dimension were large enough and were associated with the displacement of the FSI.

Temperature and EC fluctuated simultaneously at the semidiurnal frequency. The fluctuations, however, were inverted when comparing the results of observation points located at different layer boundaries (Figure 4.12), but no changes were detected in the intralayer zones. This is explained by the change in inclination (verticality) of the FSI during seaward/landward movements associated with sea tides within each layer. For example, during high tides, the FSI moved landwards and both the FSI and the thermal

contours were less close to vertical in high K layers and closer to vertical in low K layers compared to their respective shapes during low tides (Figure 4.15). The orientation of the FSI produced differential movements within the same layer, resulting in an opposite oscillation between top and bottom. However, adjacent observation points located at different layers (top of high K and bottom low of K or bottom of high K and top of low K) had synchronized oscillations (Figure 4.12). The proposed mechanism could explain the opposite oscillations observed for EC and temperature when comparing the observation depths in other studies that did not incorporate such an explanation (Vallejos et al., 2015). On the other hand, changes in the hydraulic gradient, related to a higher recharge, produced a decrease in salinity due to the displacement of the FSI seawards (Figure 4.15 C). The heat plume followed the FSI and became narrower because of the increment in groundwater flow and the movement of the fresh groundwater seawards.
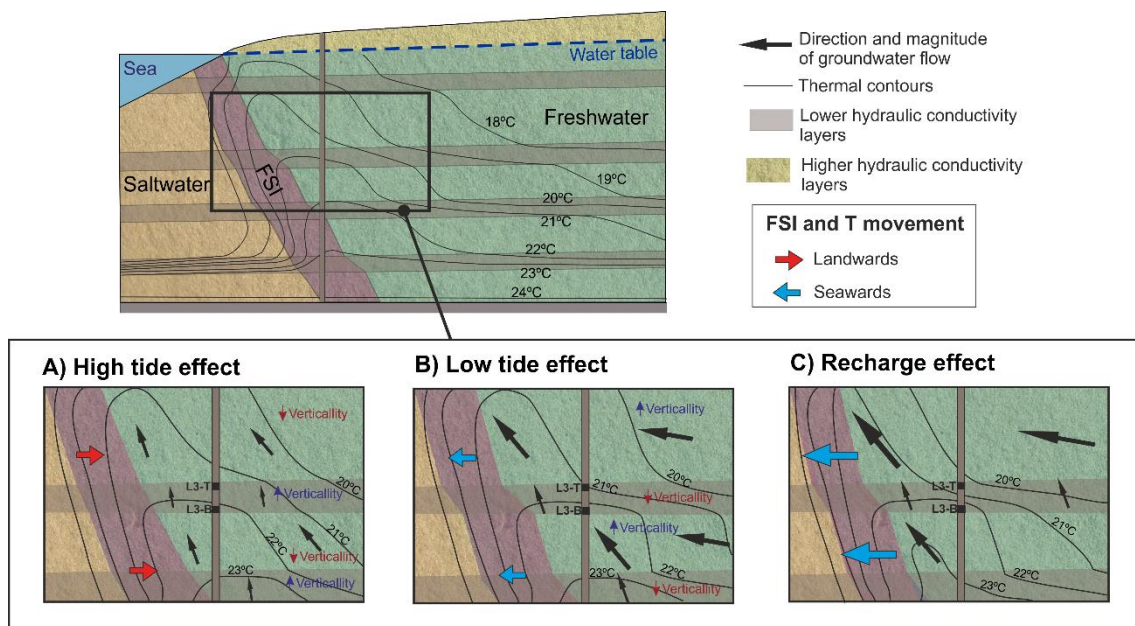

Figure 4.15.- Representation of the effect of sea tides (A,B) and the increase of recharge (C) on the FSI and groundwater temperature distribution obtained from models B and C. The movement and verticality of the thermal contours and the FSI were exaggerated to improve the visualization.

This study considered processes that are located at a depth where surface processes cannot have an immediate effect by direct transport (e.g., heat). The temperature variability was related to the changes in the position of the ascending thermal plume that accompanied the FSI position. Levanon et al. (2017) associated the salinity fluctuations near the FSI with the movement of the entire freshwater body. However, in aquifers where there is a thermal plume, the same can also be displaced as a result of the movement of groundwater, thus enabling the identification of thermal oscillations that would not be registered if the thermal contours were horizontal. This is the reason why almost simultaneous fluctuations were observed in the temperature and EC datasets. Levanon et al. (2016) showed that the hydraulic head in the FSI reacted faster than the EC, as EC fluctuations represent the actual movement of water, whereas hydraulic head fluctuations only represent pressure diffusion. Our study demonstrates that temperature fluctuations can originate from the same mechanisms that produce EC fluctuations. The close relationship between salinity and temperature distribution indicates that heat can be a

useful tool to study coastal aquifers and that the use of temperature as a natural tracer could be applied to the monitoring of the FSI location.

These relatively small variations will become important in future scenarios. Extreme droughts or rising sea levels are expected to have a greater impact on groundwater resources. The reduction of rainfall can decrease groundwater recharge to the aquifer, resulting in reduced aquifer flow and seawater intrusion (Costall et al., 2020), and a disturbance of geothermally affected groundwater temperature. Moreover, human actions such as the construction of dams, which contribute to the modification of water regimes, can induce changes in the groundwater temperature distribution in deep zones. In the study, river water flow and discharge flow from the Rules dam confirmed that the management of surface water resources generated an impact on temperature distribution. The pattern of groundwater temperature changed when the recharge increased due to the larger volume of water discharged by the Rules dam (Figure 4.6).

The Motril-Salobreña aquifer is characterized by being one of the few coastal aquifers in the Mediterranean Sea that conserves exceptional water quality and quantity (Calvache et al., 2011). The recharge originating from the melting of snow in the Sierra Nevada prevents the aquifer from incurring saltwater encroachment and, consequently, salinity and temperature oscillations due to tidal effects are smaller than under low groundwater recharge. However, other coastal Mediterranean aquifers with more extreme climate conditions can be the subject of study to identify thermal plume oscillations since they would have more evident effects.

6. Conclusions

Groundwater recharge variability and sea tides induce temporal changes in the distribution of temperature in sectors of coastal aquifers not directly influenced by surficial recharge, i.e., at deep locations. Data collected near the freshwater–saltwater interface area in the Motril-Salobreña aquifer, combined with a set of variable density and heat transport models, were used to understand the conceptual mechanism that produces temperature oscillations, as it has been observed for hydraulic heads.

1. Seasonal variations of aquifer recharge and sea tides produced a displacement of the fresh groundwater and the FSI and, consequently, changes in EC and temperature distribution. EC fluctuations depended on the horizontal gradient of salinity in the proximity of the FSI. However, the oscillations of temperature depended on the presence of the thermal plume generated by the upwelling flow along the FSI, which was also displaced together with the FSI.

2. The amplitude of EC and temperature oscillations associated with sea tides decreased with depth and increased in the areas where hydraulic conductivity changed. The convective heat transport was refracted at the interface between layers with different hydraulic conductivity, inducing a bending with different degrees of inclination (verticality) of the thermal contours. The desynchronization of the oscillations registered at the bottom and at the top of the same layer was produced by the variations in verticality of the thermal plume and the FSI.

3. EC and temperature fluctuations were related to hydraulic gradient variations and, hence, to groundwater recharge. The presence of the thermal plume induced a different evolution of salinity and temperature. Salinity progressively decreased as

the hydraulic gradient increased. However, the evolution of temperature depended on the position of the observation point with respect to the thermal plume.

4. The temperature distribution in coastal aquifers is highly sensitive to natural changes or those induced by humans. The position of the FSI and the thermal plume are dependent on groundwater recharge, which, in turn, depends on climate variability and/or water management. Groundwater recharge plays an important role in the amplitudes of temperature oscillations induced by the tides.

REFERENCES

An, Ran, Xiao Wei Jiang, Jun Zhi Wang, Li Wan, Xu Sheng Wang, and Hailong Li., 2015. Analyse Théorique de La Distribution de La Température de L'eau Souterraine à L'échelle D'un Bassin. Hydrogeol. J. 23, 397–404. https://doi.org/10.1007/s10040-014-1197-y

Anderson, M.P., 2005. Heat as a ground water tracer. Groundwater. https://doi.org/10.1111/j.1745-6584.2005.00052.x

Ataie-Ashtiani, B., Volker, R.E., Lockington, D.A., 1999. Tidal Effects on Sea Water Intrusion in Unconfined Aquifers. J. Hydrol. 216, 17–31. https://doi.org/10.1016/S0022-1694(98)00275-3.

Befus, K.M., Cardenas, M.B., Erler, D.V., Santos, I.R., Eyre, B.D., 2013. Heat transport dynamics at a sandy intertidal zone. Water Resour. Res. 49, 3770–3786. https://doi.org/10.1002/wrcr.20325

Blanco-Coronas, A.M., Duque, C., Calvache, M.L., López-Chicano, M., 2021a. Temperature Distribution in Coastal Aquifers: Insights from Groundwater Modeling and Field Data. J. Hydrol. 603, 126912. https://doi.org/10.1016/j.jhydrol.2021.126912.

Blanco-Coronas, A.M., López-Chicano, M., Acosta-Rodriguez, R., Calvache, M.L. Groundwater recharge-discharge estimation with differential flow gaugings in the final stretch of the Guadalfeo river (Granada). Geogaceta 2021b, 69, 91–94.

Calvache, M.L., Duque, C., Gomez Fontalva, J.M., Crespo, F., 2011. Processes affecting groundwater temperature patterns in a coastal aquifer. Int. J. Environ. Sci. Tech 8, 223–236.

Calvache, M.L., Ibáñez, S., Duque, C., Martín-Rosales, W., López-Chicano, M., Rubio, J.C., González, A., Viseras, C., 2009. Numerical modelling of the potential effects of a dam on a coastal aquifer in S. Spain. Hydrol. Process. 23, 1268–1281. https://doi.org/10.1002/hyp.7234

Calvache, M.L., Sánchez-Úbeda, J.P., Duque, C., López-Chicano, M., De La Torre, B., 2015. Evaluation of analytical methods to study aquifer properties with pumping tests in coastal aquifers with numerical modelling (Motril-salobreña aquifer). Water Resour. Manag. 30, 559–575. https://doi.org/10.1007/s11269-015-1177-6

Carr, P.A., Van der Kamp, G., 1969. Determining aquifer characteristics by the tidal methods. Water Resour. Res. 5, 1023–1031.

Costall, A.R., Harris, B.D., Teo, B., Schaa, R., Wagner, F.M., Pigois, J.P., 2020. Groundwater Throughflow and Seawater Intrusion in High Quality Coastal Aquifers. Sci. Rep. 10, 9866. https://doi.org/10.1038/s41598-020-66516-6

del Val, L. 2020. Advancing in the Characterization of Coastal Aquifers: A Multimethodological Approach Based on Fiber Optics Distributed Temperature Sensing. Ph.D. Thesis, Polytechnic University of Catalonia, Barcelona, Spain.

Domenico, P.A., Palciauskas. V.V., 1973. Theoretical analysis of forced convective heat transfer in regional groundwater flow. GSA Bulletin 84, 3803–3814. https://doi.org/10.1130/0016-7606(1973)84<3803:TAOFCH>2.0.CO;2

Duque, C. Influencia Antrópica Sobre la Hidrogeología del Acuífero Motril-Salobreña. Ph.D. Thesis, University of Granada, Granada, Spain, 2009.

Duque, C., Calvache, M.L., Engesgaard, P., 2010. Investigating river-aquifer relations using water temperature in an anthropized environment (Motril-Salobreña aquifer). J. Hydrol. 381, 121–133. https://doi.org/10.1016/j.jhydrol.2009.11.032

Duque, C., Calvache, M.L., Pedrera, A., Martín-Rosales, W., López-Chicano, M., 2008. Combined time domain electromagnetic soundings and gravimetry to determine marine intrusion in a detrital coastal aquifer (Southern Spain). J. Hydrol. 349, 536–547. https://doi.org/10.1016/j.jhydrol.2007.11.031

Duque, C., López-Chicano, M., Calvache, M.L., Martín-Rosales, W., Gómez-Fontalva, J.M., Crespo, F., 2011. Recharge sources and hydrogeological effects of irrigation and an influent river identified by stable isotopes in the Motril-Salobreña aquifer (Southern Spain). Hydrol. Process. 25, 2261–2274. https://doi.org/10.1002/hyp.7990

Erskine, A.D., 1991. The Effect of Tidal Fluctuation on a Coastal Aquifer in the UK. Groundwater. 29, 556–562. https://doi.org/10.1111/j.1745-6584.1991.tb00547.x.

Fidelibus, M.D., Pulido-Bosch, A., 2019. Groundwater temperature as an indicator of the vulnerability of Karst coastal aquifers. Geosciences. 9, 23. https://doi.org/10.3390/geosciences9010023.

Geng, X., Boufadel, M., 2017. Spectral responses of gravel beaches to tidal signals. Sci. Rep. 7, 40770. https://doi.org/10.1038/srep40770.

Harbaugh, A.W., Banta, E.R., Hill, M.C., Mcdonald, M.G., 2000. MODFLOW-2000, The U.S. Geological Survey modular ground-water model user guide to modularization concepts and the ground-water flow procesS, Geological Survey. CO McDonald Morrissey Associates.

Heiss, J.W., Michael, H.A., 2014. Saltwater-freshwater mixing dynamics in a sandy beach aquifer over tidal, spring-neap, and seasonal cycles. Water Resour. Res. 50, 6747–6766. https://doi.org/10.1002/2014WR015574.

Kim, K.Y., Chon, C.M., Park, K.H., Park, Y.S., Woo, N.C., 2008. Multi-depth monitoring of electrical conductivity and temperature of groundwater at a multilayered coastal aquifer: Jeju Island, Korea. Hydrol. Process. 22, 3724–3733. https://doi.org/10.1002/hyp.6976

Kim, K.Y., Park, Y.S., Kim, G.P., Park, K.H., 2009. Dynamic freshwater-saline water interaction in the coastal zone of Jeju Island, South Korea. Hydrogeol. J. 17, 617–629. https://doi.org/10.1007/s10040-008-0372-4

Kurylyk, B.L., Irvine, D.J., Bense, V.F., 2019. Theory, tools, and multidisciplinary applications for tracing groundwater fluxes from temperature profiles. Wiley Interdiscip. Rev. Water 6, e1329. https://doi.org/10.1002/wat2.1329

La Licata, I., Langevin, C.D., Dausman, A.M., Alberti, L., 2011. Effect of tidal fluctuations on transient dispersion of simulated contaminant concentrations in coastal aquifers. Hydrogeol. J. 19, 1313–1322. https://doi.org/10.1007/s10040-011-0763-9.

Larocque, M., Mangin, A., Razack, M., Banton, O., 1998. Contribution of correlation and spectral analyses to the regional study of a large karst aquifer (Charente, France). J. Hydrol. 205, 217–231. https://doi.org/10.1016/S0022-1694(97)00155-8

Langevin, C.D., Dausman, A.M., Thorne, D., Sukop., M.C., 2008. Modeling solute and heat transport with SEAWAT. In MODFLOW and More 2008: Ground Water and Public Policy–Conference Proceedings, Golden, Colorado, 19–21 May 2008.

LeRoux, N.K., Kurylyk, B.L., Briggs, M.A., Irvine, D.J., Tamborski, J.J., Bense, V.F., 2021. Using Heat to Trace Vertical Water Fluxes in Sediment Experiencing Concurrent Tidal Pumping and Groundwater Discharge. Water Resour. Res. 57, e2020WR027904. https://doi.org/10.1029/2020WR027904.

Levanon, E., Yechieli, Y., Shalev, E., Friedman, V., Gvirtzman, H., 2013. Reliable monitoring of the transition zone between fresh and saline waters in coastal aquifers. Groundw. Monitor. Remed. 33, 101–110. https://doi.org/10.1111/gwmr.12020.

Levanon, E., Shalev, E., Yechieli, Y., Gvirtzman, H., 2016. Advances in Water Resources Fluctuations of fresh-saline water interface and of water table induced by sea tides in unconfined aquifers. Adv. Water Resour. 96, 34–42. https://doi.org/10.1016/j.advwatres.2016.06.013

Levanon, E., Yechieli, Y., Gvirtzman, H., Shalev, E., 2017. Tide-Induced Fluctuations of Salinity and Groundwater Level in Uncon-fined Aquifers—Field Measurements and Numerical Model. J. Hydrol. 551, 665–675. https://doi.org/10.1016/j.jhydrol.2016.12.045.

Li, L., Barry, D.A., Stagnitti, F., Parlange, J.Y., Jeng, D.S., 2000. Beach water table fluctuations due to spring-neap tides: Moving boundary effects. Adv. Water Res. 23, 817–824. http://doi.org/10.1016/S0309-1708(00)00017-8.

Li, L., Horn, D.P., Baird, A.J., 2006. Tide-induced variations in surface temperature and water-table depth in the intertidal zone of a sandy beach. J. Coast. Res. 22, 1370–1381. https://doi.org/10.2112/04-0202.1.

Ma, J., Zhou, Z., 2021. Origin of the low-medium temperature hot springs around Nanjing, China. Open Geosci. 13, 820–834. https://doi.org/10.1515/geo-2020-0269

Mao, X., Enot, P., Barry, D.A., Li, L., Binley, A., Jeng, D.S., 2006 Tidal influence on behaviour of a coastal aquifer adjacent to a low-relief estuary. J. Hydrol. 327, 110–127.

Nguyen, T.T.M., Yu, X., Pu, L., Xin, P., Zhang, C., Barry, D.A., Li, L., 2020. Effects of temperature on tidally influenced coastal unconfined aquifers. Water Resour. Res. 56, e2019WR026660. https://doi.org/10.1029/2019WR026660.

Nielsen, P., 1990. Tidal dynamics of the water table in beaches. Water Resour. Res. 26, 2127–2134. https://doi.org/10.1029/WR026i009p02127.

Raubenheimer, B., Guza, R.T., Elgar, S., 1999. Tidal Water Table Fluctuations in a Sandy Ocean Beach. Water Resour. Res. 35, 2313–2320, https://doi.org/10.1029/1999WR900105.

Olsen, J.T., 2016. Modeling the Evolution of Salinity in the Motril-Salobreña Aquifer Using a Paleo-Hydrogeological Model. Master's Thesis, University of Oslo, Oslo, Norway.

Pan, H., Lv, X., Wang, Y., Matte, P., Chen, H., Jin, G., 2018. Exploration of Tidal-Fluvial Interaction in the Columbia River Estuary Using S_TIDE. J. Geophys. Res. Ocean. 123, 6598–6619. https://doi.org/10.1029/2018JC014146

Parsons, M.L., 1970. Groundwater thermal regime in a glacial complex. Water Resour. Res. 6, 1701–172.

Pawlowicz, R., Beardsley, B., Lentz, S., 2002. Classical tidal harmonic analysis including error estimates in MATLAB using T_TIDE. Comput. Geoscien. 28, 929–937. https://doi.org/10.1016/S0098-3004(02)00013-4.

Pugh, D.T., 1996. Tides, Purges and Mean Sea Level. John Wiley & Sons Ltd., Chichester, UK.

Pollock, L.W., Hummon, W.D., 1971. Cyclic Changes in Interstitial Water Content, Atmospheric Exposure, and Temperature in a Marine Beach. Limnol. Oceanogr. 16, 522–535. https://doi.org/10.4319/lo.1971.16.3.0522.

Pool, M., Post, V.E.A., Simmons, C.T., 2014. Effects of Tidal Fluctuations on Mixing and Spreading in Coastal Aquifers: Homogeneous Case. Water Resour. Res. 50, 6910–6926. https://doi.org/10.1002/2014WR015534.

Robinson, M.A., Gallagher, D., Reay, W., 1998. Field observations of tidal and seasonal variations in groundwater discharge to tidal estuarine surface water. Groundw. Monitor Remed. 18, 83–92.

Robinson, C., Li, L., Barry, D.A., 2007. Effect of Tidal Forcing on a Subterranean Estuary. Adv. Water Resour. 30, 851–865. https://doi.org/10.1016/j.advwatres.2006.07.006.

Rotzoll, K., Gingerich, S.B., Jenson, J.W., El-Kadi, A.I., 2013. Estimating hydraulic properties from tidal attenuation in the Northern Guam Lens Aquifer, territory of Guam, USA. Hydrogeol. J. 21, 643–654. https://doi.org/10.1007/s10040-012-0949-9.

Saar, M. O., 2011. Review: Geothermal heat as a tracer of large-scale groundwater flow and as a means to determine permeability fields. Hydrogeol. J. 19, 31–52. https://doi.org/10.1007/s10040-010-0657-2

Sánchez-Úbeda, J. P., Calvache, M. L., Duque, C., López-Chicano, M., 2016. Filtering methods in tidal-affected groundwater head measurements: Application of harmonic analysis and continuous wavelet transform. Adv. Water Res. 97, 52–72. https://doi.org/10.1016/j.advwatres.2016.08.016

Sánchez-Úbeda, J.P., Calvache, M.L., López-Chicano, M., Duque, C., 2018. The Effects of Non-TIDAL Components, Depth of Measurement and the Use of Peak Delays in the Application of Tidal Response Methods. Water Res. Manag. 32, 481–495. https://doi.org/10.1007/s11269-017-1822-3.

Shumway, H.S., Stoffer, D.S., 2006. Time Series Analysis and its Applications: With R Examples, 2nd ed.; Springer Science + Business Media, LLC.: New York, NY, USA, 575p.

Szijártó, M., Galsa, A., Tóth, Á., Mádl-Szőnyi, J., 2019. Numerical investigation of the combined effect of forced and free thermal convection in synthetic groundwater basins. J. Hydrol. 572, 364–379. https://doi.org/10.1016/j.jhydrol.2019.03.003

Tabrizinejadas, S., Fahs, M., Ataie-Ashtiani, B., Simmons, C.T., di Chiara Roupert, R., Younes, A., 2020. A Fourier series solution for transient three-dimensional thermohaline convection in porous enclosures. Water Resour. Res. 56, e2020WR028111. https://doi.org/10.1029/2020WR028111

Taniguchi, M., 2000. Evaluations of the saltwater-groundwater interface from borehole temperatura in a coastal region. Geophys. Res. Lett. 27, 713-716.

Tirado-Conde, J., Engesgaard, P., Karan, S., Müller, S., Duque, C., 2019. Evaluation of temperature profiling and seepage meter methods for quantifying submarine groundwater discharge to coastal lagoons: Impacts of saltwater intrusion and the associated thermal regime. Water. 11, 1648. https://doi.org/10.3390/w11081648

Tóth, J., 1962. A theory of groundwater motion in small basins in central Alberta, Canada. J. Geophys. Res., 67, 4375–43787. https://doi.org/10.1029/JZ067i011p04375

Urish, D.W., McKenna, T.E., 2004. Tidal Effects on Ground Water Discharge through a Sandy Marine Beach. Groundwater. 42, 971–982. https://doi.org/10.1111/j.1745-6584.2004.tb02636.x.

Vandenbohede, A., Lebbe, L., 2011. Heat transport in a coastal groundwater flow system near De Panne, Belgium. Hydrogeol. J. 19, 1225–1238. https://doi.org/10.1007/s10040-011-0756-8

Vallejos, A., Sola, F., Pulido-Bosch, A., 2015. Processes Influencing Groundwater Level and the Freshwater-Saltwater Interface in a Coastal Aquifer. Water Res. Manag. 29, 679–697. https://doi.org/10.1007/s11269-014-0621-3.

Wang, Z., Gao, P., Jiang, G., Wang, Y., Hu, S., 2021. Heat Flow Correction for the High-Permeability Formation: A Case Study for Xiong'an New Area. Lithosphere, 2021. https://doi.org/10.2113/2021/9171191

Xun, Z., Chao, S., Ting, L., Ruige, C., Huan, Z., Jingbo, Z., Qin, C., 2015. Estimation of aquifer parameters using tide-induced groundwater level measurements in a coastal confined aquifer. Environ. Earth Sci. 73, 2197–2204. https://doi.org/10.1007/s12665-014-3570-5.

Yang, X., Shaoa, Q., Hoteit, H., Carrera, J., Younes, A., Fahs, M., 2021. Three-dimensional natural convection, entropy generation and mixing in heterogeneous porous medium. Adv. Water Resour. 115, 103992 https://doi.org/10.1016/j.advwatres.2021.103992

Yu, X., Xin, P., Wang, S.S.J., Shen, C., Li, L., 2019. Effects of Multi-Constituent Tides on a Subterranean Estuary. Adv. Water Resour. 124, 53–67. https://doi.org/10.1016/j.advwatres.2018.12.006.

Zheng, C., Wang., P.P., 1999. MT3DMS—A modular three-dimensional multispecies transport model for simulation of advection, dispersion and chemical reactions of contaminants in groundwater systems: Documentation and user's guide. U.S. Army Corps of Engineers Contract Report SERDP-99-1.

CHAPTER 5
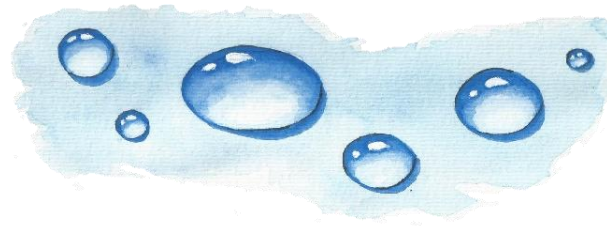
Coastal Floodings in the Guadalfeo River Plain: The Role of Groundwater

Abstract

Coastal floodings are commonly associated with land occupation by seawater and channel overflows during high tides and storms. Due to the complex behavior of the water table in coastal aquifers, groundwater inundation is poorly recognized and frequently confused with surface water flooding. Southern Mediterranean has been considered one of the most vulnerable coastal areas in the world due to flooding episodes, especially in low-lying coastal plains and deltaic areas. During recent decades, coastal areas are experiencing rapid socio-economic development and hence a population increase. This research evaluates the response of the Motril-Salobreña aquifer to flooding on the deltaic plain of the Guadalfeo river. Periodic floods occur in this area and it causes ecological damage to a wetland nature reserve "La Charca de Suárez" and economic damage to buildings, crops, and industry and tourism sector. From February 2018 to January 2021, continuous water table data had been compared with precipitation, sea level, wind direction, and sea wave height records. During the measurements period, several flood episodes took place and they could be related to water level rises registered in the piezometers. Our results showed that water table lift plays an important role in the permanence of these floodings. A higher water table reduced the unsaturated zone and hinder surface infiltration, increasing overland runoff. The high-water table events were generated by: i) the lowering of atmospheric pressure that rises sea level; ii) precipitation; iii) the decrease of the infiltration rate due to a thinner unsaturated zone; iv) high wind speeds and its direction relative to the coastline position.

_____

1. Introduction

Climate change may induce the rise of the sea level and the increase of extreme weather events (Parry et al., 2007). The vulnerability to marine inundation has increased due to sea level rise (SLR). Global sea level is estimated to have risen 0.18-0.48 m by mid-century, and 0.5-1.4 m by the end of the century (Scavia et al., 2002; Cayan et al., 2008). The consequences of SLR are the landward movement of the shoreline, beaches erosion, degradation of coastal ecosystems, acceleration of cliff retreat, damage of coastal infrastructures and humans (Jones et al., 2016; Arkema et al., 2013; Dawson et al., 2009; Rotzoll, et al., 2013; Wahl et al., 2015). Furthermore, coastal groundwater resources are expected to be degraded due to the saltwater intrusion induced by SLR. Marine floodings result in seawater infiltration into the aquifer polluting the freshwater resources. The pollution is remediated by the natural freshwater discharge of the aquifer to the sea which produces the dilution of the salt plume (Yang et al., 2013), however, it depends on the hydrodynamic state in the aquifer, such as groundwater velocity (Yang et al., 2015). Progressive salinization can affect groundwater systems when the freshwater flow is not enough, such as in overexploited aquifers.

Near the coast, fresh groundwater is forced upwards by the FSI and discharged in coastal springs and wetlands. Seasonal variations in sea level influence groundwater discharge: higher sea level results in enhanced saltwater intrusion and higher salinity of the groundwater input to the wetlands (Wood and Harrington, 2015). The conservation

of coastal wetlands requires detailed knowledge of the hydrogeological processes in coastal plains for optimal sustainable management (Price et al., 2006).

Storm surges are a common phenomenon in coastal areas worldwide (Terry, 2007; Werner et al., 2013). The range of the surge depends on the topography in the region and the position of the coastline concerning the storm track (Gönnert et al., 2001). Low-altitude locations and urban areas are susceptible to environmental and economic impacts from flooding (Housego et al., 2021). Depressed areas can experience transient floodings when the water table exceeds the land surface, known as groundwater inundations. However, they are poorly recognized and frequently confused with surface water floodings (Hughes et al., 2011). Rotzoll & Fletcher (2013) highlighted the importance of having a detailed understanding of groundwater level spatial distribution and the processes that control changes in water table height throughout the coastal zone.

In coastal regions, storm surges combined with precipitation can magnify the impact of floods (Bevacqua et al., 2019; Rahimi et al., 2020). The water table rises in response to the infiltration of precipitation (Zhang et al., 2017; Smail et al., 2019) and the infiltration capacity is reduced for subsequent events (Rotzoll and Fletcher, 2013). Thus, the integration of oceanographic, meteorological, and hydrogeological processes is needed in the study of the impact of storm hazards (Elko et al., 2019).

Although small in magnitude, sea level fluctuations cannot be neglected, and coastal communities will face a choice between coastal abandonment and adopting protective measures (Nicholls and Hoozemans, 1996). In the last decade, an increase in floods has been observed on the coast of Motril (Southeast Spain). Flooding episodes occur in the more depressed areas located near the shoreline, such as the beach, garages, roads, and wetlands. The objective of this study is to determine the contribution of groundwater to the generation of floodings in the study area, aside from other well-known factors that induce them. In addition, this study also focused on the response of La Charca de Suárez (LCS) wetlands to the floodings and evaluate potential damages under a global change scenario.

2. Research Area

The Motril-Salobreña aquifer is divided into two sectors (Duque, 2009): the western sector, which is associated with a deltaic environment, and the eastern sector, which is composed of coastal plain sediments (Figure 5.1 A). The present study is focused on the deltaic plain of the Guadalfeo River, which is constituted by pebbles, sands, and silts in variable proportions. The aquifer thickness increases from north to south until reaching more than 250 m near the coastline. The altitude of the deltaic plain ranges between 0 and 70 m a.s.l (Figure 5.1 B), however, the topographic gradient of the coastal strip is very small considering that the altitude is 6 m a.s.l. at a distance of 1500 m from the shoreline in certain areas, such as the Motril Harbor.

The coast of the province of Granada has a dry season with 400 mm mean annual rainfall. However, the region is vulnerable to extratropical Atlantic cyclones and Mediterranean storms (Ortega-Sánchez et al., 2003). Thus, rainfall events are usually associated with intense thunderstorms which cause flash floodings in the low-lying area of the deltaic plain where several buildings were constructed.

The hydrologic system is intensively managed by weirs, the Rules dam, and a large number of irrigation channels. The management has multiple purposes, such as flood control and water supply for agriculture. As a result of the construction of the Rules dam, the sediment transport through the Guadalfeo River is interrupted producing changes in the coastal sedimentation patterns. During the past decades, the sea dynamics caused erosion in Granada Beach and deposition in Poniente Beach (Bergillos et al., 2016) (Figure 5.2 A). By attempting to preserve the coast as similar as possible to natural conditions, maintenance works are frequently carried out to transport materials from Poniente Beach to Granada Beach. However, the problem is still not resolved since sand removal causes topography depressions at Poniente Beach.

The irrigation channels constitute an important asset against floodings, as they also drain the surface runoff of the entire extension of the aquifer during rainstorms. However, the farming activity is progressively abandoned and some of the channels were eliminated due to other economic interests. Nowadays, the surface runoff is concentrated in one channel that crosses the LCS reserve and discharges to the sea (Figure 5.2 B). When the sea level rises, the channel is not capable to discharge, and the upstream channels overflow.
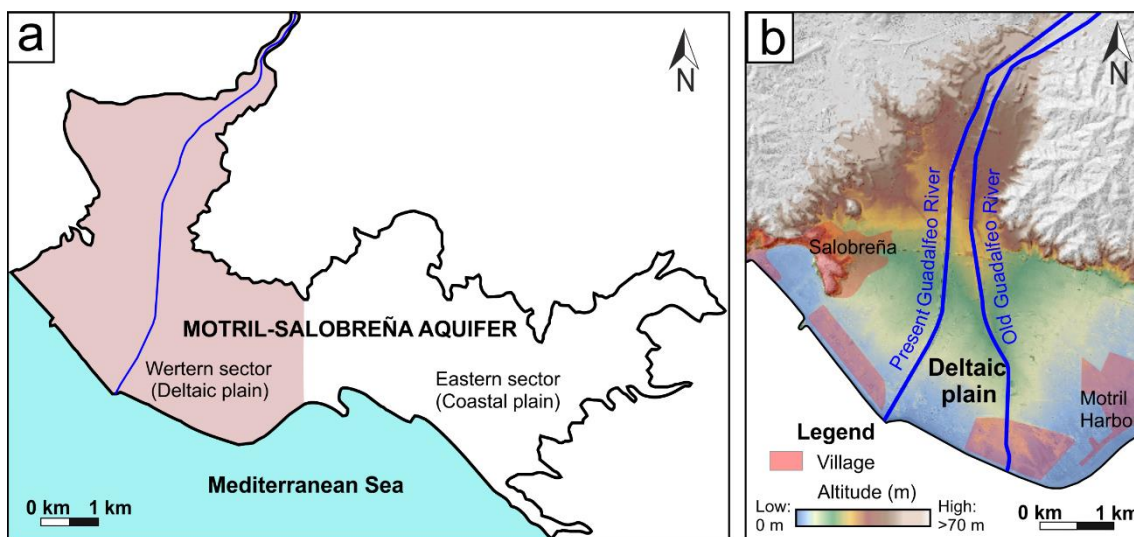

Figure 5.1.- (A) The sectors of the Motril-Salobreña aquifer considering the sedimentary environment (Modified from Sánchez-Úbeda, 2017); (B) Elevation map of the deltaic plain of the Guadalfeo River.

The Guadalfeo River, which crosses the aquifer from north to south, is characterized by being a losing stream at its northern stretch and a gaining stream at its nearest stretch to the sea (Duque et al., 2010). As the water table is situated slightly below the topography near the coastline (< 1 m), groundwater emerges in the depressed areas of the deltaic plain, such as in La Charca de Suarez (LCS) wetlands (Figure 5.2). This Protected Nature Reserve encompasses 4 lagoons located 300 m from the coastline. In general, the lagoons follow a flow-through behavior, however, the functioning of the southernmost lagoon (Lirio wetland: LW) is more complex since its limnimetric level changed related to precipitation and wind events (Blanco-Coronas et al., 2020).

Within the Deltaic Plain of the Guadalfeo River, the present study is interested in the eastern sector limited by the Mediterranean Sea (Figure 5.2 A) for being the most exposed area to the risk of flooding. It encompasses the coastal area of the municipality of Motril, the LCS wetlands, and the discharge point to the sea of the irrigation channels of the basin (Figure 5.2 B).
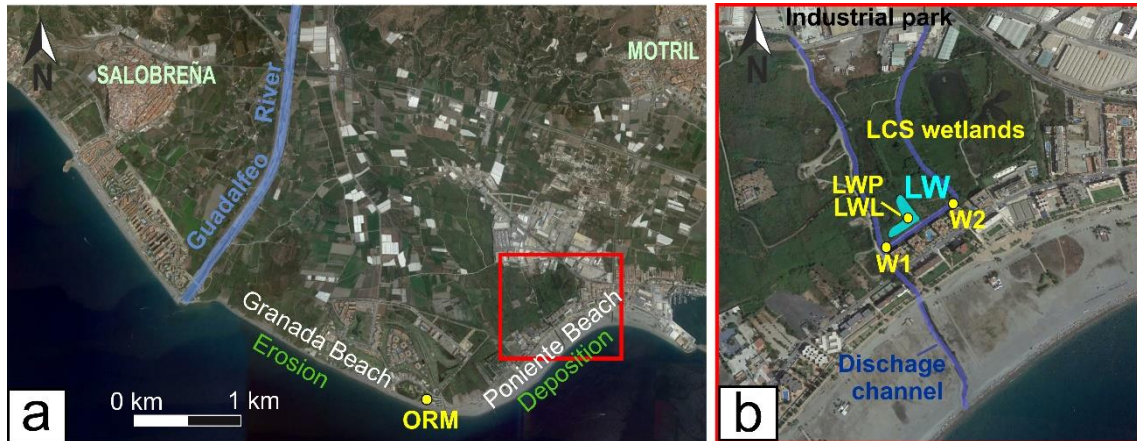

Figure 5.2.- (A) Erosion and sedimentation problems of the coastline (red rectangle corresponds to figure 5.2 B) ; (B) Location of the study area within the deltaic plain of the Guadalfeo River (Poniente Beach and La Charca de Suarez wetlands). The main channels of surface water are dark blue lines, Lirio wetland (LW) in light blue, and research boreholes in yellow points.

3. Methodology

To determine the factors associated with the creation of floodings near the coastline, field observations were conducted to detect the events and identify the affected areas, especially when the weather forecast predicted thunderstorms. Also, continuous groundwater level and limnimetric level were collected over 2 years and compared with continuous hydrometeorological data (precipitation and wind speed) and sea wave height. To identify changes in the quality of groundwater due to flooding events, continuous EC data and vertical logs of EC were registered for 5 months.

Three research wells were used to study the groundwater variations: ORM (70 m deep) at a distance of 50 m to the shoreline, and W1 and W2 (20 m deep) at a distance of 330 m to the shoreline (Figure 5.2). Pressure–temperature–EC sensors were installed at a 45-m in ORM and 6-m depth in W1 and W2, to measure at 1–hour intervals (Seametrics CT2X sensor) from 2018 to 2020. Vertical EC profiles were logged at W1 using a multiparameter probe KLL-Q-2 (accuracy: ±0.1 °C; resolution 0.01 °C) in different months of 2019.

To study the relationship between groundwater and limnimetric level during floodings, one limnimetric tube (LWL) and one piezometric tube (LWP) were sunk into the bottom of LW at its southern sector (Figure 5.2 B). Pressure-temperature sensors were configured to measure at 1–hour intervals (Seametrics LevelSCOUT smart pressure sensors) during 2020. The pressure measurements obtained from the LevelScouts and CT2X sensors were compensated by a barometric pressure sensor (Seametric BaroScout). EC of water samples collected in LW was also measured by the multiparameter probe KLL-Q-2 from June to October 2019.

Hourly precipitation and inland wind speed and direction datasets were obtained from the nearest meteorological station (60.Motril) that belongs to the SAIH Hidrosur network (Junta de Andalucía). The hourly data of sea wave height and offshore wind speed and direction were obtained from the State Harbors of the Spanish Ministry of Development from the SIMAR point located off the Motril coast (SIMAR 2042080).

4. Results

4.1. Description of the Flooding Events

During 2018 and 2019, several floods occurred near the coastline of Motril. The root causes that induced the flooding were different for each event, which entailed contrasts in the extension of the affected zone and the permanence of the sheet of water.

Flooding 1 (F1)

On 1st March 2018 started the first flooding of the period (F1), which endured until 2nd of March. 105.4 mm of rainfall accumulated in a 48-h period. The highest inland wind speed observed was 4.6 m/s with the general wind direction being SW (Figure 5.3), and the offshore wind speed was 20.38 m/s. The affected zone was the LCS wetland, the industrial park, and the Poniente beach where channels and lagoons overflowed.
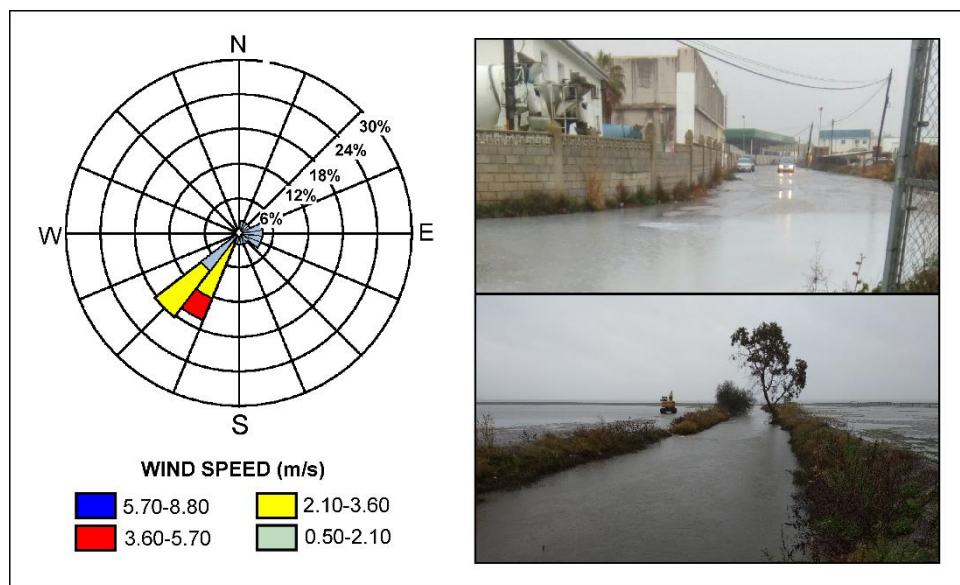

Figure 5.3.- Inland wind direction and speed during the 1st and 2nd of March 2018, and some of the affected areas during the flooding F1: the industrial park and the beach (Pictures taken by the staff of LCS)

Flooding 2 (F2)

On 18th March 2018 occurred the second flooding of the period (F2) endured until 19th of March. It was a consequence of the 57.9 mm of rain received the previous day and the inland wind speed of 4.06 m/s blowing from the SW (Figure 5.4). The maximum wind speed observed offshore was 17.87 m/s. Compared with the climate conditions during F1, precipitations were considerably less, and the wind blew from the SW 30% of the time. The

affected zones were a large area of the beach, the LCS wetlands, and the industrial park, as well as the effects of the previous flooding event.
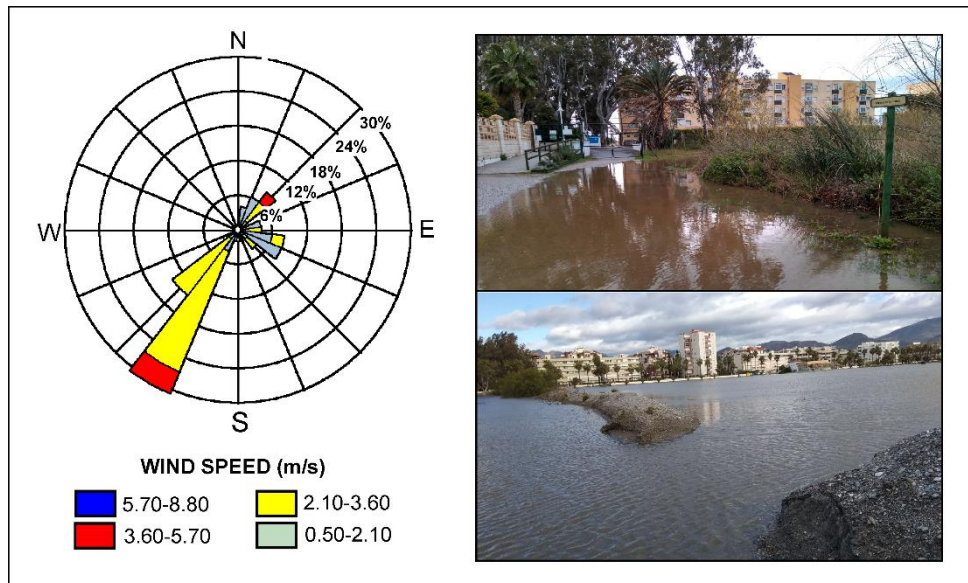

Figure 5.4.- Wind direction and speed during the days 18th and 19th of March 2018, and some of the affected areas during the flooding F2: LCS reserve and the beach (Pictures taken by the staff of LCS).

Flooding 3 (F3)

On 18th October 2018 occurred the third flooding of the period (F3), after 20 mm of rainfall in an 8 h period and high winds with a maximum speed of 3.09 m/s blowing from the NNE (Figure 5.5). The maximum wind speed measured offshore was 13.07 m/s. It was observed high water levels at the channels and small puddles at the beach, however, the affected surface was very limited compared to F1 and F2.
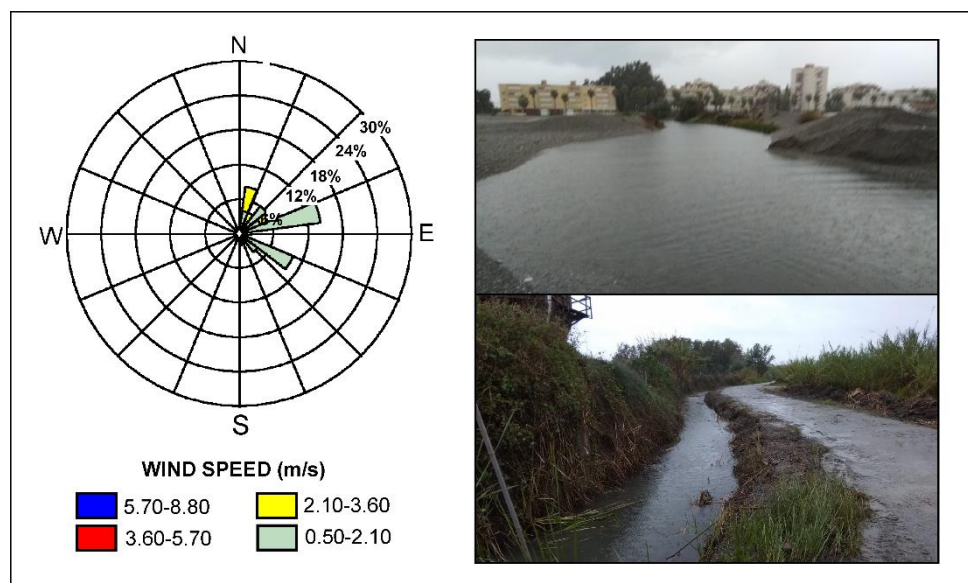
Figure 5.5.- Wind direction and speed during the days 18th October 2018, and some of the affected areas during the flooding F3: the beach and channels of LCS wetlands (Pictures taken by the staff of LCS).

Flooding 4 (F4)

The fourth flooding of the period (F4) was on 19th November 2018. 25 mm of rainfall were accumulated in 24 h and the highest wind speed observed was 3.3 m/s coming from SW (Figure 5.6). The maximum wind speed observed offshore was 14.88 m/s. The affected zone was the LCS wetland due to overflowing channels, however, the beach was not flooded, and the sea was relatively calm.
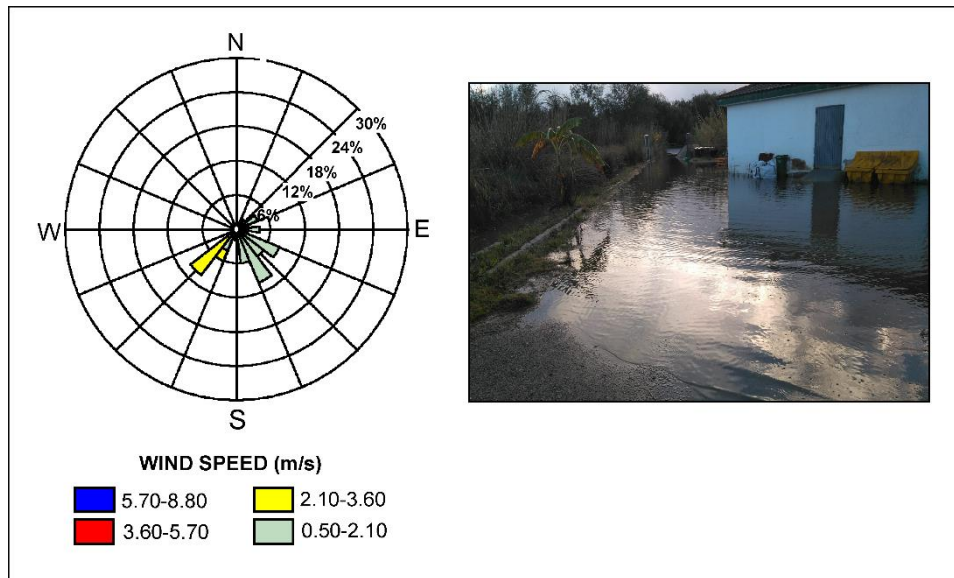

Figure 5.6.- Wind direction and speed during the day of 19th November 2018, and some of the affected areas during the flooding F4: LCS reserve (Pictures taken by the staff of LCS).

Flooding 5 (F5)

On 1st February 2019, the fifth flooding of the period (F5). 26 mm of rainfall were accumulated in 12 h and the highest wind speed observed was 6.7 m/s blowing from W (Figure 5.7). The maximum wind speed observed offshore was 17.9 m/s. The affected zone was the Poniente beach.

Flooding 6 (F6)

On 26th March 2019 started the sixth flooding of the period (F6) and endured until 30th of March. There was no precipitation but high winds with a maximum velocity of 4 m/s blowing from SE (Figure 5.8). The maximum wind speed observed offshore was 20.03 m/s. The affected areas were the beach and nearby infrastructures, such as roads and garages. F6 was the longest flooding of the research period.
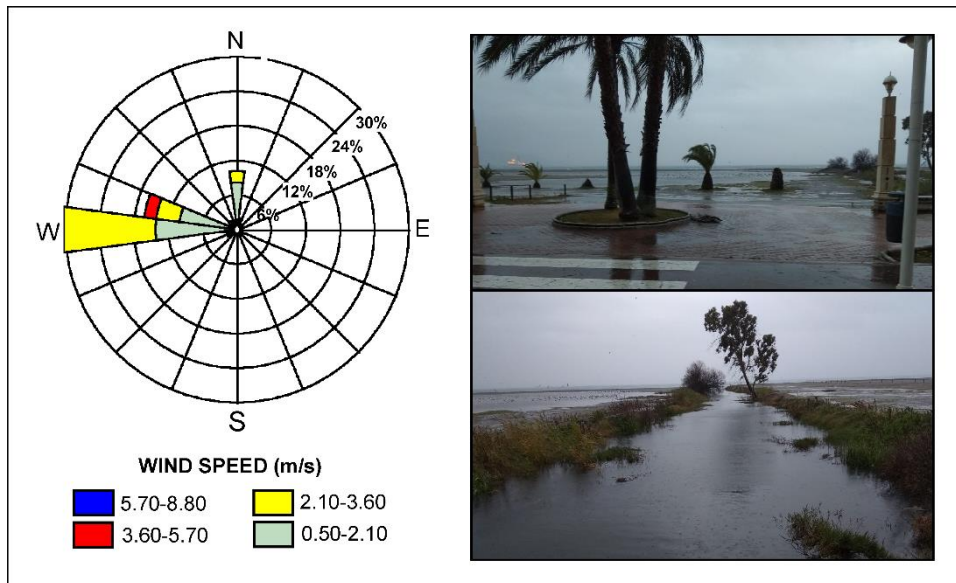
Figure 5.7.- Wind direction and speed during the days 1ˢᵗ February 2019, and the affected areas during the flooding F5: beach and the channel outlet to the sea (Pictures taken by the staff of LCS).
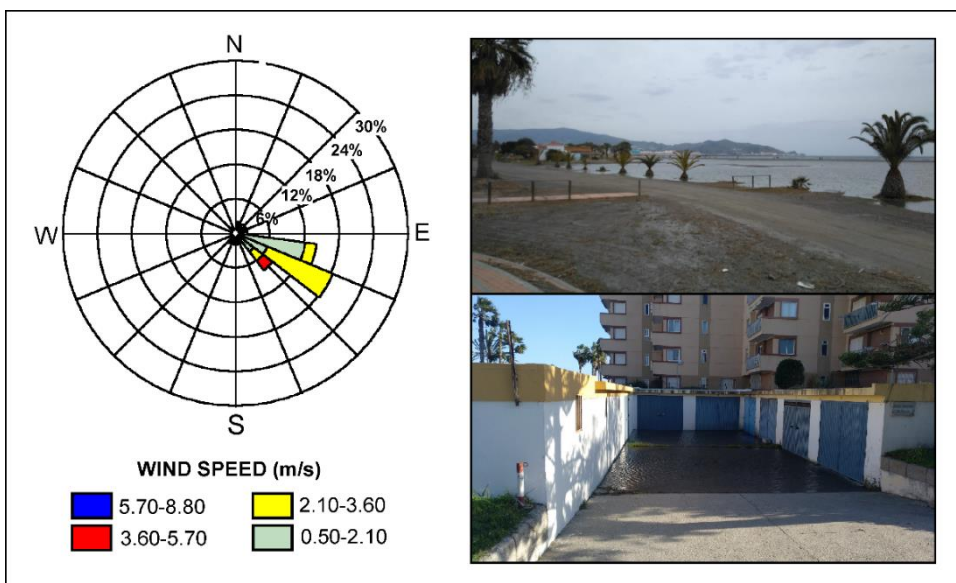

Figure 5.8.- Wind direction and speed during the day of 26ᵗʰ March 2019, and some of the affected areas during the flooding F6: Poniente beach, garages of buildings located near the beach, and roads.

<u>Flooding 7 (F7)</u>

This flooding event (F7) occurred in continuity with F6 (31ˢᵗ March 2019). 6 mm of rainfall in 15 h and a wind speed of 1.17 m/s coming from SW caused the beach to flood again when the water sheet of F6 had almost disappeared (Figure 5.9). The maximum wind speed observed offshore was 6.59 m/s.
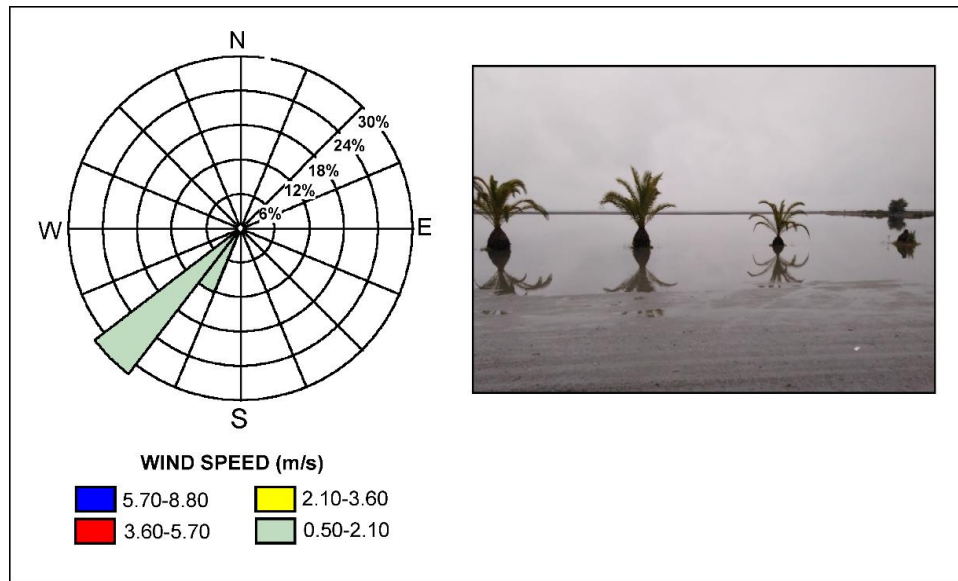
Figure 5.9.- Wind direction and speed during the day of 31st March 2019, and some of the affected areas during the flooding F7: beach (Pictures taken by the staff of LCS).

4.2. Groundwater Level Fluctuations during Flooding Events

The groundwater levels measured in wells ORM, W1, and W2 (Figure 5.10) showed that the water table was raised when flood events occurred. Most of the flood events were linked to precipitation except for the F6. The presence of heavy rains did not always entail the creation of floods or high elevation of groundwater level, as shown in September 2018. The groundwater level was less stable and had faster reactions in ORM than in W1 and W2. For instance, the water table in ORM started to increase 10 hours before W1 and W2 during F1 and F2. Fluctuations had greater magnitude in ORM than in the other observation wells during the measurement period, although the difference in magnitude was smaller during intense rainfall. Those different reactions were especially visible during the summer of 2018, registered without precipitation or flooding events.
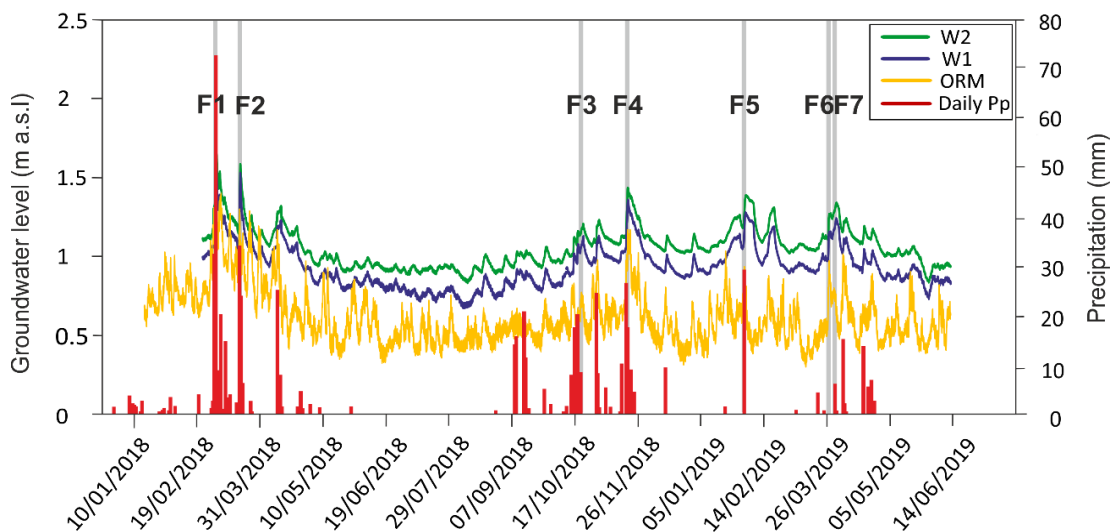

Figure 5.10.- Groundwater level (m a.s.l.) measured in the wells of LCS nature reserve (W1 and W2) and of the old river mouth (ORM), and daily precipitations (mm).

Despite the similarity of groundwater level registrations of the three observation points, data obtained at ORM was more unstable. Thus, it was chosen to compare with other parameters to determine the origin of the fluctuations (Figure 5.11). The groundwater level peaks reflected the close relationship between the sea level changes and the groundwater level nearby the coastline, not only during floodings or precipitation but also throughout the measurement period. In the last cases, the groundwater level peaks were produced in parallel with sea wave height peaks. On the other hand, the groundwater level was even more similar to the atmospheric pressure record but inversely, i.e., the maximum in the groundwater, and the minimum in the atmospheric pressure.
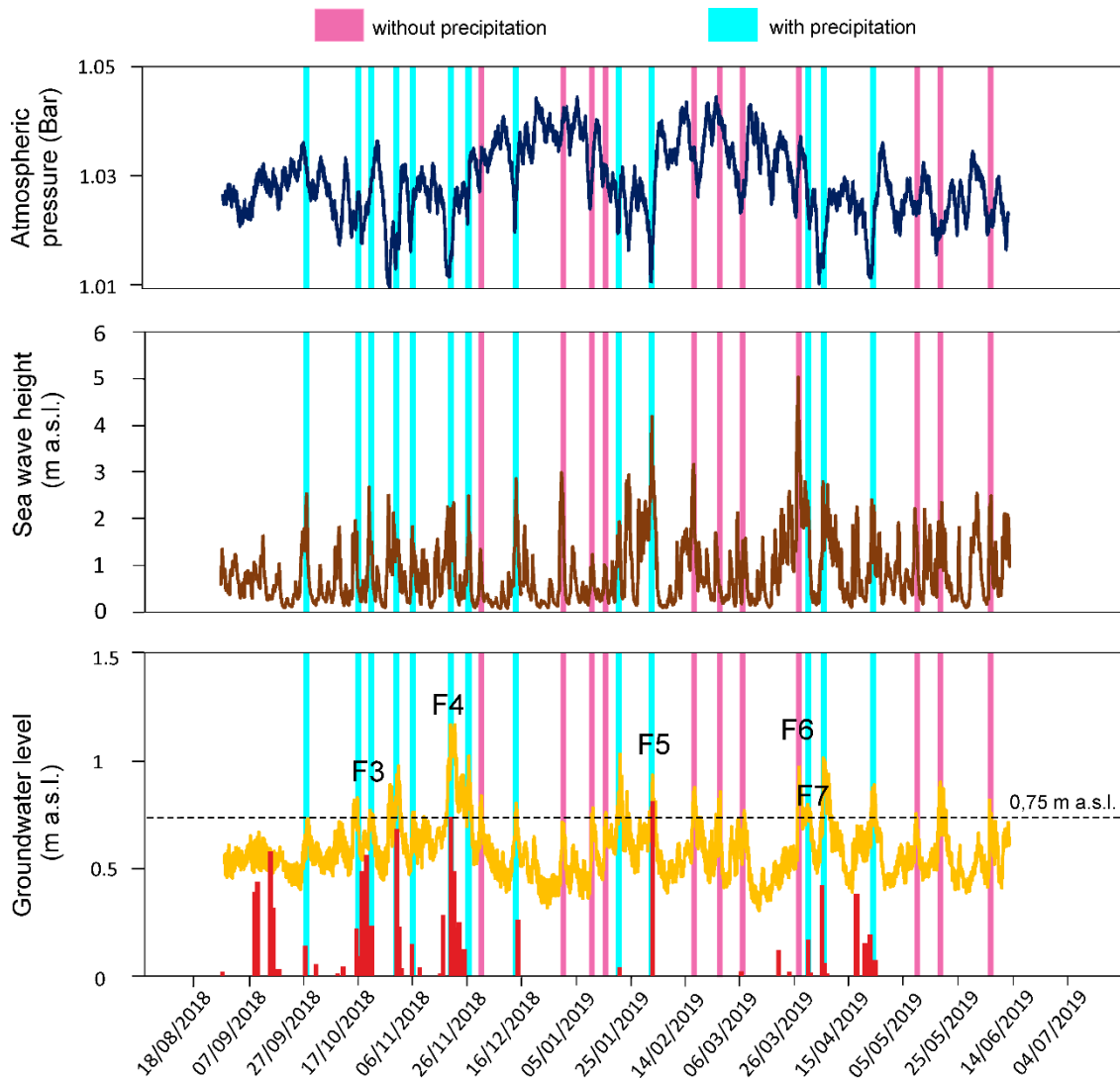

Figure 5.11.- Atmospheric pressure (Bar), Sea wave height (m a.s.l.), water table in ORM (m a.s.l.), and daily precipitations in red (mm). The blue and pink lines indicate when water level reached 0,75 m a.s.l.

4.3. *LCS Wetlands Functioning during Flooding Events and Potential Hazards*

Although LCS wetlands had a flow-through functioning under normal conditions with groundwater inflows in the northern section and groundwater outflows in the southern section (Blanco-Coronas et al., 2020), the hydrodynamics was often changed. At the southern sector of the LW lagoon, the groundwater level surpassed the limnimetric level several times during the period from June 2020 to January 2021 (Figure 5.12). The most significant peak occurred during the flooding event F8 after an accumulation of 40.6 mm of rainfall: the limnimetric level rose about 0.58 m and the piezometric level rose 0.67 m in less than 24 hours, resulting in an inversion of the hydraulic gradient. The other inversions of the hydraulic gradient in the southern part of the lagoon were associated with strong winds prevailing from SW and SE. They caused the aquifer to recharge the LW at the southern section and thus, the lagoon changed from a flow-through lagoon to an influent lagoon.
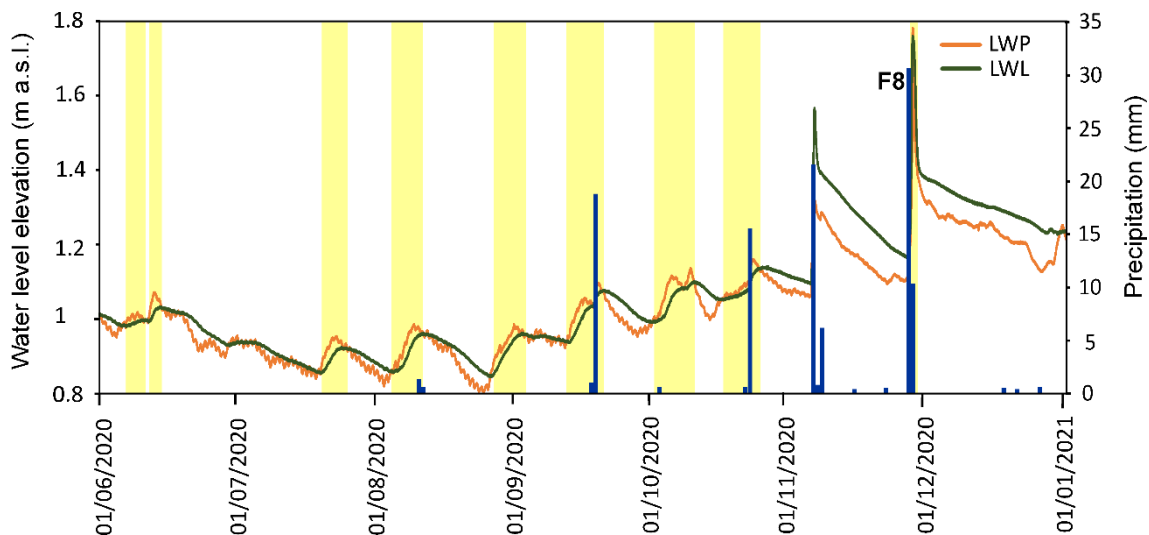

Figure 5.12.- Groundwater level and limnimetric level (m a.s.l.) measured in LW and daily precipitation in blue (mm). The yellow areas represent the inversion of the hydraulic gradient.

Water samples obtained in LW from June to October 2019 showed that EC values ranged from 1400 to 1800 µS/cm (Figure 5.13 A). Until July, there is a rising trend of salinity when the maximum was reached, followed by a continuous decrease in the salinity. The vertical logs of EC in W1 (Figure 5.13 B) increased salinity from March 2019 to June 2019. On March 2019, EC was about 2400 µS/cm from -1 to -12 m and then started to increase until reaching 3500 µS/cm at -15 m. On April 2019, EC was about 2800 µS/cm from -2 m to -12 m and then started to increase until reaching 4200 µS/cm at -15 m. On May 2019, EC was about 2800 µS/cm from -2 m to -10 m and then started to increase until reaching 4200 µS/cm at -12 m. Thus, during the three months, the lowest increase was about 380 µS/cm at - 6 m and about 1740 µS/cm at -12 m.
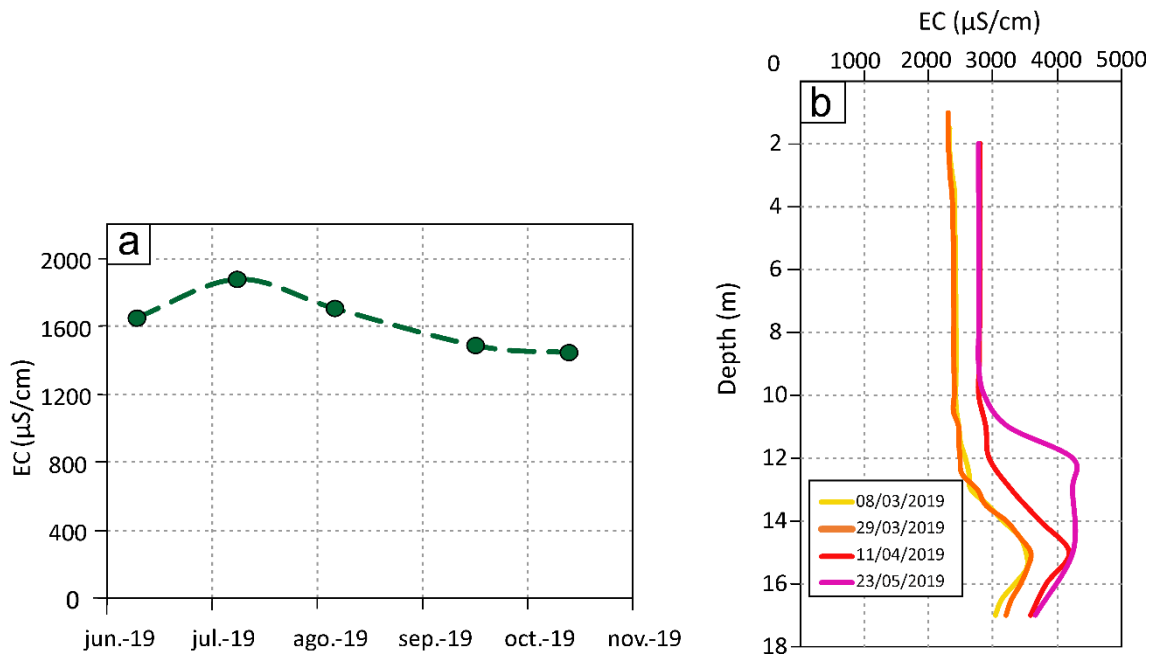
Figure 5.13.- (A) Monthly registration of electrical conductivity (EC) in LW. (B) Vertical logs of electrical conductivity in W1.

5. Discussion

The reason for the inundations in the deltaic plain of the Guadalfeo River was the combination of different sources: precipitation, marine inundations, and groundwater rise, as has been shown in other coastal areas (Rahimi, et al. 2020). Although the study area is subjected to a semi-arid climate, precipitations were concentrated as intense events during autumn and spring. During floodings, the amount of precipitation falling in the study area caused the increment of the overland runoff in the drainage basin. The magnitude of the floodings was increased when rainfall coincided with higher sea levels, as in the case of F1 and F2: the discharge capacity of the channel diminished since the sea behaved as a hydraulic barrier.

During storm surges, strong winds drove water toward the shoreline and incremented the sea level locally. The sea invaded the more depressed areas located at the beach due to the action of the sea waves, often caused during low barometric pressure. The direction of the wind during floodings was predominantly SE and SW, which influenced storm surges more than other registered directions that had less presence. The importance of wind direction was confirmed when the single action of the wind blowing from SE, perpendicular to the coast, caused flooding F6. Gönnert et al. (2001) also associated the magnitude of floodings with the direction of the wind relative to the coastline position.

The water table was incremented until 0.7 m nearer the coastline during sea level lifts due to storm surges, and thus it was positioned nearest to the topography. As described by Rotzoll and Fletcher (2013), the unsaturated zone of the aquifer become almost negligible and provoked a decrease in the infiltration capacity of the soil, which hindered the infiltration of the surface water. Therefore, floodings were larger due to high groundwater levels. On the other hand, the water table remained high for 5 days during F6, conserving the surface water sheet over those days at distant points from the shoreline,

such as depressed areas and garages, that marine inundation did not reach. This could be considered direct groundwater inundation, even if it is initially triggered by a marine inundation according to Rotzoll and Fletcher (2013). The role of barometric pressure in these events must be considered too as it induced greater wave action and increased the water table, as described in Vallejos et al., (2015). Therefore, the role of groundwater table in coastal floodings must be contemplated and studied in conjunction with the previous factors (precipitation, atmospheric pressure, wind speed and direction, and infiltration rate).

The functioning of LCS wetlands was very sensitive to coastal hydrodynamics, especially the lagoon LW which changed its behavior from flow-through under normal conditions to effluent lagoon not only during marine floodings, (Blanco-Coronas et al., 2020) but also during strong wind periods. Changes in the surrounding hydrologic system can produce salinization of coastal wetlands, as observed in the lagoons of the Guadalhorce River Mouth in Málaga (Nieto-López et al., 2020). The origin of the salinization of LW is unknown: the evaporation could have incremented the solute concentration, commonly observed in dry or semi-arid climate regions. Casamitjana et al. (2019) identified in NE Spain that the enrichment in salts in a lagoon due to evaporation salinized the aquifer due to infiltration during the dry seasons and, once the autumn cyclonic storm events began, the infiltrated water was returned to the lagoons. However, in the present study, groundwater salinity had been increasing before summer at the closest piezometer W1 and before the salinization of LW (Figure 5.13 B). This area was predisposed to be affected by seawater intrusion due to the proximity of the discharge channel to the sea. A potential origin of salinity in the study area is related to saline water encroaching inland throughout the channel during marine floodings and then it was infiltrated, resulting in the salinization of groundwater. Thus, the rise of salinity detected in LW could be linked to groundwater discharge to the lagoon because of inversions of the hydraulic gradient, similar to the process produced in the Piccaninnie Ponds on the coast of South Australia (Wood and Harrington, 2015).

Although the aquifer has good groundwater quality at the current time, this fact should be studied in depth. If marine flooding events are repeated in the future combined with hydraulic gradient inversion, lagoons can be fed with more saline groundwater endangering the current wetland status. The predicted sea-level rise and the decrease of freshwater recharge can induce progressive salinization as the fresh groundwater flow will not be enough to flush the saline plume.

The flooding processes near the shoreline of the Guadalfeo River plain have been repeated in the last few years. In addition to the climate component, this phenomenon has been exacerbated by other factors induced by human intervention. On one hand, the elimination of discharge points of surface water to the sea and the concentration into one drainage channel produced its overflow and increased the surface of the flooded terrain. On the other hand, the extraction of sand produced depressions of the topography of the beach that behaved as floodable areas during the events.

6. Conclusions

During the period between 2018 and 2020, eight coastal floodings were identified at the deltaic plain of the Guadalfeo River. The buildings, infrastructures, and the Protected Nature Reserve of La Charca de Suárez were affected.

The floodings were induced by several factors common to other study sites: rainfall, storm surges, and barometric pressure. However, the results of this research highlighted the role of groundwater, which was commonly neglected in flood studies. During storm surges, the local sea level rise, induced by strong winds, caused an increase in the height of the groundwater level. In topographically lower areas, the water table magnified the duration and extent of flood impacts. It diminished the unsaturated zone of the soil avoiding the runoff water infiltration and even it caused groundwater floodings on certain occasions.

Intense precipitations did not always produce flooding in the study area. Most of the floodings were induced by the combination of precipitation with storm surges and the rise of the water table and they had a duration of up to 2 days. However, precipitation was absent during one of the floodings (F6) and the storm surge was the main cause of the longest inundation registered in the study period (5 days). In this case, the direction of the wind had an important role in the elevation of the water table, especially when it blew perpendicular to the coast.

The hydrodynamics of the lagoons were changed several times due not only to coastal floodings but also to the decrease of atmospheric pressure that produced high winds. Also, the quality state of the lagoon LW was endangered by its progressive salinization during the dry period, which occurred a short time after the increase of salinity in groundwater. The inversion of the hydraulic gradient could deteriorate the ecosystem of the lagoons of LCS. Due to the complexity of the hydrodynamics in coastal systems, the behavior of groundwater should be considered in order to face more frequent and longer inundations in the future.

REFERENCES

Arkema, K.K., Guannel, G., Verutes, G., Wood, S.A., Guerry, A., Ruckelshaus, M., Kareiva, P., Lacayo, M., Silver, J.M., 2013. Coastal habitats shield people and property from sea-level rise and storms. Nat. Clim. Chang., 3, 913–918.

Bergillos, R.J., Rodríguez-Delgado, C., Millares, A., Ortega-Sánchez, M. Losada, M.A. 2016. Impact of river regulation on a Mediterranean delta: Assessment of managed versus unmanaged scenarios. Water Resour. Res. 52, 5132-5148. https://doi.org/10.1002/2015WR018395

Bevacqua, E., Maraun, D., Vousdoukas, M. I., Voukouvalas, E., Vrac, M., Mentaschi, L., Windmann, M., 2019. Higher Probability of Compound Flooding from Precipitation and Storm Surge in Europe under Anthropogenic Climate Change. Sci. Adv. 5 (9), 5531. https://doi.org/10.1126/sciadv.aaw5531

Blanco-Coronas, A.M., López-Chicano, M., Calvache, M.L., Benavente, J., Duque, C., 2020. Groundwater-Surface water interactions in "La Charca de Suárez" Wetlands, Spain. Water, 12(2), 344. https://doi.org/10.3390/w12020344

Casamitjana, X., Mencló, A., Quintana, X.D., Soler, D., Compte, J., Martinoy, M., Pascual, J., 2019. Modeling the salinity fluctuations in salt marsh lagoons. J. Hydrol. 575, 1178-1187. https://doi.org/10.1016/j.jhydrol.2019.06.018

Cayan, D.R., Bromirski, P.D., Hayhoe, K., Tyree, M., Dettinger, M.D., Flick, R.E. 2008. Climate change projections of sea level extremes along the California coast. Climatic Change 87 (Suppl 1), 57–73. https://doi.org/10.1007/s10584-007-9376-7

Dawson, R.J., Dickson, M.E., Nicholls, R.J., Hall, J.W., Walkden, M.J.A., Stansby, P.K., Mokrech, M., Richards, J., Zhou, J., Milligan, J., Jordan, A., Pearson, S., Rees, J., Bates, P.D., Koukoulas, S., Watkinson, A.R., 2009. Integrated analysis of risks of coastal flooding and cliff erosion under scenarios of long term change. Clim. Chang., 95, 249–288.

Duque, C., 2009. Influencia antrópica sobre la hidrogeología del acuífero Motril-Salobreña. Doctoral thesis. University of Granada. 196 pp.

Duque, C., Calvache, M.L., Engesgaard, P., 2010. Investigating river-aquifer relations using water temperature in an anthropized environment (Motril-Salobreña aquifer). J. Hydrol. 381, 121–133. https://doi.org/10.1016/j.jhydrol.2009.11.032

Elko, N., Dietrich, J., Cialone, M., Stockdon, H., Bilskie, M., Boyd, B., et al., 2019. Advancing the understanding of storm processes and impacts. Shore and Beach, 87, 41– 55.

Gönnert, G., Dube, S.K., Murty, T., Siefert, W., 2001. Global storm surges, Die Küste— Archive for research and technology on the North Sea and Baltic Sea coast. Kuratorium Forsch. Küsteningenieurwesen. 63, 623.

Housego, R., Raubenheimer, B., Elgar, S., Cross, S., Legner, C., Ryan, D., 2021. Coastal flooding generated by ocean wave-and surge-driven groundwater fluctuations on a sandy barrier island. J. Hydrol., 603, 126920. https://doi.org/10.1016/j.jhydrol.2021.126920

Hughes, A.G., Vounaki, T., Peach, D.W., Ireson, A.M., Jackson, C.R., Butler, A.P., Bloomfield, J.P., Finch, J., Wheater, H.S., 2011. Flood risk from groundwater: Examples from a Chalk catchment in southern England. J. Flood Risk Manag. 4(3): 143–155. https://doi.org/10.1111/j.1753-318X.2011.01095.x

Nicholls, F.J., Hoozemans, F.M.J., 1996. The Mediterranean: vulnerability to coastal implications of climate change. Ocean Coast. Manag. 31, 105-132. https://doi.org/10.1016/S0964-5691(96)00037-3

Nieto-López, J.M., Barberá, J.A., Andreo, B., Ramírez-González, J.M., Rendón-Martos, M., 2020. Hydro-environmental changes assessment after Guadalhorce River mouth channelization. An example of hydromodification in southern Spain. Catena. 189, 104461. https://doi.org/10.1016/j.catena.2020.104461

Ortega-Sánchez, M., Losada, M.A., Baquerizo, A., 2003. On the development of large-scale cuspate features on a semi-reflective beach: Carchuna Beach, southern Spain, Mar. Geol., 198, 209–223. https://doi.org/10.1016/S0025-3227(03)00126-9

Parry, M.L., Canziani, O.F., Palutikof, J.P., van der Linden, P.J., Hanson, C.E., 2007. Climate change 2007: impacts, adaptation and vulnerability. Contribution of Working Group II to the fourth assessment report of the Intergovernmental Panel on Climate Change. Cambridge: Cambridge University Press.

Price, R.M., Swart, P.K., Fourqurean, J.W., 2006 Coastal groundwater discharge – an additional source of phosphorus for the oligotrophic wetlands of the Everglades. Hydrobiologia, 569, 23-26. https://doi.org/10.1007/s10750-006-0120-5

Rahimi, R., Tavakol-Davani, H., Graves, C., Gomez, A., Valipour, M. F., 2020. Compound inundation impacts of coastal climate change: Sea-level rise, groundwater rise, and coastal watershed precipitation. Water, 12(2776), 2776. https://doi.org/10.3390/w12102776

Rotzoll, K., Fletcher, C.H., 2013. Assessment of groundwater inundation as a consequence of sea-level rise. Nat. Clim. Chang., 3, 477–481. https://doi.org/10.1038/nclimate1725

Sánchez-Úbeda, J.P., López-Chicano, M., Calvache, M.L., Purtschert, R., Engesgaard, P., Martín-Montañés, C., Sültenfuβ, J., Duque, C., 2018b. Groundwater Age Dating in Motril-Salobreña Coastal Aquifer with Environmental Tracers ($\delta18O/\delta2H$, 3H/3He, 4He, 85Kr, and 39Ar). In: Calvache M., Duque C., Pulido-Velazquez D. (eds) Groundwater and Global Change in the Western Mediterranean Area. Environ. Earth Sci. Springer, Cham. https://doi.org/10.1007/978-3-319-69356-9_33

Scavia, D., Field, J.C., Boesch, D.F.,Buddemeier, R., Cayan, D.R., Burkett, V., Fogarty, M., Harwell, M., Howarth, R., Mason, C., Reed, D.J., Royer, T.C., Sallenger, A.H., Titus, J.G., 2002. Climate change impacts on U.S. coastal and marine ecosystems. Estuaries, 25, 149-164.

Smail., R., Pruitt, A.H., Mitchell, P.D., Colquhoun, J.B. 2019. Cumulative deviation from moving mean precipitation as a proxy for groundwater level variation in Wisconsin. J. Hydrol. X, 100045. https://doi.org/10.1016/j.hydroa.2019.100045

Terry, J.P. 2007. Tropical cyclones: climatology and impacts in the South Pacific. Springer, New York, London.

Vallejos, A., Sola, F., Pulido-Bosch, A.. 2015. Processes Influencing Groundwater Level and the Freshwater-Saltwater Interface in a Coastal Aquifer. Water Resour Manage 29, 679–697. https://doi.org/10.1007/s11269-014-0621-3

Wahl, T., Jain, S., Bender, J., Meyers, S.D., Luther, M.E., 2015. Increasing risk of compound flooding from storm surge and rainfall for major US cities. Nat. Clim. Chang., 5, 1093–1097. https://doi.org/10.1038/nclimate2736

Werner, A.D., Bakker, M., Post, V.E.A., Vandenbohede, A., Lu, C., Ataie-Ashtiani, B., Simmons, C.T., Barry, D.A., 2013. Seawater intrusion processes, investigation and management: recent advances and future challenges. Adv. Water Resour. 51, 3–26. https://doi.org/10.1016/j.advwatres.2012.03.004

Wood, C., Harrington, G.A., 2015. Influence of Seasonal Variations in Sea Level on the Salinity Regime of a Coastal Groundwater–Fed Wetland. Groundwater, 53. https://doi.org/ 10.1111/gwat.12168

Yang, J., Graf, T., Herold, M., Ptak, T., 2013. Modelling the effects of tides and storm surges on coastal aquifers using a coupled surface-subsurface approach. J. Contam. Hydrol. 149, 61–75. https://doi.org/10.1016/j.jconhyd.2013.03.002

Yang, J., Graf, T., Ptak, T., 2015. Sea level rise and storm surge effects in a coastal heterogeneous aquifer: a 2D modelling study in northern Germany. Grundwasser 20, 39–51. https://doi.org/10.1007/s00767-014-0279-z

Zhang, J., Wu, J., Hua, P., Zhao, Z., Wu, L., Fan, G., Bai, Y., Kaeseberg, T., Krebs, P., 2017. The influence of land use on source apportionment and risk assessment of polycyclic aromatic hydrocarbons in road-deposited sediment Environ. Pollut., 229, 705-714 https://doi.org/ 10.1016/j.envpol.2017.07.019

CHAPTER 6
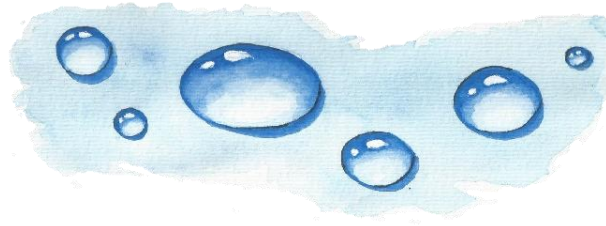
Conclusions

1. Conclusions

The investigation derived from this Ph.D. has provided a deeper understanding of the hydrodynamic processes of coastal aquifers related to groundwater temperature distribution near the saltwater-freshwater interface, surface water ecosystem exchange in coastal aquifers, and coastal flooding events involving groundwater. Several methodologies were tested specifically in the Motril-Salobreña aquifer to characterize in detail natural coastal patterns. Current natural and human-induced perturbations, such as local sea-level variations or seasonal changes in groundwater recharge and surface temperature, were examined and interpreted to understand how they altered the natural functioning of the system. Even though these processes can be considered technical details in the big picture, a high sensitivity of coastal aquifers to changes was observed. Given that they are expected to be stronger in the context of Global Change, their study made it possible to anticipate the reaction of coastal aquifers in the future. The outcomes of each chapter are summarized:

- *Groundwater-Surface Water Interactions in "La Charca De Suarez" Wetland*

The Nature Reserve of "La Charca de Suárez", has a complex hydrodynamic behavior between lagoons and the aquifer due to spatial and temporal variations. The initially considered predominant inlet to the lagoon system (surface water) is not the only input as the four lagoons depended entirely or partially on groundwater. Although the general flow-through functioning of the wetlands with groundwater inflows in the northern sector and aquifer recharge in the southern sector, variations in flow patterns were detected for each of the lagoons, an interesting feature considering that all the lagoons are located close to each other. The Aneas lagoon changed to influent lagoon during wet climate periods but also because of the anthropic water supply. On the other hand, the Lirio lagoon behaved as an effluent lagoon during flooding episodes in the coastal strip caused by precipitation and/or sea wave storms. The maintenance of the required inlets of surface water not only preserved the good state of wetlands but also the subjacent aquifer as surface water infiltration in the Aneas lagoon prevented saltwater intrusion.

- *Temperature Distribution in Coastal Aquifers*

A synthetic theoretical model of temperature distribution for coastal aquifers focussed on the saline wedge area was proposed for the understanding of heat interactions with different origins (surface water recharge, sea infiltration, and geothermal heat). Each heat source induced a thermal signal within the aquifer, causing variations in temperature at different depths. Recharge temperature and seawater temperature produced seasonal temperature oscillations within the surficial zone and the saltwater domain, respectively. The geothermal heat induced an increment of the groundwater temperature with depth. Numerical modeling revealed the existence of an ascending thermal plume whose position and shape depend on the freshwater-saltwater interface. The difference in temperature between the surface and the basement of the aquifer contributed to determining the width of the freshwater-saltwater interface and the position of its toe. The flow patterns associated with the saline wedge generated a thermal barrier coinciding with the position of the freshwater-saltwater interface that separated the temperature of the saltwater and freshwater domains. The sensitivity analysis applied to different hydraulic

and thermic parameters for a range of realistic values in the experimental site showed that hydraulic conductivity and thermal input in the base of the aquifer were the main parameters influencing temperature distribution.

- *Salinity and Temperature Variations vear the Freshwater-Saltwater Interface*

Changes in groundwater temperature at deep locations of coastal aquifers were not the consequence of a thermal signal produced by surface water recharge. Instead, they were induced by the seaward/landward displacement of the fresh groundwater and the freshwater-saltwater interface due to sea tides and seasonal variations of groundwater recharge. The salinity fluctuations depended on the horizontal gradient of salinity in the proximity of the freshwater-saltwater interface. However, the oscillations of temperature depended on the thermal plume, which was also displaced together with the freshwater-saltwater interface. Aquifer heterogeneity increased the horizontal thermal gradient due to the presence of the thermal plume: thermal contours were bent by the refraction of flowlines at the interface between layers with different hydraulic conductivity. The amplitude of temperature oscillations associated with sea tides decreased with depth, but it increased with the horizontal thermal gradient of the thermal plume. On the other hand, groundwater recharge variability induced different evolution of salinity and temperature. The increase of hydraulic gradient produced the progressive decrease of salinity, however, the evolution of temperature depended on the location of the observation point concerning the thermal plume.

- *The Role of Groundwater in Coastal Floodings*

Several coastal floodings took place at the deltaic plain of the Guadalfeo River and caused economic damage to buildings and other infrastructures and environmental damage to "La Charca de Suárez" wetlands. Most of the floodings were produced by several factors common to other study sites: precipitations, storm surges, and barometric pressure. However, the results of this Ph.D. highlighted the role of groundwater, which was commonly neglected in flood studies. During storm surges, the local sea level rise, induced by strong winds and sea waves invaded the more depressed areas located at the beach, and, as a consequence, the groundwater level rose. As a result, the infiltration capacity of the soil diminished due to the almost negligible unsaturated zone of the aquifer, producing groundwater floodings in depressed areas of the study area. Most of the floodings were induced by a combination of different factors. The affected area was bigger during floodings produced by the combination of precipitation and storm surges; however, the longest flooding was caused by the action of only a storm surge and the rise of the water table. Furthermore, coastal phenomena changed the hydrodynamics of "La Charca de Suárez" wetlands, without the existence of floodings. The increase in salt concentrations in the Lirio lagoon could be the result of variations in hydraulic gradient induced by climate conditions but also by changes in the topographic surface due to human intervention.

2. Open Research Issues

The findings of this Ph.D. thesis contribute to the improvement of the knowledge of coastal hydrogeology. Nevertheless, a few issues highlight the need for in-depth investigation:

- The Ph.D. thesis comprises the first study that determines the connection of the Motril-Salobreña aquifer with "La Charca de Suárez" wetlands. The water balance of the lagoons shows that the main inlet to the system was surface water, however, it was calculated for five months during the winter-spring period. Although the climate of May was extremely dry in comparison with other years and the study period covered both the wet and the dry moments of the year, it is interesting to further study for a longer term. On the other hand, groundwater-surface water interaction was calculated as net exchange flow rather than individual groundwater inflow/outflow rates. Even seepage meters were constructed and installed to measure flow rates, the restrictions to access the study area to avoid disturbance and protect fauna only enabled measurements once per month. Other methodologies could be developed or applied in the study area to solve this problematic characteristic of protected reserves. For example, the automated seepage meter, which is a modification of the conventional seepage meter made by Rosenberry (2008), would allow continuous monitoring of seepage flux, in addition to other instrumentation specifically designed for groundwater-surface water interaction studies (Rosenberry et al., 2020).

- Temperature data is difficult to obtain at deep locations of coastal aquifers because long wells for conventional water supply are not commonly drilled due to the presence of the saline wedge. In addition, it is difficult to ensure reliable temperature data as it can be altered by the mixing of waters due to vertical flow inside the casing of the well. Even with the careful obtention of measurements in this study, the comparison of temperature data from boreholes of different characteristics, e.g. nested wells or well clusters, could be applied to acquire more accurate results of thermal propagation, as it was performed for hydraulic head and salinity in the coast of Israel (Levanon et al., 2017). Also, other methodologies such as fiber-optic distributed temperature sensing (FO-DTS) could provide additional information (del Val, 2020).

- The synthetic model of temperature distribution in coastal aquifers proposed in this Ph.D. thesis was compared with field measurements obtained from the Motril-Salobreña aquifer. Although the model results were consistent with observations, it would be needed to verify it compared with other study areas, especially, where temperature input can differ from the experimental site, i.e. extreme air temperatures or higher geothermal gradients. Also, places affected by intensive groundwater pumping where the geometry of the freshwater-saltwater interface can be modified, as occurred in the Andarax coastal aquifer (Stein et al., 2020). The theoretical model of heat distribution was a key part of understanding temperature oscillations measured in deep parts of the aquifer and its relationship with the salinity oscillations. While the influence of tidal forces and recharge variations were measured and simulated numerically; long-term phenomena, such as global sea-level rise, should be considered in future studies and, hence, longer time series must be obtained for this purpose.

- The detailed understanding of processes that controlled the hydrodynamics of coastal aquifers demonstrated the role of groundwater in the existence of coastal flooding. Here, different methodologies could complement the initial findings to assess coastal floodings in the Motril-Salobreña aquifer, such as numerical modeling, analytical methods and others explained in Bosserelle et al. (2022). Furthermore, since the relation of the salinization processes of the lagoon with inversions of hydraulic gradient was an unconfirmed hypothesis with strong implications for the management of the natural reserve of "La Charca de Suárez", the origin of salinity enrichment should be determined to support it. The use of stable isotopes to track water origins could be an excellent tool, as it was successfully implemented in other similar and proximal study areas (Skrzypek et al., 2016; Gil-Márquez et al., 2017).

REFERENCES

Bosserelle, A. L., Morgan, L. K., Hughes, M. W., 2022. Groundwater rise and associated flooding in coastal settlements due to sea-level rise: A review of processes and methods. Earth's Future, 10, e2021EF002580. https://doi.org/10.1029/2021EF002580

del Val, L., 2020. Advancing in the Characterization of Coastal Aquifers: A Multimethodological Approach Based on Fiber Optics Distributed Temperature Sensing. Ph.D. Thesis, Polytechnic University of Catalonia, Barcelona, Spain.

Gil-Márquez, J.M., Barberá, J.A., Andreo, B., Mudarra, M., 2017. Hydrological and geochemical processes constraining groundwater salinity in wetland areas related to evaporitic (karst) systems. A case study from Southern Spain. J. Hydrol. 544, 538-554. https://doi.org/10.1016/j.jhydrol.2016.11.062.

Levanon, E., Yechieli, Y., Gvirtzman, H., Shalev, E., 2017. Tide-induced fluctuations of salinity and groundwater level in unconfined aquifers – Field measurements and numerical model. J. Hydrol. 551, 665–675. https://doi.org/10.1016/j.jhydrol.2016.12.045

Rosenberry, D., 2008. A seepage meter designed for use in flowing water. J. Hydrol. 359. 118-130. 10.1016/j.jhydrol.2008.06.029

Rosenberry, D., Duque, C., Lee, D., 2020. History and evolution of seepage meters for quantifying flow between groundwater and surface water: Part 1 – Freshwater settings. Earth-Science Rev. 204. 103167. 10.1016/j.earscirev.2020.103167

Stein, S., Sola, F., Yechieli, Y., Shalev, E., Sivan, O., Kasher, R., Vallejos, A., 2020. The effects of long-term saline groundwater pumping for desalination on the fresh – saline water interface: field observations and numerical modeling. Sci. Total Environ. 732, 139249. https://doi.org/10.1016/j.scitotenv.2020.139249

Skrzypek, G., Dogramaci, S., Grierson, P.F., 2013. Geochemical and hydrological processes controlling groundwater salinity of a large inland wetland of northwest Australia, Chem. Geol. 357, 164-177, https://doi.org/10.1016/j.chemgeo.2013.08.035.

APPENDIX
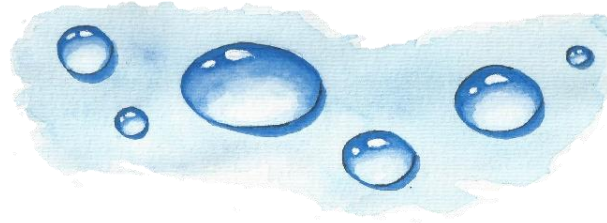
Supplementary files of Chapter 4

Figure A1.- Simulation results of model B at the observation points: L1-T (-20 m), L1-B (-31 m), L2-T (-80 m), L2-B (-96 m), L4-T (-169 m), L4-B (-182 m), L2-I (-88 m), H2-I (-70 m), L3-I (-131 m), H3-I (-110 m), L4-I (-175 m) and H4-I (-155 m).
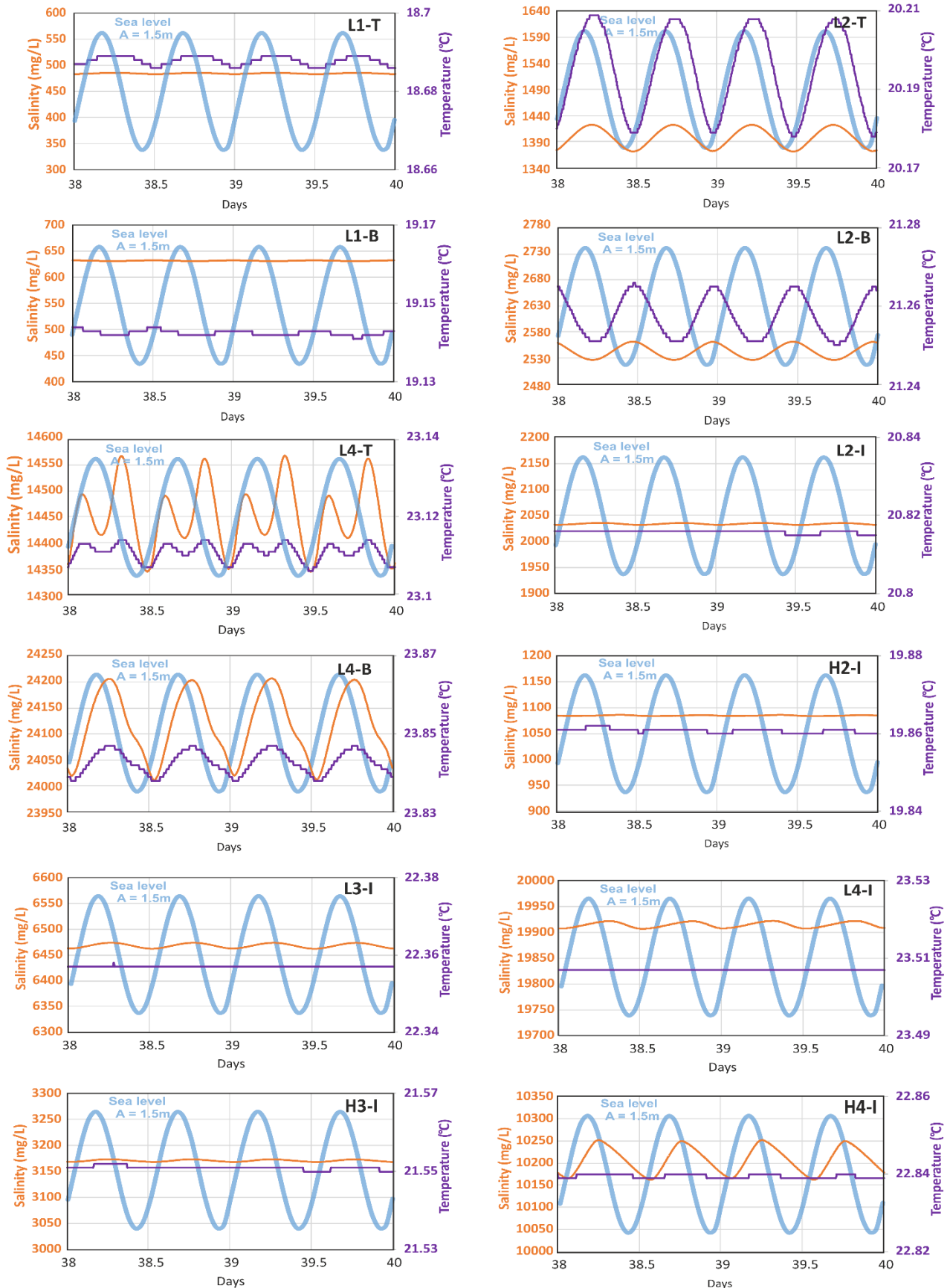
Figure A2.- Simulation results of model C at the observation points: L1-T (-20 m), L1-B (-31 m), L3-T (-124 m), L3-B (-139 m), L1-I (-26 m), L2-I (-88 m), L3-I (-131 m), H2-I (-70 m), H3-I (-110 m) and H4-I (-155 m)